PHYSICALLY BASED CLOSED-FORM SOLUTIONS FOR FILM CONDENSATION OF PURE VAPORS IN VERTICAL TUBES

by

Quang Tan Le

A Thesis Presented to the Faculty of Graduate Studies

In Partial Fulfillment of the Requirements for the Degree of

Master of Science

Department of Mechanical and Manufacturing Engineering

University of Manitoba

Winnipeg, Manitoba, Canada

ABSTRACT

This work analytically solves the governing equations of the laminar film condensation from pure vapors in vertical tubes to find the condensate film thickness. The solution is then extended to turbulent flow conditions for steam. All other relevant quantities are derived from the film thickness solution. For laminar film condensation of quiescent vapors, an exact explicit solution and an approximate closed-form solution were found by using a new definition of the dimensionless film thickness, the Lambert W-function, and a logarithmic function approximation. For laminar mixed-convection film condensation with interfacial shear stress, an approximate closed-form solution was found by using a new definition of the pressure gradient. For turbulent film condensation of steam, correlations of the turbulent vapor and liquid viscosities were formed by asymptotically comparing this approximate laminar closed-form solution to a turbulent flow numerical solution. The present solutions compared very well to published numerical and experimental data.

ACKNOWLEDGEMENTS

I would like to express my gratitude to my advisors, Dr. S.J. Ormiston and Dr. H.M. Soliman, for their advice and constructive criticism.

Many thanks for the support from the department of Mechanical Engineering Technology, Red River College, Winnipeg, Manitoba, Canada.

TABLE OF CONTENTS

LIST OF FIGURES

Figure *Page*

LIST OF TABLES

NOMENCLATURE

C_P	specific heat [J kg^{-1} K^{-1}]
f	friction factor
g	gravitational acceleration [m s^{-2}]
h_{fg}	latent heat of vaporization [J kg^{-1}]
h	local heat transfer coefficient [W m^{-2} K^{-1}]
Ja	Jakob number ($C_p\Delta T/h_{fg}$)
k	thermal conductivity [W m^{-1} K^{-1}]
L	tube length [m]
$\dot{m}$	mass flow rate [kg s^{-1}]
Nu	local Nusselt number ($h\ 2r_o/k_L$)
P	pressure [N m^{-2}]
Pr	Prandtl number ($\mu C_p/k$)
r	radial coordinate [m]
r_o	radius of tube [m]
Re	Reynolds number
T	temperature [K]
ΔT	inlet-to-wall temperature difference (T_{in}-T_{wall}) [K]
u	axial velocity [m s^{-1}]
u^*	dimensionless axial velocity (u/u_{in})
v	radial velocity [m s^{-1}]
v^*	dimensionless radial velocity (v/u_{in})

x	quality ($\dot{m}_v/(\dot{m}_v + \dot{m}_L)$)
X	dimensionless film thickness variable $(1-\delta_+)/2$
z	axial coordinate [m]
z^*	dimensionless axial coordinate (z/r_o)

Subscripts

eff	effective
fc	forced convection
i	interface
in	inlet
L	liquid
nc	natural convection
Nu	Nusselt laminar analysis
sat	saturated
v	vapor
wall	wall

Superscripts

t	turbulent

Greek

δ	condensate film thickness [m]
δ^*	dimensionless condensate film thickness (δ/r_o)

δ_+	dimensionless film thickness variable $(1-\delta^*)^2$
η	radial transformed coordinate (Equation (4.8.1))
μ	dynamic viscosity [N s m^{-2}]
ν	kinematic viscosity [m^2 s^{-1}]
ρ	density [kg m^{-3}]
ρ_+	additional vapor density induced by motion [kg m^{-3}]
τ	shear stress [N m^{-2}]

CHAPTER 1

INTRODUCTION

Condensation is a process of phase changing from vapor to liquid. This occurs when the vapor contacts and transfers its heat to a cooler medium or surface. The study of condensation is very important for many science, engineering, and industrial applications. Some typical examples of these applications are in heat exchangers, desalination processes, and nuclear power generation. The condensation process can be classified by many different ways: geometry configurations such as channel, tube, internal, external, horizontal, and vertical; species of fluid such as steam, refrigerant, and mixture containing a non-condensable gas; condensing phenomena such as film-wise, drop-wise, and fog; and flow regime such as laminar and turbulent. Since the original work of Nusselt (1916), a large number of works have been done to contribute to the understanding of this complex process. These works resulted in many condensing models, many correlations to calculate condensing film thickness and heat transfer coefficient, and a large database of condensing data.

The methods of studying condensation can be grouped as analytical, experimental, and numerical. Analytical methods can be defined as analytically solving the governing equations from a condensing model, either complete or simplified, with various boundary conditions of a particular configuration. The result can be an exact or approximate closed-form solution, an equation or a set of equations that must be solved numerically or with an iterative procedure. To the best of author's knowledge, Nusselt's (1916) analysis

of laminar film condensation from quiescent vapors on a vertical isothermal flat plate is the only closed-form solution using an analytical method. Other typical analytical works are Rohsenow (1956), Carey (1992) and Ghiaasiaan (2008).

In the experimental studies of condensation, apparatuses were setup to produce and measure condensing data. Typical data sets contain the inlet pressure and temperature, the wall temperature distribution along the condenser, and the condensing mass flow rate. Typically, temperatures and mass flow rate of the cooling medium were also collected. From these data, the condensing film thickness and heat transfer coefficient were calculated by heat and mass transfer equations. Some typical works of this kind are Goodykoontz and Dorsch (1967), Kuhn (1995), and Kim (2000).

With the availability of modern advanced computing power, numerical analysis of condensation is becoming more common place. In this approach, the governing equations are discretized using, for example, a finite difference or a finite volume method. The resulting algebraic equations are linearized and the boundary conditions are prescribed appropriately to produce a system of equations than can be solved by a variety of algorithms. The coefficients of the linearized equations are updated and the loop is repeated until a suitable convergence is obtained. The solution results typically available from a numerical model are the condensate film thickness, the local heat transfer coefficient, the local velocity distribution, and the local temperature distribution. Some typical numerical solution based on a complete set of boundary layer equations are Yuann (1993) and Groff (2005). The in-house computer code that implements Groff's

numerical solution, including the Jones and Launder (1972) low k-ε turbulent model, was used as part of the present work.

Some studies of condensation resulted in correlations to compute the condensate film thickness, the local or average heat transfer coefficient, and the local or average Nusselt number. The sources of data used to produce the correlations were both numerical and experimental studies. Examples of correlations produced from experimental data are those of Shah (1978, 2009) and Vierow and Schrock (1991). An example of a correlation for film thickness based on an approximate analytical study is that of Muñoz-Cobo et al. (1996).

While many of the previous studies of condensation helped to improve the understanding and analysis of this complex process, the main drawback of these studies is in their solutions and applications. A simpler solution based on a correlation is not sensitive to local variable and is often not very accurate in its applicable range while a more accurate solution usually requires a complicated procedure that is beyond practical engineering application. Furthermore, despite the fact that almost a century has elapsed since Nusselt's analysis, there is no other closed-form solution available. The focus of the present work is on developing a closed-form solution for film thickness of pure vapor downward mixed-convection condensation in vertical tubes. The closed-form solution is developed in three steps. First, an exact explicit solution is derived for quiescent vapor with laminar condensate flow that is based on the complete parabolic governing differential equations. Although the condensation from quiescent vapor in vertical tubes

is not practically sustainable, this solution can be applied to condensation on the inside of a concave vertical surface with curvature r_o. Second, the solution approach in the first step is extended to obtain an approximate closed-form solution for mixed-convection laminar vapor and laminar condensate flow. This solution applies for any vapor. Third, the solution in the second step is used as the basis of a closed-form solution for mixed-convection turbulent vapor and turbulent condensate flow based on correlating the numerical results for steam. The accuracy of these closed-form solutions is demonstrated in each of the three steps. Since the resulting solutions are closed-form, they are suitable for practical engineering application.

CHAPTER 2

LITERATURE REVIEW

Film condensation is a complex heat and mass transfer phenomenon that has a wide scope of applications and a large body of literature. A recent detailed review of condensation inside tubes was given by Dalkilic and Wongwises (2009). Because the focus of the present work is on simplified solutions for film condensation analyses, the scope of this literature review will be limited to physically based analyses and empirical correlations for film condensation from a pure vapor on vertical flat plates and in vertical tubes. The term "physically based analyses" refers to analyses based on governing equations that were derived from physical principles such as conservation of mass, momentum, and energy.

2.1. Film Condensation on Vertical Flat Plates

The subject of these works was a cooled vertical isothermal flat plate maintained at a temperature below the saturation temperature and exposed to pure quiescent or downward flowing saturated vapor. The condensation starts at the top of the plate and forms a growing liquid film flowing downward because of gravity. In some cases, the shear stress at the interface between the liquid and the vapor was considered. The condensate flow is laminar at the beginning, wavy-laminar in the transitional regime, and then fully turbulent. The objective of these works was to compute one or more of: the local condensate film thickness, the local or average heat transfer coefficient, and the local or average Nusselt number.

2.1.1. Physically Based Analyses of Quiescent Vapors

To the best of the author's knowledge, the analytical work of Nusselt (1916) was the earliest and the only one that produced a closed-form solution. Nusselt made several assumptions to simplify the analysis: laminar liquid film, constant properties, quiescent saturated pure vapor, negligible shear stress at the liquid-vapor interface, negligible momentum transfer along the condensing film, and heat transfer across the liquid film by conduction only. The most distinguishable feature of his work was the derivation of an equation for the condensate mass flow rate from both the momentum equation and from an energy balance. By equating these two equations and integrating, the result of his analysis was closed-form solutions for local film thickness, heat transfer coefficient, and Nusselt number as functions of axial coordinate, z.

Rohsenow (1956) added the effect of energy convection in the film to Nusselt's analysis. By neglecting the energy advection in the condensate, Nusselt assumed that the temperature profile in the condensate was linear. Therefore, Rohsenow showed that the temperature profile in the condensate could be nonlinear. The result of Rohsenow's analysis was a use of an effective latent heat of condensation, which was important for liquids with high subcooling or Jakob number.

Sparrow and Gregg (1959) used a boundary-layer analysis with a similarity transformation and included the effects of convection and fluid acceleration in the condensate. In this technique, the partial differential governing equations were transformed to ordinary differential equations using similarity variables. Once that was

achieved, numerical integration was used to compute the film thickness and the temperature profile. A special case, in which the fluid acceleration was excluded, compared well to Rohsenow (1956). Note that Sparrow and Gregg also tried to include variable wall temperature in the analysis but concluded that this type of similarity analysis could not be used for either polynomial or exponential wall temperature profile. Koh et al. (1961) used stream function in the similarity transformation of the laminar flow boundary layer equations and also considered the interfacial shear stress. However, the interfacial shear stress was not induced by vapor flow. Instead, the liquid flow induced motion in the quiescent vapor near the film. From this point of view, the condensate velocity and flow rate were reduced. It was clear that the effect of this type of interfacial shear was very small and they concluded that it was practically unimportant. Shang and Wang (1997) used dimensionless variables to transform the governing equations of the liquid and of the quiescent superheated vapor. In a two-step numerical procedure, the vapor was treated as quiescent and with shear force induced by downward flowing laminar condensate film. Fujii et al. (1997) also used stream functions to transform the governing equations and then solved them with a numerical method. The condensate flow was assumed laminar. The quiescent saturated vapor was in the near-critical region. They reported that the effect of the liquid axial convection, for steam and carbon dioxide, was significant in the near-critical region. Xu et al. (2008) also used boundary layer analysis with a similarity transformation. Instead of numerical integration, the solution method was the homotopy analysis method. This work did not produce an actual solution set for the condensation, however. Its main purpose was to demonstrate the applicability of its mathematical formulation by showing different approximations of

the transformed variables obtained with various orders of the homotopy analysis method. These approximations can then be used, by additional analyses, to find a more desirable physical quantity such as the heat flux at the wall.

Lee (1964) considered the turbulent flow in the condensate by adding the eddy kinematic viscosity and eddy thermal diffusivity in the governing equations by Deissler's and von Karman's expressions in appropriate regions. Transformations were performed on the governing equations to become a first order differential equation, which were then solved by a numerical method. The solution set included the velocity profile, the temperature profile, and the film thickness. Chen (1986) also considered the turbulent condensate flow by using Prandtl's mixing length theory with surface damping effect at the wall and the interface. The system of equations was transformed by various dimensionless groups and then solved by a finite difference method. In this work the full turbulent regime was assumed to start at the liquid Reynolds number of 450 while the Reynolds number of the transitional regime was 175.

2.1.2. Physically Based Analyses of Mixed Convection

Ghiaasiaan (2008) proposed one of the most interesting approaches to account for the vapor flow and its resulting interfacial shear stress in the analysis of laminar film condensation. He defined the pressure gradient as the body force of a modified vapor density and equated it to the sum of the regular body force and an additional constant component of pressure gradient in the vapor phase, which was responsible for the vapor motion. A procedure similar to that of the Nusselt analysis was then performed and

resulted in a system of three equations with five unknowns. This result was clearly impractical although the approach was very logical.

Rohsenow et al. (1956) considered the effect of vapor shear stress on the film by analyzing the force balance on an element of the liquid. They neglected the vertical momentum flow across the element's face to reduce the shear stress to a linear profile across the film and constant along the vertical direction. For the turbulent flow regime, an assumed universal velocity distribution was used in the liquid. An interesting discussion was included in the authors' closure section where the authors suggested that a fictitious vapor density may be used to replace the molecular vapor density in order to simplify the analysis. This may be the earliest mention of this concept which was used in other works such as Muñoz-Cobo (1996), Carey (1992), and Ghiaasiaan (2008). A variant of this vapor density function and its associated pressure gradient were used successfully in Chapter 4 of the present work. Note that in the earlier works, the fictitious vapor density replaced the molecular vapor density as a whole. In the present work, the vapor density function is an additional component of the total density.

Jacobs (1966) used a coordinate transformation to reduce the governing equations of the vapor and liquid flows to a set of ordinary differential equations. The unknowns in these equations were the laminar dimensionless film thickness and interface velocity. These quantities were expanded by series, truncated after the linear term, and then solved by numerical integration. Fujii and Uehara (1972) essentially used the same formulation and solution method as proposed by Jacobs (1966). However, they used a better

approximation of the power series and a better numerical method. The solutions were used to form correlations for local and average Nusselt numbers. The correlations were grouped by natural convection, forced convection, and mixed convection.

Denny et al. (1971) studied laminar flow of a steam-air mixture but also considered pure vapor. The similarity transformation used stream function to transform the vapor's momentum, species, and energy equations. They were then approximated by fully implicit finite difference scheme and solved by iteratively marching down the vertical direction. A parametric study was performed to determine the optimized value of various numerical parameters such as step size, number of nodes, and initial guesses. Shu and Wilks (1995) presented a general methodology to solve a system of differentio-integral equation which is commonly associated with two-phase flow. The continuous transformation was stated to be applicable to any characteristic coordinate. They only showed the completed transformation and the iterative solution for a vertical plate, however. Winkler et al. (1999) performed a transformation by different parameters for free and forced convection cases. The transformed equations were solved by finite difference method and studies were done for both saturated and superheated vapors. The effect on the heat flux of the latter was found to be insignificant. Nusselt number correlations were formed for saturated steam in the cases of free and forced convection. They compared well with Shu and Wilks (1995). Fujii et al. (1996) also used stream function to transform the governing equations and then solved them with a numerical method. Both vapor and liquid flows were assumed laminar. Similar to their later study in

1997 of free convection, the saturated vapor was in the near-critical region, which had a significant effect in the liquid axial convection for steam and carbon dioxide.

Ünsal (1988) derived an algebraic equation for average heat transfer coefficient of laminar mixed convective condensation on inclined surfaces. The solution method was a first-order perturbation with a linearized stability analysis to approximately determine 17 coefficients. Some terms were dropped by an order of magnitude analysis. Although the solution was called closed-form, it was a correlation composed of the perturbation coefficients and other dimensionless parameters.

Chin (1995) and Chin et al. (1998) developed numerical solution for the complete governing equations of condensation from mixed-convection vapor-gas mixtures over an isothermal flat plate. The plate could be oriented at any angle from horizontal to vertical. The inertia and energy convection was treated as input parameters so the effects of using complete and simplified governing equations could be studied for laminar condensation. The solution was based on a finite volume method.

2.1.3. Empirical Correlations

Several other researchers extended the Nusselt analysis to include the effect of film waviness and turbulence by correlating experimental works. The most common ones were Labuntsov (1957), Kutateladze (1963), Kutateladze and Gogonin (1979), and Kutateladze et al. (1980). These works produced expressions for the average modified Nusselt number applicable for the transitional and full turbulent flow. The data used for

these correlations were obtained from many different experimental studies. The authors stated that the validity of these formulae cannot be fully assessed on the basis of the experimental data presented due to the large scatter in the experimental points. Chen et al. (1987) also presented a similar correlation to account for both film waviness and turbulence. Beside the uncertainty due to the large scatter in the data points, there was another shortcoming in all of these works. These correlations were relations between the average modified Nusselt number and the condensate Reynolds number, which might require an iterative solution.

2.2. Mixed Convection Film Condensation in Vertical Tubes

The objective of these works was to study the film condensation in vertical tubes. They all started with mixed convection and ignored the quiescent vapor case for the obvious reason that the condensation in tubes from quiescent vapor cannot be sustained for long tubes. The four most difficult quantities to determine in these analyses are: interfacial temperature, interfacial shear stress, velocity profile, and turbulence. Interfacial temperature was excluded from this review since only pure vapor was considered. Interfacial shear stress, which cannot be ignored in the mixed convection scenario, was usually dealt with by using a single phase flow friction factor. The velocity profile was commonly assumed as parabolic or some universal profile. Turbulence was treated by either a mixing length model or a low Reynolds number k-ε model.

2.2.1. Physically Based Analyses and Correlations

Mixed convection film condensation in vertical tubes can be analyzed using a procedure similar to the Nusselt (1916) analysis, only in a cylindrical coordinate system. Blangetti et al. (1982) used this approach and derived a system of three equations, including a cubic equation to compute the dimensionless film thickness. The coefficients of these equations included terms involving the local film Reynolds number and the interfacial shear stress. Turbulence was modeled using the liquid eddy viscosity with and without a wall damping effect. The dependency among these quantities required an iterative procedure to compute the film thickness. Carey (1992) defined a fictitious vapor density that combined the gravitational, frictional, and momentum components of the pressure gradient. The frictional component was based on a single-phase flow friction factor. The momentum component was based on an approximation of the void fraction and an order of magnitude analysis among its terms to obtain a simplified expression. The result was a system of four equations, including a quartic equation to compute the film thickness. The coefficients of these equations included terms of the interfacial shear stress and the fictitious vapor density. Turbulence was accounted for by a correlation with Von Karman's mixing-length model. Again, the interdependency of these terms required an iterative procedure for the solution. Dalkilic et al. (2009) used the same technique as Carey to create a laminar film condensation model. They computed the local heat transfer coefficient and compared it to experimental data for R134a. The deviation was reported to be between 60.7% and 64.1%. Note that the deviation was high because the model was laminar while the experimental data were for turbulent flows. These works demonstrate the difficulties and the limitations related to this type of analysis; such as the interfacial

shear stress, the pressure gradient, the closure conditions, and the solution techniques; these espects are all successfully dealt with in the present work.

A typical work that used an approximate integral analysis with an assumed velocity profile was reported by Lucas and Moser (1979). Their main objective was to compare the laminar heat transfer by flows with uniform and with fully developed inlet velocities, which were concluded to be similar. The comparison was also made for horizontal and vertical tubes. In this case, the integral analysis was shown to be inappropriate for horizontal tubes due to the annular flow assumption. Dobran and Thorsen (1980) solved a simplified set of boundary layer equations with assumed velocity and temperature profiles. They started with the complete set of parabolic laminar boundary layer equations and a fully developed inlet velocity profile. These equations were then simplified by five dimensionless parameters: vapor Froude-to-Reynolds number ratio, Buoyancy number, vapor-to-liquid viscosity ratio, liquid Prandtl number, and Subcooling number. With assumed vapor and liquid parabolic axial velocity profiles and an assumed liquid parabolic temperature profile, the governing equations were simplified and reduced to three nonlinear ordinary differential equations. The numerical solution of these equations compared well to Nusselt's solution in appropriate ranges of parameters and offered significant insights of their hydrodynamic effects. Pohner and Desai (1989) converted the integral forms of the mass, momentum, and energy equilibrium to their differential forms. The result was a set of equations of seven dependent variables. Closure was obtained by assumed velocity profiles and temperature profile. The interfacial shear stress was computed from a friction factor for both laminar and turbulent

vapor cases. An iterative procedure was employed to compute the laminar flow heat transfer coefficient. Chen and Ke (1993) considered turbulent vapor flow and turbulent condensate flow. The turbulent model divided the annular flow to three regions: the inner region near the wall, the interface region, and the outer region at the vapor core. Using an assumed self-similar velocity profile and a correlation for the interfacial shear stress, the governing equations were reduced to a set of integro-differential equations of various dimensionless variables such as dimensionless velocities and dimensionless properties. These equations were solved by an iterative numerical procedure marching along the axial coordinate. The results compared well to the experimental data of Goodykoontz and Dorsch (1966) except at the inlet and end sections. The disagreement at the inlet section was attributed to liquid entrainment and the disagreement at the end section was attributed to slug flow. Kim et al. (2011) assumed the liquid to be Couette flow. The liquid momentum equation was therefore simplified without the pressure gradient term. The derivation required the vapor-liquid interfacial velocity which was supplied by an empirical power-law velocity profile. An iterative procedure was used to compute the film thickness with various guess values of power-law. The value of power-law was thus an important parameter and was determined to be 2 after comparison with the experimental data of Lee and Kim (2008).

Another analytical approach is solving a simplified set of boundary layer equations combined with other assumptions, correlations, and theories. A typical work that used this approach was Yao and Ghiaasiaan (1996). They numerically solved a simplified set of boundary layer equations which modeled the liquid film and the gaseous layer near the

liquid-vapor interface as Couette flows. The results compared well to the experimental data of Siddique (1993). Du and Wang (2003) used Kelvin-Helmholtz instability theory to account for the interfacial waviness and studied this influence on the condensing heat transfer in small diameter tubes from 1.94 mm to 6 mm. Oh and Revankar (2005) also solved a simplified set of boundary layer equations with the interfacial shear stress computed from a friction factor. The resulting average heat transfer coefficient was compared well with experimental data. Zhou et al. (2010) used a finite difference method to solve for the local condensing film thickness and the average heat transfer coefficient of a four-tube-bundle passive condenser. The model's results agreed within 25% of their own experimental data.

Muñoz-Cobo et al. (1996) developed an approximate formula to calculate the turbulent condensate film thickness by polynomial functions of the axial location *z*. They performed a force balance on an element of the condensate film thickness, expanded the resulting function using a Taylor series, and then integrated along the radial direction with other Taylor series approximations to obtain two levels of correlation: without and with interfacial shear stress. For a limiting case of pure vapor where the tube radius is approaching infinity (i.e., a flat plate) while the Reynolds number is approaching zero (i.e., neglecting interfacial shear stress), the correlated film thickness should approach Nusselt film thickness. However, this correlation approaches $1.189\delta_{Nu}$ in this limiting case. When including the effect of the interfacial shear stress, the approximate condensate film thickness must be obtained by an expression that required other parameters: shear stress at the interface, interface-to-wall temperature difference, and a fictitious mixture

density. The steps to calculate these parameters required an iterative procedure involving several other parameters: the friction factor at the interface, the condensing mass flow rate per unit area, the interface velocity, and the interface temperature. For example, the fictitious mixture density requires the mass flow rate, the mass flow rate requires the velocity profile, and the velocity profile requires the fictitious mixture density. Similarly, the film thickness requires the film-side interface shear stress, the film-side interface shear stress requires the interface friction factor, and the interface friction factor requires the film thickness. The knowledge of these values is limited and therefore so is the practical use of this solution procedure.

Yuann (1995) numerically solved the complete set of parabolic governing equations together with a low Reynolds number k-ε turbulence model. Film surface waviness was also accounted for by an empirical correlation. Panday (2003) solved the full coupled parabolic governing equations in the liquid and vapor boundary layer equations. He coupled the phases via an enthalpy balance at the interface. Turbulence was modeled using Pletcher's mixing length.

Groff (2005) and Groff et al. (2007) also solved the complete set of parabolic governing equations with a combination of mixing length and low Reynolds number k-ε turbulent models in vapor and condensate flow. The solutions of these works are possible only by full numerical procedure with computer code due to the complexity of the governing equations. The Groff (2005) solution procedure was used as part of the development of the present work.

2.2.2. Empirical Correlations

Shah (1978, 2009) developed a general correlation for heat transfer during film condensation inside pipes of all orientations (vertical, horizontal, and inclined) for 22 various fluids (freons, steam, methanol, benzene, trichloro-ethylene, toluene, and ethanol). He analyzed 1189 experimental data points from 39 independent studies of many authors. The correlation was a set of simple expressions that used the well known Dittus-Boelter equation, reduced pressure, and vapor quality. The correlations are applicable in the laminar, transitional, and fully turbulent flow regimes. Although the calculated mean approximate percentage difference was 14.4%, Shah stated that the error could be a combination of the correlation error and the errors associated with related experimental data. Shah's correlation predicted a zero heat transfer coefficient at the tube's entrance, where the vapor quality is unity. At the end of condensation, where the vapor quality is zero, Shah predicted a heat transfer coefficient equivalent to a tube full of saturated liquid. In reality, the heat transfer should be very high near the tube's entrance since the film thickness is very small, and in many situations there is not enough liquid to fill the tube at the end of condensation.

Siddique et al. (1993) proposed that Nusselt number can be correlated as a function of mixture Reynolds number, Schmidt number, noncondensable gas mass fraction, and Jakob number. They argued that, for turbulent flow of a condensing film, waviness can break up the gaseous laminar sub-layer, destabilize it and thus enhance the mass transfer. They also stated that the sub-layer of high Schmidt number fluid is thin and the effect of interface waviness is more profound. For a steam-air mixture, since the Schmidt number

is small, the concentration layer is thicker compared to the hydrodynamic layer and the interface waviness is not effective in breaking it up. Therefore, the dependency on Schmidt number can be removed to get the correlation that required local mixture Reynolds number, Jakob number, and air mass fractions at the wall and the core. A logarithmic transformation and a linear regression analysis were used to find the coefficients of the correlation. Siddique's experiment used a condensing tube 2.54-m length with a 0.046-m diameter. The noncondensable gases used with steam were air and helium with gas mass fractions of 10% to 35%. The operating pressure was 100 to 500 kPa.

Revankar et al. (2010) used heat and mass analogy model together with the relation of interfacial shear and friction factor to simulate a limited set of experiment data. The experiment used a condensing tube of 0.984-m length and 0.0266-m diameter. The air mass fraction was 0 to 10%. The operating pressure was 100 to 400 kPa. In turn, the experimental data of steam were used to validate the model. The model was then used to generate a large set of artificial data for the development of a correlation. A non-parametric regression algorithm called alternating conditional expectation (ACE) was used. The correlation predicts a total condensation Nusselt number for laminar and turbulent flow. They reported that the correlations compared well with the experimental data of Kuhn (1995).

Vierow and Schrock (1991) proposed a degradation factor method for a correlation where the computed heat transfer coefficient is related to the Nusselt heat transfer coefficient by

two factors. In the formulation, the enhancing factor f_1, which relates to Reynolds number, and the degradation factor f_2, which relates to the noncondensable gas mass fraction, seem to be independent. However, the simplicity of each factor suggests that they must be used together. For example, with pure vapor, the degradation factor f_2 becomes unity and the correlation becomes too simple to be effective. The data used for the fitting of correlation's coefficients came from the testing facility with a condensing tube length and inside diameter of 2.1 m and 0.022 m, respectively. The mixture was steam-air with the air mass fraction of 0 to 14%. The operating pressure range was 30 to 450 kPa.

Continuing the work of Vierow and Schrock (1991), Kuhn (1997) modified the enhancing factor f_1 with $f_{1\text{shear}}$ and $f_{1\text{other}}$. The factor $f_{1\text{shear}}$ represents the effect of interfacial shear. The factor $f_{1\text{other}}$ represents the effect of other deviations such as film waviness and depends on the condensate Reynolds number. With the inclusion of interfacial shear, the film thickness δ_{shear} must be computed separately by another equation which requires the blowing parameter for momentum transfer, the condensate film flow rate per unit perimeter, and the Blasius turbulent friction factor. The practical use of this correlation depends on the availability of condensation flow rate per unit perimeter and shear stress which also depends on the local bulk mixture velocity, the interface velocity, and the condensate mass flux. Kuhn's experiment used a condensing tube 2.4-m length with a 0.0475-m diameter. The noncondensable gases were air and helium with gas mass fractions of 0 to 40%. The operating pressure was 100 to 500 kPa.

Park and No (1999) also used a degradation factor method and proposed a correlation for the heat transfer coefficient but considered that the effect of the mixture Reynolds number is weaker than the liquid Reynolds numbers. The practical use of this correlation, however, is limited by the need to know the liquid Reynolds number. Their test facility used a tube length and diameter of 2.4 m and 0.0475 m, respectively. The air mass fraction was 10% to 40%. The operating pressure was 170 to 500 kPa.

Lee and Kim (2008) also proposed a correlation using a degradation factor method but took into consideration the interfacial shear stress. For pure vapor condensation, the factor f_2 does not become unity. Their condensing tube had a length of 2.8 m and a diameter of 0.013 m. They used steam and nitrogen gas with a mass fraction from 0 to 40%. The operating pressure was 100 to 130 kPa. Note that the tube diameter of this experimental setup is the smallest one used to generate data for correlation development.

Aglar and Tanrikut (2008) also used a degradation method and included both the steam-air mixture Reynolds number and the condensate Reynolds number in the correlation. The coefficients were calculated by their experimental data at the Middle East Technical University. The tube diameter and length were 0.033 m and 2.158 m, respectively. The ranges of parameters used in the experiment were: inlet pressure from 1.8 to 5.5 bar, inlet mixture Reynolds number from 45000 to 94000, and air mass fraction from 0 to 0.52. The data were reduced by Kuhn's algorithm and fitted by the Marquardt-Levenberg nonlinear method. The mean approximate percentage difference between the correlation and the experiment was 19.4%. Similar to Siddique, the film waviness was ignored in the

development of this correlation since the Schmidt-number of air-vapor mixture is small. For small Schmidt-number mixtures, the concentration layer is thicker compared to the hydrodynamic layer and the film waviness is not effective in breaking it up.

2.3. Conclusions

From the above literature review, a number of conclusions can be drawn:

1. Nusselt's analysis is the only closed-form solution available. It applies to laminar condensation from a quiescent vapor on a vertical flat plate.
2. Other analytical works included the effects of subcooling, turbulence, interfacial shear stress, and surface waviness. They required, however, an iterative solution procedure.
3. Nusselt's solution was used as the starting point for many theoretical correlations. Therefore the effect of the tube's curvature was ignored or absorbed into the correlation coefficients.
4. Some empirical correlations are very simple but not very accurate.
5. More elaborate empirical correlations are more accurate but require an iterative solution procedure.

It is the goal of the present work to develop, from fundamental physical balances, closed-form solutions for laminar and turbulent downward flow of mixed convection film condensation from pure vapors in vertical tubes. The solution should use simple and accurate functions that require only readily available parameters such as the tube radius, the inlet Reynolds number, the inlet saturation temperature or pressure, the constant or

variable wall temperature, and the required axial location. The calculation procedure should be as straight forward as substituting these input parameters into the function without the need for iteration.

CHAPTER 3

LAMINAR FILM CONDENSATION OF QUIESCENT VAPOR

3.1. Mathematical Model

The literature review indicated that many correlations are based on the Nusselt analytical solution of vertical flat plate condensation. Many of these correlations produced good results even for vertical tube applications. This agreement indicates that curvature might not have a significant influence on the film thickness and the resulting heat transfer coefficient. It is possible, however, that the effect of curvature was absorbed in the correlation's coefficients. For smaller tubes, it is unlikely that Nusselt's analysis is reasonable, and the effect of interfacial shear is needed for practical situations. As a starting point in the development of a mixed convection model, the present work starts with the equivalent of Nusselt's analysis, only in cylindrical coordinates as shown in Figure 3.1. A new closed-form solution is developed as described below.

The assumptions for this analysis are:

1. The vapor is pure, saturated, and quiescent.
2. The temperature in the vapor is uniform.
3. The wall temperature is constant.
4. Shear stress at the liquid-vapor interface is negligible.
5. The condensate flow is laminar.
6. Fluid properties are constant.
7. Radial pressure gradient is negligible.

8. Axial conduction in the condensate is negligible.
9. Heat transfer in the liquid film is only by conduction in the radial direction.
10. Advection of momentum and axial diffusion of momentum in the liquid are negligible.

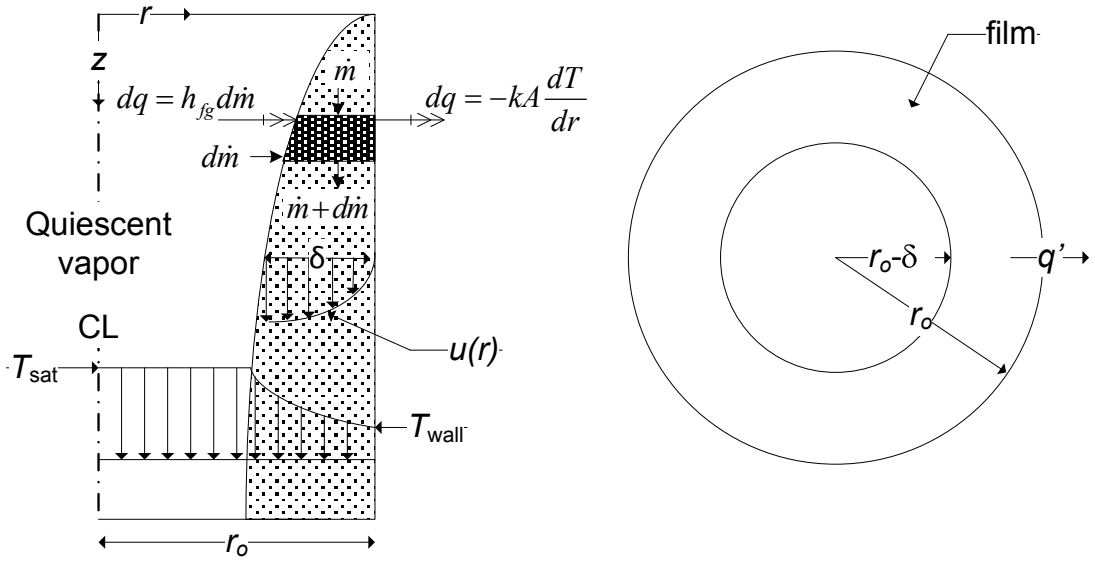

a) side view b) top view

Figure 3.1: Laminar film condensation without interfacial shear stress

Using the coordinate system in Figure 3.1, the governing equations of the liquid film are, therefore:

$$\frac{1}{r}\frac{\partial}{\partial r}\left(r\mu_L \frac{\partial u_L}{\partial r}\right) = \frac{dP}{dz} - \rho_L g \tag{3.1.1}$$

$$k_L \frac{1}{r}\frac{\partial}{\partial r}\left(r\frac{\partial T_L}{\partial r}\right) = 0 \tag{3.1.2}$$

The control volume in Figure 3.1 shows two balances that are made on a differential control volume encompassing the entire liquid film for a height of *dz*. The energy flows,

indicated by double arrows, show the balance of energy transfer by latent heat and energy transfer at the wall. The mass flows, indicated by single arrows, show the mass addition by condensation. In the analysis in this work, the overall mass balance in the liquid is enforced implicitly. Therefore, the differential form of the continuity equation does not appear in the set of governing equations for the liquid.

The axial pressure gradient is:

$$\frac{dP}{dz} = \rho_V g \tag{3.1.3}$$

From the assumptions and the no slip condition at the wall, the boundary conditions for the film are:

$$\left.\frac{\partial u_L}{\partial r}\right|_{r=r_o-\delta} = 0 \tag{3.1.4}$$

$$u_L\big|_{r=r_o} = 0 \tag{3.1.5}$$

$$T_L\big|_{r=r_o} = T_{\text{wall}} \tag{3.1.6}$$

$$T_L\big|_{r=r_o-\delta} = T_{\text{sat}} \tag{3.1.7}$$

3.2. Condensate Radial Velocity Profile

The condensing film velocity profile can be obtained from the liquid axial momentum Equation (3.1.1) with the pressure gradient from Equation (3.1.3). Substituting Equation (3.1.3) into Equation (3.1.1) yields:

$$\mu_L \frac{1}{r}\frac{d}{dr}\left(r\frac{du_L}{dr}\right) = \frac{dP}{dz} - \rho_L g = \rho_V g - \rho_L g = -g(\rho_L - \rho_V) \tag{3.2.1}$$

or

$$\frac{d}{dr}\left(r\frac{du_L}{dr}\right) = -\frac{g(\rho_L - \rho_V)}{\mu_L} r \tag{3.2.2}$$

Integrating Equation (3.2.2) with respect to radius, and evaluating the constant of integration by using Equation (3.1.4), yields:

$$r\frac{du_L}{dr} = -\frac{g(\rho_L - \rho_V)}{2\mu_L} r^2 + C_{L,1} \tag{3.2.3}$$

where

$$C_{L,1} = \frac{g(\rho_L - \rho_V)(r_o - \delta)^2}{2\mu_L} \tag{3.2.4}$$

Therefore, Equation (3.2.3) can be rewritten as:

$$r\frac{du_L}{dr} = \frac{g(\rho_L - \rho_V)}{2\mu_L}\left((r_o - \delta)^2 - r^2\right) \tag{3.2.5}$$

or

$$\frac{du_L}{dr} = \frac{g(\rho_L - \rho_V)}{2\mu_L}\left(\frac{(r_o - \delta)^2}{r} - r\right) \tag{3.2.6}$$

Now Equation (3.2.6) is integrated with respect to radius and the constant of integration is evaluated using Equation (3.1.5) to obtain:

$$u_L = \frac{g(\rho_L - \rho_V)}{2\mu_L}\left((r_o - \delta)^2 \ln(r) - \frac{r^2}{2}\right) + C_{L,2} \tag{3.2.7}$$

where

$$C_{L,2} = -\frac{g(\rho_L - \rho_V)}{2\mu_L}\left((r_o - \delta)^2 \ln(r_o) - \frac{r_o^2}{2}\right) \tag{3.2.8}$$

The radial film velocity profile is then:

$$u_L = \frac{g(\rho_L - \rho_V)}{4\mu_L}\left(2(r_o - \delta)^2 \ln\left(\frac{r}{r_o}\right) + \left(r_o^2 - r^2\right)\right) \tag{3.2.9}$$

3.3. Condensate Axial Mass Flow Rate

The axial mass flow rate of the film is obtained from the integration of the velocity profile as follows:

$$\begin{aligned}\dot{m}(z) &= \int_{r_o-\delta}^{r_o} \rho_L u_L 2\pi r dr \\ &= \frac{\pi g \rho_L(\rho_L - \rho_V)}{2\mu_L}\int_{r_o-\delta}^{r_o}\left(2(r_o - \delta)^2 r \ln\left(\frac{r}{r_o}\right) + \left(r_o^2 r - r^3\right)\right)dr\end{aligned} \tag{3.3.1}$$

The terms of the integration can be evaluated separately and then combined:

$$\int_{r_o-\delta}^{r_o} r\ln\left(\frac{r}{r_o}\right)dr = \left(\frac{r^2}{2}\left(\ln\left(\frac{r}{r_o}\right) - \frac{1}{2}\right)\right)_{r_o-\delta}^{r_o} = -\frac{r_o^2}{4} - \frac{(r_o - \delta)^2}{2}\ln\left(\frac{r_o - \delta}{r_o}\right) + \frac{(r_o - \delta)^2}{4} \tag{3.3.2}$$

$$\int_{r_o-\delta}^{r_o}\left(r_o^2 r - r^3\right)dr = \left(\frac{r_o^2 r^2}{2} - \frac{r^4}{4}\right)_{r_o-\delta}^{r_o} = \frac{r_o^4}{4} + \frac{(r_o - \delta)^4}{4} - \frac{r_o^2(r_o - \delta)^2}{2} \tag{3.3.3}$$

So that

$$\dot{m}(z)=\frac{\pi g\rho_L(\rho_L-\rho_V)}{2\mu_L}\left(\begin{array}{l}2(r_o-\delta)^2\left(-\frac{r_o^2}{4}-\frac{(r_o-\delta)^2}{2}\ln\left(\frac{r_o-\delta}{r_o}\right)+\frac{(r_o-\delta)^2}{4}\right)+\\ \frac{r_o^4}{4}+\frac{(r_o-\delta)^4}{4}-\frac{r_o^2(r_o-\delta)^2}{2}\end{array}\right)$$

$$=\frac{\pi g\rho_L(\rho_L-\rho_V)}{2\mu_L}\left(\begin{array}{l}-\frac{2(r_o-\delta)^2r_o^2}{4}-\frac{4(r_o-\delta)^4}{4}\ln\left(\frac{r_o-\delta}{r_o}\right)+\frac{2(r_o-\delta)^4}{4}+\\ \frac{r_o^4}{4}+\frac{(r_o-\delta)^4}{4}-\frac{2r_o^2(r_o-\delta)^2}{4}\end{array}\right) \tag{3.3.4}$$

$$=\frac{\pi g\rho_L(\rho_L-\rho_V)}{8\mu_L}\left(r_o^4+3(r_o-\delta)^4-4r_o^2(r_o-\delta)^2-4(r_o-\delta)^4\ln\left(\frac{r_o-\delta}{r_o}\right)\right)$$

Simplification is achieved by defining a dimensionless film thickness variable:

$$\delta_+=\left(\frac{r_o-\delta}{r_o}\right)^2 \tag{3.3.5}$$

The following terms use δ_+ in their simplification:

$$\delta=r_o\left(1-\sqrt{\delta_+}\right) \tag{3.3.6}$$

$$r_o-\delta=r_o\sqrt{\delta_+} \tag{3.3.7}$$

$$2r_o-\delta=r_o\left(1+\sqrt{\delta_+}\right) \tag{3.3.8}$$

$$\delta(2r_o-\delta)=r_o^2\left(1-\delta_+\right) \tag{3.3.9}$$

With this new dimensionless film thickness variable, Equation (3.3.4) becomes:

$$\dot{m}(z)=\frac{\pi g\rho_L(\rho_L-\rho_V)}{8\mu_L}r_o^4\left(1-4\delta_++3\delta_+^2-2\delta_+^2\ln\delta_+\right) \tag{3.3.10}$$

3.4. Condensate Radial Temperature Profile and Heat Transfer Rate

The steps in integrating the axial condensate energy Equation (3.1.2) twice are:

$$k_L \frac{1}{r}\frac{d}{dr}\left(r\frac{dT_L}{dr}\right)=0 \tag{3.4.1}$$

$$r\frac{dT_L}{dr}=C_{T,1} \tag{3.4.2}$$

$$\frac{dT_L}{dr}=C_{T,1}\frac{1}{r} \tag{3.4.3}$$

$$T_L=C_{T,1}\ln(r)+C_{T,2} \tag{3.4.4}$$

Boundary conditions given by Equations (3.1.6) and (3.1.7) are applied to obtain the condensate radial temperature profile. Equation (3.1.6) yields:

$$T_{sat}=C_{T,1}\ln(r_o-\delta)+C_{T,2} \tag{3.4.5}$$

Equation (3.1.7) yields:

$$T_{wall}=C_{T,1}\ln(r_o)+C_{T,2} \tag{3.4.6}$$

Equations (3.4.5) and (3.4.6) are solved to obtain:

$$C_{T,1}=\frac{T_{sat}-T_{wall}}{\ln\left(\frac{r_o-\delta}{r_o}\right)} \tag{3.4.7}$$

and

$$C_{T,2}=T_{wall}-\frac{T_{sat}-T_{wall}}{\ln\left(\frac{r_o-\delta}{r_o}\right)}\ln\left(r_o\right) \tag{3.4.8}$$

So that the temperature profile in the condensate is:

$$T_L = T_{wall} + \frac{T_{sat} - T_{wall}}{\ln\left(\frac{r_o - \delta}{r_o}\right)} \ln\left(\frac{r}{r_o}\right) \tag{3.4.9}$$

Fourier's law is applied for the radial conduction heat transfer rate of an element of length dz:

$$dq = -k_L A_r \frac{dT_L}{dr} = -k_L (2\pi r dz)\frac{dT_L}{dr} = -(2\pi k_L dz) r \frac{dT_L}{dr} \tag{3.4.10}$$

Now, use the constant of integration $C_{T,1}$ appearing in Equations (3.4.2) and (3.4.7) to obtain:

$$dq = -(2\pi k_L dz)\frac{T_{sat} - T_{wall}}{\ln\left(\frac{r_o - \delta}{r_o}\right)} = -\frac{2\pi k_L dz \Delta T}{\ln\left(\frac{r_o - \delta}{r_o}\right)} \tag{3.4.11}$$

The radial conduction heat transfer rate can be expressed in term of δ_+ as:

$$dq = -\frac{4\pi k_L dz \Delta T}{\ln \delta_+} \tag{3.4.12}$$

The radial conduction heat transfer rate can also be expressed as:

$$dq = h \Delta T 2\pi r_o dz \tag{3.4.13}$$

Using Equations (3.4.12) and (3.4.13) the local heat transfer coefficient is:

$$h = -\frac{2k_L}{r_o \ln \delta_+} \tag{3.4.14}$$

The local Nusselt number is:

$$\mathrm{Nu} = \frac{h2r_o}{k_L} = -\frac{2k_L}{r_o \ln \delta_+}\frac{2r_o}{k_L} = -\frac{4}{\ln \delta_+} \tag{3.4.15}$$

3.5. Condensate Film Thickness Equation

By the eighth and ninth assumptions, the condensing heat transfer rate is equal to the radial conduction heat transfer rate:

$$d\dot{m} \cdot h_{fg} = -\frac{4\pi k_L \Delta T dz}{\ln \delta_+} \tag{3.5.1}$$

or

$$\frac{d\dot{m}}{dz} = -\frac{4\pi k_L \Delta T}{h_{fg} \ln \delta_+} \tag{3.5.2}$$

From Equation (3.3.10), the derivative of mass flow rate with respect to axial direction is:

$$\begin{aligned}\frac{d\dot{m}}{dz} &= \frac{d\dot{m}}{d\delta_+}\frac{d\delta_+}{dz} \\ &= \frac{\pi g \rho_L(\rho_L - \rho_V)}{8\mu_L} r_o^4\left(-4 + 6\delta_+ - 2\left(2\delta_+ \ln \delta_+ + \delta_+\right)\right)\frac{d\delta_+}{dz} \\ &= -\frac{\pi g \rho_L(\rho_L - \rho_V)}{2\mu_L} r_o^4\left(1 - \delta_+ + \delta_+ \ln \delta_+\right)\frac{d\delta_+}{dz}\end{aligned} \tag{3.5.3}$$

Equating Equation (3.5.2) to Equation (3.5.3) and rearranging appropriate factors, one obtains:

$$-\frac{\pi g\rho_L(\rho_L-\rho_V)}{2\mu_L}r_o^4\left(1-\delta_+ +\delta_+\ln\delta_+\right)\frac{d\delta_+}{dz}=-\frac{4\pi k_L\Delta T}{h_{fg}\ln\delta_+} \tag{3.5.4}$$

Integrating both sides of Equation (3.5.4):

$$\int\left(\ln\delta_+ -\delta_+\ln\delta_+ +\delta_+\ln^2\delta_+\right)d\delta_+=\int\frac{8\mu_L k_L\Delta T}{r_o^4 h_{fg}g\rho_L(\rho_L-\rho_V)}dz \tag{3.5.5}$$

The *LHS* of Equation (3.5.5) is:

$$\begin{aligned}LHS&=\left(\delta_+\ln\delta_+-\delta_+\right)-\left(\frac{\delta_+^2}{2}\ln\delta_+-\frac{\delta_+^2}{4}\right)+\left(\frac{\delta_+^2}{2}\ln^2\delta_+-\left(\frac{\delta_+^2}{2}\ln\delta_+-\frac{\delta_+^2}{4}\right)\right)\\&=\frac{\delta_+^2}{2}\ln^2\delta_+ +\delta_+\left(1-\delta_+\right)\ln\delta_+-\delta_+ +\frac{\delta_+^2}{2}\end{aligned} \tag{3.5.6}$$

Note that the constant of integration is introduced in the *RHS* of Equation (3.5.5):

$$RHS=\frac{8\mu_L k_L\Delta Tz}{r_o^4 h_{fg}g\rho_L(\rho_L-\rho_V)}+C_3=\frac{2\delta_{Nu}^4}{r_o^4}+C_3=2\delta_{Nu}^{*4}+C_3 \tag{3.5.7}$$

where

$$\delta_{Nu}^*=\frac{\delta_{Nu}}{r_o} \tag{3.5.8}$$

and

$$\delta_{Nu}=\left(\frac{4\mu_L k_L\Delta Tz}{h_{fg}g\rho_L(\rho_L-\rho_V)}\right)^{1/4} \tag{3.5.9}$$

which is the Nusselt solution for condensation on a vertical flat plate from a quiescent vapor subject to the same assumptions as in Section 3.1.

Equating both sides by Equations (3.5.6) and (3.5.7) yields:

$$\delta_+^2 \ln^2 \delta_+ + 2\delta_+(1-\delta_+)\ln\delta_+ - 2\delta_+ + \delta_+^2 = 4\delta_{Nu}^{*4} + C_3 \tag{3.5.10}$$

Evaluating the constant of integration at $z = 0$ where $\delta = 0$, $\delta_+ = 1$, and $\delta_{Nu}^* = 0$, yields:

$$C_3 = -1 \tag{3.5.11}$$

Rearranging terms of Equation (3.5.10) produces:

$$\delta_+^2 \ln^2 \delta_+ + 2\delta_+(1-\delta_+)\ln \delta_+ + (1-\delta_+)^2 - 4\delta_{Nu}^{*4} = 0 \tag{3.5.12}$$

Rewriting the perfect square and simplifying:

$$\left(\delta_+ \ln \delta_+ + (1-\delta_+)\right)^2 - 4\delta_{Nu}^{*4} = 0 \tag{3.5.13}$$

$$\delta_+ \ln\delta_+ + (1-\delta_+) - 2\delta_{Nu}^{*2} = 0 \tag{3.5.14}$$

$$\ln \delta_+ = \frac{\delta_+ - 1 + 2\delta_{Nu}^{*2}}{\delta_+} = 1 - \frac{1 - 2\delta_{Nu}^{*2}}{\delta_+} \tag{3.5.15}$$

Equation (3.5.15) can be expressed as:

$$\ln \delta_+ = 1 - \frac{A}{\delta_+} \tag{3.5.16}$$

where

$$A = 1 - 2\delta_{Nu}^{*2} \tag{3.5.17}$$

3.6. Exact Solution of the Condensate Film Thickness

To obtain the exact analytical solution, Equation (3.5.16) is rearranged as follows:

$$\frac{A}{\delta_+} = 1 - \ln \delta_+ = \ln e - \ln \delta_+ = \ln\left(\frac{e}{\delta_+}\right) \tag{3.6.1}$$

$$e^{\frac{A}{\delta_+}} = \frac{e}{\delta_+} \tag{3.6.2}$$

$$\delta_+ e^{\frac{A}{\delta_+}} = e \tag{3.6.3}$$

$$-\frac{A}{\delta_+ e^{\frac{A}{\delta_+}}} = -\frac{A}{e} \tag{3.6.4}$$

$$-\frac{A}{\delta_+} e^{-\frac{A}{\delta_+}} = -\frac{A}{e} \tag{3.6.5}$$

The solution of Equation (3.6.5) is:

$$-\frac{A}{\delta_+} = W\left(-\frac{A}{e}\right) \tag{3.6.6}$$

where W is the Lambert W-function as defined in Corless et al. (1996). Therefore:

$$\delta_+ = \frac{-A}{W\left(-\frac{A}{e}\right)} \tag{3.6.7}$$

From Equation (3.6.7), since $\delta_+ \le 1$ and $A \le 1$, then $W(-A/e) \le -1$. So the numerical evaluation of Lambert W-function is by the secondary real branch, W_{-1}. Using Equation (3.3.6), the exact solution for δ^* is therefore:

$$\delta^* = 1 - \sqrt{\frac{-A}{W_{-1}\left(-\frac{A}{e}\right)}} \tag{3.6.8}$$

Note that the implementation of the Lambert W-function is currently available in commercial software packages such as MatLab, Mathcad, Mathematica, or Maple. The implementations are either by series expansion or high precision root search using a combination of Newton and Bisection methods. Some typical works that involved these implementations are Corless et al. (1996) and Barry et al. (1995). In order to implement the Lambert W-function on other system, it can be approximated by other analytical methods globally or by branch. Some typical works that involved these methods and provided accurate approximations for the Lambert W-function are Boyd (1997) and Barry et al. (2000). Although the expression of Equation (3.6.7) is an explicitly exact solution, it may not be classified as closed-form solution by pure mathematical arguments such as Chow (1999) and Bronstein (2008). However, the existence of an exact solution provides an excellent benchmark against which to compare an approximate solution that is more easily computed. An approximate solution to Equation (3.5.16) can be obtained by first approximating $\ln \delta_+$. The next section describes that approximation and two forms of the resulting approximate solution.

3.7. Approximate Solution of the Condensate Film Thickness Equation

3.7.1. Approximation to the Natural Logarithm

Two different expansions of Taylor series are used to approximate natural logarithm:

$$\ln \delta_+ = TS_1(\delta_+) = (\delta_+ - 1) - \frac{1}{2}(\delta_+ - 1)^2 + \frac{1}{3}(\delta_+ - 1)^3 + \ldots \text{ for } \delta_+ > 0 \tag{3.7.1}$$

$$\ln \delta_+ = TS_2(\delta_+) = \left(\frac{\delta_+ - 1}{\delta_+}\right) + \frac{1}{2}\left(\frac{\delta_+ - 1}{\delta_+}\right)^2 + \frac{1}{3}\left(\frac{\delta_+ - 1}{\delta_+}\right)^3 + \ldots \text{ for } \delta_+ \geq \frac{1}{2} \tag{3.7.2}$$

Taking the first term of each series, two approximations for $\ln \delta_+$ are:

$$\ln \delta_+ \approx f_1(\delta_+) = (\delta_+ - 1) \tag{3.7.3}$$

$$\ln \delta_+ \approx f_2(\delta_+) = \left(\frac{\delta_+ - 1}{\delta_+}\right) \tag{3.7.4}$$

Another way to approximate $\ln \delta_+$ is the average of the above approximations:

$$\ln \delta_+ \approx f_3(\delta_+) = \frac{1}{2}\left(f_1(\delta_+) + f_2(\delta_+)\right) = \frac{\delta_+^2 - 1}{2\delta_+} \tag{3.7.5}$$

The plots of these approximations versus the logarithmic function are shown in Figure 3.2 over the typical domain of δ_+. The curves in Figure 3.2 show that $f_1(\delta_+)$ and $f_2(\delta_+)$ are poor approximation of $\ln \delta_+$ for $\delta_+ < 0.9$ while $f_3(\delta_+)$ is a good approximation over the entire domain. These characteristics are used in the next subsections that discuss obtaining an approximate solution that is simple yet accurate.

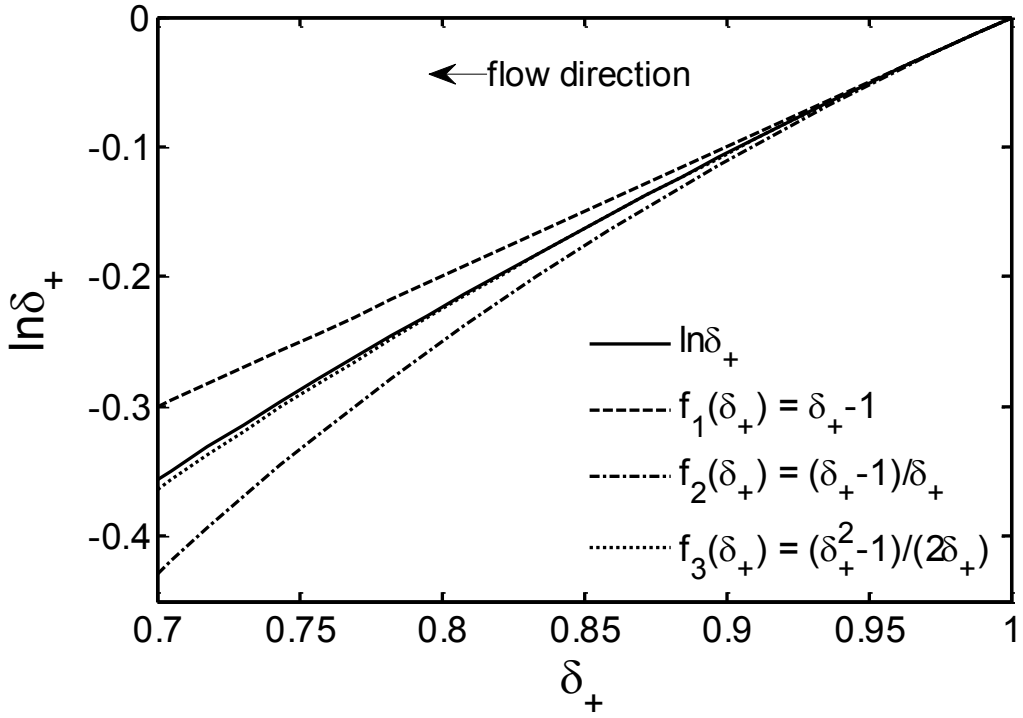

Figure 3.2: The logarithmic function and three approximations

3.7.2. First Form of the Approximate Solution

It is worthy to note that using increased number of term of Equations (3.7.1) and (3.7.2) would improve the approximation of $\ln\delta_+$ but results in cubic, quartic, or higher polynomial equation for δ_+. Because of the increased complexity in solving those higher order polynomial equations, using $f_3(\delta_+)$ is preferred in order to keep the approximate solution simple and yet still reasonably accurate. Substituting Equation (3.7.5) into Equation (3.5.16) yields:

$$\frac{\delta_+^2-1}{2\delta_+}=1-\frac{A}{\delta_+} \tag{3.7.6}$$

or

$$\delta_+^2-2\delta_++(2A-1)=0 \tag{3.7.7}$$

so

$$\delta_+ = \frac{2 \pm \sqrt{4 - 4(2A - 1)}}{2} = 1 \pm \sqrt{2(1 - A)} = 1 - \sqrt{2(1 - A)} \tag{3.7.8}$$

Note that the negative operator is used in the above equation because $\delta_+ \le 1$. Thus,

$$\delta_+ = 1 - \sqrt{2\left(1 - \left(1 - 2\delta_{Nu}^{*2}\right)\right)} = 1 - \sqrt{2 - 2 + 4\delta_{Nu}^{*2}} = 1 - 2\delta_{Nu}^{*} \tag{3.7.9}$$

Using the approximate solution of Equation (3.7.9) in Equation (3.3.6) to obtain:

$$\delta^* = 1 - \sqrt{1 - 2\delta_{Nu}^*} \tag{3.7.10}$$

Since this approximate closed-form solution has Nusselt solution of film condensation on isothermal vertical flat plate in its expression, it is worth checking its limit as the tube radius approaching infinity. This limit can be obtained by the following manipulation:

$$\begin{aligned}
\delta &= r_o - r_o\sqrt{1 - 2\frac{\delta_{Nu}}{r_o}} \\
&= r_o - \sqrt{r_o^2 - 2r_o\,\delta_{Nu}} \\
&= r_o - \sqrt{r_o^2 - 2r_o\,\delta_{Nu} + \delta_{Nu}^2 - \delta_{Nu}^2} \\
&= r_o - \sqrt{\left(r_o - \delta_{Nu}\right)^2 - \delta_{Nu}^2} \\
&= r_o - \sqrt{\left(r_o - \delta_{Nu}\right)^2\left(1 - \frac{\delta_{Nu}^2}{\left(r_o - \delta_{Nu}\right)^2}\right)}
\end{aligned} \tag{3.7.11}$$

As r_o approaches infinity:

$$r_o \to \infty \Rightarrow \frac{\delta_{Nu}^2}{\left(r_o - \delta_{Nu}\right)^2} \to 0 \tag{3.7.12}$$

Then:

$$\begin{aligned} \lim_{r_o \to \infty} \delta &\to r_o - \sqrt{\left(r_o - \delta_{Nu}\right)^2} \\ &\to r_o - \left(r_o - \delta_{Nu}\right) \\ &\to \delta_{Nu} \end{aligned} \tag{3.7.13}$$

Thus, the correct limit of the vertical flat plate condensation solution is obtained for very large radius.

3.7.3. Second Form of the Approximate Solution

This alternative approach is useful when a compact expression similar to Equation (3.5.16) cannot be obtained. One can substitute Equation (3.7.5) directly into Equation (3.5.12) to obtain:

$$\delta_+^2\left(\frac{\delta_+^2 - 1}{2\delta_+}\right)^2 + 2\delta_+\left(1 - \delta_+\right)\left(\frac{\delta_+^2 - 1}{2\delta_+}\right) + \left(1 - \delta_+\right)^2 - 4\delta_{Nu}^{*4} = 0 \tag{3.7.14}$$

Expanding all terms and simplifying:

$$\delta_+^2 \frac{\delta_+^4 - 2\delta_+^2 + 1}{4\delta_+^2} + 2\delta_+\left(1 - \delta_+\right)\left(\frac{\delta_+^2 - 1}{2\delta_+}\right) + 1 - 2\delta_+ + \delta_+^2 - 4\delta_{Nu}^{*4} = 0 \tag{3.7.15}$$

$$\frac{\delta_+^4 - 2\delta_+^2 + 1}{4} + \left(1 - \delta_+\right)\left(\delta_+^2 - 1\right) + 1 - 2\delta_+ + \delta_+^2 - 4\delta_{Nu}^{*4} = 0 \tag{3.7.16}$$

$$\delta_+^4 - 2\delta_+^2 + 1 + 4\left(1 - \delta_+\right)\left(\delta_+^2 - 1\right) + 4 - 8\delta_+ + 4\delta_+^2 - 16\delta_{Nu}^{*4} = 0 \tag{3.7.17}$$

$$\delta_+^4 - 2\delta_+^2 + 1 + 4\delta_+^2 - 4 - 4\delta_+^3 + 4\delta_+ + 4 - 8\delta_+ + 4\delta_+^2 - 16\delta_{Nu}^{*4} = 0 \tag{3.7.18}$$

$$1 - 4\delta_+ + 6\delta_+^2 - 4\delta_+^3 + \delta_+^4 - 16\delta_{Nu}^{*4} = 0 \tag{3.7.19}$$

$$\left(1 - \delta_+\right)^4 - 16\delta_{Nu}^{*4} = 0 \tag{3.7.20}$$

$$\left(\frac{1-\delta_+}{2}\right)^4 - \delta_{Nu}^{*4} = 0 \tag{3.7.21}$$

The solution of Equation (3.7.21) is the same as the solution of Equation (3.7.9). A useful form of Equation (3.7.21) is:

$$X^4 - C = 0 \tag{3.7.22}$$

where

$$X = \frac{1-\delta_+}{2} = \frac{1-\left(1-\dfrac{\delta}{r_o}\right)^2}{2} = \frac{1-\left(1-2\dfrac{\delta}{r_o}+\left(\dfrac{\delta}{r_o}\right)^2\right)}{2} = \frac{\delta}{r_o} - \frac{1}{2}\left(\frac{\delta}{r_o}\right)^2 \tag{3.7.23}$$

and

$$C = \delta_{Nu}^{*4} = \frac{4\mu_L k_L \Delta T z}{r_o^4 h_{fg} g \rho_L (\rho_L - \rho_V)} \tag{3.7.24}$$

This form of the δ_+ equation will be referred to in subsequent analyses.

3.8. Variable Wall Temperature

Most experiments of condensation in vertical tube used a cooling jacket with either parallel or counter flow. In the experiments the pure vapor saturation temperature is constant but the wall temperature varies along the tube length. This variation can be

accounted for by expressing the wall temperature by a polynomial. The inlet-to-wall temperature difference is, therefore:

$$\Delta T(z) = a_0 + a_1 z + a_2 z^2 + \cdots = \sum_{i=0}^{n} a_i z^i \tag{3.8.1}$$

With the variable wall temperature, the integration on the *LHS* of Equation (3.5.5) is unchanged. However, the integration of the *RHS* in Equation (3.5.7) must be modified.

$$\begin{aligned} RHS &= \int \frac{8\mu_L k_L}{r_o^4 h_{fg} g \rho_L (\rho_L - \rho_V)} \sum_{i=0}^{n} a_i z^i dz \\ &= \frac{8\mu_L k_L}{r_o^4 h_{fg} g \rho_L (\rho_L - \rho_V)} \sum_{i=0}^{n} a_i \frac{z^{i+1}}{i+1} + C_3 \end{aligned} \tag{3.8.2}$$

The constant of integration is evaluated as previously described and has the same value. Therefore, the final equation for the condensate film thickness and its solution will have the same format but the expressions for the Nusselt film thickness and the coefficient *C* of the quartic equation are:

$$\delta_{Nu} = \left(\frac{4\mu_L k_L}{h_{fg} g \rho_L (\rho_L - \rho_V)} \sum_{i=0}^{n} a_i \frac{z^{i+1}}{i+1} \right)^{1/4} \tag{3.8.3}$$

$$C = \frac{4\mu_L k_L}{r_o^4 h_{fg} g \rho_L (\rho_L - \rho_V)} \sum_{i=0}^{n} a_i \frac{z^{i+1}}{i+1} \tag{3.8.4}$$

For a given set of experimental data, the temperature difference, which can be computed from the reported wall temperature, is curve-fitted and the resulting coefficients are substituted into the above expressions. In all of these equations, the properties of vapor

are constant and computed at a constant saturation temperature. However, the properties of liquid are variable and computed at variable film temperatures of:

$$T_{film} = T_{wall} + 0.31\Delta T \tag{3.8.5}$$

The effect of variable wall temperatures and thus the resulting coefficient C expressed by Equation (3.8.4) is also applicable for the laminar and turbulent mixed convection condensation in Chapters 4 and 5. It is worthy to note that this important effect of variable wall temperature is absent from the literature except in full numerical works. Furthermore, Sparrow and Gregg (1959) concluded that the similarity transformation analysis cannot handle this effect.

3.9. Comparison with the Nusselt Solution

The exact and approximate solutions for film thickness in cylindrical coordinates that have just been presented apply for axisymmetric condensation from a quiescent vapor. This could be applied to vertical downward flow in a tube, but this flow could not be sustained for any reasonable length of tube. Instead, the previously presented analytical solutions should be applied for condensation on the inside of a concave vertical surface with radius r_o that is exposed to quiescent vapor. Comparisons are now made between the exact and approximate solutions derived earlier and Nusselt's classic solution for condensation on a vertical flat plate exposed to quiescent steam at atmospheric pressure. These comparisons are made for various temperature differences $\Delta T = T_{sat} - T_{wall}$ and wall radii, and are presented in Figures 3.3 to 3.6. For a small tube radius, the approximate closed-form solution (Equation (3.7.10)) slightly overestimates the film

thickness compared to the exact solution of Equation (3.6.8) as shown in Figures 3.3 and 3.4. That overestimation increases with increased temperature difference.

Note that all comparisons in the present work are quantified by the root mean square of the approximate percentage differences:

$$\mathrm{RMS} = \sqrt{\frac{\sum_{i=1}^{N}\left(\frac{\delta_{1,i} - \delta_{2,i}}{\delta_{1,i}}\right)^2}{N}} \times 100 \tag{3.9.1}$$

where δ_1 is the first data set and δ_2 is the second data set.

From Figure 3.4, the RMS deviation between the Nusselt solution and the exact explicit solution is 1.2%. This agreement indicates that the Nusselt's vertical flat plate solution is a good approximate starting point for vertical tube correlations as used in many published works. From the same figure, the RMS deviation between the exact explicit solution and the approximate closed-form solution is 2.4%. This agreement validates the accuracy of the logarithmic approximation. Note that although the Nusselt solution appears to be better than the approximate solution, it is only for quiescent case and cannot be extended to the forced or mixed convection cases. For a wall radius of 10 mm, the difference between all these curves is small for both temperature differences, as seen in Figures 3.5 and 3.6. For a wall radius above 10 mm the differences are negligible.

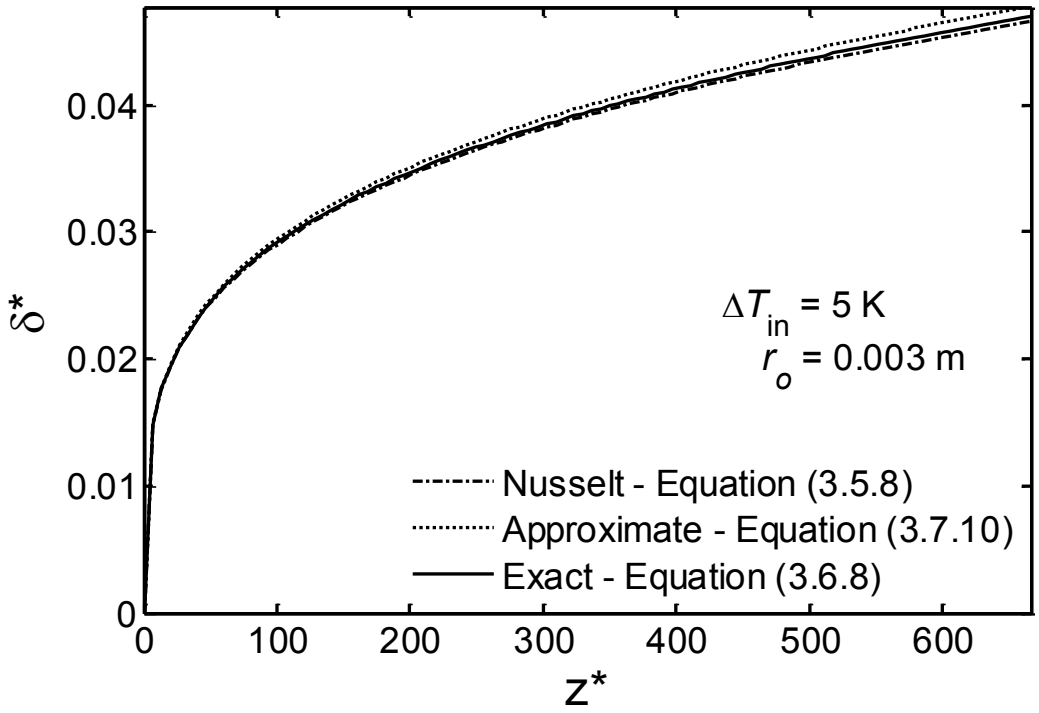

Figure 3.3: Axial film thickness variation ($\Delta T_{in} = 5$ K, $r_o = 0.003$ m)

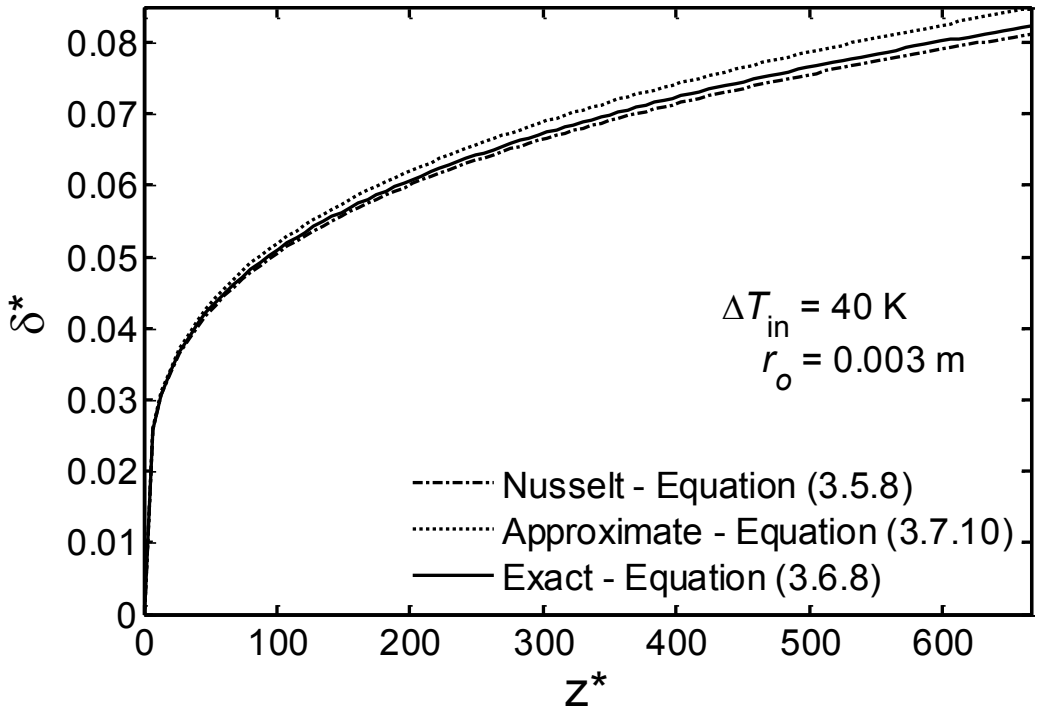

Figure 3.4: Axial film thickness variation ($\Delta T_{in} = 40$ K, $r_o = 0.003$ m)

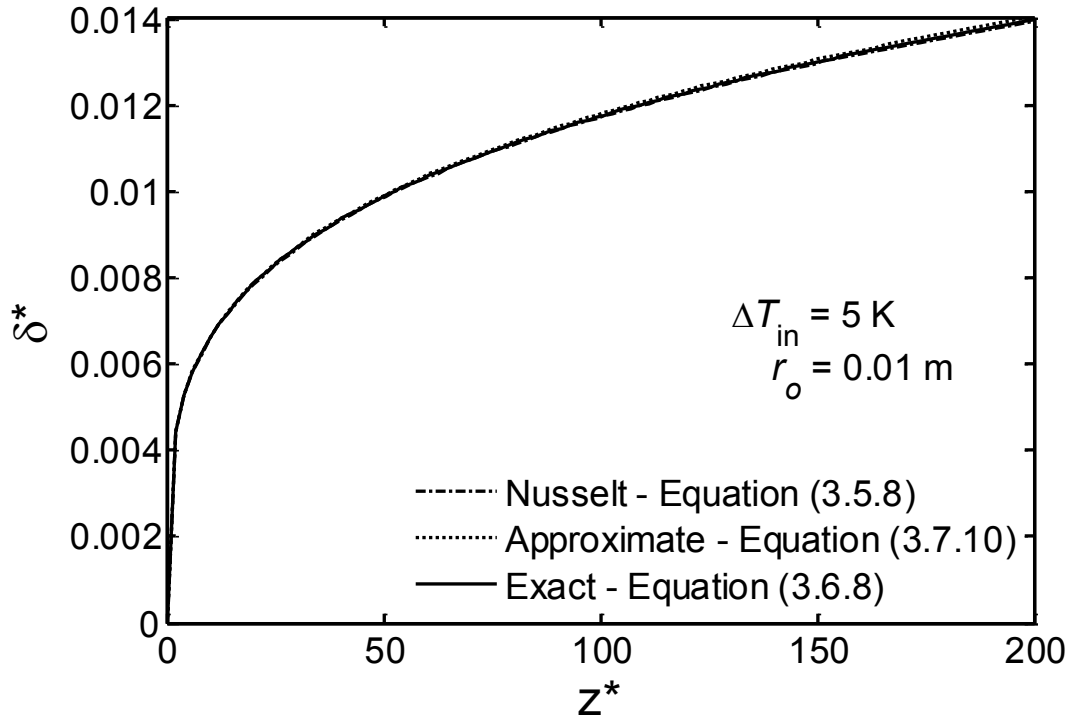

Figure 3.5: Axial film thickness variation ($\Delta T_{in} = 5$ K, $r_o = 0.01$ m)

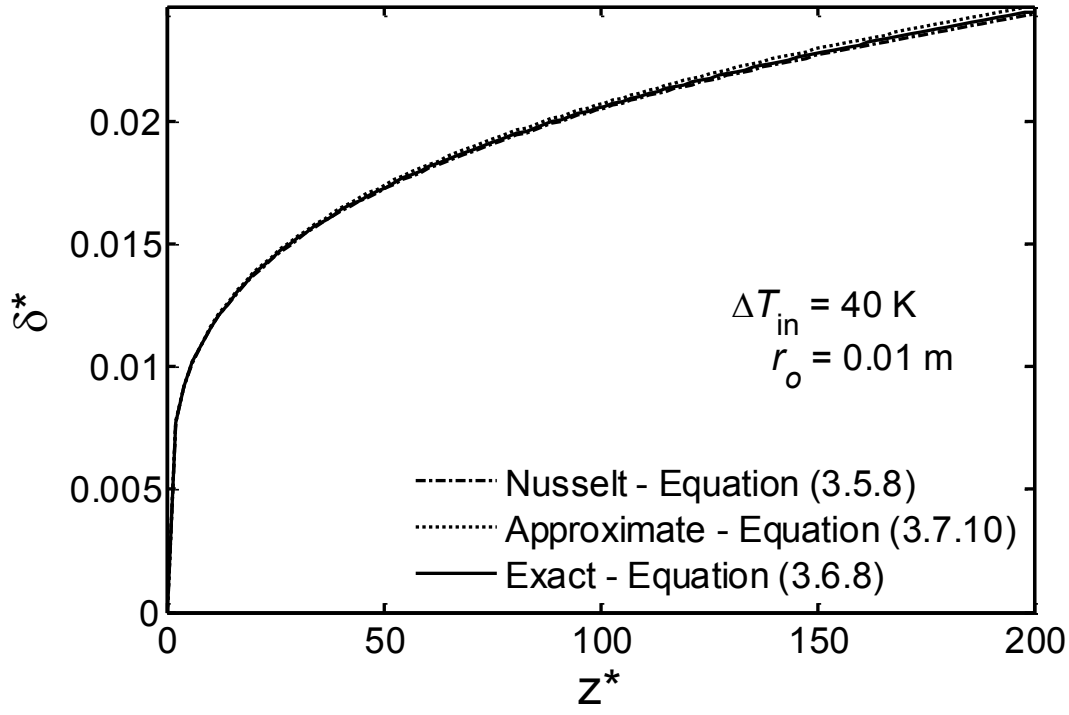

Figure 3.6: Axial film thickness variation ($\Delta T_{in} = 40$ K, $r_o = 0.01$ m)

3.10. Conclusions

From this analysis and the comparison, the following conclusions can be drawn:

1. From a practical point of view, the Nusselt solution for film condensation from quiescent pure vapor on isothermal vertical flat plate is a good approximate starting point for solution of film condensation on a curved surface.
2. The exact and approximate solutions for δ^* yield practically the same results.
3. Equation (3.7.5) is an excellent approximation of the logarithmic function, over the domain of δ_+ in this work and can be useful in subsequent analyses.

CHAPTER 4

LAMINAR MIXED-CONVECTION FILM CONDENSATION

4.1. Mathematical Model

This chapter extends the analysis of Chapter 3 with a consideration of the vapor flow and the resulting shear force at the liquid-vapor interface. Similar to the analysis in Chapter 3, the main objective of this analysis is to find a closed-form solution for the condensate film thickness. Unlike the previous analysis of quiescent vapor, which has an exact solution, the closed-form solution of the laminar mixed-convection condensation will be approximate due to its increased complexity. The solution procedure and approximation formula presented previously in the quiescent vapor scenario will be used as a basis for this analysis. The schematic of this analysis is shown in Figure 4.1.

The assumptions for this analysis are:

1. The inlet flow is a pure saturated vapor.
2. The temperature in the vapor is uniform.
3. The wall temperature is constant.
4. Continuous velocity and shear stress at the liquid-vapor interface.
5. The vapor flow and the condensate flow are laminar.
6. Fluid properties are constant.
7. Radial pressure gradient is negligible.
8. Axial conduction in the condensate is negligible.
9. Heat transfer in the liquid film is only by conduction in the radial direction.

10. Advection of momentum and axial diffusion of momentum in the liquid and the vapor are negligible.

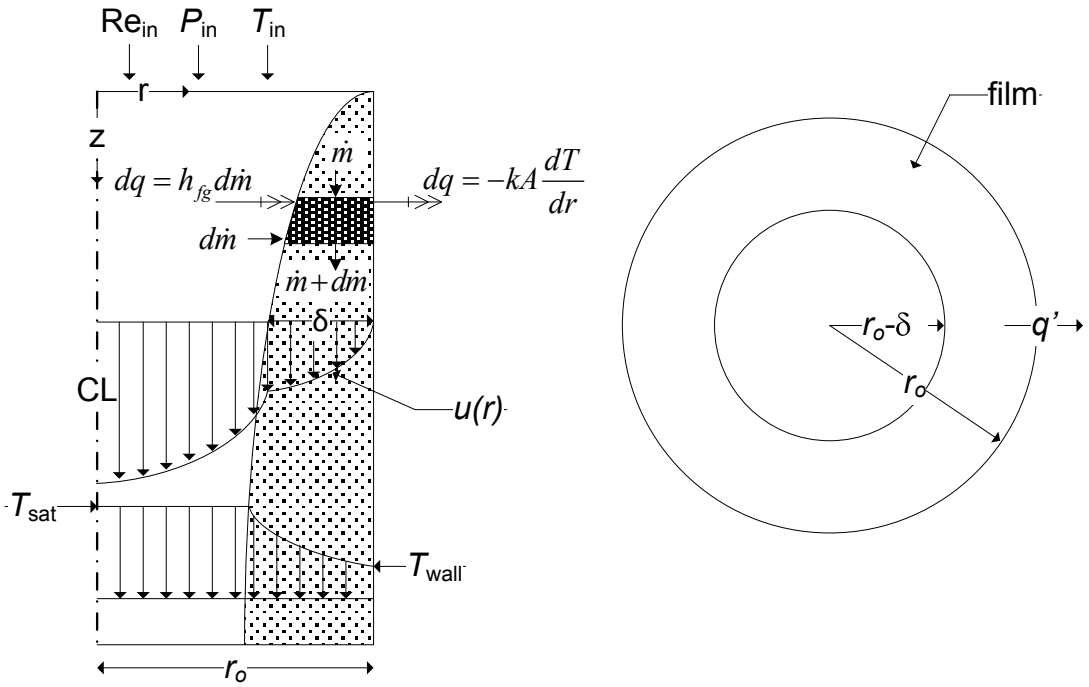

a) side view b) top view

Figure 4.1: Laminar film condensation with interfacial shear stress

The governing equations of the vapor and the liquid film are, therefore:

$$\frac{1}{r}\frac{\partial}{\partial r}\left(r\mu_V\frac{\partial u_V}{\partial r}\right)=\frac{dP}{dz}-\rho_V g \tag{4.1.1}$$

$$\frac{1}{r}\frac{\partial}{\partial r}\left(r\mu_L\frac{\partial u_L}{\partial r}\right)=\frac{dP}{dz}-\rho_L g \tag{4.1.2}$$

$$k_L\frac{1}{r}\frac{\partial}{\partial r}\left(r\frac{\partial T_L}{\partial r}\right)=0 \tag{4.1.3}$$

Similar to Chapter 3, the energy balance and the mass balance are enforced implicitly as shown in the differential control volume of Figure 4.1. Therefore, the differential form of the continuity equation does not appear in the set of governing equations. From the assumptions and the no slip condition at the wall and the interface, the boundary conditions are:

$$\left.\frac{\partial u_V}{\partial r}\right|_{r=0} = 0 \tag{4.1.4}$$

$$u_L\big|_{r=r_o} = 0 \tag{4.1.5}$$

$$u_L\big|_{r=r_o-\delta} = u_V\big|_{r=r_o-\delta} \tag{4.1.6}$$

$$\tau_i = -\mu_V \left.\frac{\partial u_V}{\partial r}\right|_{r=r_o-\delta} = -\mu_L \left.\frac{\partial u_L}{\partial r}\right|_{r=r_o-\delta} \tag{4.1.7}$$

The boundary conditions used in Chapter 3, Equations (3.1.6) and (3.1.7), still apply for temperature. In addition, the solution for T in Section 3.4 still applies in this analysis.

4.2. Vapor and Condensate Radial Velocity Profiles

To simplify the analysis, a density function ρ_+ is defined. This density function accounts for the pressure drop induced by forced flow. Ghiaasiaan (2008) used a similar definition to extend Nusselt vertical flat plate analysis with a consideration of the interfacial shear stress. He assumed constant axial pressure gradient and interfacial shear stress to produce a set of three equations with five unknowns. The present analysis does not make these assumptions. In this analysis, the axial pressure gradient is approximated by a body force that is a combination of the density function and vapor density. Note that the pressure

gradient is composed of frictional, momentum, and gravitational components. The density function ρ_+ is intended to account for both frictional and momentum components. Since the radial pressure gradient is assumed to be negligible, the density function ρ_+ is a function of axial coordinate only. Thus:

$$\frac{dP}{dz} = (\rho_V + \rho_+)g \tag{4.2.1}$$

The vapor velocity profile can be derived from Equation (4.1.1) using the new definition of pressure gradient by Equation (4.2.1):

$$\frac{1}{r}\frac{\partial}{\partial r}\left(r\mu_V \frac{\partial u_V}{\partial r}\right) = \frac{dP}{dz} - \rho_V g = (\rho_V + \rho_+)g - \rho_V g = \rho_+ g \tag{4.2.2}$$

or

$$\frac{\partial}{\partial r}\left(r\mu_V \frac{\partial u_V}{\partial r}\right) = \rho_+ g r \tag{4.2.3}$$

Integrating Equation (4.2.3) with respect to radius produces:

$$r\mu_V \frac{\partial u_V}{\partial r} = \frac{\rho_+ g}{2} r^2 + C_{V,1} \tag{4.2.4}$$

Using the boundary condition from Equation (4.1.4) yields $C_{V,1} = 0$ so Equation (4.2.4) can be rewritten as:

$$\mu_V \frac{\partial u_V}{\partial r} = \frac{\rho_+ g}{2} r \tag{4.2.5}$$

Equation (4.2.5) can be used to express the interfacial shear stress as:

$$\tau_i = -\mu_V \left.\frac{\partial u_V}{\partial r}\right|_{r=r_o-\delta} = -\frac{\rho_+ g(r_o-\delta)}{2} \tag{4.2.6}$$

The vapor velocity can be obtained by dividing Equation (4.2.5) by μ_V and integrating it with respect to radius. The constant of integration $C_{V,2}$ will be evaluated later.

$$u_V = \frac{\rho_+ g}{4\mu_V} r^2 + C_{V,2} \tag{4.2.7}$$

The liquid film velocity profile can be derived from Equation (4.1.2) using the following steps:

$$\frac{1}{r}\frac{\partial}{\partial r}\left(r\mu_L \frac{\partial u_L}{\partial r}\right) = \frac{dP}{dz} - \rho_L g = (\rho_V + \rho_+)g - \rho_L g = -(\rho_L - \rho_V - \rho_+)g \tag{4.2.8}$$

$$\frac{\partial}{\partial r}\left(r\mu_L \frac{\partial u_L}{\partial r}\right) = -(\rho_L - \rho_V - \rho_+)gr \tag{4.2.9}$$

$$r\mu_L \frac{\partial u_L}{\partial r} = -\frac{(\rho_L - \rho_V - \rho_+)g}{2} r^2 + C_{L,1} \tag{4.2.10}$$

$$\mu_L \frac{\partial u_L}{\partial r} = -\frac{(\rho_L - \rho_V - \rho_+)g}{2} r + C_{L,1}\frac{1}{r} \tag{4.2.11}$$

Equation (4.2.11) can be used to express the interfacial shear stress as:

$$\tau_i = -\mu_L \left.\frac{\partial u_L}{\partial r}\right|_{r=r_o-\delta} = \frac{(\rho_L - \rho_V - \rho_+)g(r_o-\delta)}{2} - \frac{C_{L,1}}{r_o-\delta} \tag{4.2.12}$$

Equating the interfacial shear stress from Equations (4.2.6) and (4.2.12) to solve for $C_{L,1}$ yields:

$$-\frac{\rho_+ g(r_o-\delta)}{2}=\frac{(\rho_L-\rho_V-\rho_+)g(r_o-\delta)}{2}-\frac{C_{L,1}}{r_o-\delta} \tag{4.2.13}$$

so that

$$C_{L,1}=\frac{(\rho_L-\rho_V)g(r_o-\delta)^2}{2} \tag{4.2.14}$$

The liquid velocity is then obtained by substituting Equation (4.2.14) into Equation (4.2.11), rearranging, and integrating with respect to radius:

$$\frac{\partial u_L}{\partial r}=-\frac{(\rho_L-\rho_V-\rho_+)g}{2\mu_L}r+\frac{(\rho_L-\rho_V)g(r_o-\delta)^2}{2\mu_L}\frac{1}{r} \tag{4.2.15}$$

$$u_L=-\frac{(\rho_L-\rho_V-\rho_+)g}{4\mu_L}r^2+\frac{(\rho_L-\rho_V)g(r_o-\delta)^2}{2\mu_L}\ln(r)+C_{L,2} \tag{4.2.16}$$

The constant of integration $C_{L,2}$ is determined by using Equation (4.1.5):

$$C_{L,2}=\frac{(\rho_L-\rho_V-\rho_+)gr_o^2}{4\mu_L}-\frac{g(\rho_L-\rho_V)(r_o-\delta)^2\ln(r_o)}{2\mu_L} \tag{4.2.17}$$

so that

$$u_L=\frac{(\rho_L-\rho_V-\rho_+)g}{4\mu_L}\left(r_o^2-r^2\right)+\frac{g(\rho_L-\rho_V)(r_o-\delta)^2}{2\mu_L}\ln\left(\frac{r}{r_o}\right) \tag{4.2.18}$$

The liquid film velocity profile in Equation (4.2.18) can be rearranged to identify two meaningful terms related to forced convection and natural convection:

$$u_L = -\frac{\rho_+ g}{4\mu_L}\left(r_o^2 - r^2\right) + \frac{g\left(\rho_L - \rho_V\right)}{4\mu_L}\left(\left(r_o^2 - r^2\right) + 2\left(r_o - \delta\right)^2 \ln\left(\frac{r}{r_o}\right)\right) \tag{4.2.19}$$

$$= u_{L,fc} + u_{L,nc}$$

The first term on the *RHS* of Equation (4.2.19) is due to the effect of forced convection. The second term is due to body force only; it is Equation (3.2.9) from the quiescent vapor analysis. The interface velocity, which will be used to complete the vapor velocity profile, is therefore:

$$u_i = u_{i,fc} + u_{i,nc} \tag{4.2.20}$$

where

$$u_{i,fc} = -\frac{\rho_+ g\delta\left(2r_o - \delta\right)}{4\mu_L} \tag{4.2.21}$$

and

$$u_{i,nc} = \frac{g\left(\rho_L - \rho_V\right)}{4\mu_L}\left(\delta\left(2r_o - \delta\right) + 2\left(r_o - \delta\right)^2 \ln\left(\frac{r_o - \delta}{r_o}\right)\right) \tag{4.2.22}$$

Using the boundary condition given by Equation (4.1.6), Equation (4.2.7) is set equal to Equation (4.2.20), which allows $C_{V,2}$ to be determined:

$$\frac{\rho_+ g\left(r_o - \delta\right)^2}{4\mu_V} + C_{V,2} = u_{i,fc} + u_{i,nc} \tag{4.2.23}$$

so that

$$C_{V,2} = -\frac{\rho_+ g\left(r_o - \delta\right)^2}{4\mu_V} + u_{i,fc} + u_{i,nc} \tag{4.2.24}$$

Substituting $C_{V,2}$ into Equation (4.2.7) and rewriting to show terms that depend on ρ_+, produces:

$$\begin{aligned} u_V &= \frac{\rho_+ g}{4\mu_V} r^2 - \frac{\rho_+ g\left(r_o - \delta\right)^2}{4\mu_V} + u_{i,fc} + u_{i,nc} \\ &= -\frac{\rho_+ g}{4\mu_V}\left(\left(r_o - \delta\right)^2 - r^2\right) + u_{i,fc} + u_{i,nc} \\ &= -\frac{\rho_+ g}{4\mu_V}\left(\left(r_o - \delta\right)^2 - r^2\right) - \frac{\rho_+ g\delta\left(2r_o - \delta\right)}{4\mu_L} + u_{i,nc} \end{aligned} \tag{4.2.25}$$

4.3. Derivation of the Density Function

In order to complete the solution for the velocity profiles, ρ_+ must be determined. The density function can be solved by using an overall mass balance that applies at each *z* location:

$$\dot{m}_{in} = \dot{m}_L + \dot{m}_V \tag{4.3.1}$$

The total mass flow rate in the liquid is:

$$\dot{m}_L = \int_{r_o-\delta}^{r_o} \rho_L u_L 2\pi r dr = 2\pi\rho_L \int_{r_o-\delta}^{r_o} r u_{L,fc} dr + 2\pi\rho_L \int_{r_o-\delta}^{r_o} r u_{L,nc} dr = \dot{m}_{L,fc} + \dot{m}_{L,nc} \tag{4.3.2}$$

The second integral in Equation (4.3.2) was already given in Equation (3.3.10). The first integral in Equation (4.3.2) is evaluated as follows:

$$\dot{m}_{L,fc} = 2\pi\rho_L \int_{r_o-\delta}^{r_o} r\left(-\frac{\rho_+ g}{4\mu_L}\left(r_o^2 - r^2\right)\right)dr$$

$$= -\frac{\pi\rho_L\rho_+ g}{2\mu_L}\int_{r_o-\delta}^{r_o}\left(r_o^2 r - r^3\right)dr$$

$$= -\frac{\pi\rho_L\rho_+ g}{2\mu_L}\left(r_o^2\frac{r^2}{2} - \frac{r^4}{4}\right)_{r_o-\delta}^{r_o}$$

$$= -\frac{\pi\rho_L\rho_+ g}{2\mu_L}\left(\left(\frac{r_o^4}{2} - \frac{r_o^4}{4}\right) - \left(\frac{r_o^2(r_o-\delta)^2}{2} - \frac{(r_o-\delta)^4}{4}\right)\right)$$

$$= -\frac{\pi\rho_L\rho_+ g}{2\mu_L}\left(\left(\frac{2r_o^4}{4} - \frac{r_o^4}{4}\right) - \left(\frac{2r_o^2(r_o-\delta)^2}{4} - \frac{(r_o-\delta)^4}{4}\right)\right)$$

$$= -\frac{\pi\rho_L\rho_+ g}{8\mu_L}\left(r_o^4 - 2r_o^2(r_o-\delta)^2 + (r_o-\delta)^4\right) \tag{4.3.3}$$

Using the previously defined variable change δ_+ as given in Equation (3.3.7), Equation (4.3.3) becomes:

$$\dot{m}_{L,fc} = -\frac{\pi\rho_L\rho_+ g}{8\mu_L}\left(r_o^4 - 2r_o^2\left(r_o^2\delta_+\right) + \left(r_o^4\delta_+^2\right)\right)$$

$$= -\frac{\pi\rho_L\rho_+ g}{8\mu_L} r_o^4\left(1-\delta_+\right)^2 \tag{4.3.4}$$

The liquid total mass flow rate is therefore:

$$\dot{m}_L = -\frac{\pi\rho_L\rho_+ g}{8\mu_L} r_o^4\left(1-\delta_+\right)^2 + \frac{\pi\rho_L g\left(\rho_L-\rho_V\right)}{8\mu_L} r_o^4\left(1 - 4\delta_+ + 3\delta_+^2 - 2\delta_+^2\ln\delta_+\right) \tag{4.3.5}$$

or

$$\dot{m}_L = \frac{\pi\rho_L g\left(\rho_L-\rho_V\right)}{8\mu_L} r_o^4\left(-\frac{\rho_+}{\left(\rho_L-\rho_V\right)}\left(1-\delta_+\right)^2 + \left(1 - 4\delta_+ + 3\delta_+^2 - 2\delta_+^2\ln\delta_+\right)\right) \tag{4.3.6}$$

The vapor total mass flow rate is:

$$\begin{aligned}
\dot{m}_V &= \int_0^{r_o-\delta} \rho_V u_V 2\pi r dr \\
&= 2\pi\rho_V \int_0^{r_o-\delta} r\left(-\frac{\rho_+ g}{4\mu_V}\left((r_o-\delta)^2 - r^2\right) - \frac{\rho_+ g\delta\left(2r_o-\delta\right)}{4\mu_L} + u_{i,nc}\right) dr \\
&= 2\pi\rho_V \int_0^{r_o-\delta} \left(-\frac{\rho_+ g}{4\mu_V}\left((r_o-\delta)^2 r - r^3\right) - \frac{\rho_+ g\delta\left(2r_o-\delta\right)}{4\mu_L} r + u_{i,nc} r\right) dr \\
&= 2\pi\rho_V \left(-\frac{\rho_+ g}{4\mu_V}\left((r_o-\delta)^2 \frac{r^2}{2} - \frac{r^4}{4}\right) - \frac{\rho_+ g\delta\left(2r_o-\delta\right) r^2}{8\mu_L} + \frac{u_{i,nc} r^2}{2}\right)_0^{r_o-\delta} \\
&= 2\pi\rho_V \left(-\frac{\rho_+ g(r_o-\delta)^4}{16\mu_V} - \frac{\rho_+ g\delta\left(2r_o-\delta\right)(r_o-\delta)^2}{8\mu_L} + \frac{u_{i,nc}(r_o-\delta)^2}{2}\right) \\
&= -\frac{\rho_+ \pi g\rho_V}{8}\left(\frac{(r_o-\delta)^4}{\mu_V} + \frac{2\delta\left(2r_o-\delta\right)(r_o-\delta)^2}{\mu_L}\right) + \pi\rho_V u_{i,nc}(r_o-\delta)^2 \\
&= \begin{cases} -\frac{\rho_+ \pi g\rho_V}{8}\left(\frac{(r_o-\delta)^4}{\mu_V} + \frac{2\delta\left(2r_o-\delta\right)(r_o-\delta)^2}{\mu_L}\right) + \\ \frac{\pi\rho_V g\left(\rho_L-\rho_V\right)}{4\mu_L}\left(\delta\left(2r_o-\delta\right)(r_o-\delta)^2 + 2(r_o-\delta)^4 \ln\left(\frac{r_o-\delta}{r_o}\right)\right) \end{cases}
\end{aligned} \tag{4.3.7}$$

Applying the same variable change with the derived simplification expressions from Equations (3.3.7) and (3.3.9), Equation (4.3.7) can be written as:

$$\dot{m}_V = -\frac{\rho_+ \pi g\rho_V}{8} r_o^4 \left(\frac{\delta_+^2}{\mu_V} + \frac{2\delta_+\left(1-\delta_+\right)}{\mu_L}\right) + \frac{\pi\rho_V g\left(\rho_L-\rho_V\right)}{4\mu_L} r_o^4 \left(\delta_+\left(1-\delta_+\right) + \delta_+^2 \ln\delta_+\right) \tag{4.3.8}$$

Substituting the liquid and vapor mass flow rates into Equation (4.3.1) allows solving for the density function through the following sequence of four steps:

First

$$\dot{m}_{in} = \begin{cases} -\dfrac{\pi\rho_L\rho_+ g}{8\mu_L} r_o^4\left(1-\delta_+\right)^2 + \dfrac{\pi\rho_L g\left(\rho_L-\rho_V\right)}{8\mu_L} r_o^4\left(1-4\delta_+ +3\delta_+^2 - 2\delta_+^2\ln\delta_+\right) \\ -\dfrac{\rho_+\pi g\rho_V}{8} r_o^4\left(\dfrac{\delta_+^2}{\mu_V} + \dfrac{2\delta_+\left(1-\delta_+\right)}{\mu_L}\right) + \dfrac{\pi\rho_V g\left(\rho_L-\rho_V\right)}{4\mu_L} r_o^4\left(\delta_+\left(1-\delta_+\right)+\delta_+^2\ln\delta_+\right) \end{cases} \tag{4.3.9}$$

Second, factor out $\pi g r_o^4/8$:

$$\frac{8\dot{m}_{in}}{\pi g r_o^4} = \begin{cases} -\rho_+\left(\dfrac{\rho_L\left(1-\delta_+\right)^2}{\mu_L}\right) + \dfrac{\left(\rho_L-\rho_V\right)}{\mu_L}\rho_L\left(1-4\delta_+ +3\delta_+^2 - 2\delta_+^2\ln\delta_+\right) \\ -\rho_+\left(\rho_V\left(\dfrac{\delta_+^2}{\mu_V} + \dfrac{2\delta_+\left(1-\delta_+\right)}{\mu_L}\right)\right) + \dfrac{\left(\rho_L-\rho_V\right)}{\mu_L} 2\rho_V\left(\delta_+\left(1-\delta_+\right)+\delta_+^2\ln\delta_+\right) \end{cases} \tag{4.3.10}$$

Third, collect all terms containing the density function:

$$\frac{8\dot{m}_{in}}{\pi g r_o^4} = \begin{cases} -\rho_+\left(\dfrac{\rho_L\left(1-\delta_+\right)^2}{\mu_L} + \dfrac{\rho_V\delta_+^2}{\mu_V} + \dfrac{\rho_V 2\delta_+\left(1-\delta_+\right)}{\mu_L}\right) \\ +\dfrac{\left(\rho_L-\rho_V\right)}{\mu_L}\left(\rho_L\left(1-4\delta_+ +3\delta_+^2 - 2\delta_+^2\ln\delta_+\right) + 2\rho_V\left(\delta_+\left(1-\delta_+\right)+\delta_+^2\ln\delta_+\right)\right) \end{cases} \tag{4.3.11}$$

Fourth, rearrange Equation (4.3.11) to obtain:

$$\rho_+ = -\frac{\dfrac{8\dot{m}_{in}}{\pi g r_o^4} - \dfrac{\left(\rho_L-\rho_V\right)}{\mu_L}\left(\rho_L\left(1-4\delta_+ +3\delta_+^2 - 2\delta_+^2\ln\delta_+\right) + 2\rho_V\left(\delta_+\left(1-\delta_+\right)+\delta_+^2\ln\delta_+\right)\right)}{\dfrac{\rho_L\left(1-\delta_+\right)^2}{\mu_L} + \dfrac{\rho_V\delta_+^2}{\mu_V} + \dfrac{\rho_V 2\delta_+\left(1-\delta_+\right)}{\mu_L}} \tag{4.3.12}$$

The density function can be further simplified by factoring out the $(\rho_L - \rho_V)$ and rearranging property ratios to get:

$$\rho_+ = -(\rho_L - \rho_V)\left(\frac{\frac{8\dot{m}_{in}\mu_L}{\pi g \rho_L (\rho_L - \rho_V) r_o^4} - (1 - 4\delta_+ + 3\delta_+^2 - 2\delta_+^2 \ln \delta_+) - 2\frac{\rho_V}{\rho_L}(\delta_+ - \delta_+^2 + \delta_+^2 \ln \delta_+)}{(1-\delta_+)^2 + \frac{\rho_V \mu_L}{\rho_L \mu_V}\delta_+^2 + \frac{\rho_V}{\rho_L} 2\delta_+ (1-\delta_+)} \right) \tag{4.3.13}$$

Rewriting and defining dimensionless factors M, α, and β, Equation (4.3.13) can be written as:

$$\rho_+ = -(\rho_L - \rho_V)\left(\frac{2M - (1 - 4\delta_+ + 3\delta_+^2 - 2\delta_+^2 \ln \delta_+) - 2\alpha(\delta_+ - \delta_+^2 + \delta_+^2 \ln \delta_+)}{(1-\delta_+)^2 + \beta\delta_+^2 + \alpha 2\delta_+ (1-\delta_+)} \right) \tag{4.3.14}$$

where

$$\alpha = \frac{\rho_V}{\rho_L} \tag{4.3.15}$$

$$\beta = \frac{\rho_V \mu_L}{\rho_L \mu_V} \tag{4.3.16}$$

and

$$\begin{aligned} M &= \frac{4\dot{m}_{in}\mu_L}{\pi g \rho_L (\rho_L - \rho_V) r_o^4} \\ &= \frac{4(\pi r_o^2 u_{in} \rho_V)\mu_L}{\pi g \rho_L (\rho_L - \rho_V) r_o^4} = \frac{4 u_{in} \rho_V \mu_L}{g \rho_L (\rho_L - \rho_V) r_o^2} \\ &= \frac{4\left(\frac{\mathrm{Re}_{in}\,\mu_V}{\rho_V 2 r_o}\right)\rho_V \mu_L}{g \rho_L (\rho_L - \rho_V) r_o^2} = \frac{2\mu_L \mu_V \,\mathrm{Re}_{in}}{g \rho_L (\rho_L - \rho_V) r_o^3} \end{aligned} \tag{4.3.17}$$

Expanding and regrouping by order of exponent yields:

$$\rho_+ = -(\rho_L - \rho_V)\left(\frac{2M - 1 + 2(2-\alpha)\delta_+ + (2\alpha - 3)\delta_+^2 + 2(1-\alpha)\delta_+^2 \ln \delta_+}{1 + 2(\alpha - 1)\delta_+ + (1 + \beta - 2\alpha)\delta_+^2}\right) \tag{4.3.18}$$

The density function is now expressed as a product of the difference of fluid densities and a dimensionless factor. The dimensionless factor contains terms with fluid viscosities to account for the frictional component of the pressure gradient and an inlet Reynolds number term to account for the momentum component of the pressure gradient.

Because ρ_+ in Equation (4.3.18) is a function of δ_+ only, the condensate mass flow rate (Equation (4.3.6)) is now a function of δ_+ only. Therefore, δ_+ can be solved using an analogous procedure to that in Section 3.5. Once δ_+ is known, it can be used to find the film thickness, density function, pressure gradient, and shear stress. In this analysis, however, the density function (Equation 4.3.18)) and thus the condensate mass flow rate (Equation (4.3.6)) are much more complicated algebraically compared to the analysis of Chapter 3. Therefore, the required integration cannot be readily performed analytically. To achieve a closed-form solution, the ρ_+ function in Equation (4.3.18) must be approximated.

4.4. Approximations for the Density Function

To enable integration, it is necessary to approximate the density function in the form of a single function instead of the quotient of two functions. Two possible ways to do this approximation are: (1) drop terms by order of magnitude analysis using Equation (4.3.14) or (2) perform a series expansion starting from Equation (4.3.18).

4.4.1. The First Approximation Approach

In terms of geometry, if the film thickness is small compared to tube radius, the dimensionless variable δ_+ can be approximated as unity. In term of properties, if the vapor density is small compared to the condensate density, the property ratio α can be approximated as zero. Note that these are approximations in order to find a solution and not assumptions. With these approximations, Equation (4.3.14) becomes:

$$\rho_{+1} = -(\rho_L - \rho_V)\left(\frac{2M}{\beta}\right) = -(\rho_L - \rho_V)(2B) \tag{4.4.1}$$

where

$$B = \frac{M}{\beta} = \frac{2\mu_L\mu_V \,\mathrm{Re}_{in}}{g\rho_L(\rho_L - \rho_V)r_o^3}\frac{\rho_L\mu_V}{\rho_V\mu_L} = \frac{2\mu_V\mu_V \,\mathrm{Re}_{in}}{g(\rho_L - \rho_V)\rho_V r_o^3} \tag{4.4.2}$$

Note that there are two factors of vapor viscosity in the expression of B in Equation (4.4.2). One of them is the molecular vapor viscosity at the entrance which is used to compute the inlet Reynolds number. The other is local axial vapor viscosity which also equals to the molecular vapor viscosity for laminar flow. The distinction between these two viscosities will be important later.

4.4.2. The Second Approximation Approach

By using a Taylor series expansion about $\delta_+ = 1$, the denominator of the density function, Equation (4.3.18), can be expressed as:

$$1 + 2(\alpha - 1)\delta_+ + (1 + \beta - 2\alpha)\delta_+^2 = \beta + 2(\beta - \alpha)(\delta_+ - 1) + (1 + \beta - 2\alpha)(\delta_+ - 1)^2 \tag{4.4.3}$$

Using only the first term of this series, the density function can be expressed as:

$$\rho_{+2} = -(\rho_L - \rho_V)\left(\frac{2M - 1 + 2(2-\alpha)\delta_+ + (2\alpha - 3)\delta_+^2 + 2(1-\alpha)\delta_+^2 \ln \delta_+}{\beta}\right) \tag{4.4.4}$$

4.4.3. Comparisons of Approximations to the Density Function

The plots of the original and simplified density functions, for steam at atmospheric pressure, are shown in Figures 4.2 to 4.4. Figures 4.2 and 4.3 are for large tube radius (10 mm) and low and high inlet Reynolds numbers, respectively. Figure 4.4 is for low inlet Reynolds number and small tube radius (3 mm). All these graphs show that ρ_{+1} is a reasonable approximation only for $\delta_+ > 0.98$. Although this value corresponds to small δ / r_o ratio, it accounts for a large segment of the tube near the entrance. For larger δ / r_o ratio, ρ_{+2} is an acceptable approximation for ρ_+ and should be used in general, even with a high inlet Reynolds number as shown in Figure 4.3. Note that, as can be seen in Equation (4.2.6), $\rho_+ < 0$ yields positive interfacial shear stress and thus the vapor is dragging the liquid. On the other hand, $\rho_+ > 0$ yields negative interfacial shear stress and thus the liquid is dragging the vapor. The transition at $\rho_+ = 0$, and thus zero interfacial shear stress, is normally viewed as the flow reversal. The computation should be stopped at this point because the condensation is now equivalent to the quiescent case, which is not practically sustainable in a tube. If one needs to solve for the condition of $\rho_+ = 0$, then either Equation (4.4.4) or Equation (4.3.18) can be used.

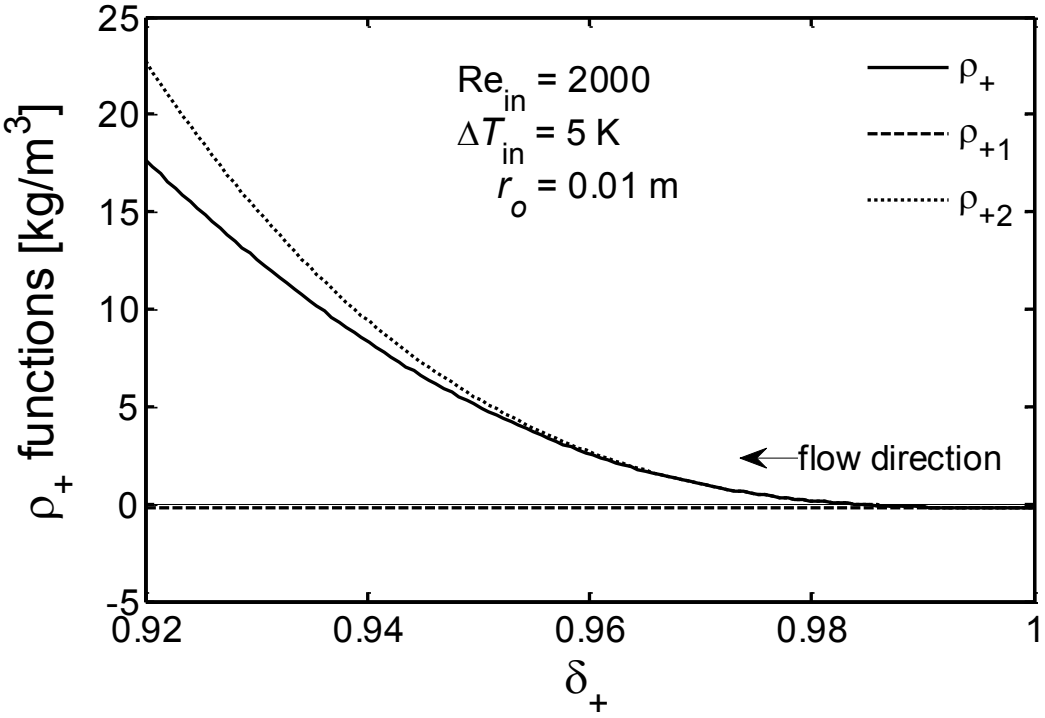

Figure 4.2: Density functions (Re_{in} = 2000, ΔT_{in} = 5 K, r_o = 0.01 m)

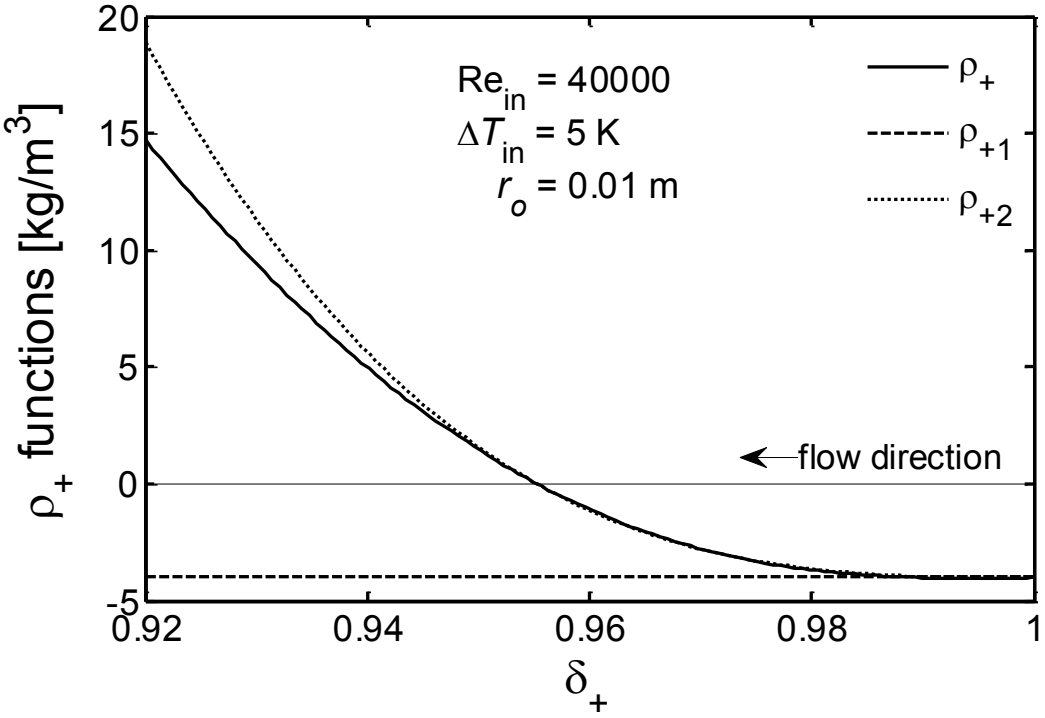

Figure 4.3: Density functions (Re_{in} = 40000, ΔT_{in} = 5 K, r_o = 0.01 m)

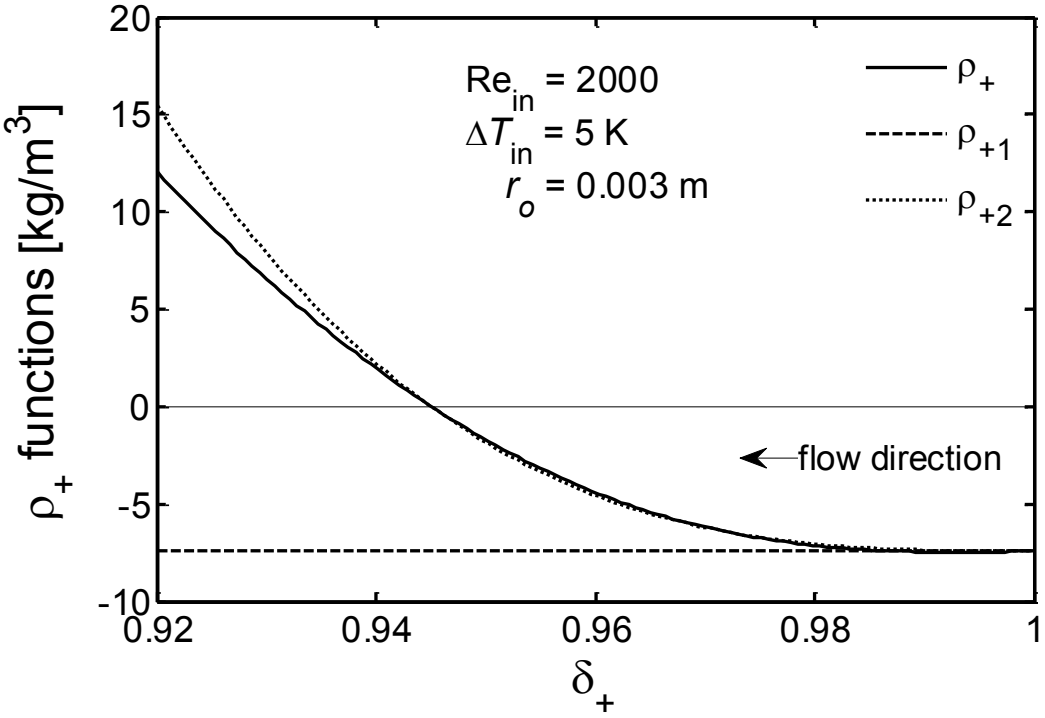

Figure 4.4: Density function ($\mathrm{Re}_{in} = 2000$, $\Delta T_{in} = 5$ K, $r_o = 0.003$ m)

4.5. Derivations of the δ_+ Equations

In this section the two approximations of the density function are used to solve for δ_+.

4.5.1. Derivation Using Density Function ρ_{+1}

Using the approximate density function ρ_{+1} from Equation (4.4.1), the condensate mass flow rate by Equation (4.3.6) becomes:

$$\dot{m}_L = \frac{\pi \rho_L g(\rho_L - \rho_V)}{8\mu_L} r_o^4 \left(2B(1-\delta_+)^2 + \left(1 - 4\delta_+ + 3\delta_+^2 - 2\delta_+^2 \ln \delta_+\right)\right) \tag{4.5.1}$$

Now, using a procedure similar to that in Section 3.5,

$$\frac{d\dot{m}_L}{dz} = \frac{d\dot{m}_L}{d\delta_+}\frac{d\delta_+}{dz}$$

$$= \frac{\pi\rho_L g(\rho_L - \rho_V)}{8\mu_L} r_o^4 \left(-4B(1-\delta_+) + \left(-4 + 6\delta_+ - 2\left(\delta_+ + 2\delta_+ \ln \delta_+\right)\right)\right)\frac{d\delta_+}{dz}$$

$$= \frac{\pi\rho_L g(\rho_L - \rho_V)}{8\mu_L} r_o^4 \left(-4B(1-\delta_+) + \left(-4 + 4\delta_+ - 4\delta_+ \ln \delta_+\right)\right)\frac{d\delta_+}{dz}$$

$$= -\frac{\pi\rho_L g(\rho_L - \rho_V)}{2\mu_L} r_o^4 \left(B(1-\delta_+) + \left(1 - \delta_+ + \delta_+ \ln \delta_+\right)\right)\frac{d\delta_+}{dz} \tag{4.5.2}$$

Equating Equation (4.5.2) to Equation (3.5.2) and rearranging appropriate factors yields:

$$-\frac{\pi\rho_L g(\rho_L - \rho_V)}{2\mu_L} r_o^4 \left(B(1-\delta_+) + \left(1 - \delta_+ + \delta_+ \ln \delta_+\right)\right)\frac{d\delta_+}{dz} = -\frac{4\pi k_L \Delta T}{h_{fg} \ln(\delta_+)} \tag{4.5.3}$$

Further rearrangement of Equation (4.5.3) leads to the following integration:

$$\int \left((1+B)\ln \delta_+ - (1+B)\delta_+ \ln \delta_+ + \delta_+ \ln^2 \delta_+\right) d\delta_+ = \int \frac{8\mu_L k_L \Delta T}{r_o^4 h_{fg} g \rho_L (\rho_L - \rho_V)} dz \tag{4.5.4}$$

The integration of each side of Equation (4.5.4) is obtained as follows:

$$LHS = \begin{cases} (1+B)\left(\delta_+ \ln \delta_+ - \delta_+\right) \\ -(1+B)\left(\frac{\delta_+^2}{2}\ln \delta_+ - \frac{\delta_+^2}{4}\right) + \left(\frac{\delta_+^2}{2}\ln^2 \delta_+ - \frac{\delta_+^2}{2}\ln \delta_+ + \frac{\delta_+^2}{4}\right) \end{cases}$$

$$= \frac{\delta_+^2}{2}\ln^2 \delta_+ + \left((1+B)\delta_+ - (2+B)\frac{\delta_+^2}{2}\right)\ln \delta_+ - (1+B)\delta_+ + (2+B)\frac{\delta_+^2}{4} \tag{4.5.5}$$

$$RHS = \frac{8\mu_L k_L \Delta T z}{r_o^4 h_{fg} g \rho_L (\rho_L - \rho_V)} + C_3 = \frac{2\delta_{Nu}^4}{r_o^4} + C_3 = 2\delta_{Nu}^{*4} + C_3 \tag{4.5.6}$$

Note that the constant of integration is introduced in the *RHS* integration. From Equations (4.5.5) and (4.5.6):

$$2\delta_+^2 \ln^2 \delta_+ + 2\left(2(1+B)\delta_+ - (2+B)\delta_+^2\right)\ln\delta_+ - 4(1+B)\delta_+ + (2+B)\delta_+^2 = 8\delta_{Nu}^{*4} + C_3 \qquad (4.5.7)$$

The constant of integration is evaluated at $z = 0$ where $\delta = 0$, $\delta_+ = 1$, and $\delta_{Nu}^* = 0$. This evaluation yields:

$$C_3 = -2 - 3B \qquad (4.5.8)$$

Thus, the δ_+ equation using ρ_{+1} becomes:

$$2\delta_+^2 \ln^2 \delta_+ + 2\left(2(1+B)\delta_+ - (2+B)\delta_+^2\right)\ln\delta_+ + 2 + 3B - 4(1+B)\delta_+ + (2+B)\delta_+^2 - 8\delta_{Nu}^{*4} = 0 \qquad (4.5.9)$$

4.5.2. Derivation Using Density Function ρ_{+2}

Using the approximate density function ρ_{+2} from Equation (4.4.4), the condensate mass flow rate by Equation (4.3.6) becomes:

$$\dot{m}_L = \frac{\pi\rho_L g(\rho_L - \rho_V)}{8\mu_L} r_o^4 \left(\begin{array}{l} \dfrac{2M - 1 + 2(2-\alpha)\delta_+ + (2\alpha - 3)\delta_+^2 + 2(1-\alpha)\delta_+^2 \ln\delta_+}{\beta}\left(1 - 2\delta_+ + \delta_+^2\right) \\ + \left(1 - 4\delta_+ + 3\delta_+^2 - 2\delta_+^2 \ln\delta_+\right) \end{array} \right) \qquad (4.5.10)$$

Expanding all terms and factors on the RHS of Equation (4.5.10) produces:

$$\dot{m}_L = \frac{\pi\rho_L g(\rho_L - \rho_V)}{8\mu_L} r_o^4 \begin{pmatrix} \frac{1}{\beta}\left(2M - 1 + 2(2-\alpha)\delta_+ + (2\alpha - 3)\delta_+^2 + 2(1-\alpha)\delta_+^2 \ln \delta_+\right) \\ -\frac{2}{\beta}\left((2M-1)\delta_+ + 2(2-\alpha)\delta_+^2 + (2\alpha-3)\delta_+^3 + 2(1-\alpha)\delta_+^3 \ln \delta_+\right) \\ +\frac{1}{\beta}\left((2M-1)\delta_+^2 + 2(2-\alpha)\delta_+^3 + (2\alpha-3)\delta_+^4 + 2(1-\alpha)\delta_+^4 \ln \delta_+\right) \\ +\left(1 - 4\delta_+ + 3\delta_+^2 - 2\delta_+^2 \ln \delta_+\right) \end{pmatrix} \tag{4.5.11}$$

Rewriting and grouping coefficients yields:

$$\dot{m}_L = \frac{\pi\rho_L g(\rho_L - \rho_V)}{8\mu_L} r_o^4 \left(a_0 + a_1\delta_+ + a_2\delta_+^2 + a_3\delta_+^3 + a_4\delta_+^4 + a_5\delta_+^2 \ln \delta_+ + a_6\delta_+^3 \ln \delta_+ + a_7\delta_+^4 \ln \delta_+\right) \tag{4.5.12}$$

where

$$a_0 = 1 + \frac{1}{\beta}(2M - 1) \tag{4.5.13}$$

$$a_1 = \frac{2}{\beta}(2-\alpha) - \frac{2}{\beta}(2M-1) - 4 \tag{4.5.14}$$

$$a_2 = \frac{1}{\beta}(2\alpha - 3) - \frac{4}{\beta}(2-\alpha) + \frac{1}{\beta}(2M-1) + 3 \tag{4.5.15}$$

$$a_3 = \frac{2}{\beta}(2-\alpha) - \frac{2}{\beta}(2\alpha - 3) \tag{4.5.16}$$

$$a_4 = \frac{1}{\beta}(2\alpha - 3) \tag{4.5.17}$$

$$a_5 = \frac{2}{\beta}(1-\alpha) - 2 \tag{4.5.18}$$

$$a_6 = \frac{4}{\beta}(\alpha - 1) \tag{4.5.19}$$

$$a_7 = \frac{2}{\beta}(1-\alpha) \tag{4.5.20}$$

Again, following the procedure in Section 3.5.

$$\begin{aligned}
\frac{d\dot{m}_L}{dz} &= \frac{d\dot{m}_L}{d\delta_+}\frac{d\delta_+}{dz} \\
&= \frac{\pi\rho_L g(\rho_L-\rho_V)}{8\mu_L} r_o^4 \begin{pmatrix} a_1 + 2a_2\delta_+ + 3a_3\delta_+^2 + 4a_4\delta_+^3 + \\ a_5(\delta_+ + 2\delta_+\ln\delta_+) + a_6(\delta_+^2 + 3\delta_+^2\ln\delta_+) + a_7(\delta_+^3 + 4\delta_+^3\ln\delta_+) \end{pmatrix}\frac{d\delta_+}{dz} \\
&= \frac{\pi\rho_L g(\rho_L-\rho_V)}{8\mu_L} r_o^4 \begin{pmatrix} a_1 + (2a_2+a_5)\delta_+ + (3a_3+a_6)\delta_+^2 + (4a_4+a_7)\delta_+^3 + \\ 2a_5\delta_+\ln\delta_+ + 3a_6\delta_+^2\ln\delta_+ + 4a_7\delta_+^3\ln\delta_+ \end{pmatrix}\frac{d\delta_+}{dz} \\
&= \frac{\pi\rho_L g(\rho_L-\rho_V)}{8\mu_L} r_o^4 (b_1 + b_2\delta_+ + b_3\delta_+^2 + b_4\delta_+^3 + b_5\delta_+\ln\delta_+ + b_6\delta_+^2\ln\delta_+ + b_7\delta_+^3\ln\delta_+)\frac{d\delta_+}{dz}
\end{aligned} \tag{4.5.21}$$

where

$$b_1 = a_1 = \frac{2}{\beta}(2-\alpha) - \frac{2}{\beta}(2M-1) - 4 = \frac{2}{\beta}(3-\alpha-2M) - 4 \tag{4.5.22}$$

$$b_2 = 2a_2 + a_5 = \frac{2}{\beta}(5\alpha + 2M - 11) + 4 \tag{4.5.23}$$

$$b_3 = 3a_3 + a_6 = \frac{2}{\beta}(13 - 7\alpha) \tag{4.5.24}$$

$$b_4 = 4a_4 + a_7 = \frac{2}{\beta}(3\alpha - 5) \tag{4.5.25}$$

$$b_5 = 2a_5 = \frac{4}{\beta}(1-\alpha) - 4 \tag{4.5.26}$$

$$b_6 = 3a_6 = \frac{12}{\beta}(\alpha - 1) \tag{4.5.27}$$

$$b_7 = 4a_7 = \frac{8}{\beta}(1-\alpha) \tag{4.5.28}$$

Rearranging Equation (4.5.21) to Equation (3.5.2) and integrating yields:

$$\int \begin{pmatrix} b_1 \ln \delta_+ + b_2 \delta_+ \ln \delta_+ + b_3 \delta_+^2 \ln \delta_+ + b_4 \delta_+^3 \ln \delta_+ + \\ b_5 \delta_+ \ln^2 \delta_+ + b_6 \delta_+^2 \ln^2 \delta_+ + b_7 \delta_+^3 \ln^2 \delta_+ \end{pmatrix} d\delta_+ = \int -\frac{32 \mu_L k_L \Delta T}{\rho_L g (\rho_L - \rho_V) h_{fg} r_o^4} dz \tag{4.5.29}$$

The integrations of both sides of Equation (4.5.29) are:

$$LHS = \begin{cases} b_1\left(\delta_+ \ln \delta_+ - \delta_+\right) + b_2\left(\frac{\delta_+^2 \ln \delta_+}{2} - \frac{\delta_+^2}{4}\right) + b_3\left(\frac{\delta_+^3 \ln \delta_+}{3} - \frac{\delta_+^3}{9}\right) + \\ b_4\left(\frac{\delta_+^4 \ln \delta_+}{4} - \frac{\delta_+^4}{16}\right) + b_5\left(\frac{\delta_+^2 \ln^2 \delta_+}{2} - \frac{\delta_+^2 \ln \delta_+}{2} + \frac{\delta_+^2}{4}\right) + \\ b_6\left(\frac{\delta_+^3 \ln^2 \delta_+}{3} - \frac{2\delta_+^3 \ln \delta_+}{9} + \frac{2\delta_+^3}{27}\right) + b_7\left(\frac{\delta_+^4 \ln^2 \delta_+}{4} - \frac{\delta_+^4 \ln \delta_+}{8} + \frac{\delta_+^4}{32}\right) \end{cases} \tag{4.5.30}$$

and

$$RHS = -\frac{32 \mu_L k_L \Delta T z}{r_o^4 h_{fg} g \rho_L (\rho_L - \rho_V)} - C_3 = -\frac{8\delta_{Nu}^4}{r_o^4} - b_8 = -8\delta_{Nu}^{*4} - C_3 \tag{4.5.31}$$

The constant of integration is evaluated at $z = 0$ where $\delta = 0$, $\delta_+ = 1$, and $\delta_{Nu}^* = 0$ to obtain:

$$C_3 = b_1 + \frac{1}{4}b_2 + \frac{1}{9}b_3 + \frac{1}{16}b_4 - \frac{1}{4}b_5 - \frac{2}{27}b_6 - \frac{1}{32}b_7 \tag{4.5.32}$$

Finally Equations (4.5.30), (4.5.31), and (4.5.32) are combined and rearranged to get an equation where all functions f_i are associated with constants b_i. Thus the δ_+ equation using ρ_{+2} is:

$$b_1 f_1 + b_2 f_2 + b_3 f_3 + b_4 f_4 + b_5 f_5 + b_6 f_6 + b_7 f_7 + 8\delta_{Nu}^{*4} = 0 \tag{4.5.33}$$

where

$$f_1 = \delta_+ \ln \delta_+ - \delta_+ + 1 \tag{4.5.34}$$

$$f_2 = \frac{\delta_+^2 \ln \delta_+}{2} - \frac{\delta_+^2}{4} + \frac{1}{4} \tag{4.5.35}$$

$$f_3 = \frac{\delta_+^3 \ln \delta_+}{3} - \frac{\delta_+^3}{9} + \frac{1}{9} \tag{4.5.36}$$

$$f_4 = \frac{\delta_+^4 \ln \delta_+}{4} - \frac{\delta_+^4}{16} + \frac{1}{16} \tag{4.5.37}$$

$$f_5 = \frac{\delta_+^2 \ln^2 \delta_+}{2} - \frac{\delta_+^2 \ln \delta_+}{2} + \frac{\delta_+^2}{4} - \frac{1}{4} \tag{4.5.38}$$

$$f_6 = \frac{\delta_+^3 \ln^2 \delta_+}{3} - \frac{2\delta_+^3 \ln \delta_+}{9} + \frac{2\delta_+^3}{27} - \frac{2}{27} \tag{4.5.39}$$

$$f_7 = \frac{\delta_+^4 \ln^2 \delta_+}{4} - \frac{\delta_+^4 \ln \delta_+}{8} + \frac{\delta_+^4}{32} - \frac{1}{32} \tag{4.5.40}$$

4.6. Approximate Solution for the Condensate Film Thickness

Equations (4.5.9) and (4.5.33) cannot be solved in closed-form for δ_+ because of the logarithm terms, so a root search must be used. Because the value of δ_+ is in the proximity of unity, using an initial guess of one will always yield a successful root search solution. An approximate solution can be found, however, by using the logarithmic

approximation presented in Chapter 3. Substituting the logarithmic approximation $f_3(\delta_+)$ (Equation (3.7.5)) into Equation (4.5.9), expanding terms, then collecting terms, and simplifying yields:

$$\left(1-4\delta_+ +6\delta_+^2-4\delta_+^3+\delta_+^4\right)+\left(2B-6B\delta_+ +6B\delta_+^2-2B\delta_+^3\right)-16\delta_{Nu}^{*4}=0 \tag{4.6.1}$$

or

$$\left(\frac{1-\delta_+}{2}\right)^4+B\left(\frac{1-\delta_+}{2}\right)^3-\delta_{Nu}^{*4}=0 \tag{4.6.2}$$

Equation (4.6.2) can then be written as:

$$X^4+BX^3-C=0 \tag{4.6.3}$$

where

$$X=\frac{1-\delta_+}{2}=\frac{1-\left(1-\dfrac{\delta}{r_o}\right)^2}{2}=\frac{1-\left(1-2\dfrac{\delta}{r_o}+\left(\dfrac{\delta}{r_o}\right)^2\right)}{2}=\frac{\delta}{r_o}-\frac{1}{2}\left(\frac{\delta}{r_o}\right)^2 \tag{4.6.4}$$

$$B=\frac{M}{\beta}=\frac{2\mu_L\mu_V\,\mathrm{Re}_{in}}{g\rho_L(\rho_L-\rho_V)r_o^3}\frac{\rho_L\mu_V}{\rho_V\mu_L}=\frac{2\mu_V\mu_V\,\mathrm{Re}_{in}}{g(\rho_L-\rho_V)\rho_V r_o^3} \tag{4.6.5}$$

$$C=\delta_{Nu}^{*4}=\frac{4\mu_L k_L\Delta Tz}{r_o^4 h_{fg}g\rho_L(\rho_L-\rho_V)} \tag{4.6.6}$$

Note that when $B=0$, Equation (4.6.3) is the same as Equation (3.7.22) which corresponds to the case of quiescent vapor (natural convection condensation). An interesting fact to note is that Rohsenow (1956), Carey (1992), Ghiaasiaan (2008), and Dalkilic (2009) also derived an equation similar to Equation (4.6.3) within their individual system of equations. The variables and coefficients in their equations were not

expressed in terms of known functions as Equations (4.6.4), (4.6.5), and (4.6.6), however. They were expressions related to one or more of: an assumed velocity profile, a friction factor interfacial shear stress, or the film thickness. Therefore, they all required an iterative procedure to find a solution.

The solution of the quartic Equation (4.6.3) can be obtained by a standard procedure such as the one given by Spiegel (1968). It is a two-step process where the first step is finding a real solution for the following cubic equation:

$$y^3 + 4Cy + B^2C = 0 \tag{4.6.7}$$

To solve for y, define Q, R, D, S, and T as follows:

$$Q = \frac{4}{3}C \tag{4.6.8}$$

$$R = -\frac{1}{2}B^2C \tag{4.6.9}$$

$$D = Q^3 + R^2 = \frac{64}{27}C^3 + \frac{1}{4}B^4C^2 = C^2\left(\frac{64}{27}C + \frac{1}{4}B^4\right) \tag{4.6.10}$$

$$S = \sqrt[3]{R + \sqrt{D}} = \sqrt[3]{-\frac{1}{2}B^2C + \sqrt{C^2\left(\frac{64}{27}C + \frac{1}{4}B^4\right)}} = \sqrt[3]{C\left(\sqrt{\left(\frac{64}{27}C + \frac{1}{4}B^4\right)} - \frac{1}{2}B^2\right)} \tag{4.6.11}$$

$$T = \sqrt[3]{R - \sqrt{D}} = \sqrt[3]{-\frac{1}{2}B^2C - \sqrt{C^2\left(\frac{64}{27}C + \frac{1}{4}B^4\right)}} = -\sqrt[3]{C\left(\sqrt{\left(\frac{64}{27}C + \frac{1}{4}B^4\right)} + \frac{1}{2}B^2\right)} \tag{4.6.12}$$

Because the discriminant $D > 0$, there is only one real solution y_1 for Equation (4.6.7). Because $S > 0$, $T < 0$, and $|S| < |T|$, then $y_1 < 0$ and y_1 is given by:

$$y_1 = S + T = \sqrt[3]{C\left(\sqrt{\left(\frac{64}{27}C + \frac{1}{4}B^4\right)} - \frac{1}{2}B^2\right)} - \sqrt[3]{C\left(\sqrt{\left(\frac{64}{27}C + \frac{1}{4}B^4\right)} + \frac{1}{2}B^2\right)} \tag{4.6.13}$$

Then, in the second step, the solutions for the quartic equation are the solutions of the following double quadratic equation:

$$X^2 + \frac{1}{2}\left(B \pm \sqrt{B^2 + 4y_1}\right)X + \frac{1}{2}\left(y_1 \mp \sqrt{y_1^2 + 4C}\right) = 0 \tag{4.6.14}$$

The discriminants of Equation (4.6.14) are:

$$\begin{aligned} D_q &= \left(\frac{1}{2}\left(B \pm \sqrt{B^2 + 4y_1}\right)\right)^2 - 4\left(\frac{1}{2}\left(y_1 \mp \sqrt{y_1^2 + 4C}\right)\right) \\ &= \frac{1}{4}\left(B^2 \pm 2B\sqrt{B^2 + 4y_1} + B^2 + 4y_1\right) - 2y_1 \pm 2\sqrt{y_1^2 + 4C} \\ &= \frac{1}{2}B^2 \pm \frac{1}{2}B\sqrt{B^2 + 4y_1} - y_1 \pm 2\sqrt{y_1^2 + 4C} \end{aligned} \tag{4.6.15}$$

Using only the positive discriminant reduces the number of solutions to two. Only one real positive solution is selected:

$$D_q = \frac{1}{2}B^2 + \frac{1}{2}B\sqrt{B^2 + 4y_1} - y_1 + 2\sqrt{y_1^2 + 4C} \tag{4.6.16}$$

$$X = -\frac{1}{4}\left(B + \sqrt{B^2 + 4y_1}\right) + \frac{1}{2}\sqrt{\frac{1}{2}B^2 + \frac{1}{2}B\sqrt{B^2 + 4y_1} - y_1 + 2\sqrt{y_1^2 + 4C}} \tag{4.6.17}$$

From Equations (4.6.4)

$$\delta_+ = 1 - 2X \tag{4.6.18}$$

Therefore, using Equation (3.3.6), the film thickness based on the ρ_{+1} and $f_3(\delta_+)$ approximations is:

$$\delta = r_o\left(1-\sqrt{\delta_+}\right) = r_o\left(1-\sqrt{1-2X}\right) \tag{4.6.19}$$

where X is determined by Equation (4.6.17) and y_1 is determined by Equation (4.6.13).

An attempt was made to find a closed-form solution for Equation (4.5.33), using the ρ_{+2} and the $f_3(\delta_+)$ approximation for $\ln\delta_+$, but this produces a sixth order polynomial which is not readily solvable in closed-form.

Therefore, three analytical solutions for the condensate film thickness have been presented in this chapter. One solution uses the ρ_{+1} approximate density function and requires a root search to solve Equation (4.5.9) for δ_+. A second solution uses the ρ_{+2} approximate density function and requires a root search to solve Equation (4.5.33) for δ_+. The third solution, which uses the ρ_{+1} approximate density function and the $f_3(\delta_+)$ approximation for $\ln\delta_+$, involves the solution of a quartic Equation (4.6.3) for δ_+. Once the δ_+ is found, δ or δ^* can be easily computed.

Figure 4.5 is a plot of the dimensionless film thickness, from steam at atmospheric pressure, for the three solution approaches mentioned above and the results from the Groff (2005) numerical solution. The inset figure magnifies the four lines and shows that the quartic-based solution ρ_{+1q} is closer to the more accurate solution based on ρ_{+2} than

the ρ_{+1}-based solution. This is due to the cancelation of two approximations used: the ρ_{+1} approximation produces a higher interfacial shear stress and thus reduces the film thickness while the logarithmic approximation used in the quartic-based solution applies a smaller value of δ_+ and thus increases the film thickness. For the input parameters of this example, the RMS deviation between the results for the ρ_{+2}-based approach and the ρ_{+1q}-based approach is 0.25%. The RMS deviation between the numerical solution and the ρ_{+1q}-based approach is 2.6%. The RMS deviation between the numerical solution and the ρ_{+2}-based approach is 2.4%.

Figure 4.6 shows a similar comparison as in Figure 4.5 but with a smaller tube radius of 0.003 m. For the input parameters of this example, the RMS deviation between the results for the ρ_{+2}-based approach and the ρ_{+1q}-based approach is 1.9%. The RMS deviation between the numerical solution and the ρ_{+1q}-based approach is 7.3%. The RMS deviation between the numerical solution and the ρ_{+2}-based approach is 5.9%. The higher deviations associated with small radius are expected because the ρ_{+1} approximation is not as good as the ρ_{+2} approximation, as seen in Figure 4.4. Note that the maximum deviation is near the inlet where the vapor velocity is high or at the end of condensation where the liquid velocity is high.

From the comparisons, for a tube radius of 0.005 m or more, Equation (4.6.19) is an excellent approximate closed-form solution. For a tube radius of 0.005 m or less, the solution based on ρ_{+2} should be used.

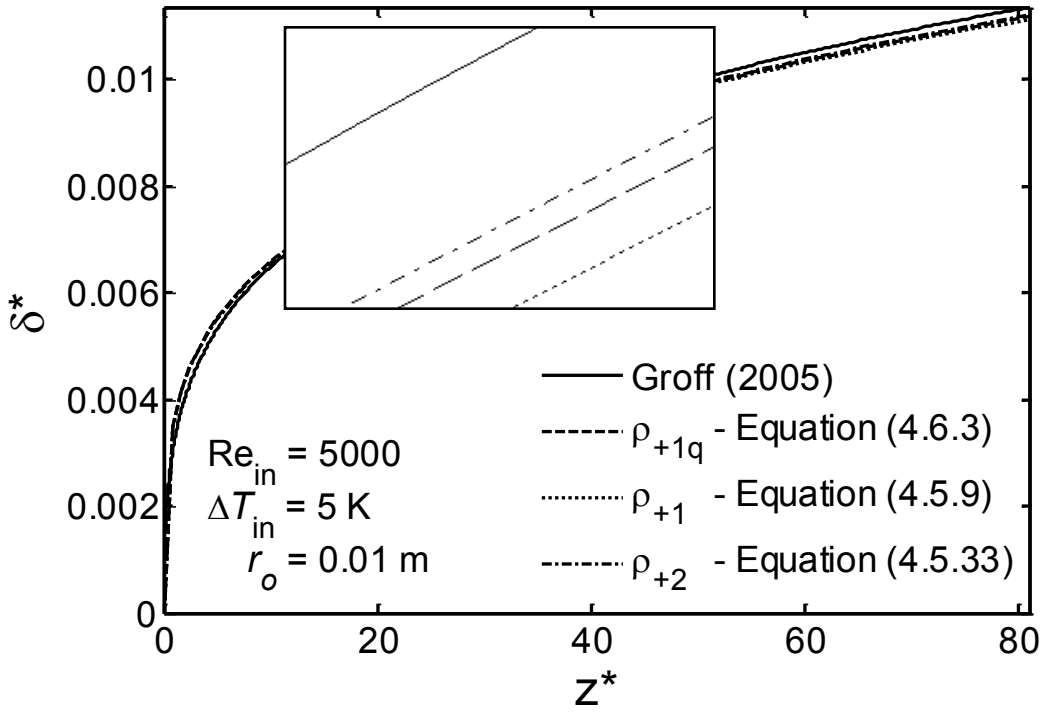

Figure 4.5: Film thickness comparison (Re_{in}= 5000, ΔT_{in} = 5 K, r_o = 0.01 m)

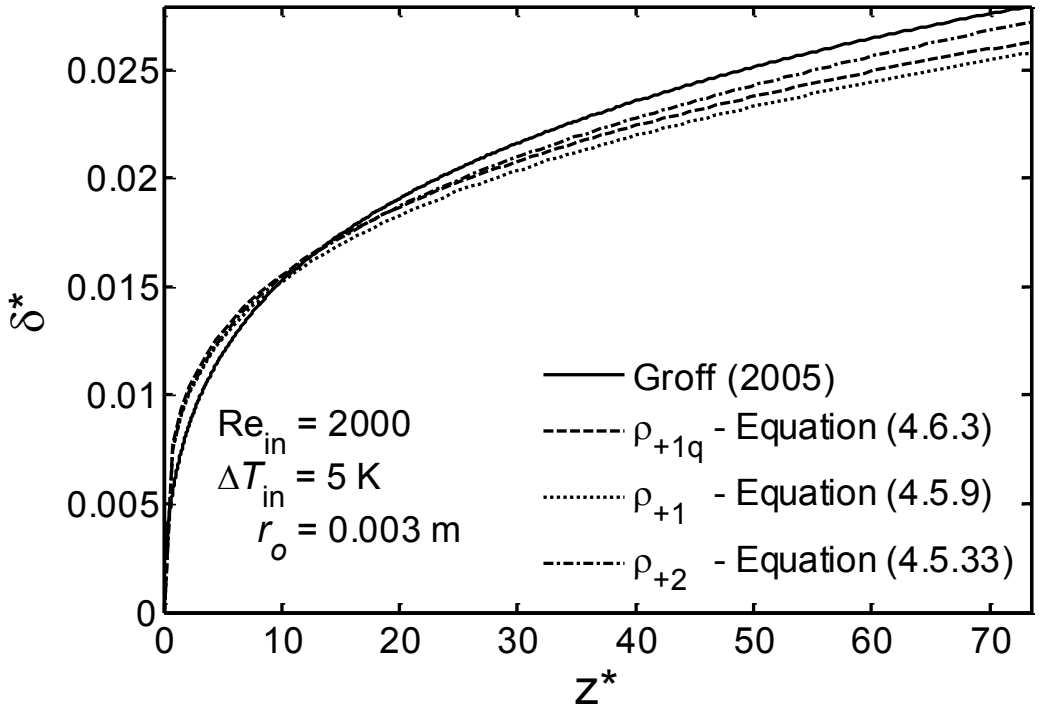

Figure 4.6: Film thickness comparison (Re_{in}= 2000, ΔT_{in} = 5 K, r_o = 0.003 m)

4.7. Observations about the Behavior of the Solutions

A better understanding of the behavior of the analytical solutions can be obtained by examining the results of the solutions in more detail.

4.7.1. Inlet Quantities

At the inlet, $z = 0$ and $\delta = 0$. Therefore, $\delta_+ = 1$ using Equation (3.3.5) and $\rho_+ = \rho_{+1}$ from Equations (4.3.18) and (4.4.1). The inlet vapor velocity profile, the inlet pressure gradient, and the inlet interfacial shear stress can be computed by substituting these quantities into Equations (4.2.25), (4.2.1), and (4.2.6), respectively. They are:

$$u_{V,\text{in}} = -\frac{\rho_{+1} g}{4\mu_V}\left(r_o^{\,2} - r^2\right) = \frac{2u_{\text{in}}}{r_o^2}\left(r_o^{\,2} - r^2\right) \tag{4.7.1}$$

$$\left(\frac{dP}{dz}\right)_{in} = \left(\rho_V + \rho_{+1}\right)g = \rho_V g - \frac{8\mu_V u_{in}}{r_o^2} \tag{4.7.2}$$

$$\tau_{in} = -\rho_{+1}\frac{g\left(r_o - \delta\right)}{2} = \frac{4\mu_V u_{in}}{r_o} \tag{4.7.3}$$

Note that u_{in} is the average inlet vapor velocity used to compute the inlet Reynolds number. These expressions reveal that the inlet vapor velocity profile is fully developed profile, the inlet pressure gradient is the same as the pressure gradient of single phase flow, and the inlet interfacial shear stress is the same as the shear stress obtained by using the Darcy-Weisbach friction factor for fully developed laminar single phase flow.

4.7.2. Interfacial Shear Stress

The plots of the dimensionless interfacial shear stress for the condensation of steam at atmospheric pressure, using Equations (4.2.6) and (4.7.3), are shown in Figures 4.7 to 4.9 over the typical range of δ_+ for a variety of tube radii, inlet Reynolds numbers, and temperature differences. These results show that the interfacial shear stress depends more on the tube radius and the inlet Reynolds number than on the temperature difference. Note that the positive shear stress means the vapor is dragging the liquid while the negative shear stress means the liquid is dragging the vapor.

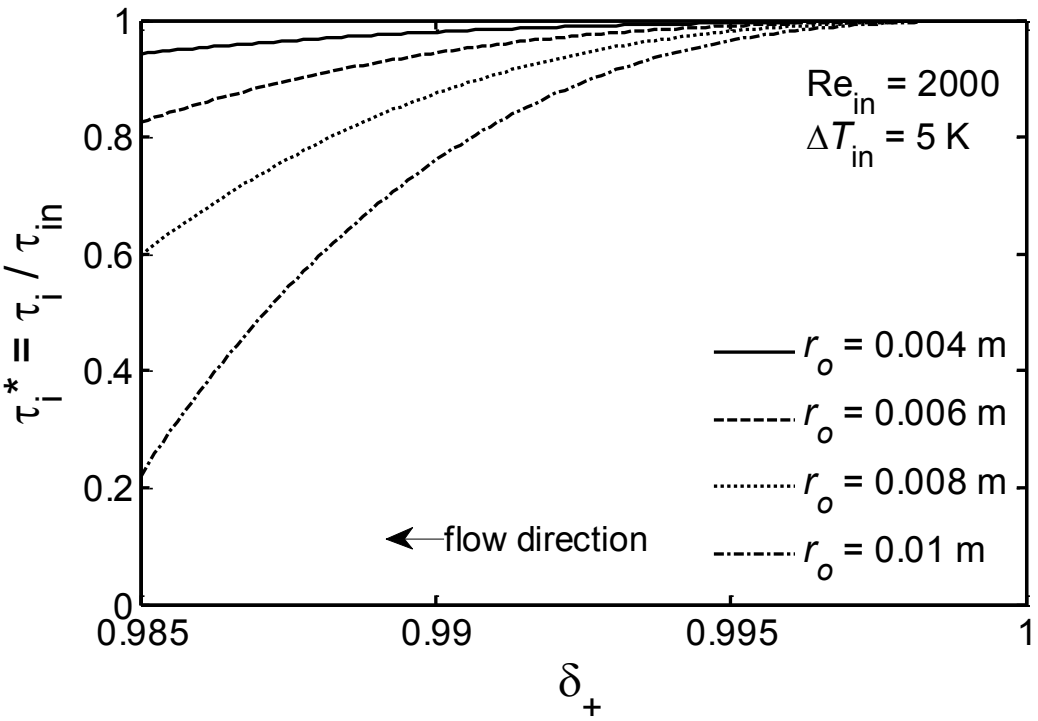

Figure 4.7: Interfacial shear stress (Re_{in} = 2000, ΔT_{in} = 5 K)

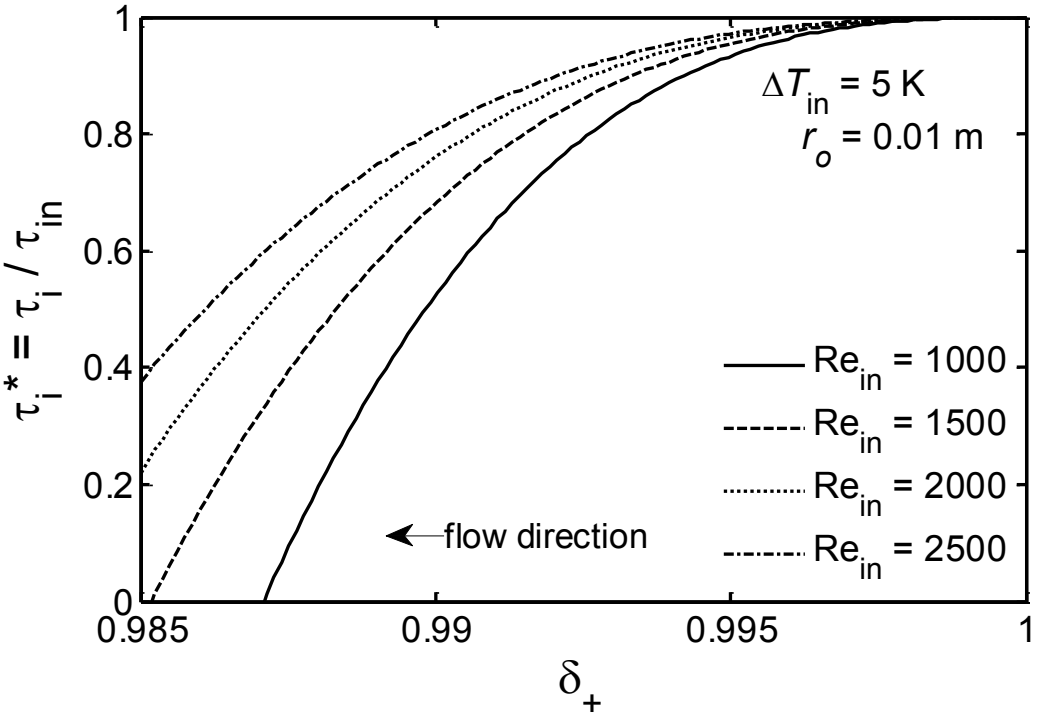

Figure 4.8: Interfacial shear stress (ΔT_{in} = 5 K, r_o = 0.01 m)

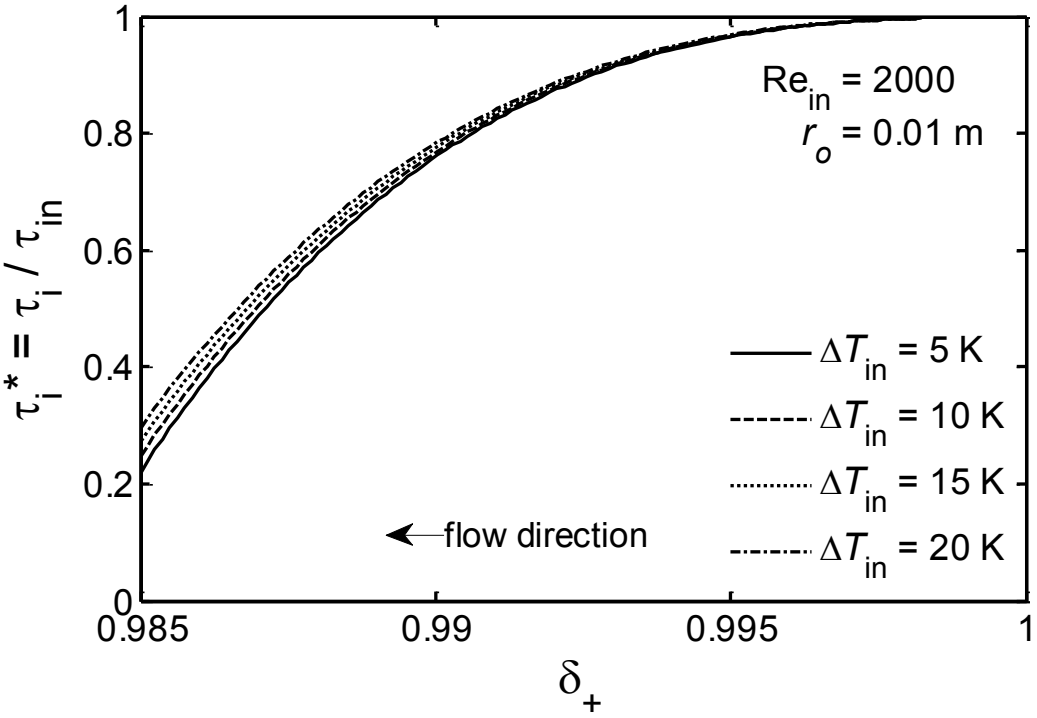

Figure 4.9: Interfacial shear stress (Re_{in} = 2000, r_o = 0.01 m)

4.7.3. Vapor and Liquid Reynolds Numbers

The validity of this analysis is for laminar vapor and condensate flows. As such, the Reynolds number of the vapor should be less than 2300 and that of the condensate should be less than 30. To understand the conditions under which the vapor and liquid Reynolds number were close to those limits, their axial variations were examined under the assumption $\delta << r_o$. In that case:

$$\mathrm{Re}_V = \frac{2\dot{m}_V}{\pi\mu_V(r_o - \delta)} \approx \frac{2\dot{m}_V}{\pi\mu_V r_o} \tag{4.7.4}$$

and

$$\mathrm{Re}_L = \frac{2\dot{m}_L}{\pi\mu_L(r_o - \delta)} \approx \frac{2\dot{m}_L}{\pi\mu_L r_o} \approx \frac{\mu_V}{\mu_L}\frac{2(\dot{m}_{in} - \dot{m}_V)}{\pi\mu_V r_o} \approx \frac{\mu_V}{\mu_L}(\mathrm{Re}_{in} - \mathrm{Re}_V) \tag{4.7.5}$$

Plots of axial vapor and condensate Reynolds numbers for various inlet Reynolds numbers and temperature differences are shown in Figures 4.10 to 4.13. The zero local axial vapor Reynolds number corresponds to the end of condensation as shown in Figures 4.10 and 4.11. Figures 4.12 and 4.13 show that the condensate Reynolds number depends more on the inlet-to-wall temperature difference than on the inlet Reynolds number.

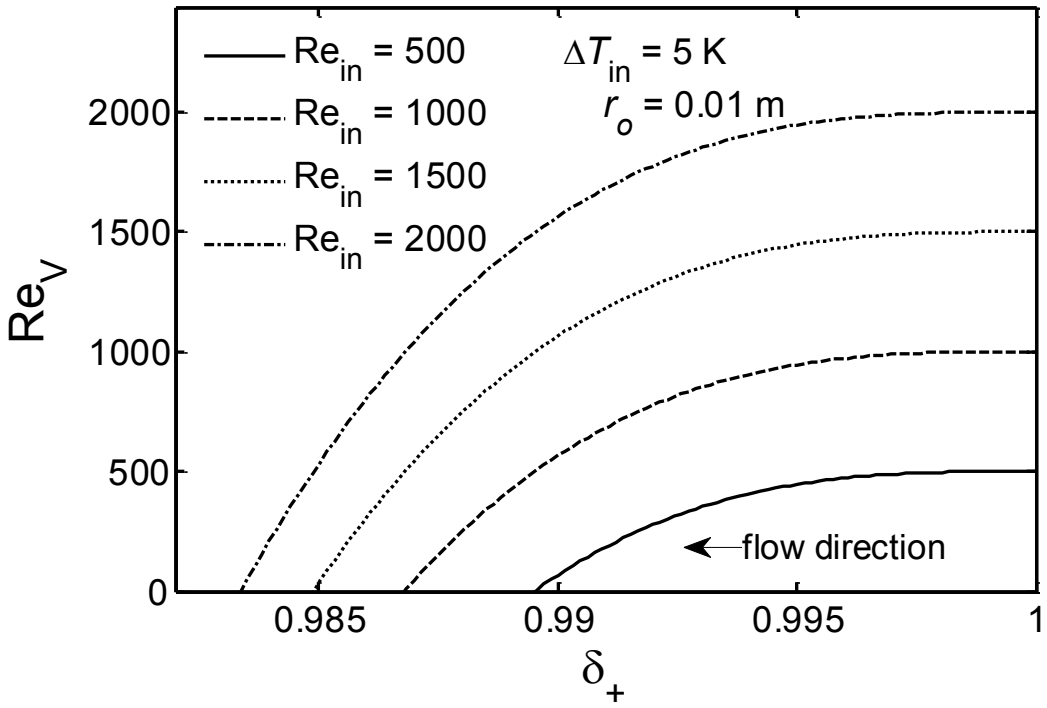

Figure 4.10: Vapor axial Reynolds number (ΔT_{in} = 5 K, r_o = 0.01 m)

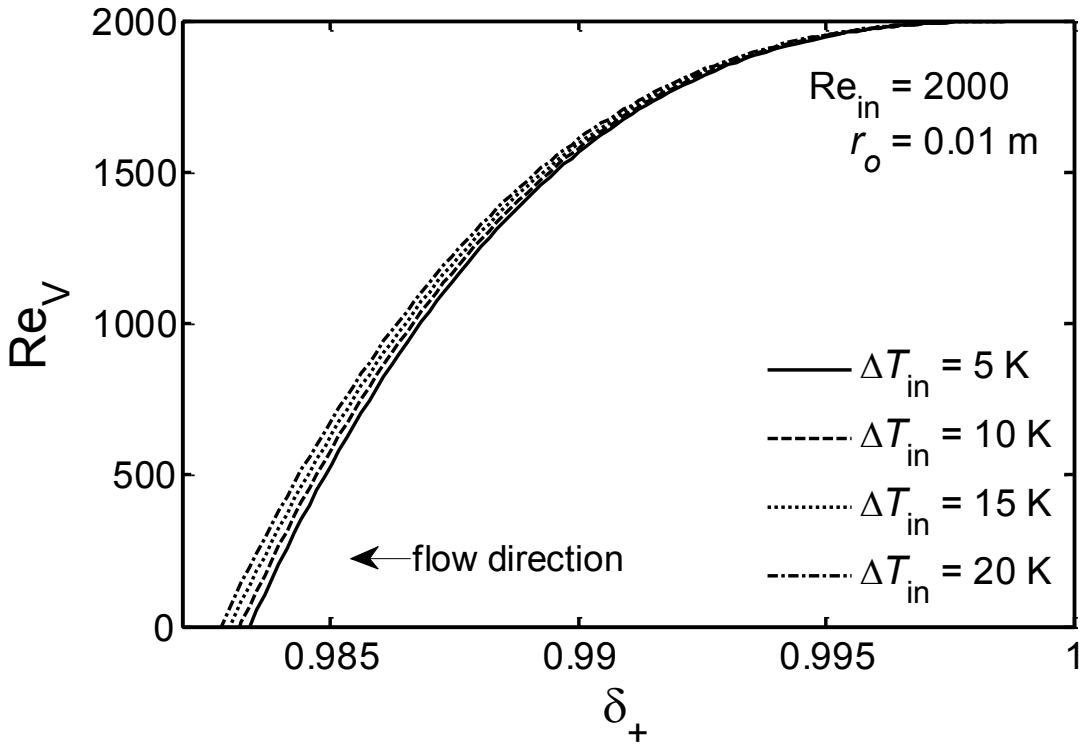

Figure 4.11: Vapor axial Reynolds number (Re_{in} = 2000, r_o = 0.01 m)

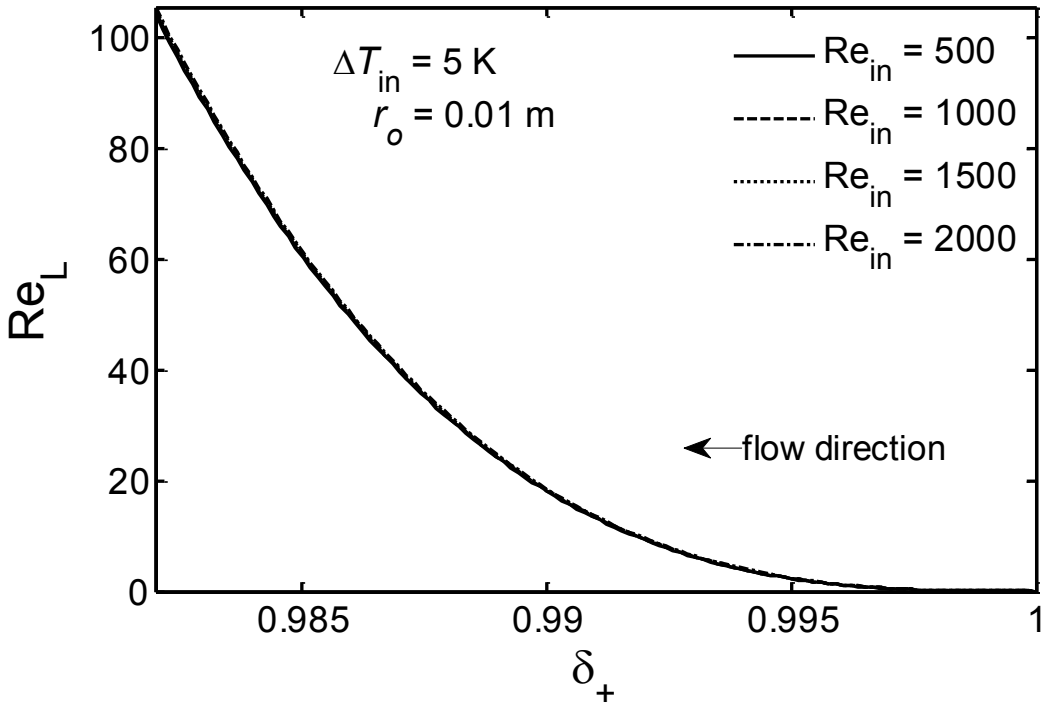

Figure 4.12: Liquid axial Reynolds number (ΔT_{in} = 5 K, r_o = 0.01 m)

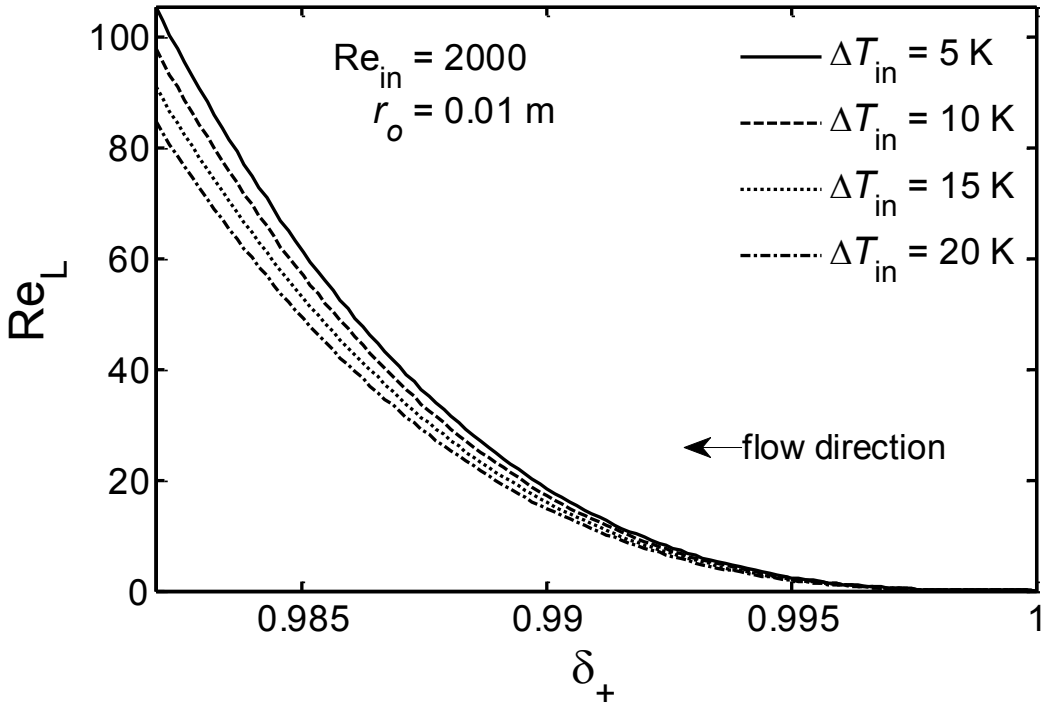

Figure 4.13: Liquid axial Reynolds number (Re$_{in}$ = 2000, r_o = 0.01 m)

4.8. Comparison with the Numerical Solution of Groff (2005)

This section compares the condensate film thickness and velocity profiles computed using the closed-form solution (ρ_{+1q}-based method) with the results produced using the numerical solution of Groff (2005). The vapor is steam at atmospheric pressure.

The dimensionless film thickness is plotted for a variety of inlet Reynolds numbers and temperature differences in Figures 4.14 to 4.19. The RMS deviation between the numerical solution and the closed-form solution is indicated on the graphs. For low inlet Reynolds number and small temperature difference (low condensation rate), the agreement is excellent as shown in Figures 4.14 and 4.15. The agreement is still reasonable up to inlet Reynolds number of 10000 as shown in Figure 4.16, which can be considered as the transitional regime before full turbulence. For higher inlet Reynolds number in Figure 4.17 and higher temperature difference (higher condensation rate) in Figures 4.18 and 4.19, the present solution does not agree well with the numerical solution because the present solution assumes laminar flow profile while the numerical solution has a turbulent model.

The maximum deviation is either near the inlet or at the end of condensation, depending on the input parameters. For high inlet Reynolds number in Figure 4.17, it is near the inlet where the vapor is turbulent in numerical solution. For high temperature difference in Figure 4.18, it is at the end of condensation where the liquid is turbulent in numerical solution. This observation is very important to the development of turbulent viscosities in Chapter 5.

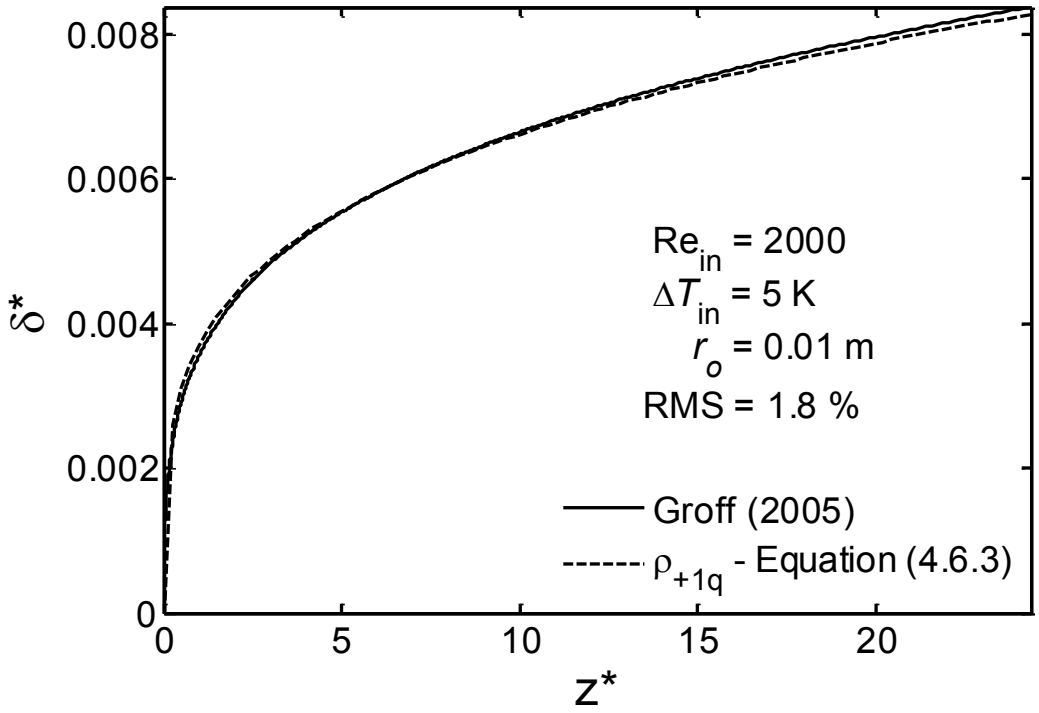

Figure 4.14: Film thickness (Re_{in} = 2000, ΔT_{in} = 5 K, r_o = 0.01 m)

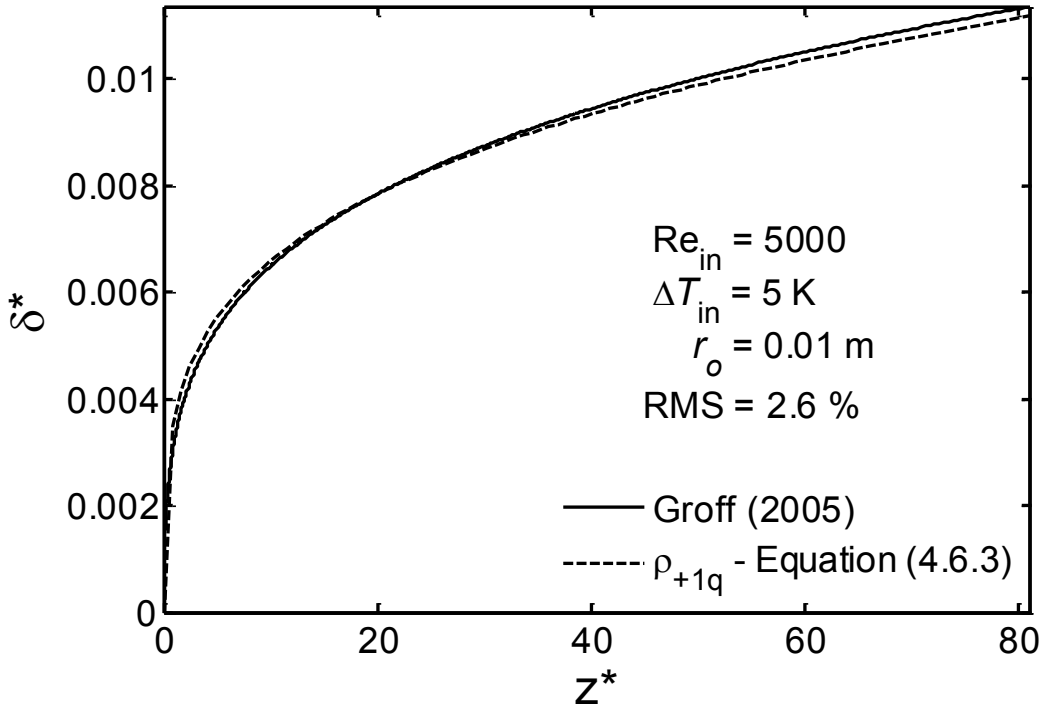

Figure 4.15: Film thickness (Re_{in} = 5000, ΔT_{in} = 5 K, r_o = 0.01 m)

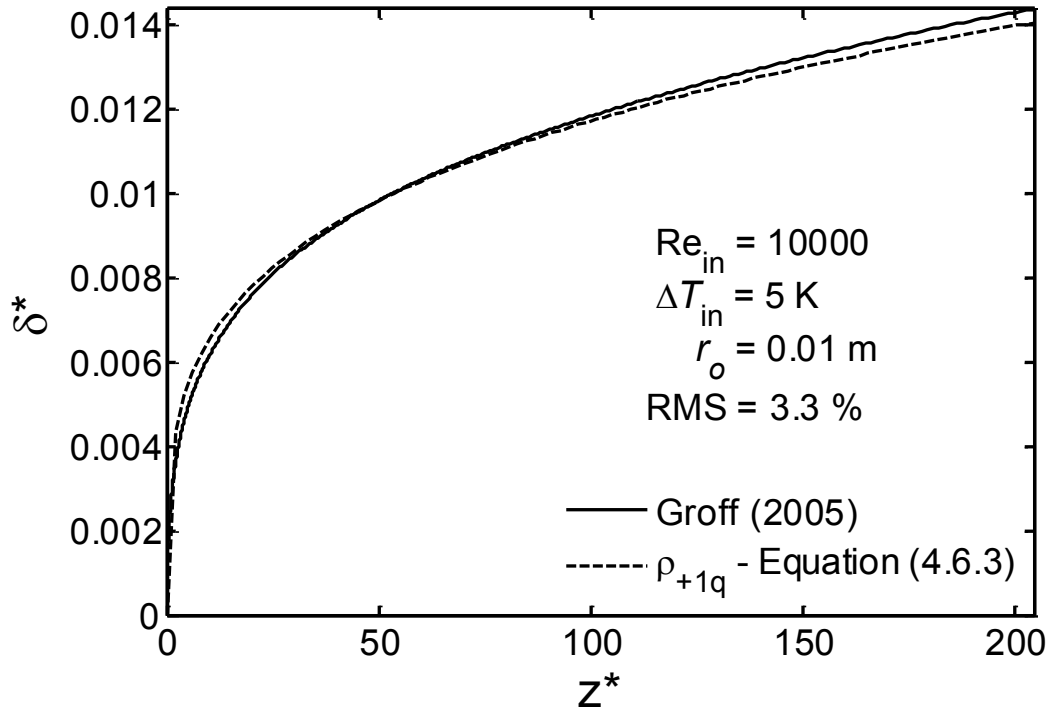

Figure 4.16: Film thickness (Re_{in} = 10000, ΔT_{in} = 5 K, r_o = 0.01 m)

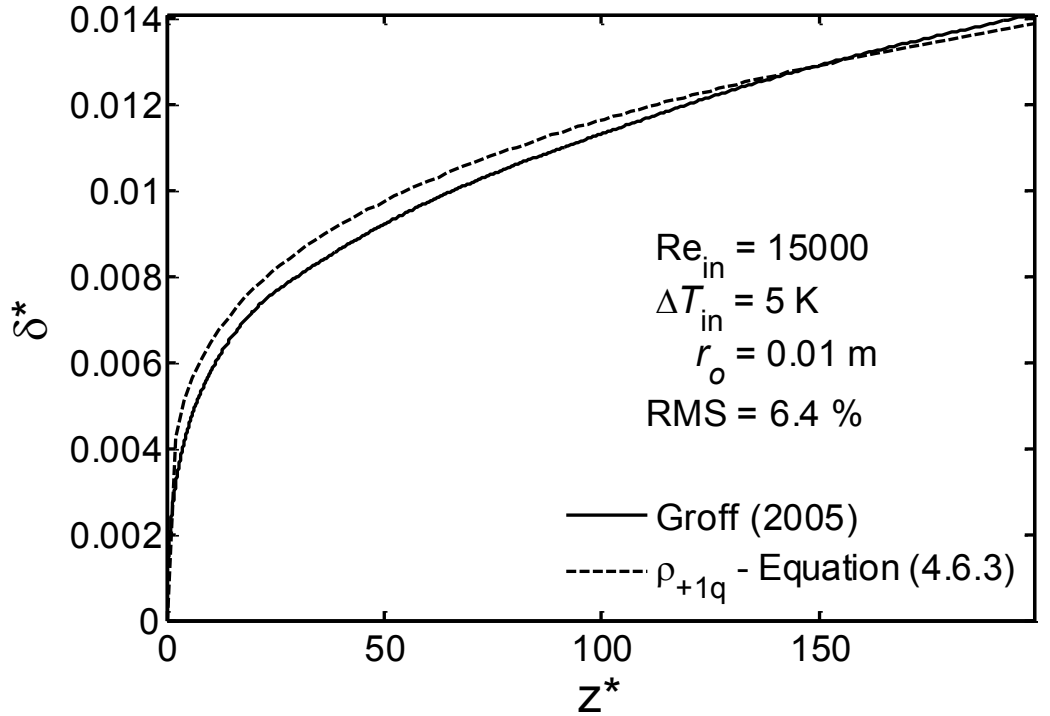

Figure 4.17: Film thickness (Re_{in} = 15000, ΔT_{in} = 5 K, r_o = 0.01 m)

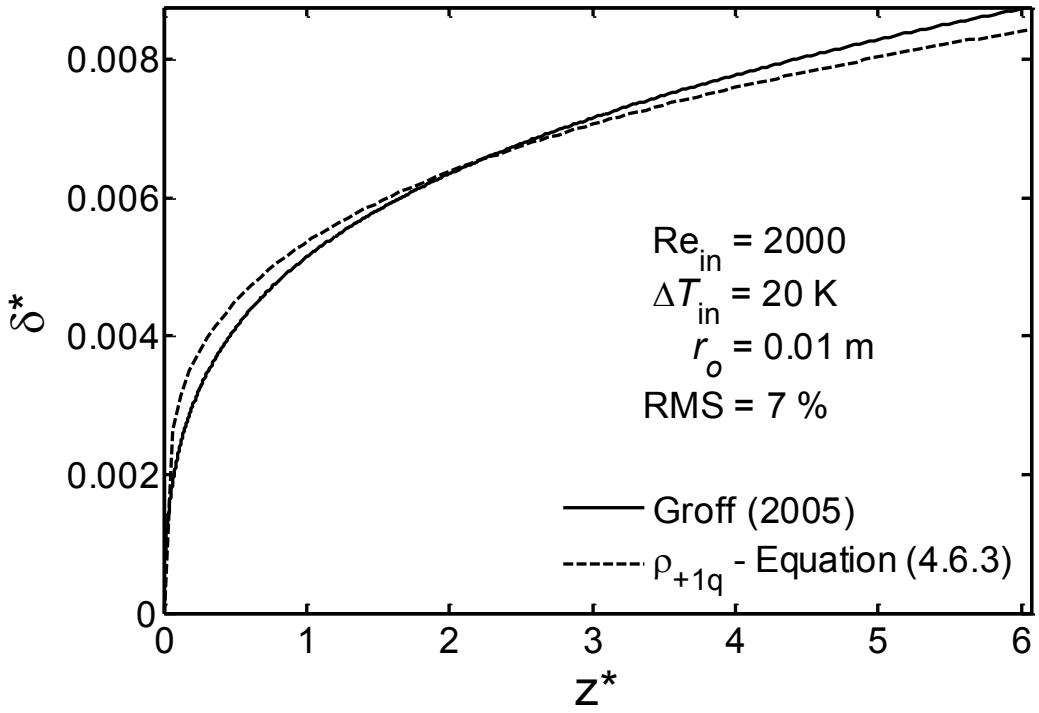

Figure 4.18: Film thickness (Re_{in} = 2000, ΔT_{in} = 20 K, r_o = 0.01 m)

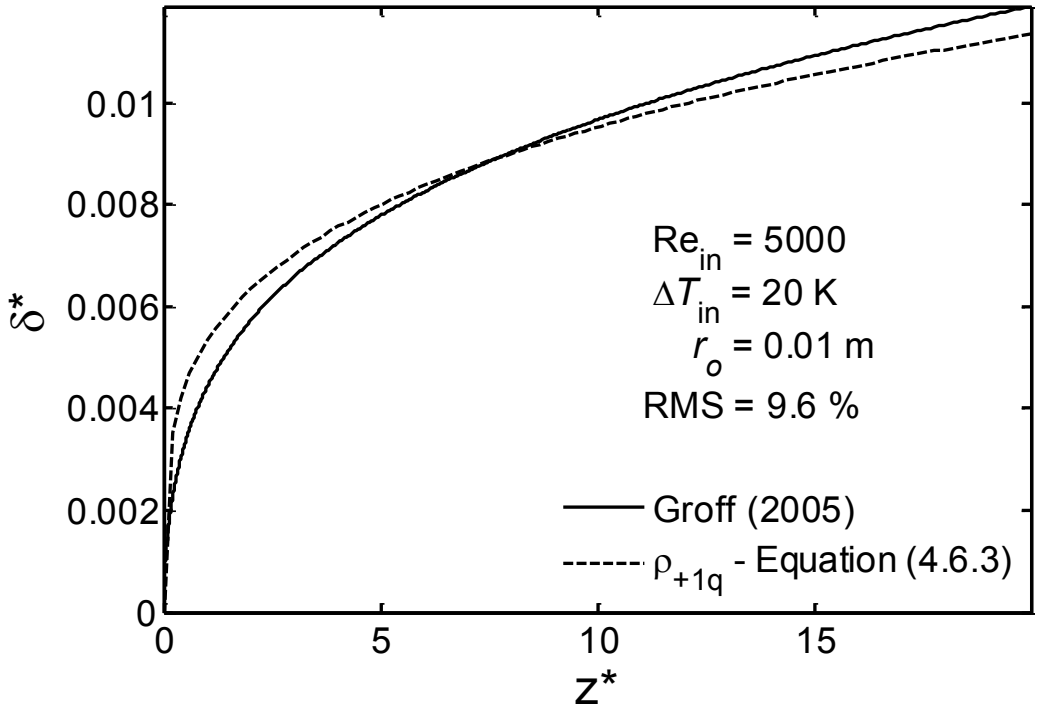

Figure 4.19: Film thickness (Re_{in} = 5000, ΔT_{in} = 20 K, r_o = 0.01 m)

The velocity profiles of two typical cases are shown in Figures 4.20 to 4.24 for $r_o = 0.01\,\text{m}$ and Figures 4.25 to 4.28 for $r_o = 0.005\,\text{m}$. Note that the horizontal axes of these figures are transformed from the radial coordinate by:

$$\eta = \begin{cases} \dfrac{r}{r_o - \delta} & 0 \le r \le r_o - \delta,\ 0 \le \eta \le 1 \\ 2 - \dfrac{r_o - r}{\delta} & r_o - \delta \le r \le r_o,\ 1 \le \eta \le 2 \end{cases} \tag{4.8.1}$$

Figure 4.20 and Figure 4.25 show that the velocity profiles do not match near the inlet. This discrepancy occurs because the present analytical solution has a fully developed vapor velocity profile while the numerical solution uses a uniform inlet vapor velocity profile. In these two figures, the numerical solution results show a very large jump in liquid velocity profile at the inlet. This is a numerical aberration caused by the uniform inlet vapor velocity profile. This numerical error does not affect subsequent liquid velocity profiles. Figures 4.20 to 4.24 and Figures 4.26 to 4.28 show that the average vapor velocities from the present solution are consistent with the numerical solution results except near the end of condensation where the flow reversal is about to occur as shown in Figure 4.24. The liquid velocity profiles of the present solution and the numerical solution are in very good agreement at all other *z* locations.

Although the difference of the vapor velocity profiles is large and thus resulting a large difference of their slopes at the interface, the difference in the interface shear stress is actually very small because of the small value of the vapor viscosity. On the other hand, the condensate viscosity is much larger so the condensate velocity profiles must be similar to ensure similar interfacial shear stress values.

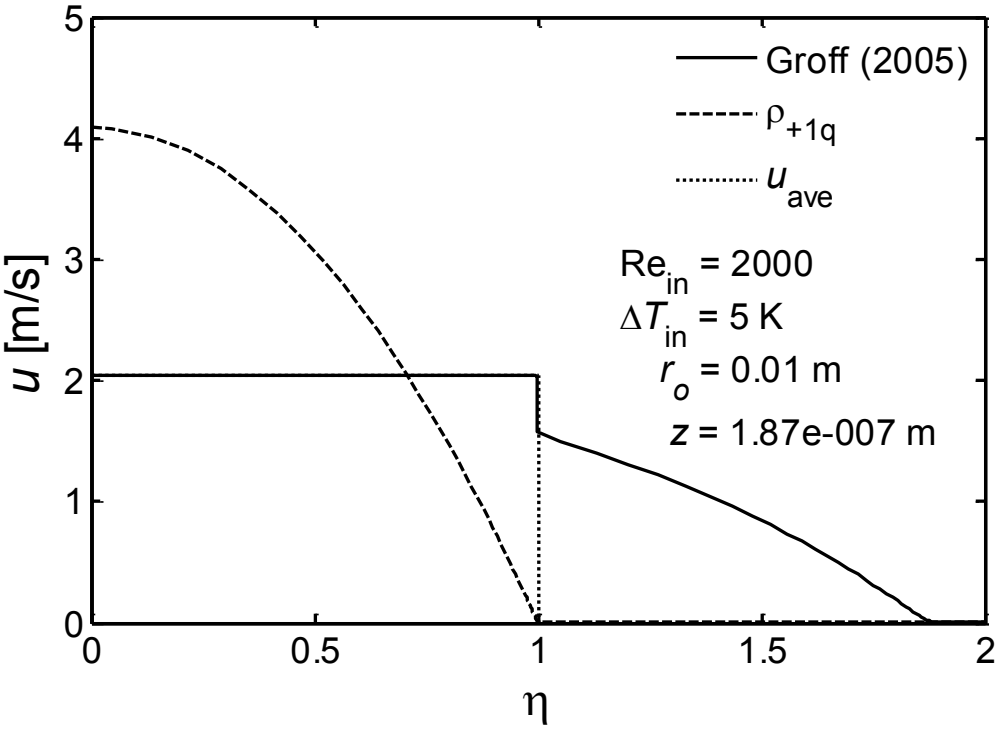

Figure 4.20: Velocity profile (Re_{in} = 2000, ΔT_{in} = 5 K, r_o = 0.01 m, z = $1.87 \cdot 10^{-7}$ m)

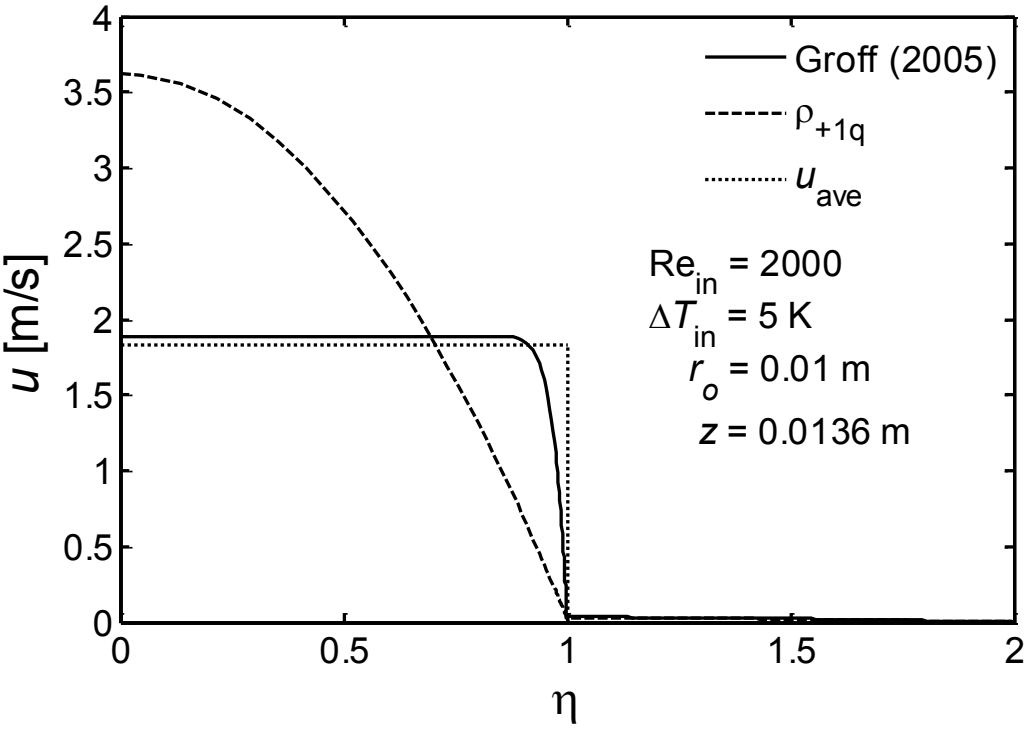

Figure 4.21: Velocity profile (Re_{in} = 2000, ΔT_{in} = 5 K, r_o = 0.01 m, z = 0.0136 m)

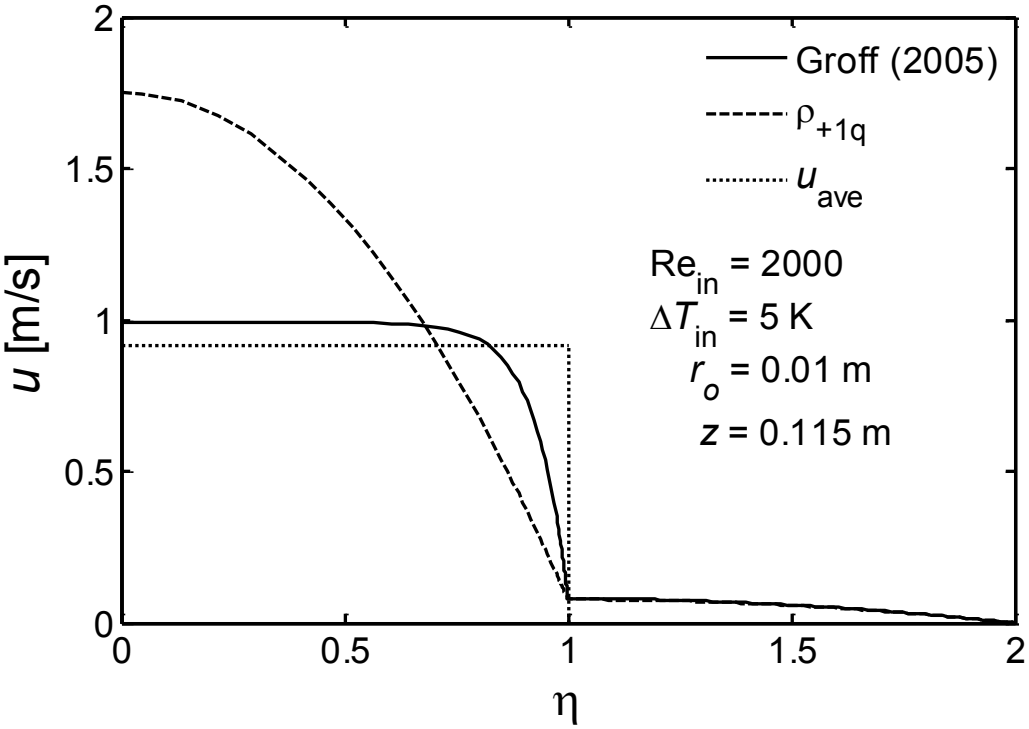

Figure 4.22: Velocity profile (Re_{in} = 2000, ΔT_{in} = 5 K, r_o = 0.01 m, z = 0.115 m)

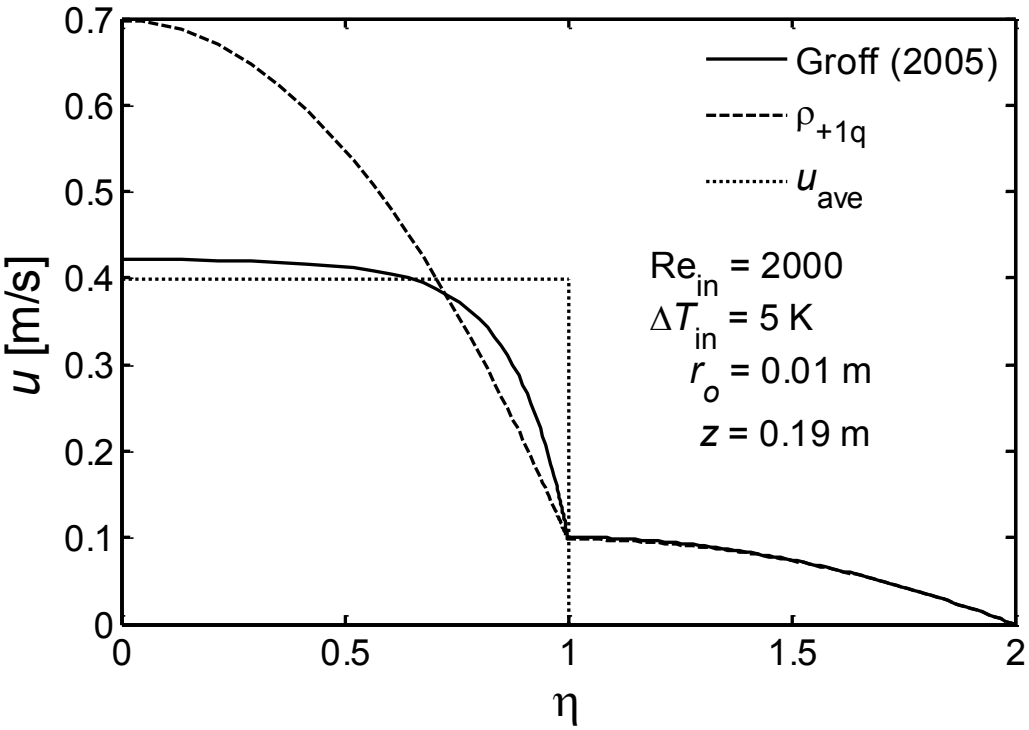

Figure 4.23: Velocity profile (Re_{in} = 2000, ΔT_{in} = 5 K, r_o = 0.01 m, z = 0.19 m)

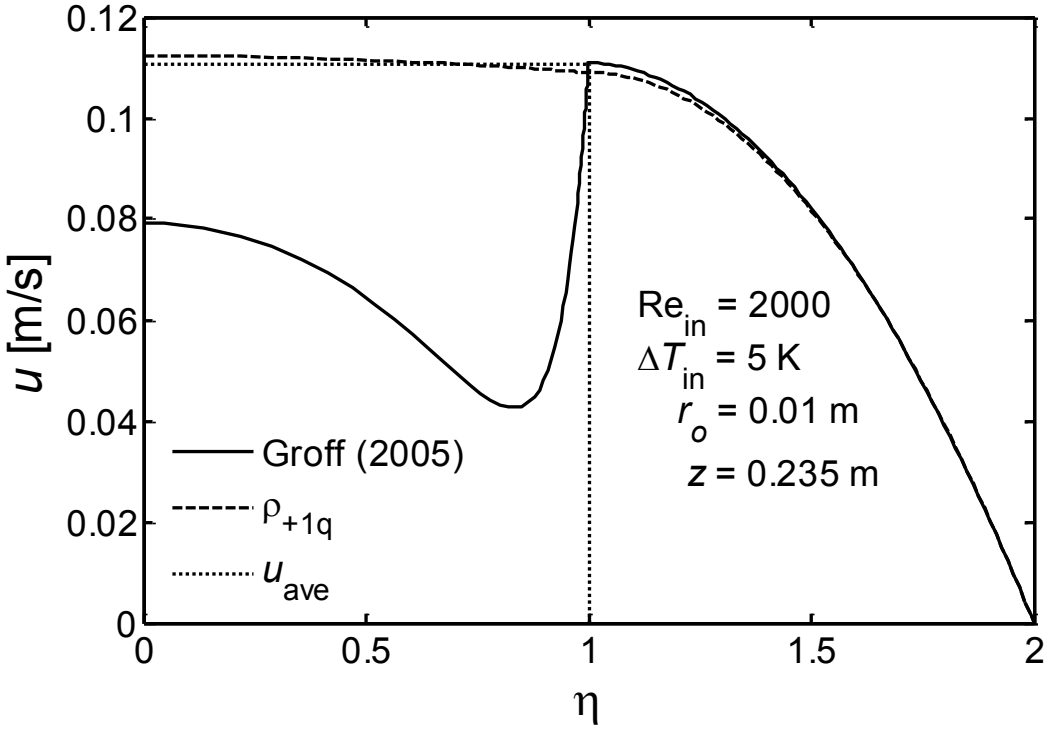

Figure 4.24: Velocity profile (Re_{in} = 2000, ΔT_{in} = 5 K, r_o = 0.01 m, z = 0.235 m)

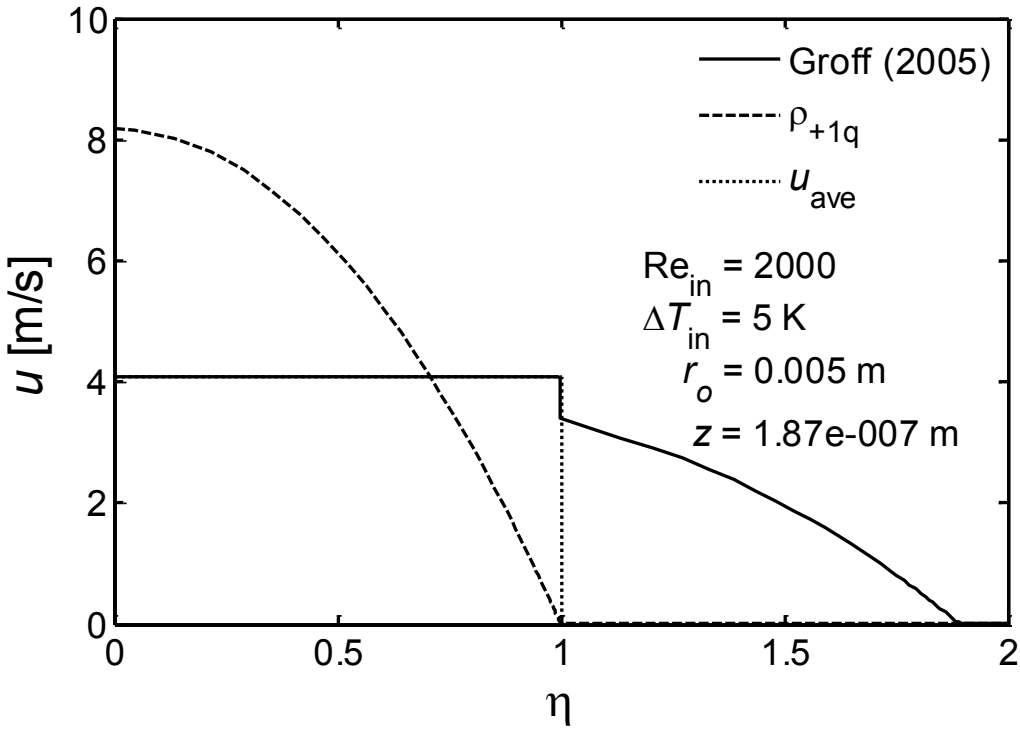

Figure 4.25: Velocity profile (Re_{in} = 2000, ΔT_{in} = 5 K, r_o = 0.005 m, z = $1.87 \cdot 10^{-7}$ m)

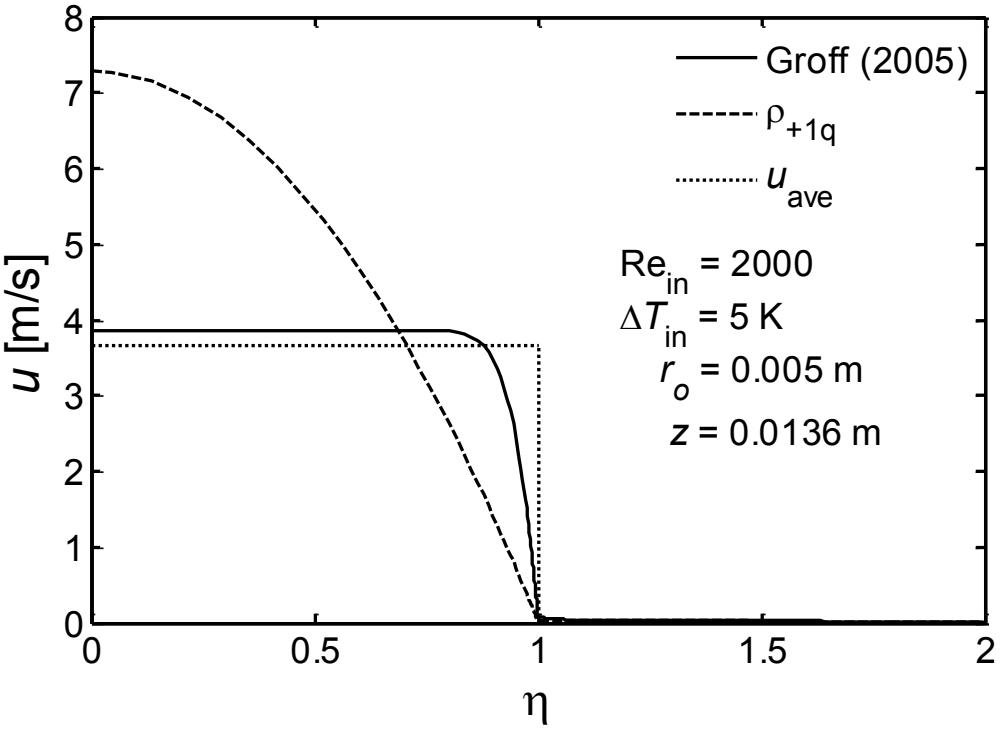

Figure 4.26: Velocity profile (Re_{in} = 2000, ΔT_{in} = 5 K, r_o = 0.005 m, z = 0.0136 m)

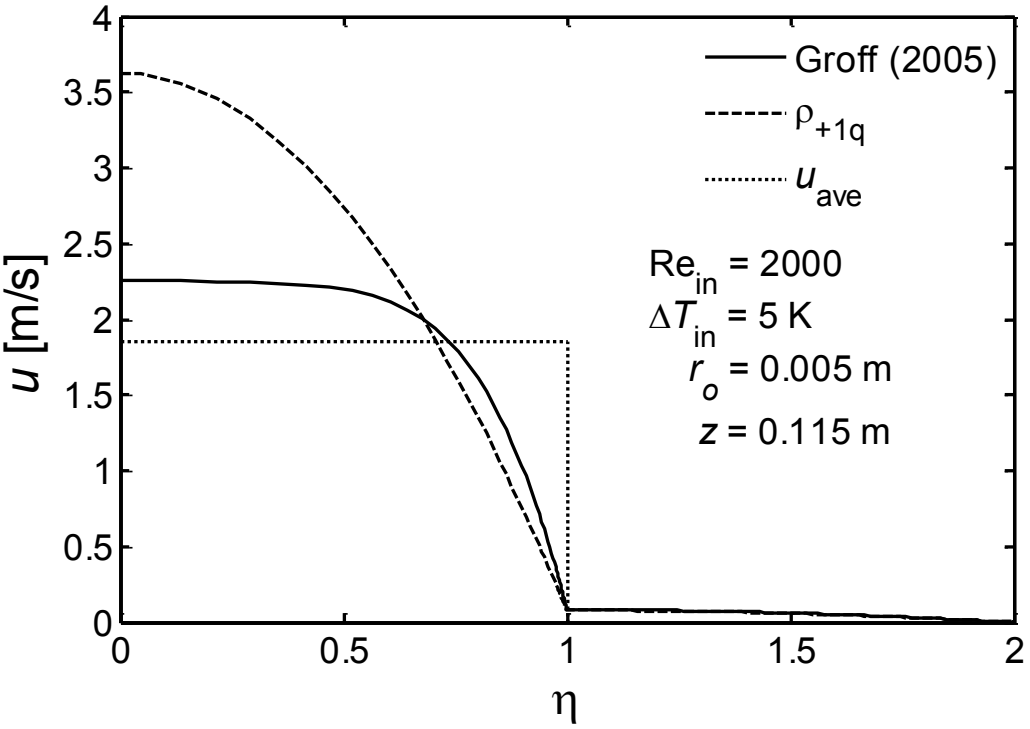

Figure 4.27: Velocity profile (Re_{in} = 2000, ΔT_{in} = 5 K, r_o = 0.005 m, z = 0.115 m)

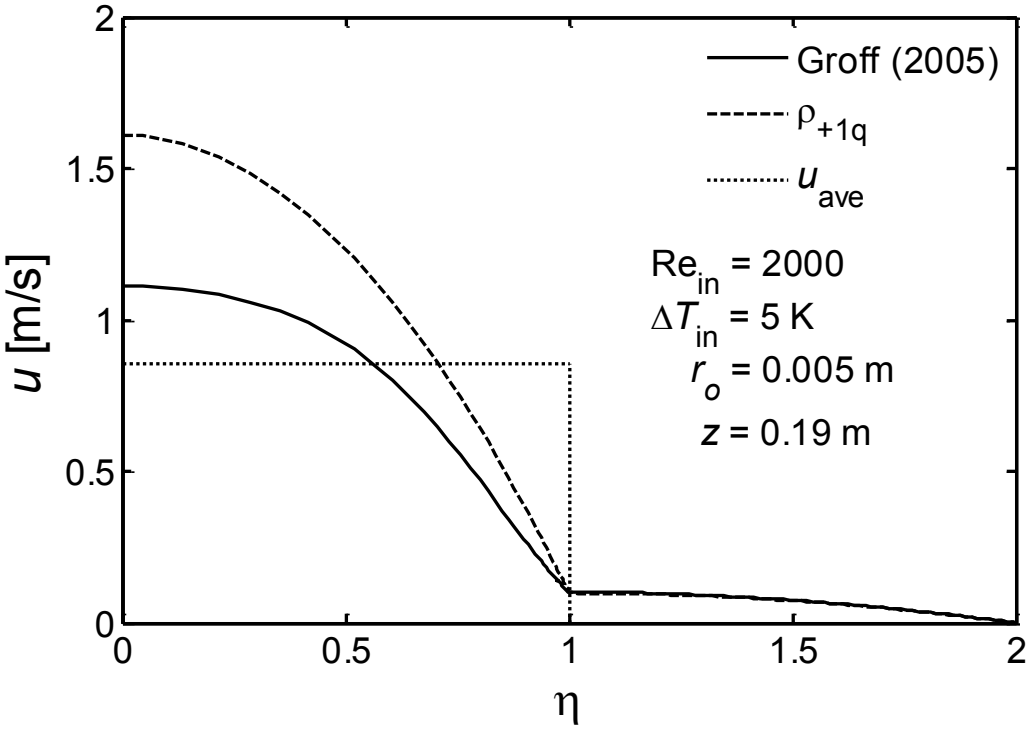

Figure 4.28: Velocity profile (Re_{in} = 2000, ΔT_{in} = 5 K, r_o = 0.005 m, z = 0.19 m)

4.9. Conclusions

From this analysis and the comparisons, the closed-form solution based on the quartic δ_+ Equation (4.6.3) gives an accurate approximation for the film thickness and other related quantities of the laminar mixed-convection condensation in vertical tubes. The RMS deviation of the film thickness is typically less than 2% compared to the numerical solution method of Groff (2005) in the laminar flow regime.

CHAPTER 5

TURBULENT MIXED-CONVECTION FILM CONDENSATION

5.1. Introduction

This chapter extends the analysis of mixed-convection laminar film condensation from a pure vapor in a vertical tube to turbulent flow of vapor and condensate. The extension begins by replacing molecular viscosity and thermal conductivity with effective quantities that are based on molecular and turbulent components.

$$\mu_{V,eff} = \mu_V + \mu_V^t \tag{5.1.1}$$

$$\mu_{L,eff} = \mu_L + \mu_L^t \tag{5.1.2}$$

$$k_{L,eff} = k_L + k_L^t = k_L + \frac{\mu_L^t C_{P,L}}{\mathrm{Pr}_L^t} = k_L + \mu_L^t C_{P,L} \tag{5.1.3}$$

These effective properties use the eddy viscosity approximation to model turbulent effects. Note that the liquid turbulent Prandtl number was assumed to be unity. Note also that the turbulent viscosities in these expressions are constants at each axial location. Equations (5.1.1) to (5.1.3) are used in the previous ρ_{+1q}-based solution approach. In this case, the equations are written as:

$$X^4 + BX^3 - C = 0 \tag{5.1.4}$$

$$X = \frac{\delta}{r_o} - \frac{1}{2}\left(\frac{\delta}{r_o}\right)^2 \tag{5.1.5}$$

$$B = \frac{2\mu_{V,eff}\mu_V \,\mathrm{Re}_{\mathrm{in}}}{g(\rho_L - \rho_V)\rho_V r_o^3} \tag{5.1.6}$$

$$C = \frac{4\mu_{L,eff} k_{L,eff} \Delta T z}{g h_{fg} \rho_L (\rho_L - \rho_V) r_o^4} \tag{5.1.7}$$

Recall the discussion of Equation (4.4.2) where there are two factors of molecular vapor viscosity. One of them is the molecular vapor viscosity at the entrance which is used to compute inlet Reynolds number. The other is the local vapor viscosity and is replaced by the effective vapor viscosity.

Recall also that in Chapter 4, when the molecular properties were known, the laminar versions of Equation (5.1.6) and (5.1.7) were used to compute *B* and *C* and the equivalent of Equation (5.1.4) was solved for *X* to yield δ at any *z* location. In the case of turbulent flow of liquid and vapor, the turbulent viscosities μ_L^t and μ_V^t are not known in the absence of a model for turbulence effects. That turbulence model could be additional equations to solve or it could be correlation equations for the turbulent viscosities. In the present work, the latter approach is adopted. The correlation equations for the turbulent viscosities are to be determined using a given set of data for $\delta(z)$, either from experiments or from a numerical model. Once those correlation equations are obtained, the closed-form solution can be used to predict δ over the range for which the correlation equations are valid.

The challenge lies in determining the correlation equations for the turbulent viscosities. If δ is known at a given *z*, then *X* can be computed from Equation (5.1.5). This leaves a single Equation (5.1.4) from which to determine both *B* and *C*. The approach adopted is

based on noting the following two characteristics of the B and C coefficients: (1) B contains vapor viscosity only and C contains liquid viscosity only, and (2) computing either B or C with molecular properties is like assuming laminar flow for either the vapor or the liquid.

Keeping the two characteristics above in mind, it is useful to examine a comparison of the laminar analysis with results of the Groff (2005) numerical model for a turbulent flow case as shown in Figure 5.1. In the figure, LL refers to "Laminar vapor, Laminar liquid", which are the results using the fully laminar model from Chapter 4. The LL model initially over-predicts the film thickness because the turbulent vapor effects on thinning the film are significant near the inlet. Further along in z, the LL model under-predicts the film thickness because the turbulent effects in the film are more significant than the laminar model can predict. The cross-over point between these two regimes is referred to here as the TTP (Turbulent Transitional Point). This is not a point of transition to turbulent flow, but rather the transition from turbulent-vapor-dominated flow to turbulent-film-dominated flow relative to the LL model. This observation is very similar to the comparison and discussion of Figures 4.17 and 4.18. In Figure 4.17, the maximum deviation is near the inlet because the inlet Reynolds number is high resulting turbulent-vapor-dominated flow. In Figure 4.18, the maximum deviation is at the end of condensation because the temperature difference is high resulting high condensation rate and thus turbulent-film-dominated flow.

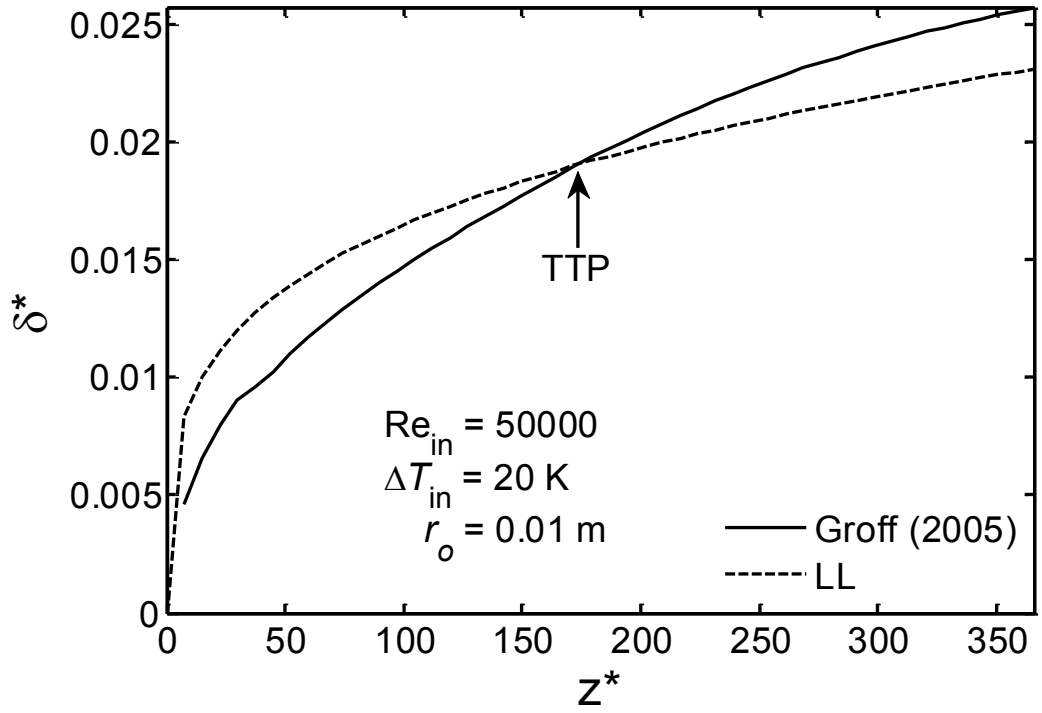

Figure 5.1: Turbulent Transitional Point

It is therefore proposed that the flow could be modeled approximately as follows. For small *z* where the film starts out laminar and the turbulent vapor effects are significant, a TL (Turbulent vapor, Laminar liquid) model could be used. Likewise, for large *z* where vapor effects are diminishing and turbulent film effects are significant, an LT (Laminar vapor, Turbulent liquid) model could be used.

The strategy employed to correlate the turbulent viscosities relates directly to the concept of TL and LT models. To correlate the vapor turbulent viscosity, *B* is written with turbulent properties and *C* is computed from molecular properties; this corresponds to a TL model and should match data asymptotically as *z* approaches zero. To correlate the liquid turbulent viscosity, *C* is written in term of turbulent properties and *B* is computed

with molecular properties; this corresponds to an LT model and should match data asymptotically as *z* becomes large. It is expected that the general model, referred to as TT (Turbulent vapor, Turbulent liquid) will be somewhere between the two asymptotes and that it will use the combination of correlated vapor and liquid turbulent viscosities. The next sections describe the correlation of the vapor and liquid turbulent viscosities.

5.2. Correlation of the Vapor Turbulent Viscosity

Given the turbulent film thickness δ variable with *z* from an experiment or a numerical solution, the value of X at the corresponding *z* is computed by Equation (5.1.5):

$$X = \frac{\delta}{r_o} - \frac{1}{2}\left(\frac{\delta}{r_o}\right)^2 \tag{5.2.1}$$

In order to compute turbulent vapor viscosity, the condensate film flow is assumed to be laminar. Therefore the coefficient *C* is computed by Equation (5.1.7) with molecular liquid viscosity and thermal conductivity:

$$C_{\text{lam}} = \frac{4\mu_L k_L \Delta T z}{g h_{fg} \rho_L (\rho_L - \rho_V) r_o^4} \tag{5.2.2}$$

From Equation (5.1.4), the turbulent coefficient *B* is:

$$B_{TL} = \frac{C_{\text{lam}} - X^4}{X^3} \tag{5.2.3}$$

where TL refers to the assumed turbulent vapor flow and laminar film flow.

Equation (5.1.6) can also be used to compute the turbulent coefficient *B*:

$$B_{TL} = \frac{2\mu_{V,eff}\mu_V \,\mathrm{Re}_{\mathrm{in}}}{g(\rho_L - \rho_V)\rho_V r_o^3} \tag{5.2.4}$$

Therefore:

$$\mu_V^t = \frac{B_{TL} g\rho_V (\rho_L - \rho_V) r_o^3}{2\,\mathrm{Re}_{\mathrm{in}}\,\mu_V} - \mu_V \tag{5.2.5}$$

Note that the vapor turbulent viscosity depends largely on the vapor Reynolds number, has all positive values, has highest value at the entrance, and is zero at the end of condensation. Therefore the vapor turbulent viscosity is correlated as a power function of the axial average vapor Reynolds number, which can be computed from Equation (4.7.4). The proposed correlation is written in dimensionless form as:

$$\frac{\mu_V^t}{\mu_V} = C_V \left(\frac{\mathrm{Re}_V}{\mathrm{Re}_{\mathrm{in}}} \right)^4 \tag{5.2.6}$$

After examining many data sets, it was found that the fourth power in Equation (5.2.6) provides the correct trend. The choice of the power allowed the correlation process to focus on one coefficient, namely C_V. Now consider a plot of the turbulent vapor viscosity for a typical case as presented in Figure 5.2. The values of μ_V^t are computed from the Groff (2005) numerical model results using Equation (5.2.5) with data from Equations (5.2.1), (5.2.2), and (5.2.3). Because the condensate film is assumed to be laminar by Equation (5.2.2), the computed values of vapor turbulent viscosity are less than the actual values. This has the effect of shifting the curve downward as can be seen in Figure 5.2. Note that the computed vapor turbulent viscosity is very high at the tube

entrance, reduces to zero quickly at the TTP, and then has negative values after this point. At the tube entrance, the correlation and the data from numerical solution do not match well, but this is over a small region. At the TTP, the effect of turbulent-vapor-dominated flow is exactly cancelled out by the effect of turbulent-film-dominated flow. Therefore, if the condensate film is assumed to be laminar by Equation (5.2.2), the vapor turbulent viscosity must be zero at the TTP. The negative values after the TTP are also due to holding condensate film laminar. With the choice of correlating function, the negative values are diminished to zero and the curve is shifted up as shown in Figure 5.2.

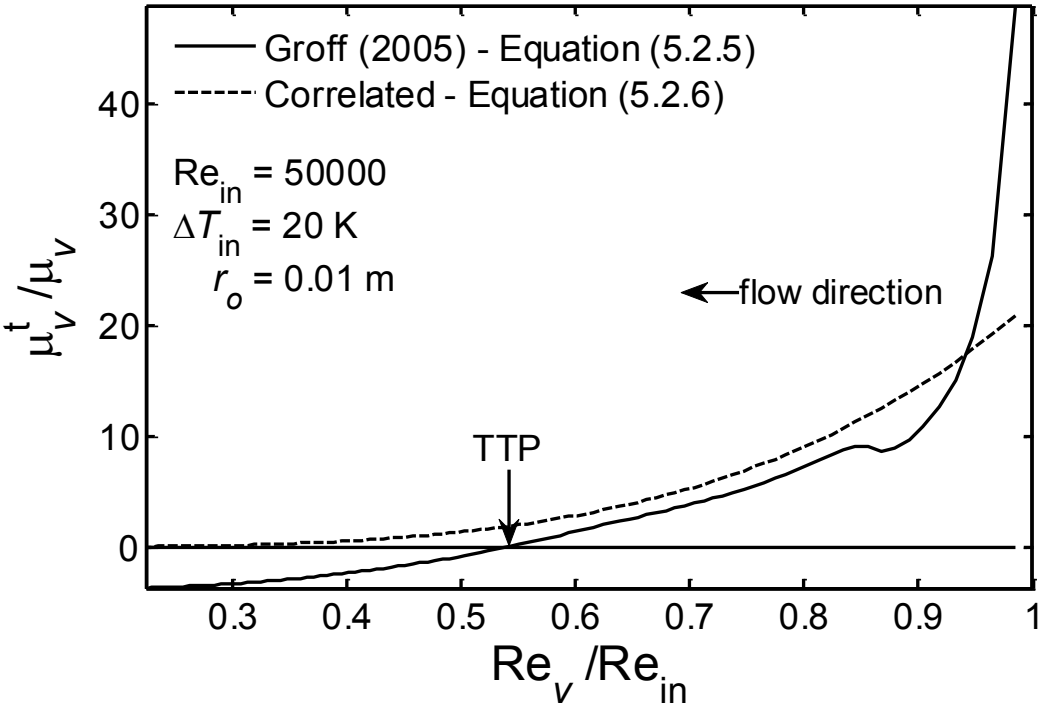

Figure 5.2: Typical vapor turbulent viscosity correlation

A variety of cases were run using the specific parameters given in Table 5.1. The correlation did not include every possible combination of those sets of values. For the

inlet Reynolds number range, the temperature difference and tube radius are fixed at 10 K and 0.01 m, respectively. For the temperature difference range, the inlet Reynolds number and tube radius are fixed at 30000 and 0.01 m, respectively. For the tube radius range, the inlet Reynolds number and temperature difference are fixed at 30000 and 30 K, respectively. Once the correlation was completed, it was tested with all values.

Table 5.1: Ranges of correlation parameters

$\mathrm{Re_{in}}(\times 10^{-3})$	5	10	20	30	50	70	90			
ΔT_{in} [K]	5	10	15	20	30	40				
r_o [m]	0.005	0.01	0.02	0.03	0.04	0.06	0.08	0.1	0.15	0.2
P_{in} [kPa]	50	101	200	400	600	800	1000			

The correlation is kept as simple as possible by using only one coefficient function per parameter except for the inlet Reynolds number. It is proposed as:

$$C_V = C_{P_{in}} \cdot C_{r_o} \cdot C_{\Delta T_{in}} \cdot C_{1,\mathrm{Re}_{in}} + C_{2,\mathrm{Re}_{in}} \tag{5.2.7}$$

In the proposed correlation, $C_{P_{in}}$ is the coefficient function for the inlet saturation pressure, C_{r_o} is the coefficient function for the tube radius, $C_{\Delta T_{in}}$ is the coefficient function for the inlet-to-wall temperature difference, and $C_{1,\mathrm{Re}_{in}}$ and $C_{2,\mathrm{Re}_{in}}$ are the coefficient functions for the inlet Reynolds number. The inlet Reynolds number coefficient is divided to two terms. One term is related to other parameters while the

other term is independent. This is done to ensure that the inlet Reynolds number is the main driving factor of the vapor turbulent viscosity, especially at high inlet Reynolds number. The typical plots of C_V are shown in Figures 5.3 to 5.6 with the resulting coefficient functions, which are simple and easily recognizable as first and second order polynomials.

Figure 5.3 shows that the coefficient function $C_{1,\mathrm{Re}_{in}}$ is zero once the inlet Reynolds number is greater than 90000. This value can be considered as the critical inlet Reynolds number where C_V is equal to $C_{2,\mathrm{Re}_{in}}$ and the vapor turbulent viscosity depends only on the inlet Reynolds number.

As can be seen in Figure 5.5, the critical tube radius is about 0.09 m. After this limit, the dependency on tube radius of C_V coefficient is reducing to limiting value of zero and the configuration can be considered as vertical flat plate.

As can be seen in the term $(1-7\cdot10^{-7}\cdot P_{\mathrm{in}})$ of Figure 5.6, the pressure dependency of vapor turbulent viscosity is found to be insignificant. This is due to two observations. Firstly, the vapor turbulent viscosity may be 20 times larger than the vapor molecular viscosity as shown in Figure 5.2. Secondly, the vapor molecular viscosity depends weakly on the saturation pressure in the range of 50-1000 kPa, about 40% variation in this range, which can be observed in many published data. Therefore, pressure dependency of vapor turbulent viscosity can be ignored.

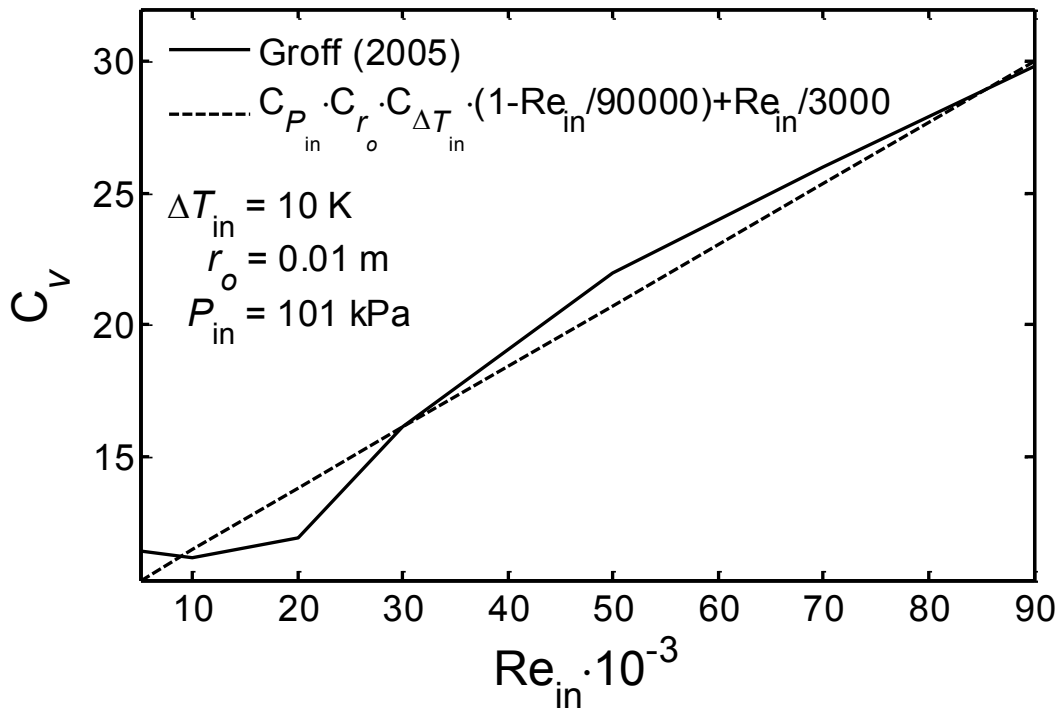

Figure 5.3: C_V versus Re_{in}

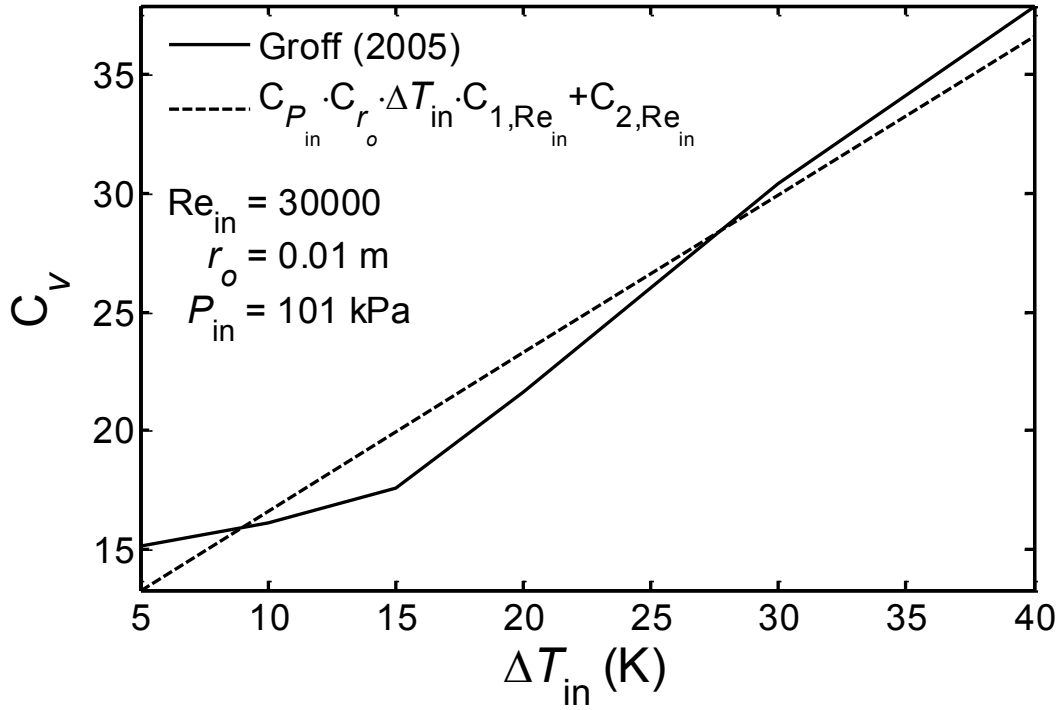

Figure 5.4: C_V versus ΔT_{in}

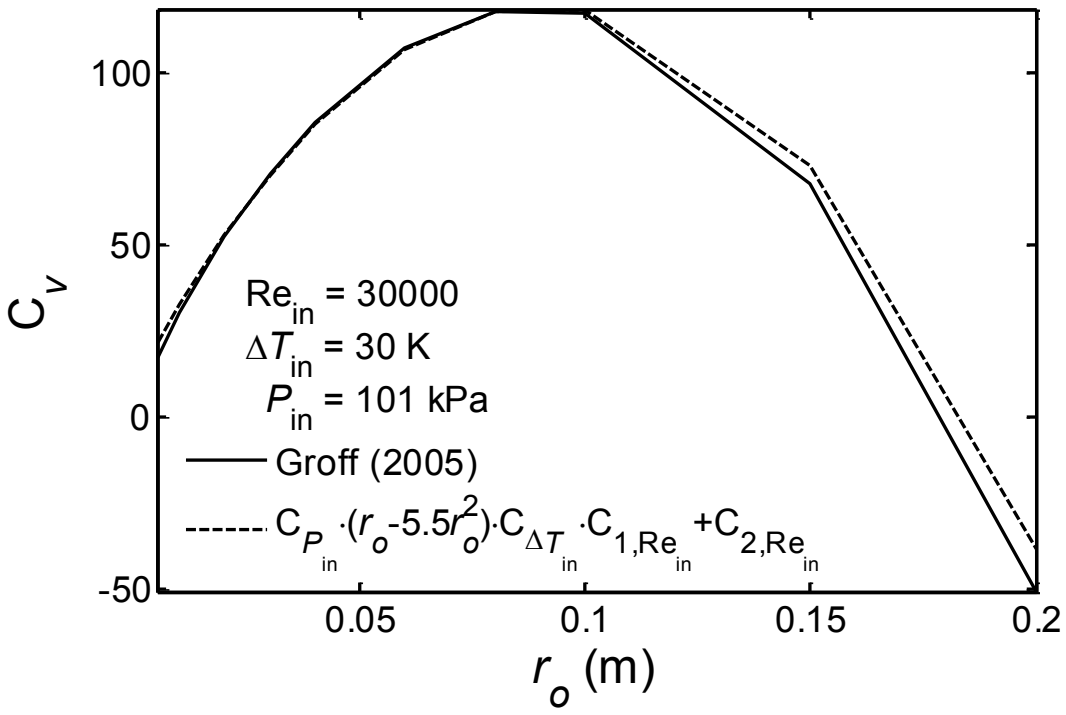

Figure 5.5: C_V versus r_o

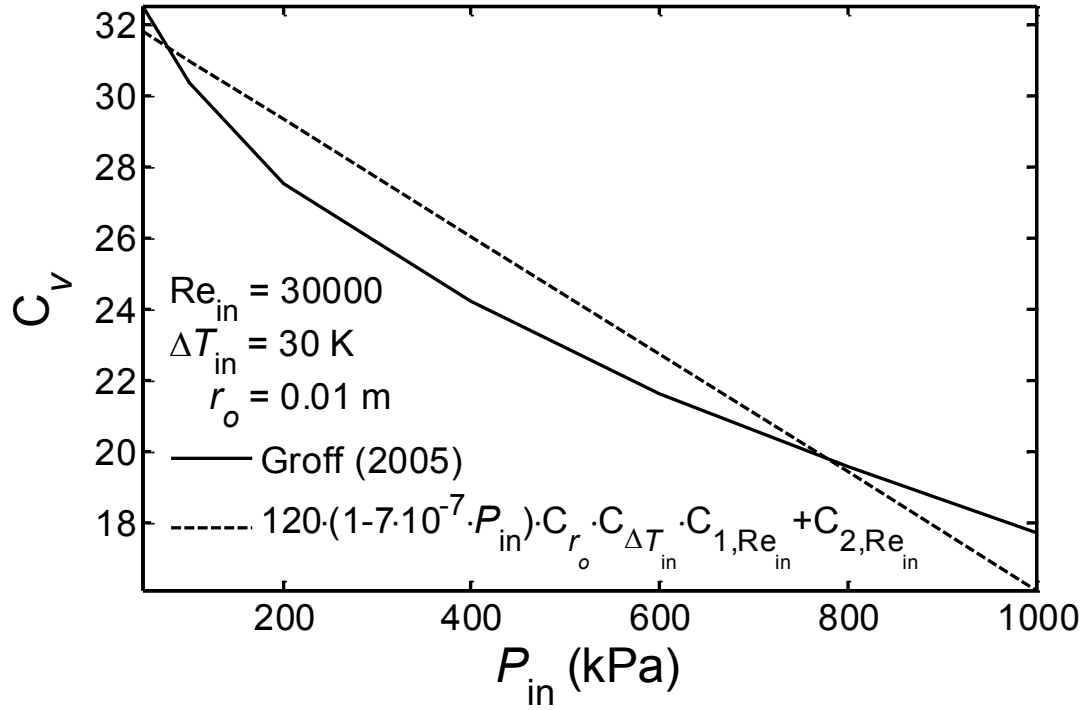

Figure 5.6: C_V versus P_{in}

The final correlation equation for C_V, applicable for the range of parameters in Table 5.1, is:

$$C_V = 120\left(r_o - 5.5r_o^2\right)\left(\Delta T_{in}\right)\left(1 - \frac{\mathrm{Re}_{in}}{90000}\right) + \frac{\mathrm{Re}_{in}}{3000} \tag{5.2.8}$$

Note that once the first term on the RHS of Equation (5.2.8) is zero, then the configuration can be considered as vertical flat plate and the vapor correlation depends only on the inlet Reynolds number. The performance of this correlation will be evaluated in Chapter 7.

5.3. Correlation of the Liquid Turbulent Viscosity

Given the turbulent film thickness δ from an experiment or a numerical solution, X is computed from Equation (5.1.5):

$$X = \frac{\delta}{r_o} - \frac{1}{2}\left(\frac{\delta}{r_o}\right)^2 \tag{5.3.1}$$

Because the vapor flow is assumed to be laminar, B is computed from Equation (5.1.6) with molecular vapor viscosity:

$$B_{\mathrm{lam}} = \frac{2\,\mathrm{Re}_{\mathrm{in}}\,\mu_V\mu_V}{g\rho_V\left(\rho_L - \rho_V\right)r_o^3} \tag{5.3.2}$$

The turbulent coefficient C is computed by the quartic equation:

$$C_{LT} = X^4 + B_{\mathrm{lam}}X^3 \tag{5.3.3}$$

where LT referred to the assumed laminar vapor flow and turbulent liquid flow.

Equation (5.1.7) can also be used to compute coefficient *C*:

$$C_{LT} = \frac{4\mu_{L,eff} k_{L,eff} \Delta Tz}{g h_{fg} \rho_L (\rho_L - \rho_V) r_o^4} \tag{5.3.4}$$

In order to isolate μ_L^t, the following expansion is made:

$$\mu_{L,eff} k_{L,eff} = (\mu_L + \mu_L^t)(k_L + \mu_L^t C_{PL}) = C_{PL}(\mu_L^t)^2 + (\mu_L C_{PL} + k_L)\mu_L^t + \mu_L k_L \tag{5.3.5}$$

From Equations (5.3.4) and (5.3.5), the liquid turbulent viscosity is the solution of equation:

$$C_{PL}(\mu_L^t)^2 + (\mu_L C_{PL} + k_L)\mu_L^t + \mu_L k_L - \frac{C_{LT} g h_{fg} \rho_L (\rho_L - \rho_V) r_o^4}{4\Delta Tz} = 0 \tag{5.3.6}$$

Consider a plot of the turbulent liquid viscosity from the above computation for a typical case in Figure 5.7. The turbulent liquid viscosity is computed by Equation (5.3.6) with data from Groff (2005) numerical solution using Equations (5.3.1), (5.3.2), and (5.3.3). Because the vapor flow is assumed to be laminar in Equation (5.3.2), the values of computed turbulent liquid viscosity are less than the actual values. This has the effect of shifting the curve downward as can be seen in Figure 5.7. Near the inlet, the shifting is more significant because the vapor flow is stronger. The shifting is diminishing along the tube to zero-shifting at the end of condensation. Note that the computed liquid turbulent viscosity is negative at the beginning to compensate for the holding of the laminar vapor, zero at the TTP, and then growing after that. The choice of a linear function effectively eliminates the negative values and shifts the curve upward without violating the zero-

shifting at the end of condensation. Therefore, the liquid turbulent viscosity is correlated as a linear function of the axial average laminar liquid Reynolds number Re_L, which is computed by Equation (4.7.5):

$$\frac{\mu_L^t}{\mu_L} = C_L \,\mathrm{Re}_L \tag{5.3.7}$$

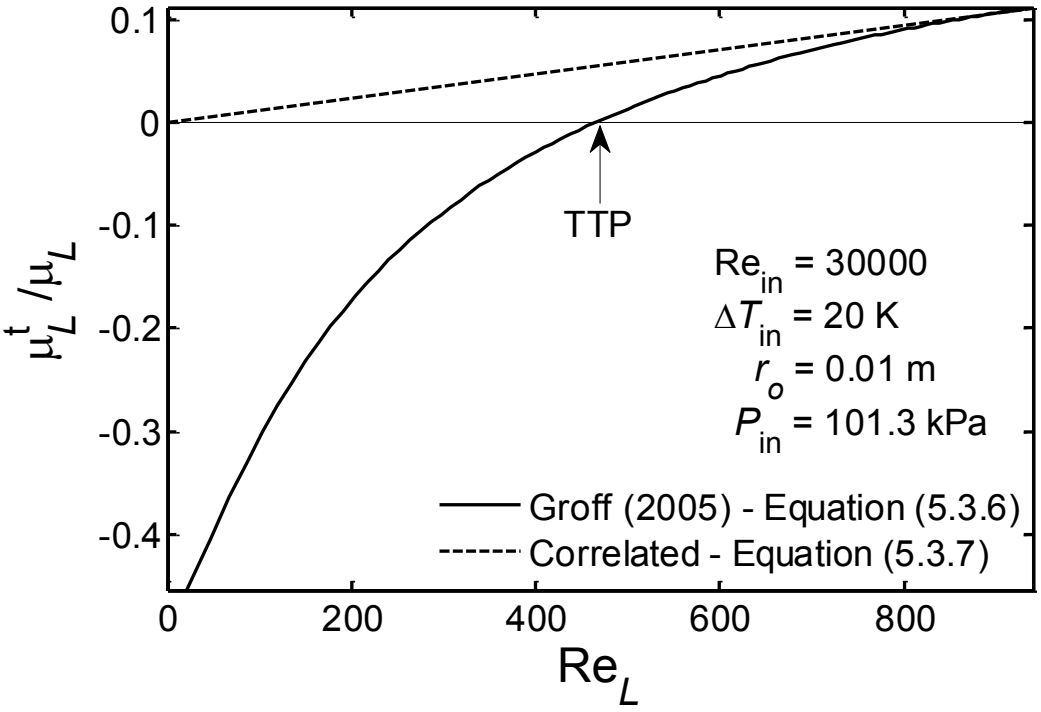

Figure 5.7: Typical liquid turbulent viscosity correlation

The correlating task is now finding the composition of the coefficient C_L using the same parameters in Table 5.1 in a similar method to that used to correlate the vapor turbulent viscosity. The correlation is again kept simple by using one coefficient function per parameter. The proposed correlation for C_L is:

$$C_L = C_{P_{in}} \cdot C_{r_o} \cdot C_{\Delta T_{in}} \cdot C_{\mathrm{Re}_{in}} \tag{5.3.8}$$

In the proposed correlation, $C_{P_{in}}$ is the coefficient function for the inlet saturation pressure, C_{r_o} is the coefficient function for the tube radius, $C_{\Delta T_{in}}$ is the coefficient function for the inlet-to-wall temperature difference, and $C_{\mathrm{Re}_{in}}$ is the coefficient function for the inlet Reynolds number. The typical plots of these correlations are shown in Figures 5.8 to 5.11 with the resulting coefficients for correlating parameters. All coefficient functions are simple, commonly recognizable, and thus easily formed.

Figure 5.8 shows that the liquid turbulent viscosity is inversely proportional to the inlet Reynolds number. The square root function is simply chosen and is sufficient to capture the trend. A constant of 2300 is tested and added to avoid singularity at the zero inlet Reynolds number. As can be seen in Figure 5.9, the liquid turbulent viscosity is linearly proportional to the temperature difference. The dependency of C_L on tube radius is diminishing at about 0.1 m, as can be seen in Figure 5.10, indicates that a vertical flat plate approximation is approached for $r_o > 0.1\,\mathrm{m}$. Figure 5.11 shows that the trend of the inlet saturation pressure coefficient function is similar to that of the inlet Reynolds number and thus a simple square root function is chosen.

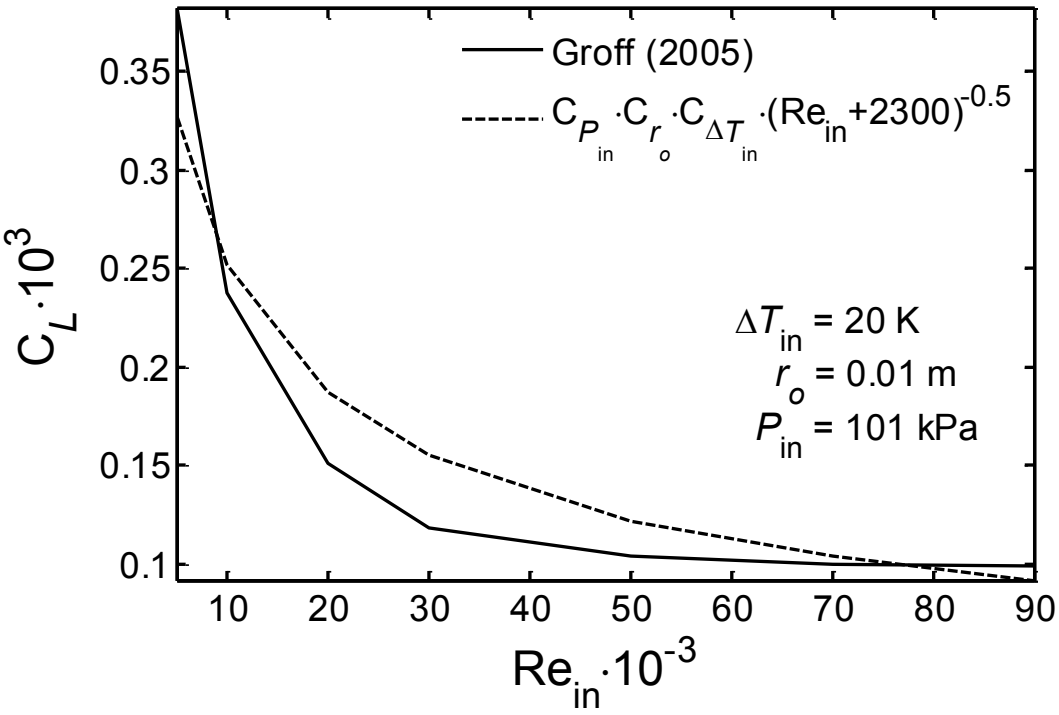

Figure 5.8: C_L versus Re_{in}

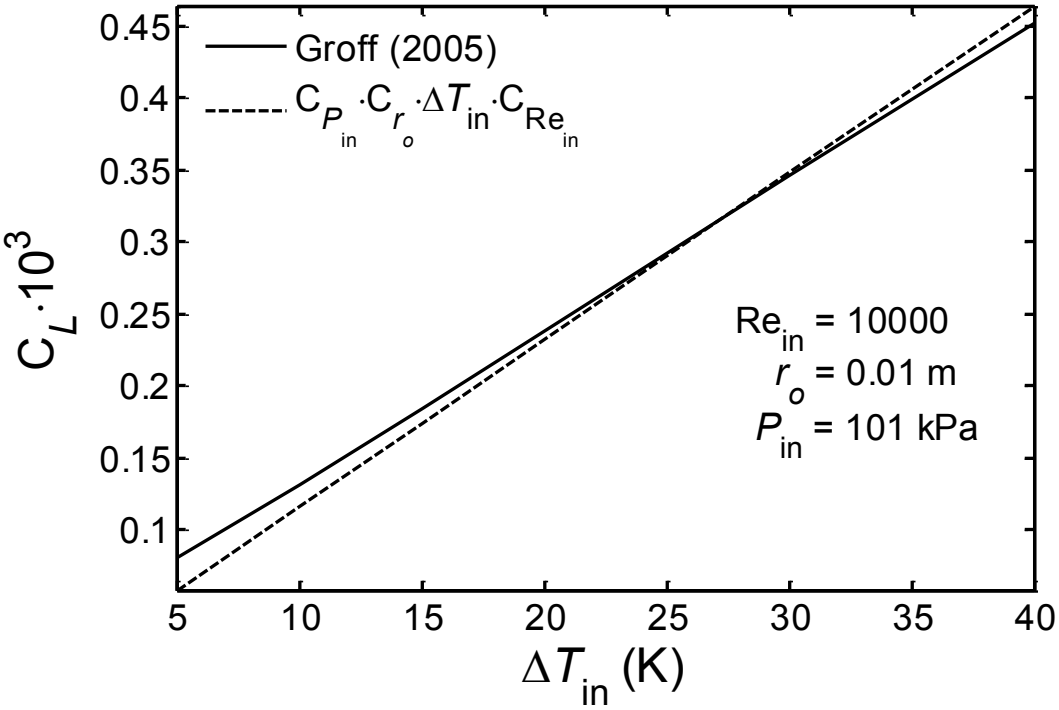

Figure 5.9: C_L versus ΔT_{in}

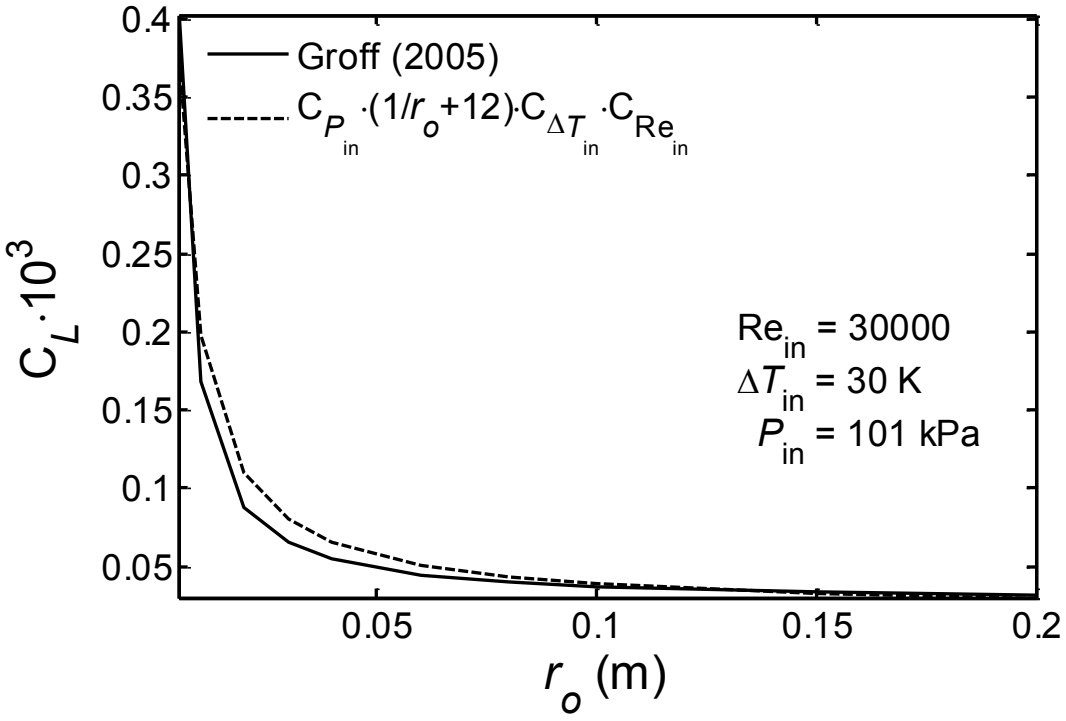

Figure 5.10: C_L versus r_o

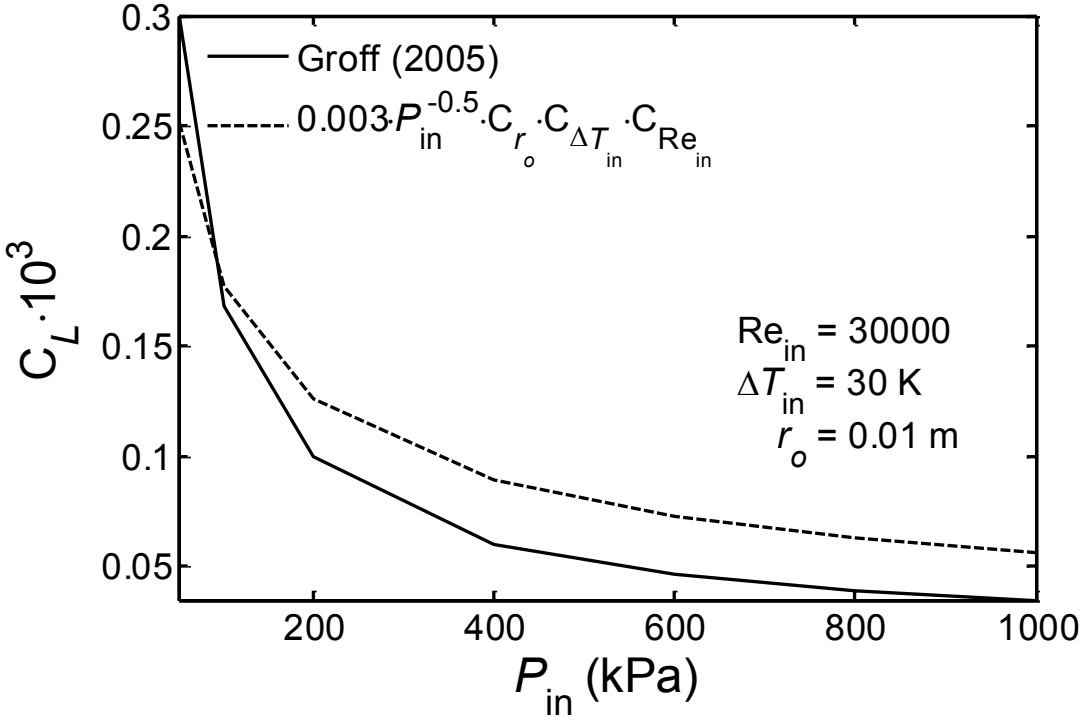

Figure 5.11: C_L versus P_{in}

Combining the coefficient functions from Figures 5.8 to 5.11, the final correlation equation for C_L, applicable in the ranges of parameters in Table 5.1, is:

$$C_L = 0.003\left(\frac{1}{\sqrt{P_{\text{in}}}}\right)\left(\frac{1}{r_o}+12\right)\left(\Delta T_{\text{in}}\right)\left(\frac{1}{\sqrt{\text{Re}_{\text{in}}+2300}}\right) \tag{5.3.9}$$

Note that the present correlation equations do not account for transitions to turbulent at $\text{Re}_V = 2300$ and $\text{Re}_L = 30$. As can be seen from Figures 5.12 and 5.13, the values of turbulent viscosities are very small at these values. Therefore, they can be ignored to maintain the simplicity of the correlations.

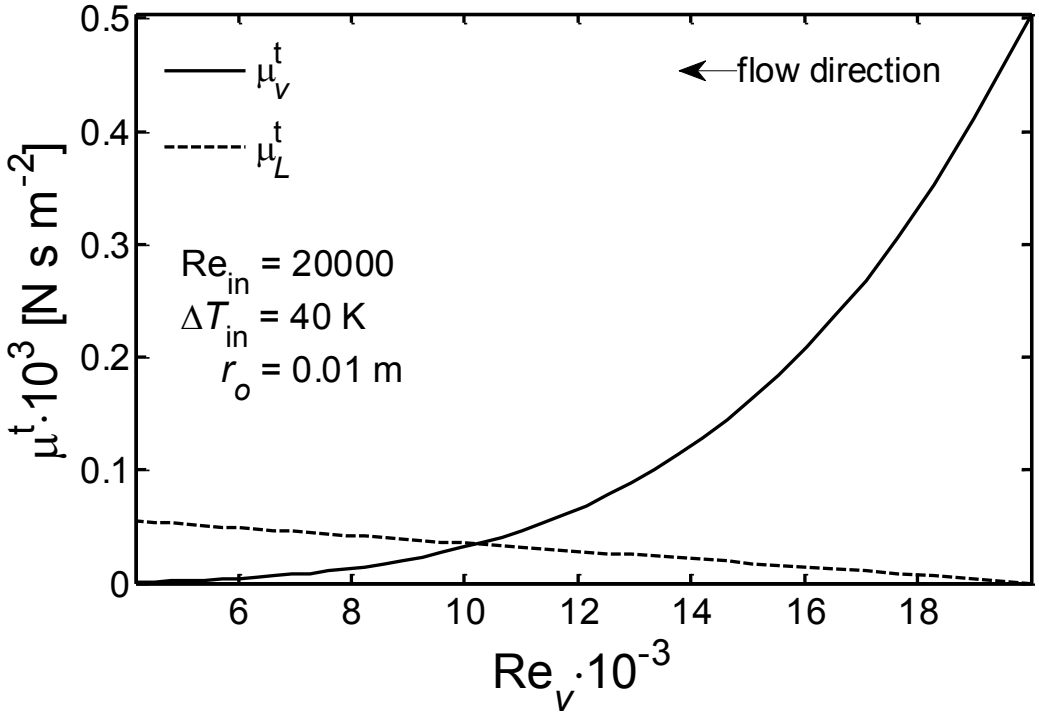

Figure 5.12: Typical turbulent viscosities versus vapor axial average Reynolds number

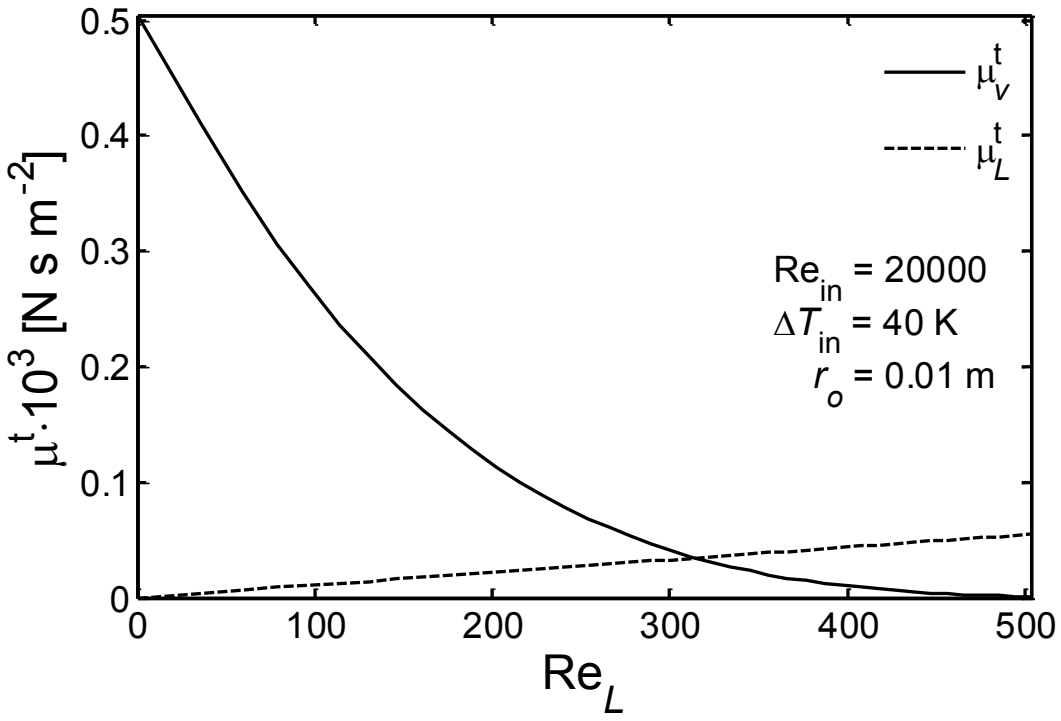

Figure 5.13: Typical turbulent viscosities versus liquid axial average Reynolds number

CHAPTER 6

SUMMARY OF THE SOLUTION PROCEDURE

This chapter presents the solution procedure to compute the condensate film thickness and other quantities for laminar and turbulent flows. The solution procedure is based on the closed-form solution of the quartic equation and recommended for tube radius larger than 0.005 m. For smaller tube radius, the film thickness should be computed from the root search of Equation (4.5.33).

6.1. Inputs to the Procedure

Input parameters to the solution procedure are:

Tube radius: r_o

Inlet Reynolds number: $\mathrm{Re}_{\mathrm{in}}$

Inlet saturation temperature or pressure: T_{in} or P_{in}

Wall temperature: T_{wall}

Axial location: z

If the wall temperature is constant, the inlet-to-wall temperature difference is:

$$\Delta T_{\mathrm{in}} = T_{\mathrm{in}} - T_{\mathrm{wall}} \tag{6.1.1}$$

If the wall temperature is not constant, the inlet-to-wall temperature differences at each known location are computed and curve fitted by a polynomial as:

$$\Delta T(z) = a_0 + a_1 z + a_2 z^2 + \cdots = \sum_{i=0}^{n} a_i z^i \tag{6.1.2}$$

The value of ΔT at a given z location is computed by the polynomial. The film temperature is then computed by:

$$T_{film} = T_{wall} + 0.31\Delta T \tag{6.1.3}$$

Vapor properties μ_V and ρ_V are computed at T_{in}.

Liquid properties μ_L, ρ_L, k_L, and C_{PL} are computed at T_{film}.

6.2. Laminar Flow Solution Procedure

Step 1: Compute the coefficients of the laminar quartic equation

Vapor mixed-convection coefficient:

$$B = \frac{2\mu_V \mu_V \,\mathrm{Re}_{in}}{g(\rho_L - \rho_V)\rho_V r_o^3} \tag{6.2.1}$$

If the wall temperature is constant, the liquid condensation coefficient is:

$$C = \frac{4\mu_L k_L \Delta T\, z}{r_o^4 h_{fg} g \rho_L (\rho_L - \rho_V)} \tag{6.2.2}$$

If the wall temperature is variable, the liquid condensation coefficient is:

$$C = \frac{4\mu_L k_L}{r_o^4 h_{fg} g \rho_L (\rho_L - \rho_V)} \sum_{i=0}^{n} a_i \frac{z^{i+1}}{i+1} \tag{6.2.3}$$

Step 2: Solve the quartic equation and the condensate film thickness

Solution of the intermediate cubic equation:

$$y_1 = \sqrt[3]{C\left(\sqrt{\left(\frac{64}{27}C+\frac{1}{4}B^4\right)}-\frac{1}{2}B^2\right)} - \sqrt[3]{C\left(\sqrt{\left(\frac{64}{27}C+\frac{1}{4}B^4\right)}+\frac{1}{2}B^2\right)} \tag{6.2.4}$$

Solution of the quartic equation:

$$X = -\frac{1}{4}\left(B+\sqrt{B^2+4y_1}\right)+\frac{1}{2}\sqrt{\frac{1}{2}B^2+\frac{1}{2}B\sqrt{B^2+4y_1}-y_1+2\sqrt{y_1^2+4C}} \tag{6.2.5}$$

Dimensionless film thickness variable:

$$\delta_+ = 1-2X \tag{6.2.6}$$

Condensate film thickness:

$$\delta = r_o\left(1-\sqrt{\delta_+}\right) \tag{6.2.7}$$

Step 3: Compute other quantities of interest

Depending on the requirement and the dependency of expressions, these quantities can be computed individually or combined together.

Local heat transfer coefficient:

$$h = -\frac{2k_L}{r_o \ln \delta_+} \tag{6.2.8}$$

Local Nusselt number:

$$\mathrm{Nu} = -\frac{4}{\ln \delta_+} \tag{6.2.9}$$

Coefficients of the density function:

$$\alpha = \frac{\rho_V}{\rho_L} \tag{6.2.10}$$

$$\beta = \frac{\rho_V \mu_L}{\rho_L \mu_V} \tag{6.2.11}$$

$$M = \frac{2\mu_L \mu_V \,\mathrm{Re}_{in}}{g\rho_L(\rho_L - \rho_V) r_o^3} \tag{6.2.12}$$

Density function:

$$\rho_+ = -(\rho_L - \rho_V)\left[\frac{2M - 1 + 2(2-\alpha)\delta_+ + (2\alpha - 3)\delta_+^2 + 2(1-\alpha)\delta_+^2 \ln \delta_+}{1 + 2(\alpha - 1)\delta_+ + (1 + \beta - 2\alpha)\delta_+^2}\right] \tag{6.2.13}$$

Liquid mass flow rate:

$$\dot{m}_L = -\frac{\pi\rho_L\rho_+ g}{8\mu_L} r_o^4 (1-\delta_+)^2 + \frac{\pi\rho_L g(\rho_L - \rho_V)}{8\mu_L} r_o^4 (1 - 4\delta_+ + 3\delta_+^2 - 2\delta_+^2 \ln \delta_+) \tag{6.2.14}$$

Vapor mass flow rate:

$$\dot{m}_V = -\frac{\rho_+ \pi g \rho_V}{8} r_o^4 \left[\frac{\delta_+^2}{\mu_V} + \frac{2\delta_+(1-\delta_+)}{\mu_L}\right] + \frac{\pi\rho_V g(\rho_L - \rho_V)}{4\mu_L} r_o^4 \left[\delta_+(1-\delta_+) + \delta_+^2 \ln \delta_+\right] \tag{6.2.15}$$

Vapor Reynolds number:

$$\mathrm{Re}_V = \frac{2\dot{m}_V}{\pi\mu_V(r_o - \delta)} \tag{6.2.16}$$

Liquid Reynolds number:

$$\mathrm{Re}_L = \frac{2\dot{m}_L}{\pi\mu_L(r_o - \delta)} \tag{6.2.17}$$

Pressure gradient:

$$\frac{dP}{dz} = (\rho_V + \rho_+)g \tag{6.2.18}$$

Interfacial shear stress:

$$\tau_i = -\frac{\rho_+ g(r_o - \delta)}{2} \tag{6.2.19}$$

Interfacial velocity:

$$u_i = -\frac{\rho_+ g\delta(2r_o - \delta)}{4\mu_L} + \frac{g(\rho_L - \rho_V)}{4\mu_L}\left[\delta(2r_o - \delta) + 2(r_o - \delta)^2 \ln\left(\frac{r_o - \delta}{r_o}\right)\right] \tag{6.2.20}$$

Liquid velocity profile:

$$u_L = -\frac{\rho_+ g}{4\mu_L}(r_o^2 - r^2) + \frac{g(\rho_L - \rho_V)}{4\mu_L}\left[(r_o^2 - r^2) + 2(r_o - \delta)^2 \ln\left(\frac{r}{r_o}\right)\right] \tag{6.2.21}$$

Vapor velocity profile:

$$u_V = -\frac{\rho_+ g}{4\mu_V}\left((r_o - \delta)^2 - r^2\right) + u_i \tag{6.2.22}$$

6.3. Turbulent Flow Solution Procedure

Step 4: Compute effective viscosities and thermal conductivity

Vapor turbulent viscosity coefficient:

$$C_V = 120\left(r_o - 5.5r_o^2\right)\left(\Delta T_{in}\right)\left(1 - \frac{\mathrm{Re}_{in}}{90000}\right) + \frac{\mathrm{Re}_{in}}{3000} \tag{6.3.1}$$

Vapor turbulent viscosity:

$$\mu_V^t = \mu_V C_V \left(\frac{\mathrm{Re}_V}{\mathrm{Re}_{in}}\right)^4 \tag{6.3.2}$$

where Re_V is computed by Equation (6.2.16).

Vapor effective viscosity:

$$\mu_{V,eff} = \mu_V + \mu_V^t \tag{6.3.3}$$

Liquid turbulent viscosity coefficient:

$$C_L = 0.003\left(\frac{1}{\sqrt{P_{in}}}\right)\left(\frac{1}{r_o} + 12\right)\left(\Delta T_{in}\right)\left(\frac{1}{\sqrt{\mathrm{Re}_{in} + 2300}}\right) \tag{6.3.4}$$

Liquid turbulent viscosity:

$$\mu_L^t = \mu_L C_L \,\mathrm{Re}_L \tag{6.3.5}$$

where Re_L is computed by Equation (6.2.17).

Liquid effective viscosity:

$$\mu_{L,eff} = \mu_L + \mu_L^t \tag{6.3.6}$$

Liquid effective thermal conductivity:

$$k_{L,eff} = k_L + \mu_L^t C_{PL} \tag{6.3.7}$$

Step 5: Compute the coefficients of the turbulent quartic equation

Turbulent vapor mixed-convection coefficient:

$$B = \frac{2\mu_{V,eff}\mu_V \,\mathrm{Re}_{in}}{g(\rho_L - \rho_V)\rho_V r_o^3} \tag{6.3.8}$$

If the wall temperature is constant, the turbulent liquid condensation coefficient is:

$$C = \frac{4\mu_{L,eff}k_{L,eff}\Delta T\, z}{r_o^4 h_{fg} g\rho_L(\rho_L - \rho_V)} \tag{6.3.9}$$

If the wall temperature is variable, the turbulent liquid condensation coefficient is:

$$C = \frac{4\mu_{L,eff}k_{L,eff}}{r_o^4 h_{fg} g\rho_L(\rho_L - \rho_V)} \sum_{i=0}^{n} a_i \frac{z^{i+1}}{i+1} \tag{6.3.10}$$

Step 6: Repeat Step 2 to determine the turbulent film thickness using the new values of B and C.

Step 7: Repeat Step 3 to determine the updated values of the quantities of interest.

Note that all new quantities are turbulent and should be computed using effective vapor and liquid viscosities.

CHAPTER 7

COMPARISON WITH TURBULENT DATA

7.1. Comparison with Groff (2005)

Because the correlations for the turbulent viscosities are derived from numerical solution of Groff (2005), any computation using them is expected to compare well with the numerical solution. The purpose of this section is to present a comparison that demonstrates the performance of the correlations. The input parameters for Figures 7.1 to 7.12 are within the range of data in Table 5.1. The RMS deviation for film thickness between the numerical solution and the closed-form turbulent solution TT (Turbulent vapor, Turbulent liquid) is shown with the input parameters on the graphs.

Figures 7.1 to 7.7 use increasing inlet Reynolds number and inlet-to-wall temperature difference. The RMS deviation in all of these comparisons is less than 4% for film thickness. The location of maximum deviation is usually near the inlet or at the end of condensation with no particular trend because the effects of all input parameters are blended together in the turbulent viscosity correlations. Figures 7.8 and 7.9 use a smaller radius of 0.005 m, combined with low and high inlet saturation pressure of 101 kPa and 400 kPa, respectively. The higher deviations of 9.3% and 5.1% in these comparisons are consistent with the ρ_{+1} approximation which is not accurate for small radius as can be seen in Figure 4.4. Figure 7.10 uses a larger tube radius of 0.03 m with an expected smaller deviation of 0.96% due to the higher accuracy of ρ_{+1} associated with larger tube

radius. Figure 7.11 and Figure 7.12 use higher saturation pressures with acceptable deviations of 2.5% and 1.7%, respectively.

These comparisons satisfactorily demonstrate the accuracy of the closed-form solution and the performance of the turbulent viscosity correlations. They also confirm that the TL model and the LT model form lower and upper bounds on the film thickness value; the TT model is in between these bounds. The spacing of the bounds is proportional to the inlet Reynolds number and the temperature difference. The spacing of the bounds is inversely proportional to the tube radius and the inlet saturation pressure.

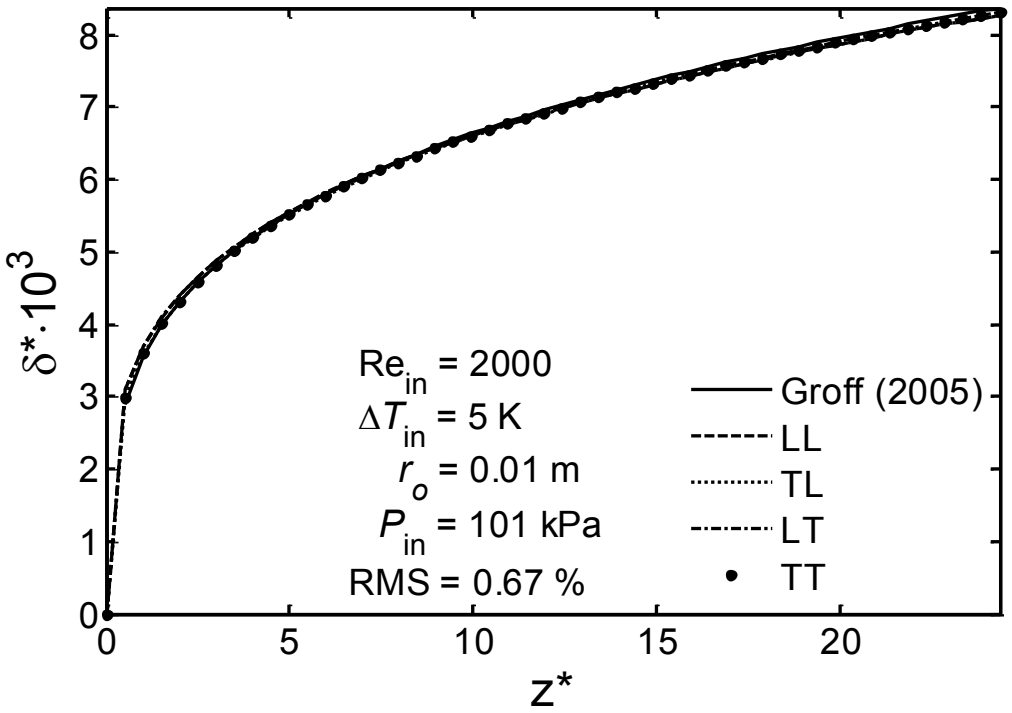

Figure 7.1: Comparison with code (Re_{in} = 2000, ΔT_{in} = 5 K, r_o = 0.01 m, P_{in} = 101 kPa)

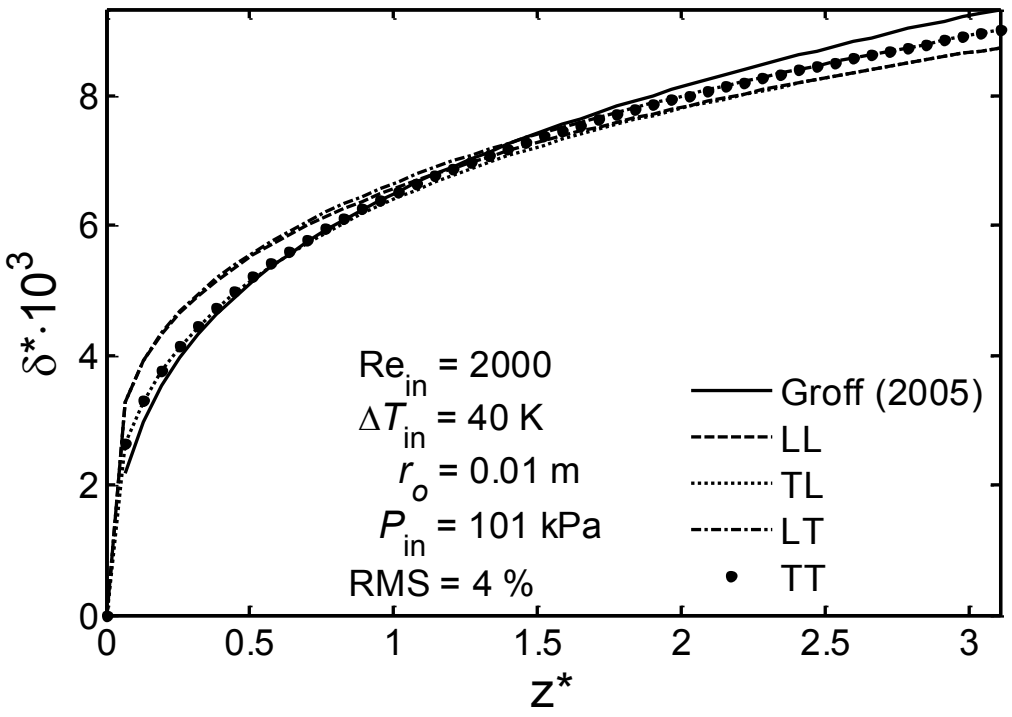

Figure 7.2: Comparison with code (Re_{in} = 2000, ΔT_{in} = 40 K, r_o = 0.01 m, P_{in} = 101 kPa)

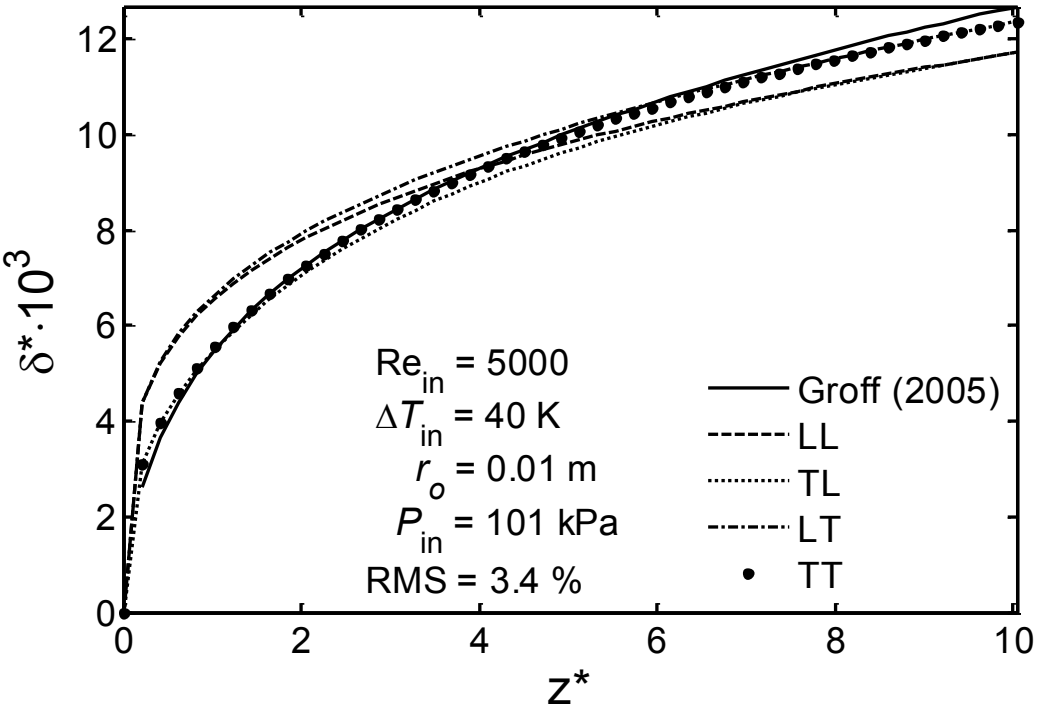

Figure 7.3: Comparison with code (Re_{in} = 5000, ΔT_{in} = 40 K, r_o = 0.01 m, P_{in} = 101 kPa)

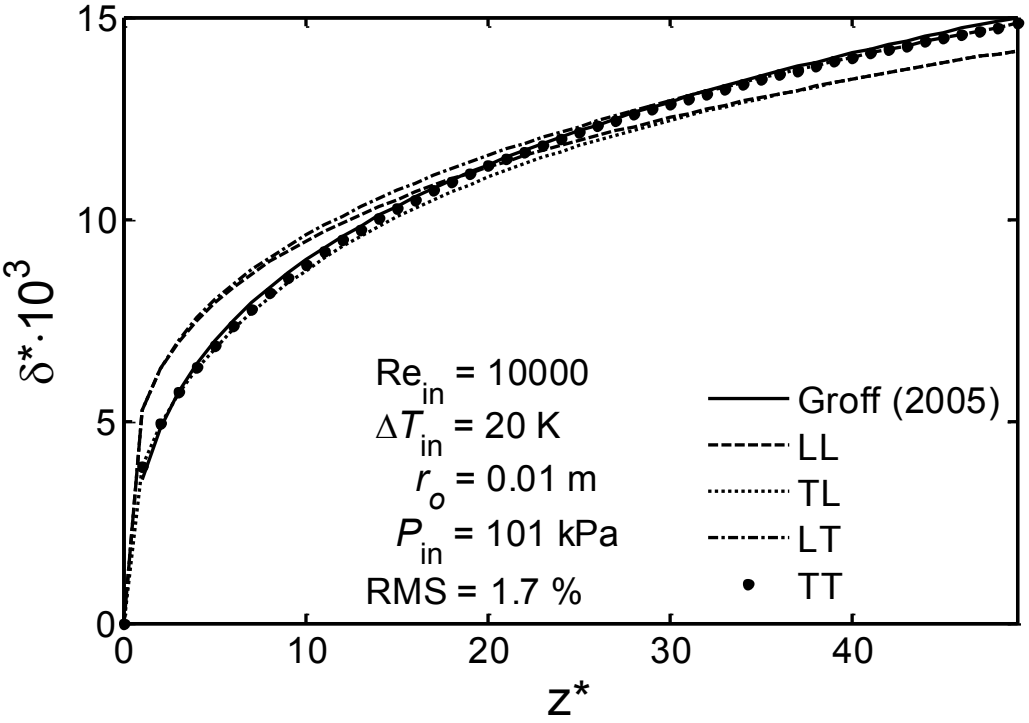

Figure 7.4: Comparison with code (Re_{in}= 10000, ΔT_{in}= 20 K, r_o = 0.01 m, P_{in} = 101 kPa)

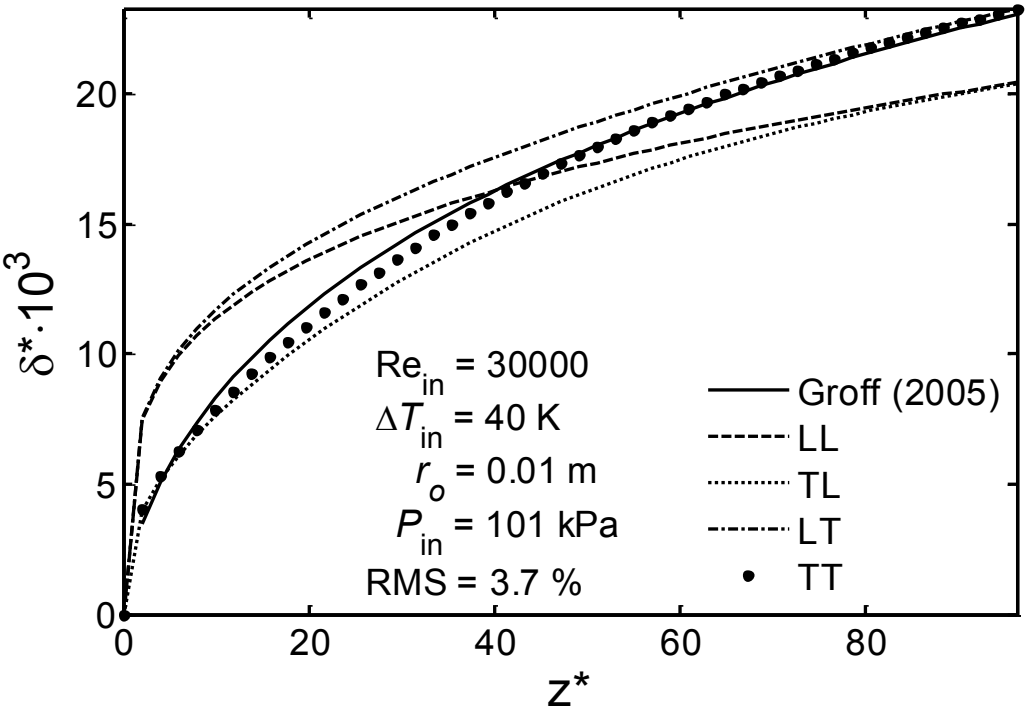

Figure 7.5: Comparison with code (Re_{in} = 30000, ΔT_{in}= 40 K, r_o = 0.01 m, P_{in}= 101 kPa)

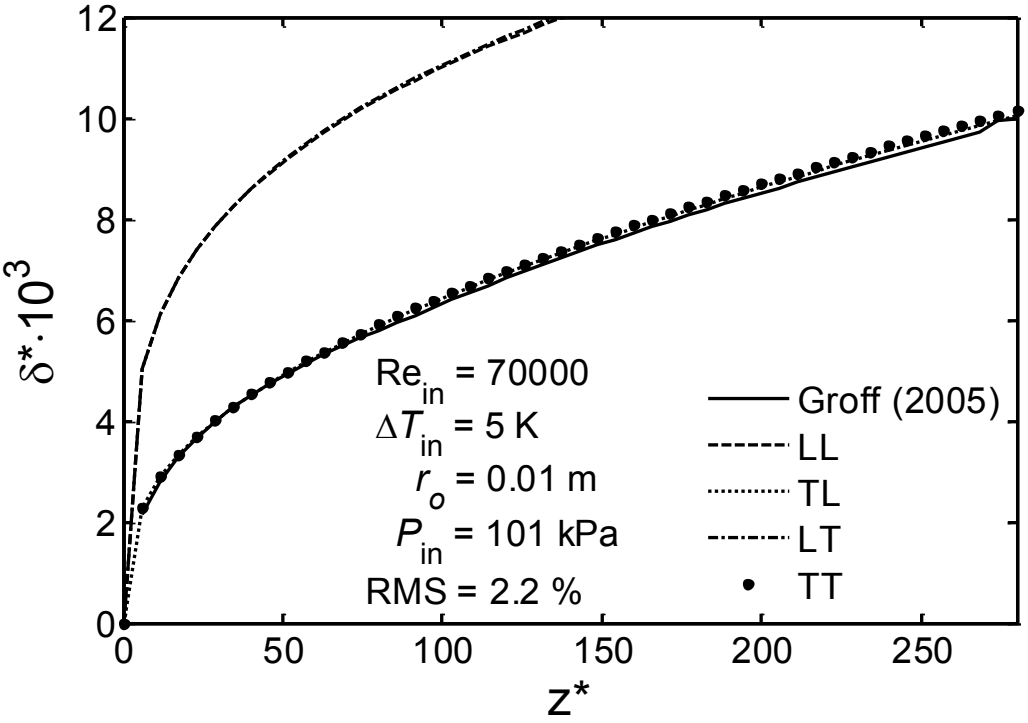

Figure 7.6: Comparison with code (Re_{in} = 70000, ΔT_{in} = 5 K, r_o = 0.01 m, P_{in}= 101 kPa)

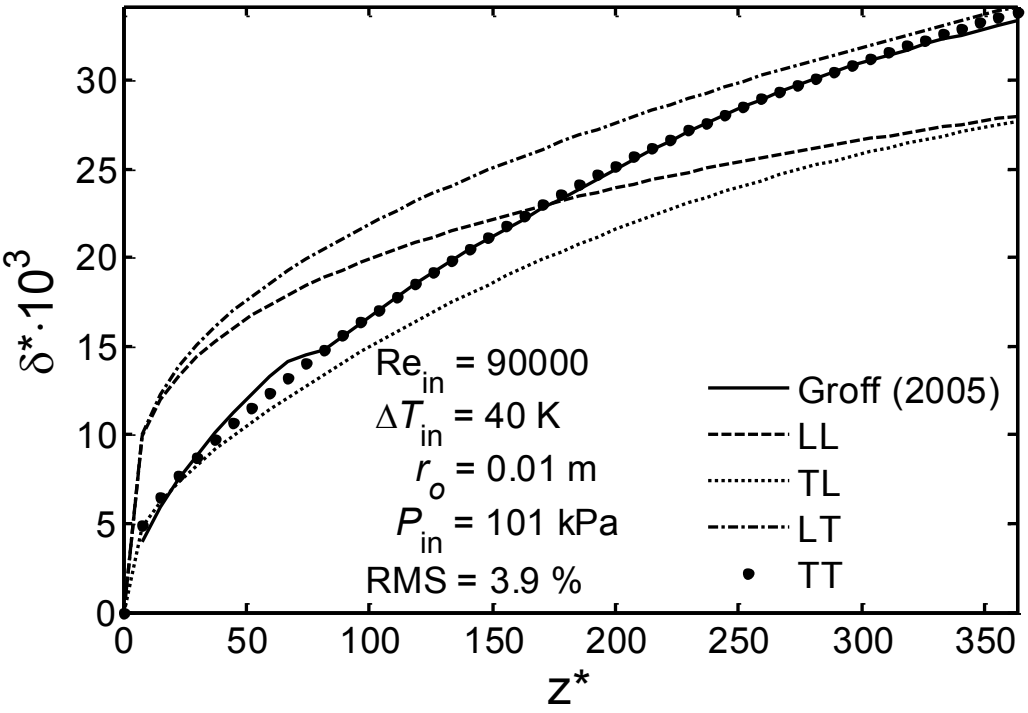

Figure 7.7: Comparison with code (Re_{in} = 90000, ΔT_{in}= 40 K, r_o = 0.01 m, P_{in}= 101 kPa)

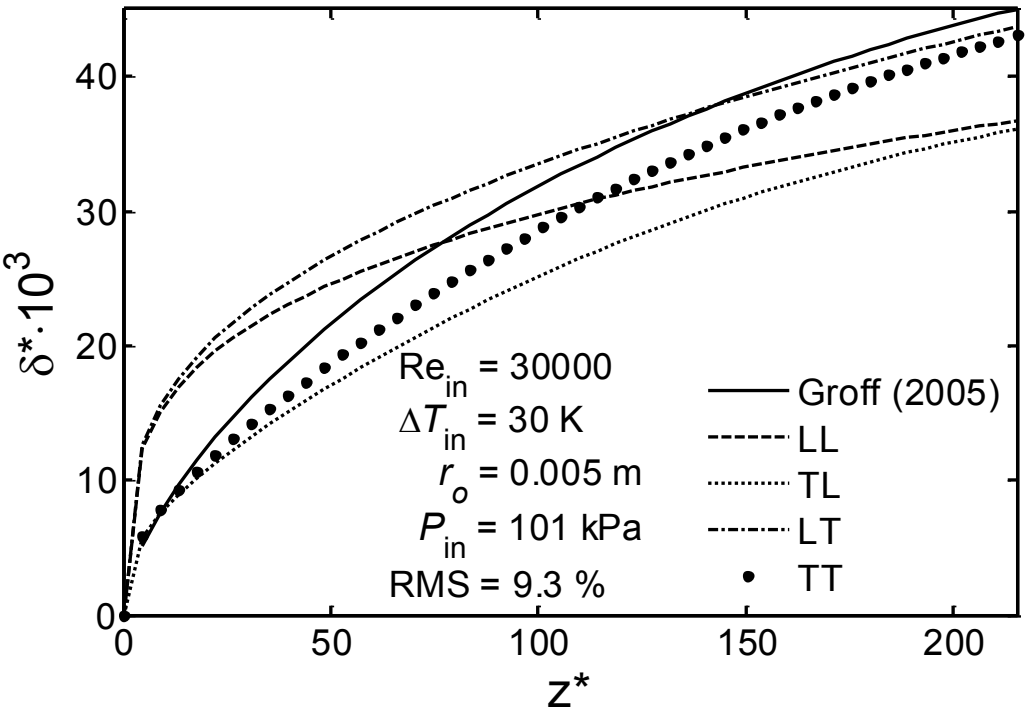

Figure 7.8: Comparison with code (Re_{in}= 30000, ΔT_{in}= 30 K, r_o= 0.005 m, P_{in}=101 kPa)

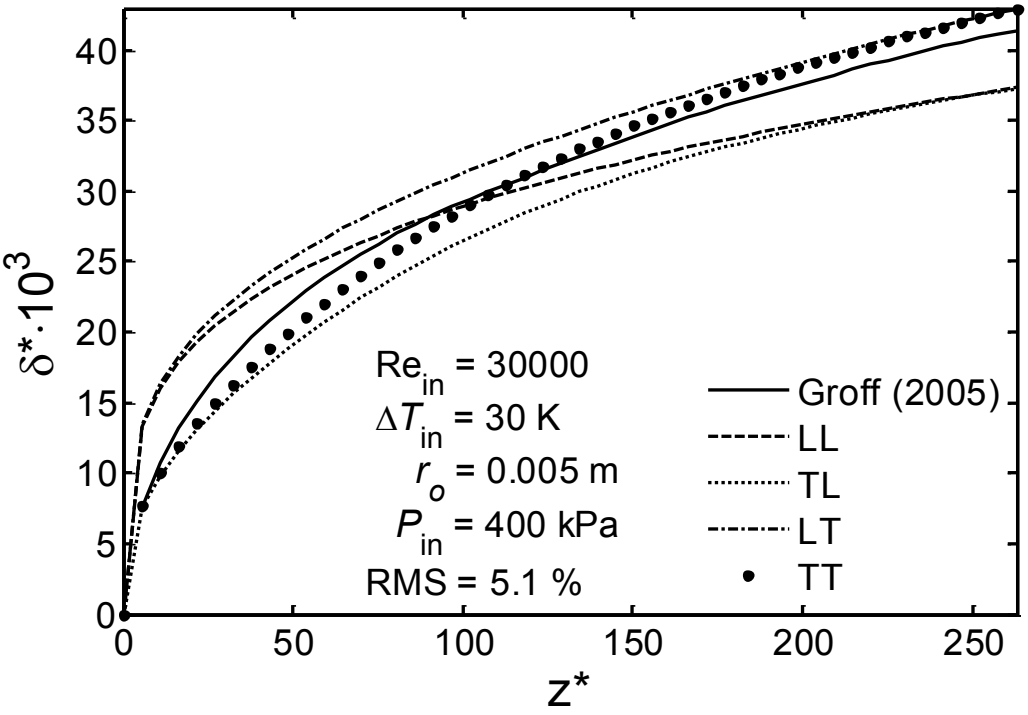

Figure 7.9: Comparison with code (Re_{in}= 30000, ΔT_{in}= 30 K, r_o= 0.005 m, P_{in}=400 kPa)

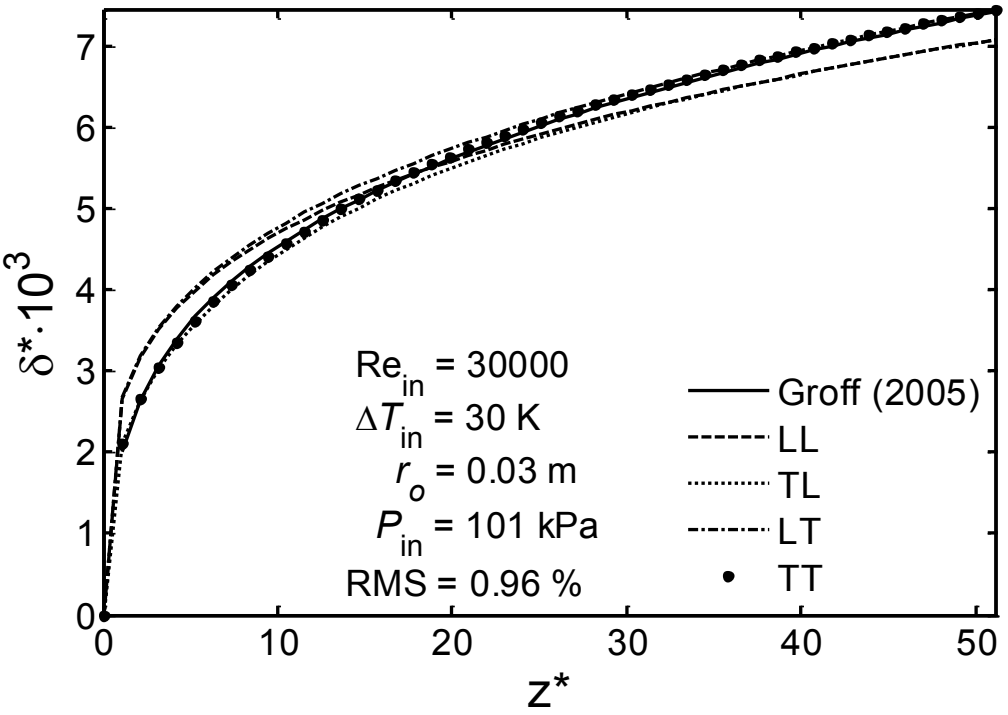

Figure 7.10: Comparison with code (Re_{in} = 30000, ΔT_{in}= 30 K, r_o = 0.03 m, P_{in} =101 kPa)

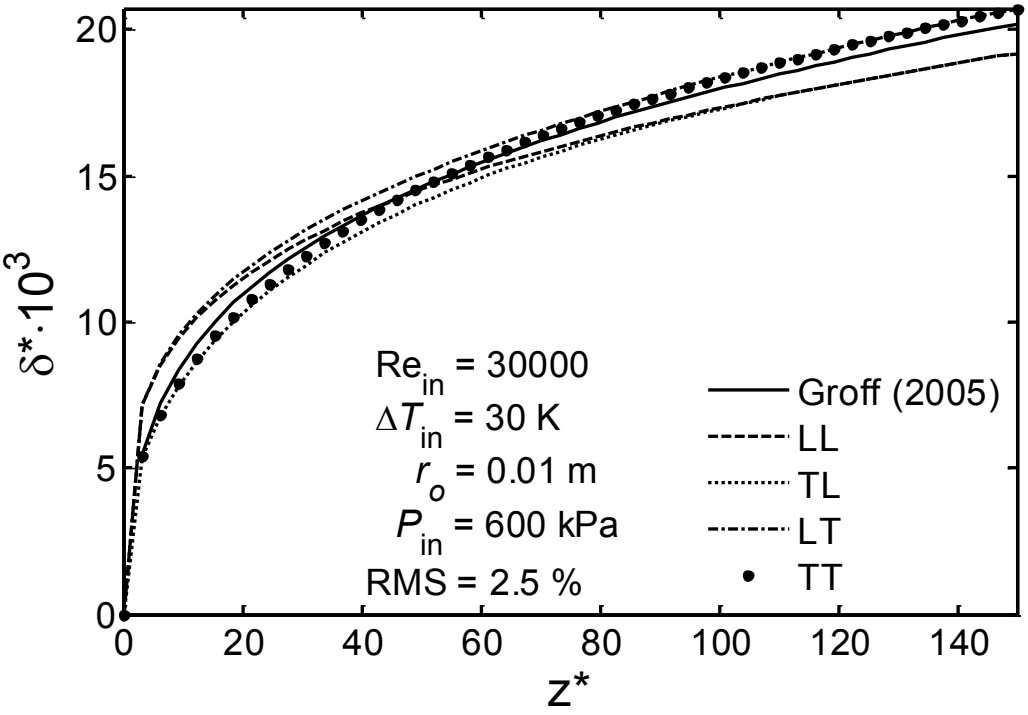

Figure 7.11: Comparison with code (Re_{in} = 30000, ΔT_{in}= 30 K, r_o = 0.01 m, P_{in}= 600 kPa)

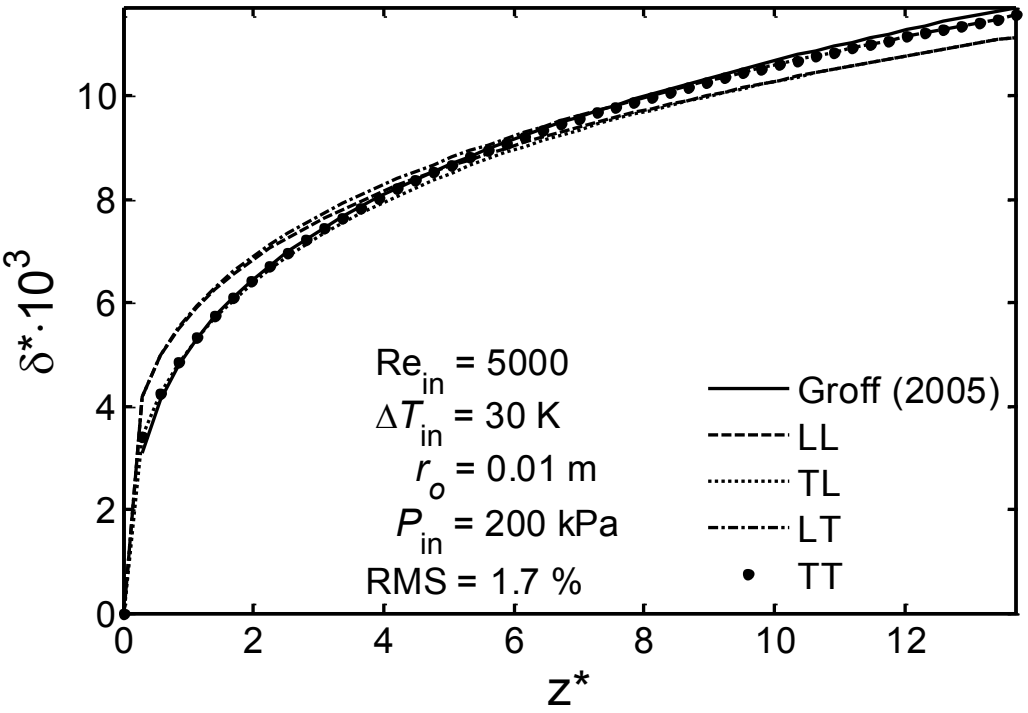

Figure 7.12: Comparison with code (Re_{in} = 5000, ΔT_{in} = 30 K, r_o = 0.01 m, P_{in} = 200 kPa)

7.2. Comparison with Kuhn (1995)

All comparisons with the experiments of Kuhn (1995) are for pure steam with the inlet Reynolds numbers from 15000 to 37000. The inlet saturation pressures range from 108 kPa to 496 kPa. The tube radius is 0.024 m. The first comparison to Kuhn run 1.1-1 is shown in Figures 7.13 to 7.16. Figure 7.13 shows the experimental temperature difference variation and the polynomial fitting that was used. Note that the wall temperatures and the polynomials are different for each run. Figure 7.14 compares the film thickness between Kuhn run 1.1-1 and the closed-form solution TT model using both variable wall temperature and constant mean wall temperature. The RMS deviation between the experimental film thickness and the closed-form solution TT model using variable wall temperature is 8.2%. The deviation between the variable wall temperature result and constant mean wall temperature result is clearly obvious. Figure 7.15 compares the local heat transfer coefficient. The RMS deviation between the local heat transfer coefficient result from Kuhn run 1.1-1 and the closed-form solution TT model using variable wall temperature is 8.5%. The deviation between the variable wall temperature result and the constant mean wall temperature result is again clearly obvious. Figure 7.16 compares the interfacial shear stress which shows a large difference of 26% due to the computation method. Kuhn used a friction factor and the interfacial velocity to compute the interfacial shear stress. The final form of the expression used is given by Equation (7.2.1). The interfacial velocity was computed by another expression which depended on the interfacial shear stress so iteration was required.

$$\tau_i = \frac{1}{2}\left(0.046\,\mathrm{Re}_V^{-0.2}\right)\rho_V\left(u_V - u_i\right)^2 \tag{7.2.1}$$

Figures 7.17 to 7.30 compare the film thickness and the local heat transfer for the remaining runs. Only the closed-form solution TT model using variable wall temperature is used. Figures 7.13 to 7.24 are for high inlet Reynolds number with increasing saturation pressure and temperature difference. Figures 7.25 to 7.30 are for low inlet Reynolds number with increasing saturation pressure and temperature difference. The agreements of film thickness and local heat transfer coefficient are good for all runs, where the maximum RMS deviations are 8.8% and 15%, respectively. The location of the larger deviation is usually near the inlet with no predicable trend. At the second half of the tube, the agreements are better than that of the first half. This may due to liquid droplets being entrained into vapor during the experiment and/or the surface waviness, which are not accounted for in the present analysis.

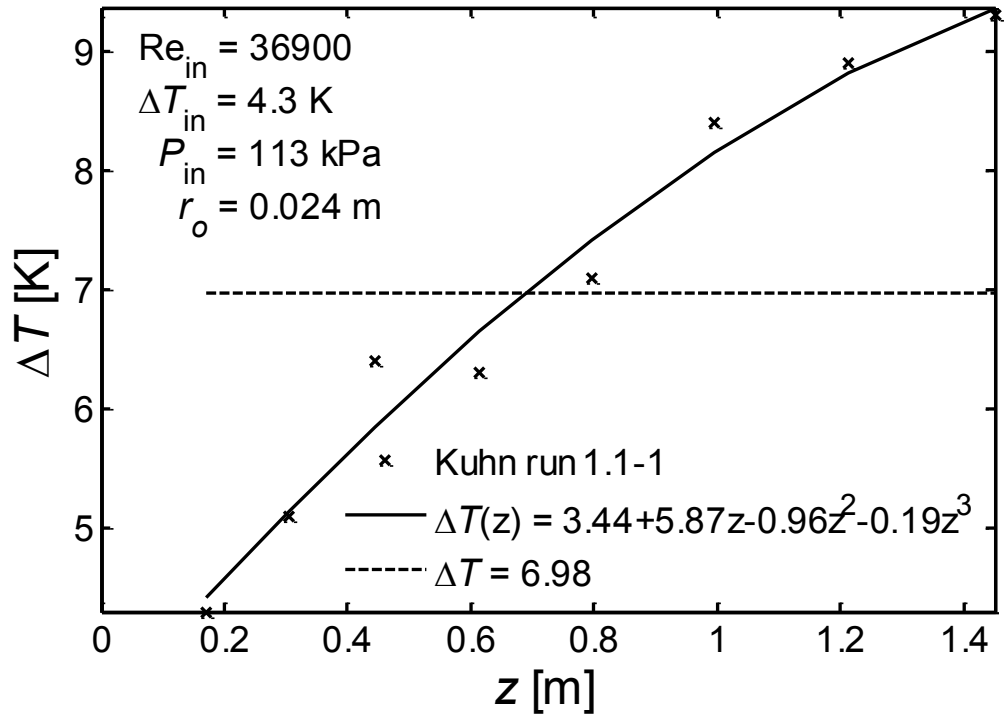

Figure 7.13: Kuhn run 1.1-1 - Temperature difference

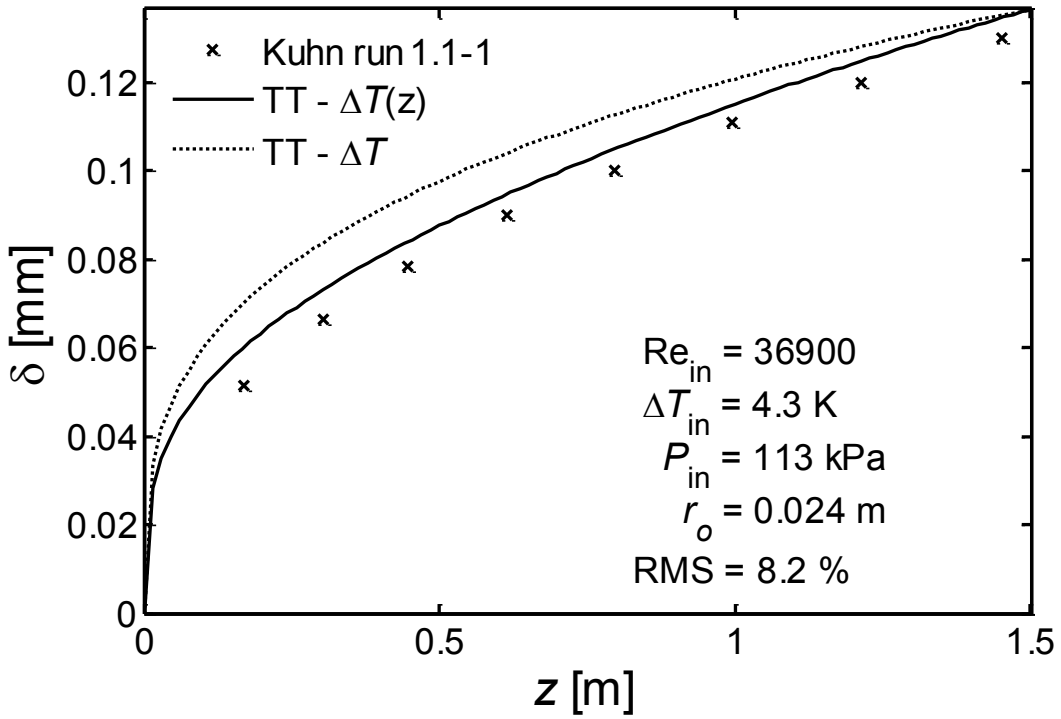

Figure 7.14: Kuhn run 1.1-1 - Film thickness

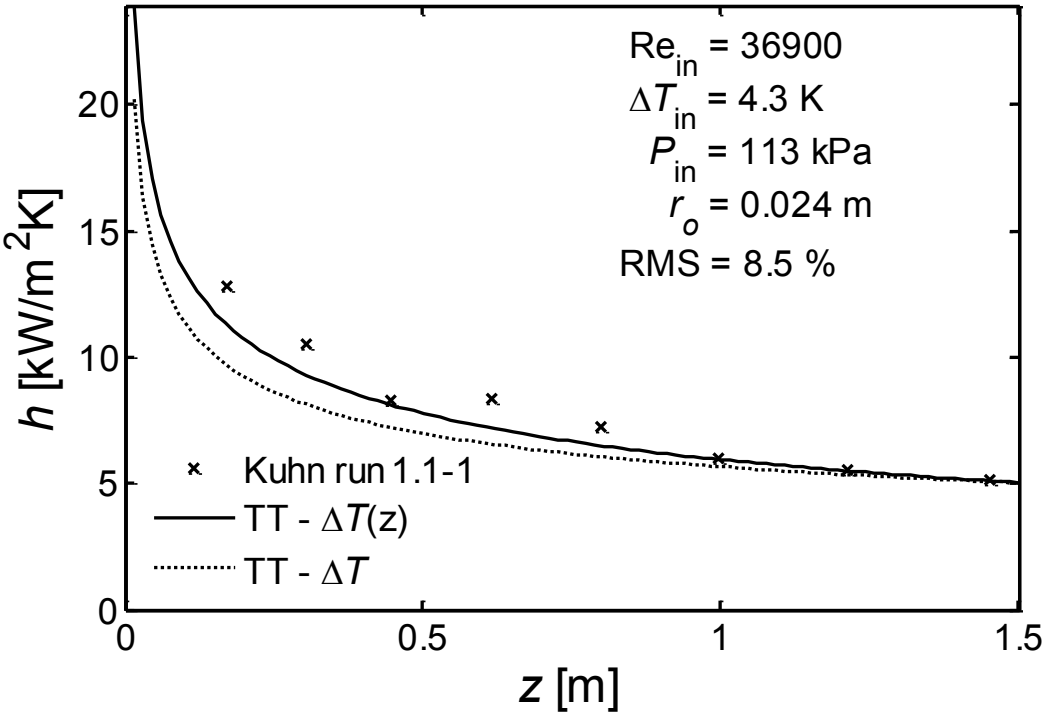

Figure 7.15: Kuhn run 1.1-1 - Local heat transfer coefficient

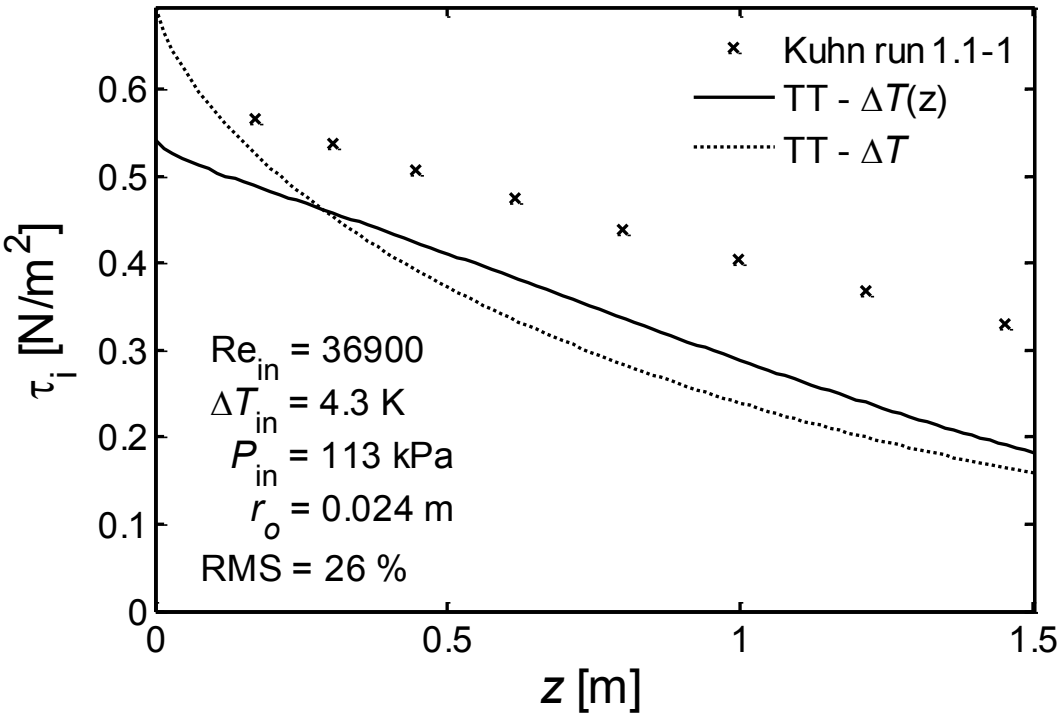

Figure 7.16: Kuhn run 1.1-1 - Interfacial shear stress

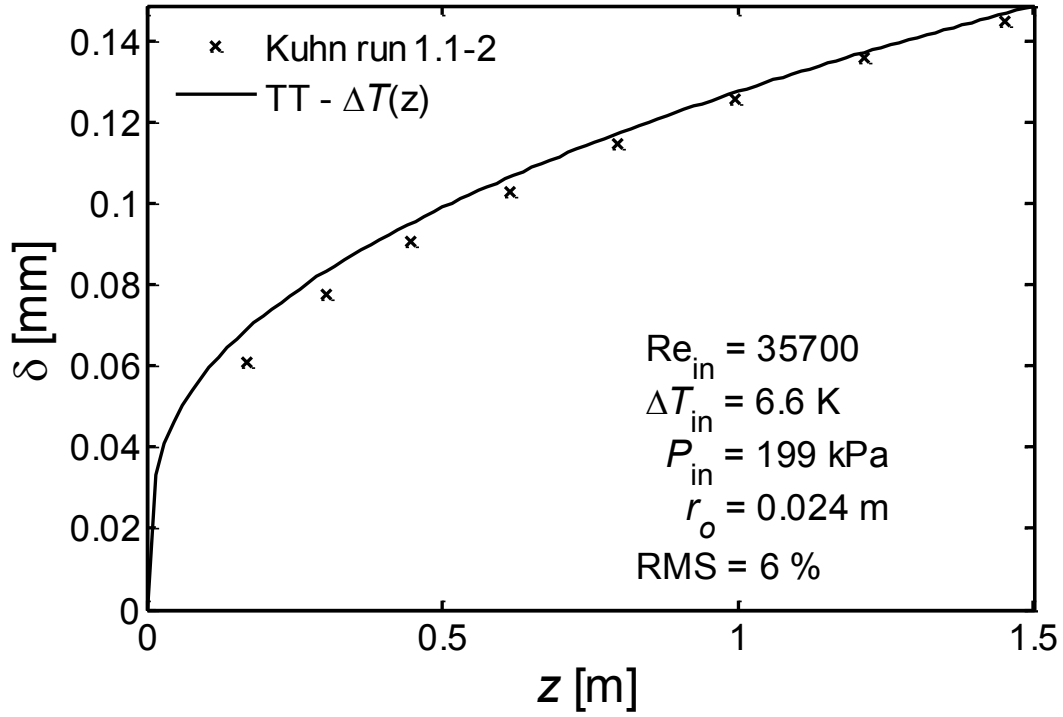

Figure 7.17: Kuhn run 1.1-2 - Film thickness

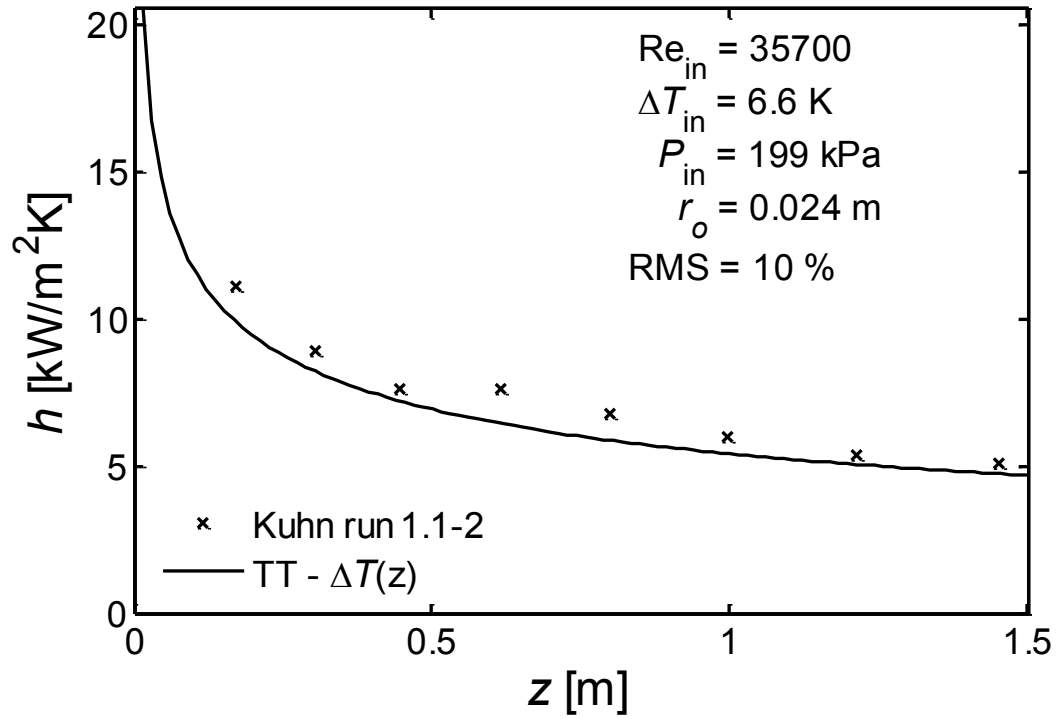

Figure 7.18: Kuhn run 1.1-2 - Local heat transfer coefficient

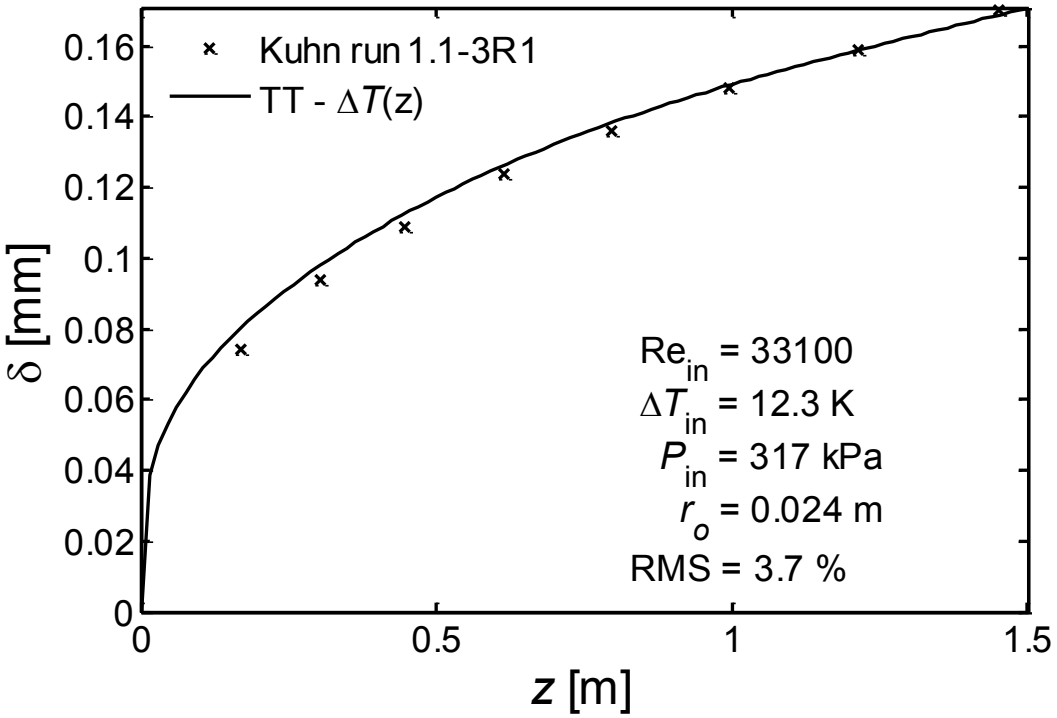

Figure 7.19: Kuhn run 1.1-3R1 - Film thickness

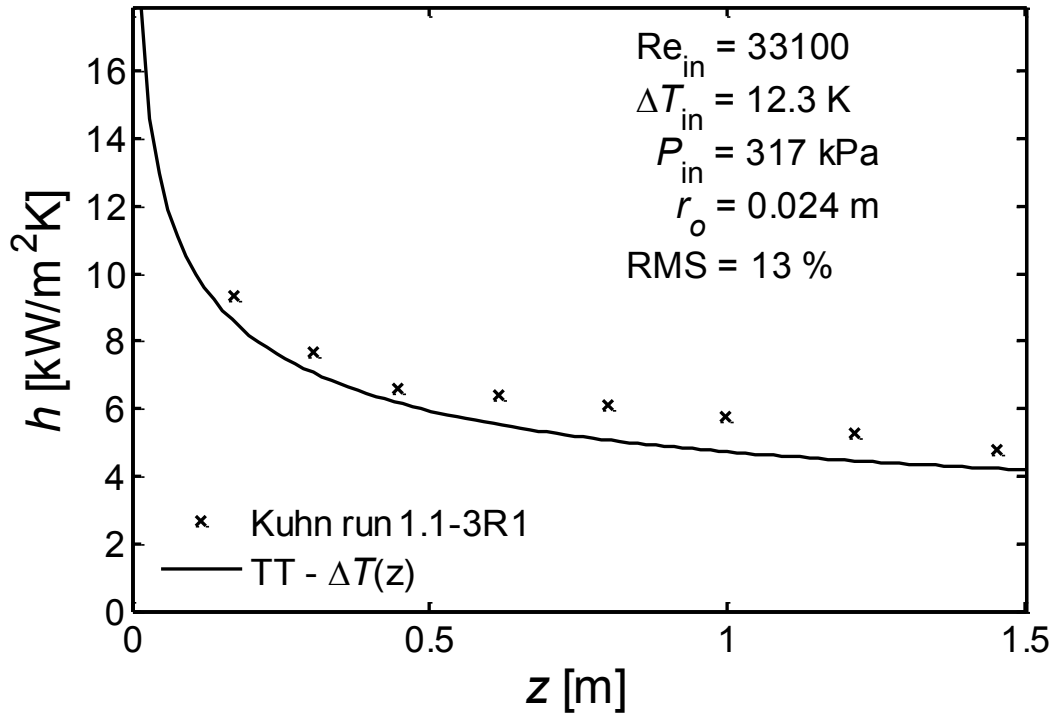

Figure 7.20: Kuhn run 1.1-3R1 - Local heat transfer coefficient

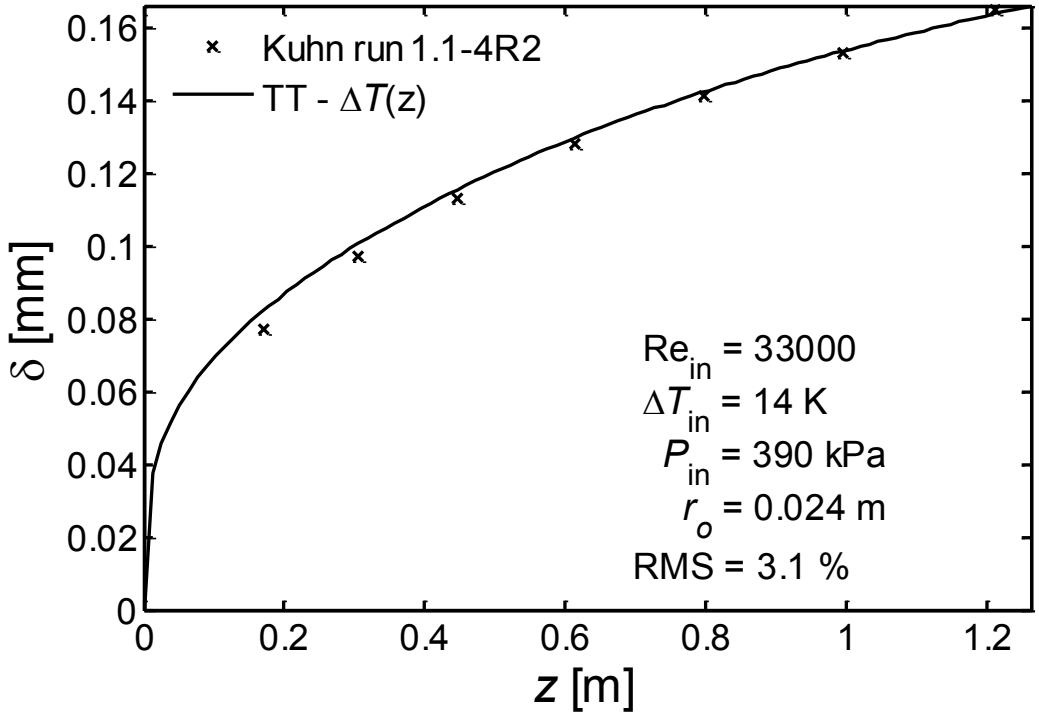

Figure 7.21: Kuhn run 1.1-4R2 - Film thickness

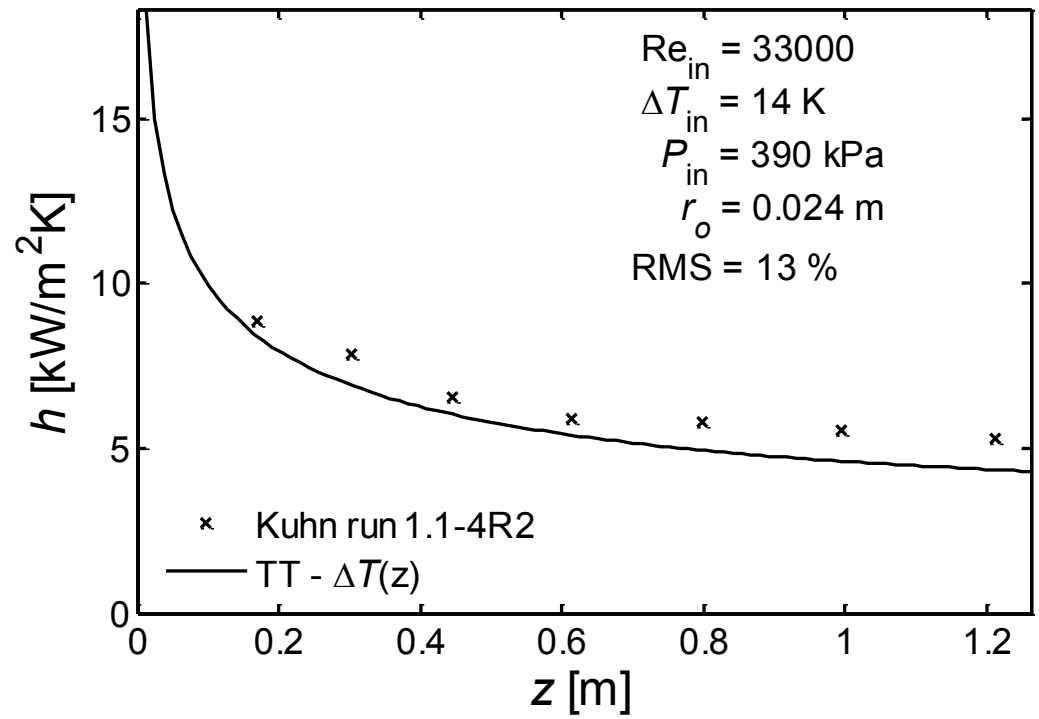

Figure 7.22: Kuhn run 1.1-4R2 - Local heat transfer coefficient

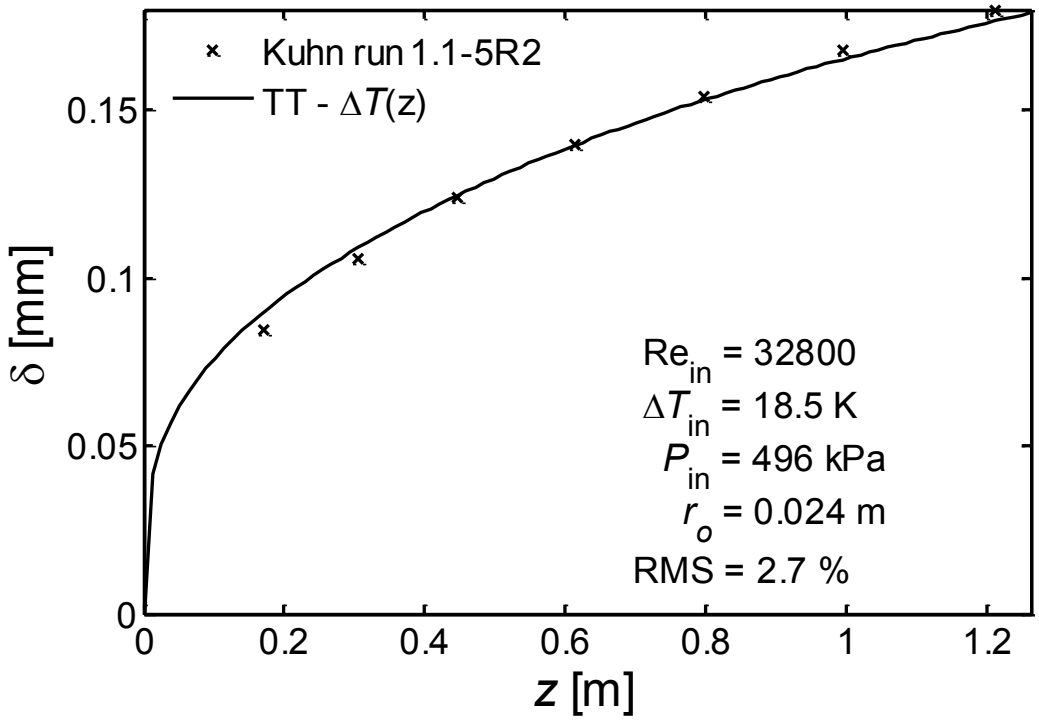

Figure 7.23: Kuhn run 1.1-5R2 - Film thickness

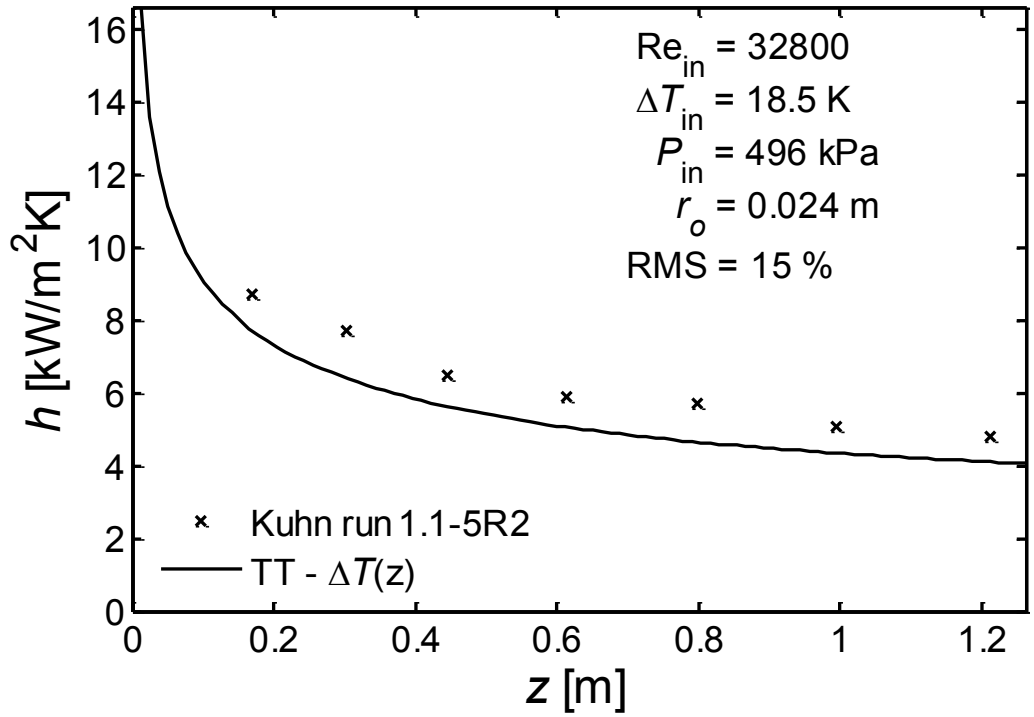

Figure 7.24: Kuhn run 1.1-5R2 - Local heat transfer coefficient

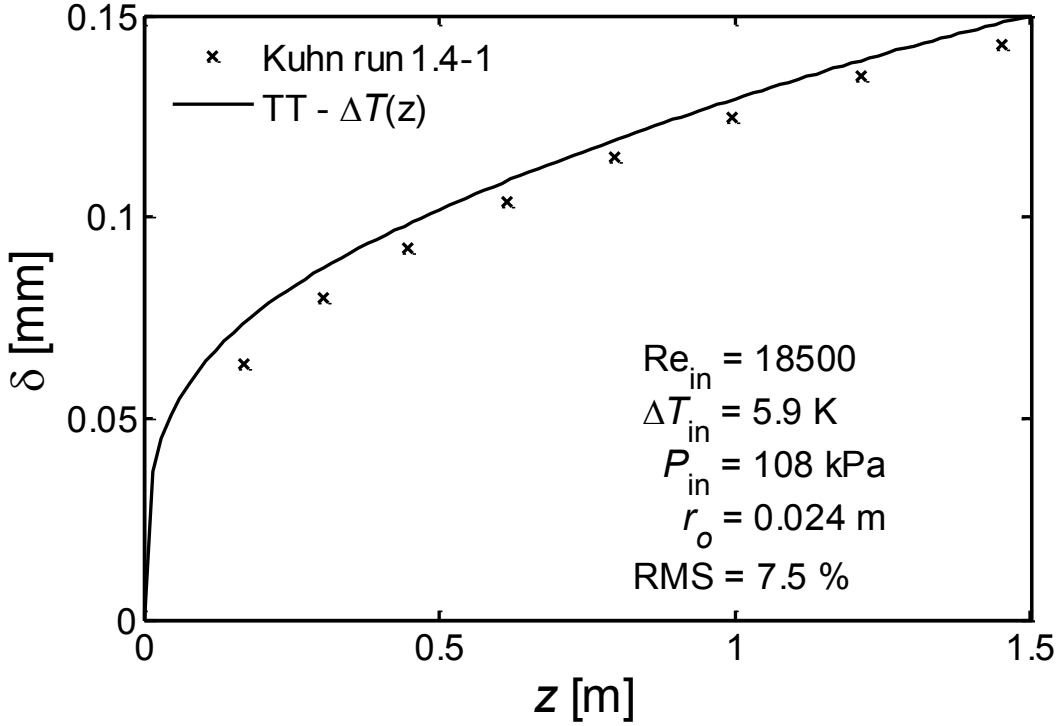

Figure 7.25: Kuhn run 1.4-1 - Film thickness

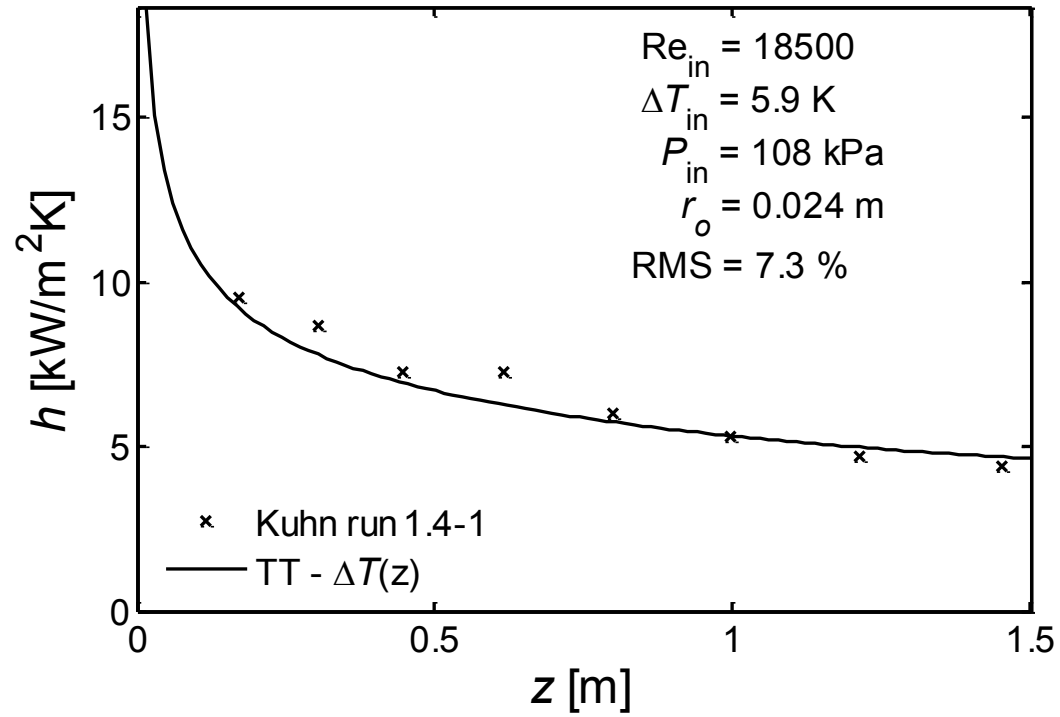

Figure 7.26: Kuhn run 1.4-1 - Local heat transfer coefficient

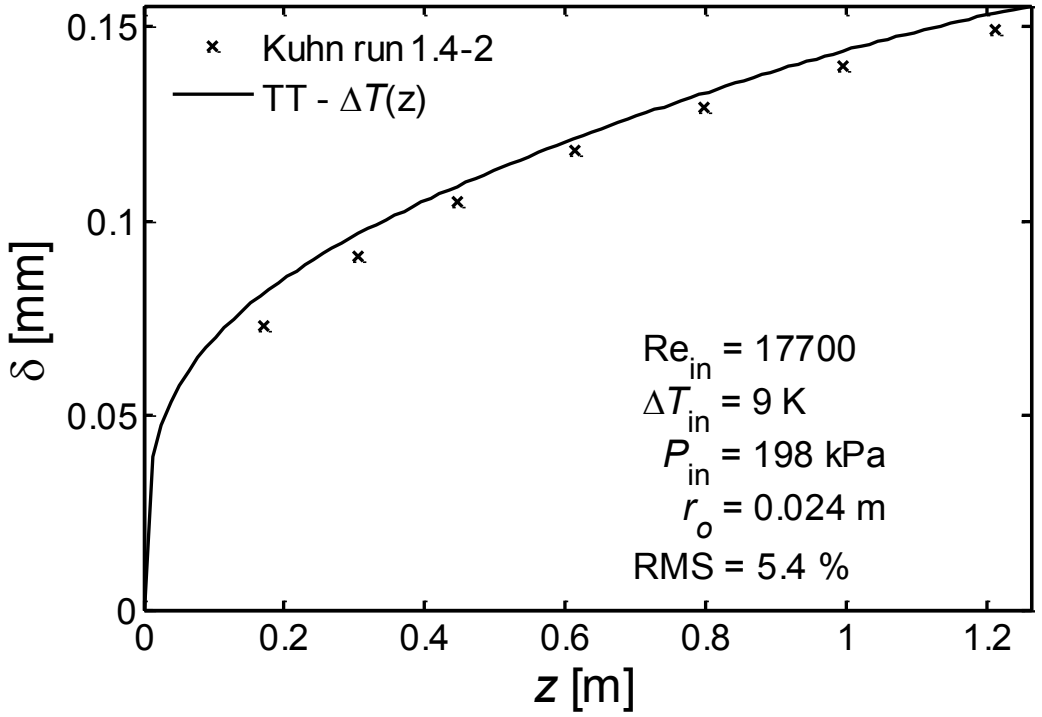

Figure 7.27: Kuhn run 1.4-2 - Film thickness

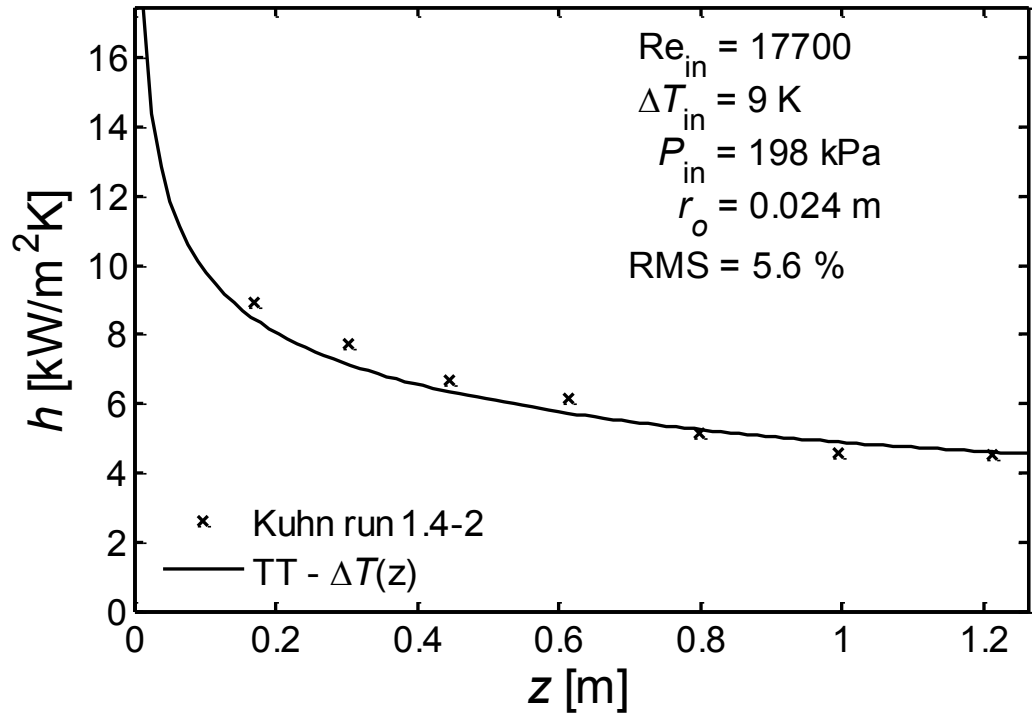

Figure 7.28: Kuhn run 1.4-2 - Local heat transfer coefficient

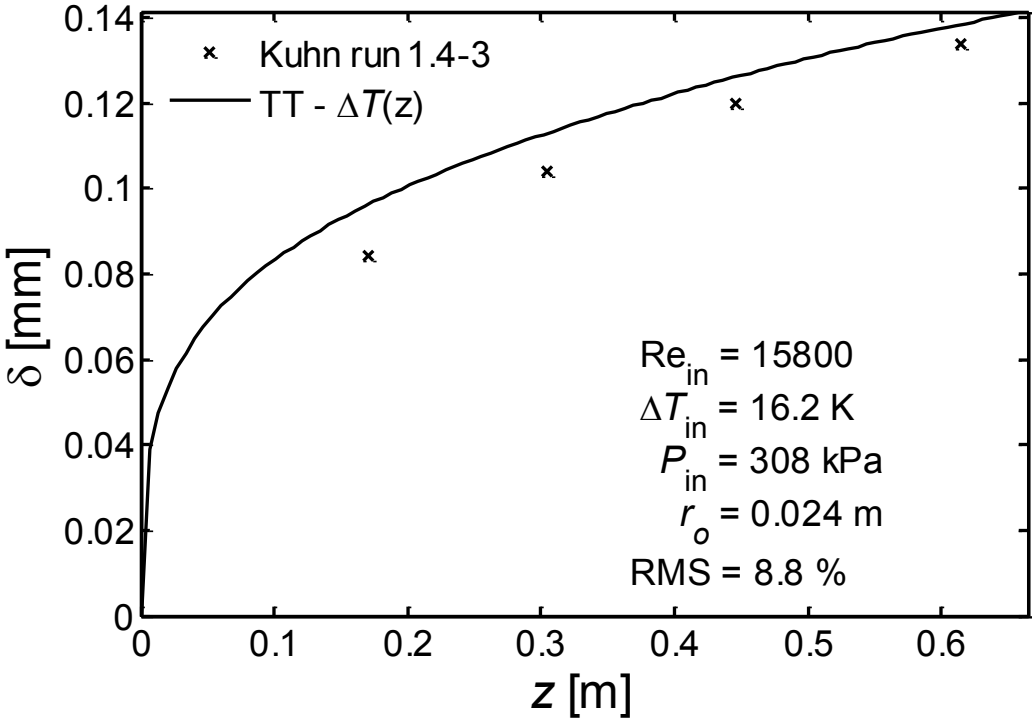

Figure 7.29: Kuhn run 1.4-3 - Film thickness

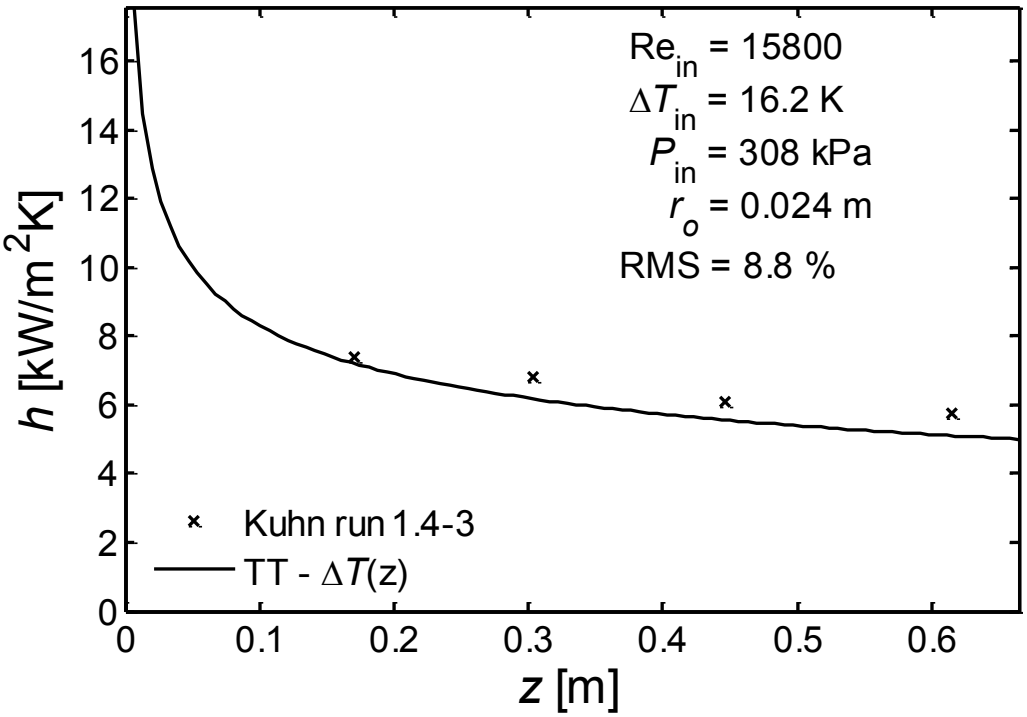

Figure 7.30: Kuhn run 1.4-3 - Local heat transfer coefficient

7.3. Comparison with Yuann (1993)

Yuann (1993) performed experiments for condensation in a vertical tube of radius 0.025 m. Two pure steam cases were selected for comparison. Each comparison consists of three figures. Figures 7.31 to 7.33 compare the closed-form solution TT model using variable wall temperature with Yuann run 276-40-0. Figure 7.31 shows the inlet-to-wall temperature difference variation and its polynomial fitting. Figure 7.32 compares the film thickness with a RMS deviation of 19%. Figure 7.33 compares the local heat transfer coefficient with a RMS deviation of 14%. As can be observed in Figures 7.32 and 7.33, the large differences occur at the first half of the tube where the effects of surface waviness and liquid entrainment are not accounted for in the present analysis. The errors in data acquisition and data reduction during the experiment can also contribute to these large differences. Figures 7.34 to 7.36 show similar comparisons to Yuann run 483-40-0. Note that Figure 7.35 shows an abnormally high film thickness at the end of condensation which is an indication of possible measurement error.

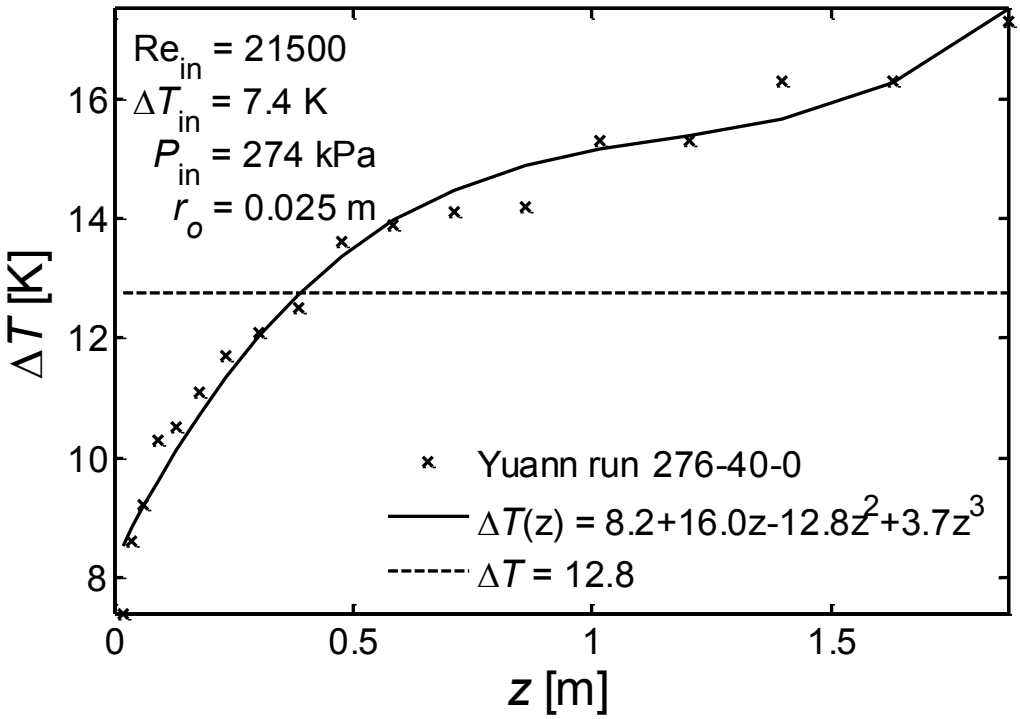

Figure 7.31: Yuann run 276-40-0 - Temperature difference

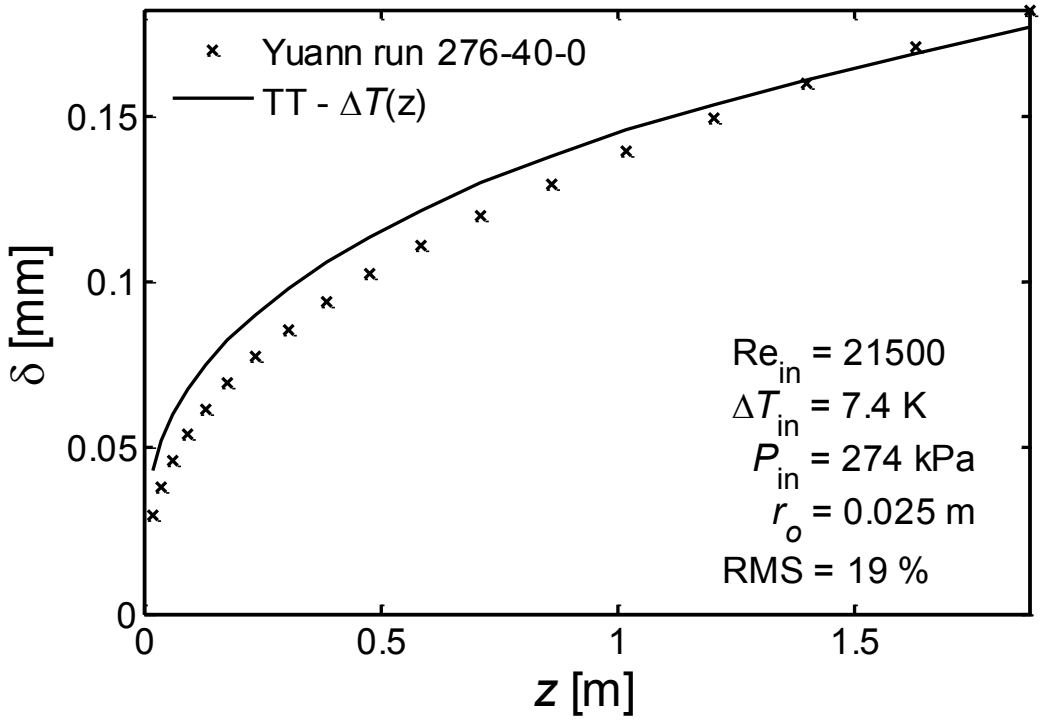

Figure 7.32: Yuann run 276-40-0 - Film thickness

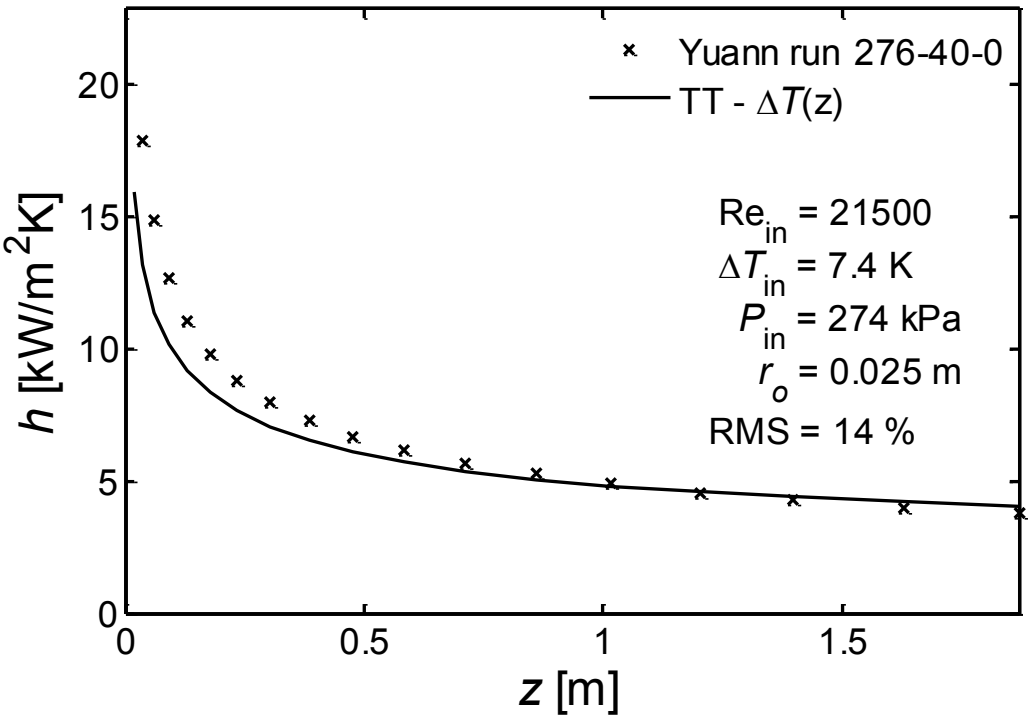

Figure 7.33: Yuann run 276-40-0 - Local heat transfer coefficient

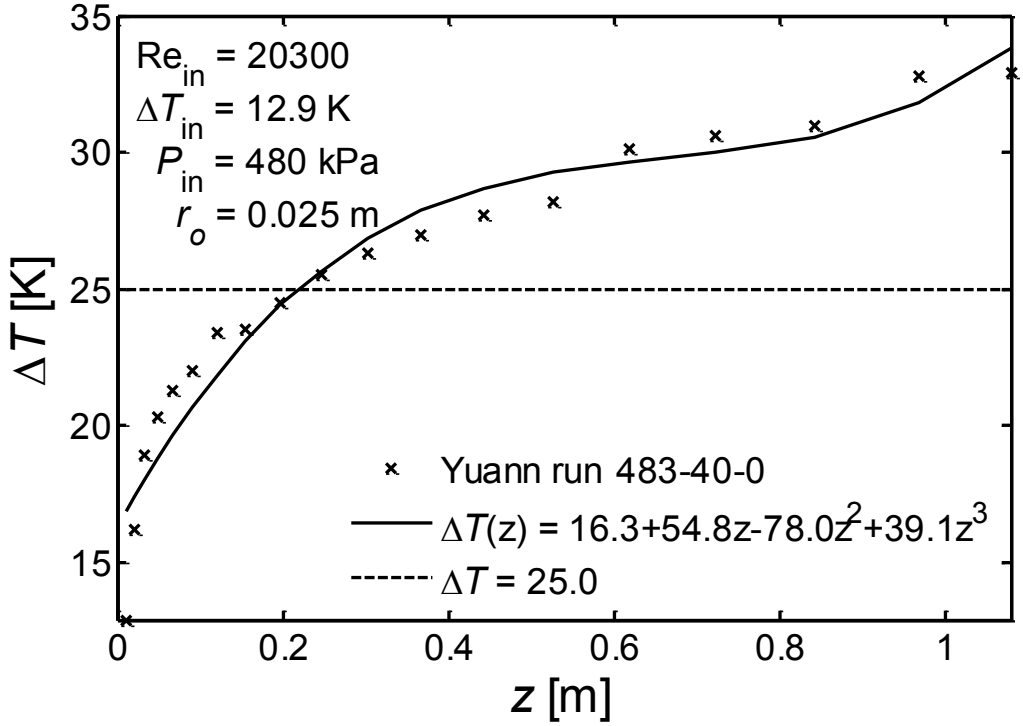

Figure 7.34: Yuann run 483-40-0 - Temperature difference

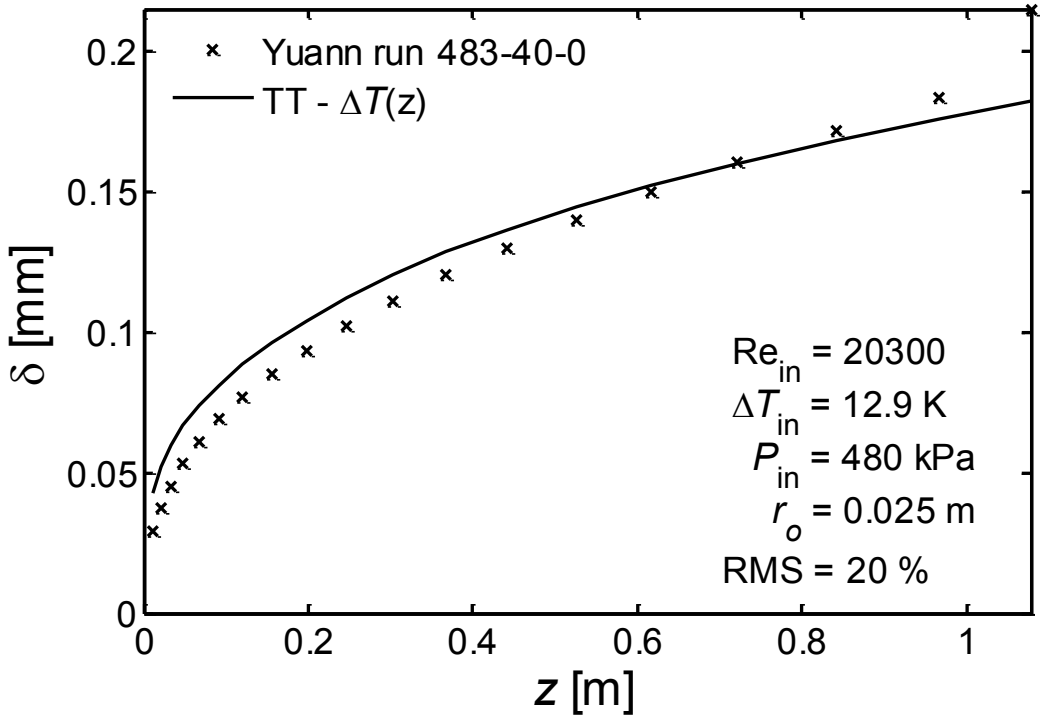

Figure 7.35: Yuann run 483-40-0 - Film thickness

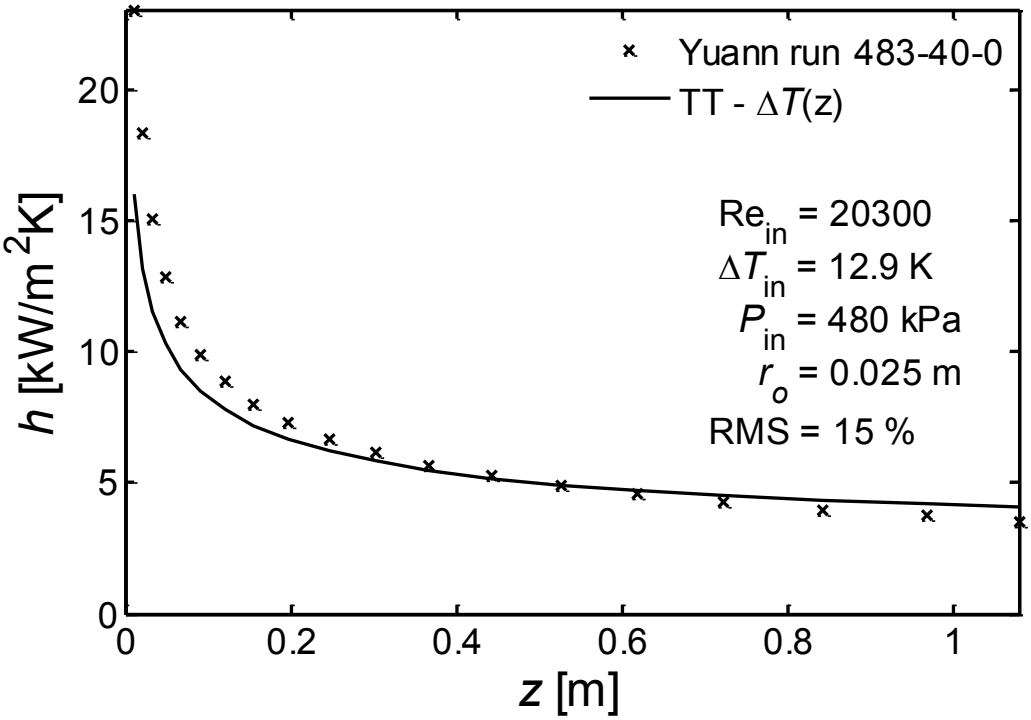

Figure 7.36: Yuann run 483-40-0 - Local heat transfer coefficient

7.4. Comparison with Goodykoontz and Dorsch (1966)

Goodykoontz and Dorsch performed 14 runs of pure steam condensation in a vertical tube with diameter of 0.0159 m. The comparison with the data of Goodykoontz and Dorsch is restricted to the local heat transfer coefficient for fourteen cases. The inlet-to-wall temperature difference variation of run 1 and its polynomial fitting are shown in Figure 7.37. Note that the wall temperatures and the polynomials are different for each run. A common trend can be observed in Figures 7.38 to 7.51 where the experiment local heat transfer coefficients drop sharply at the end of condensation. There is no physically possible explanation for this behavior but experimental errors. Some runs with very high inlet Reynolds number such as runs 3 (Figure 40) and 4 (Figure 41), show very high heat transfer coefficient at the first half of the tube. This indicates that the film thickness is very small due to liquid entrainment in high velocity vapor. The effect of liquid entrainment is not accounted for in the present analysis.

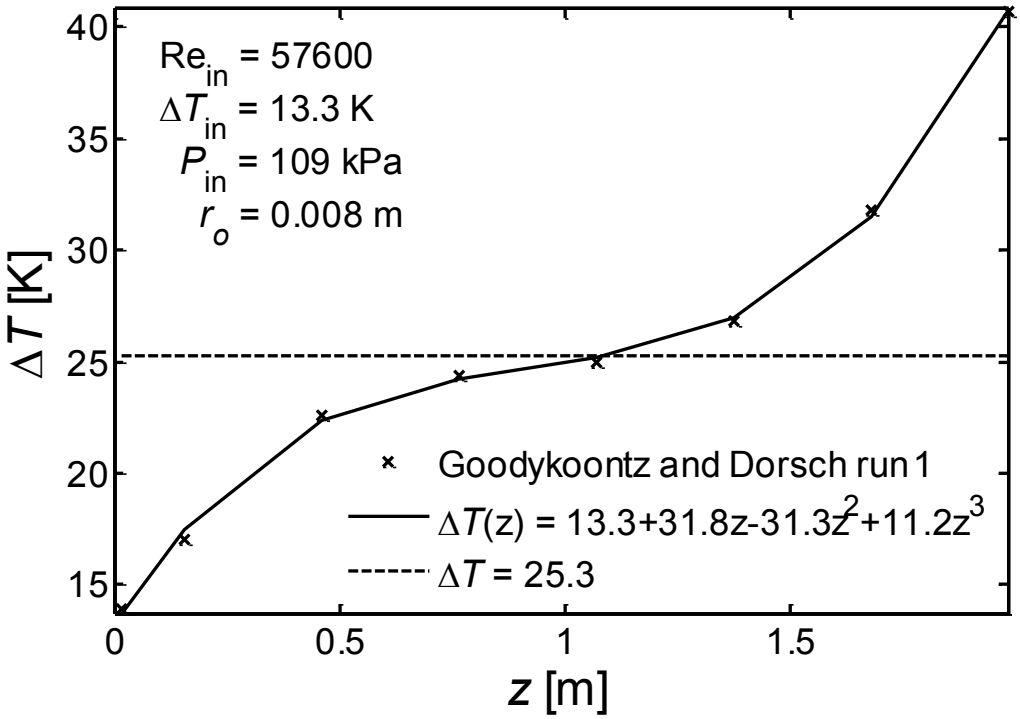

Figure 7.37: Goodykoontz-Dorsch run 1 - Temperature profile

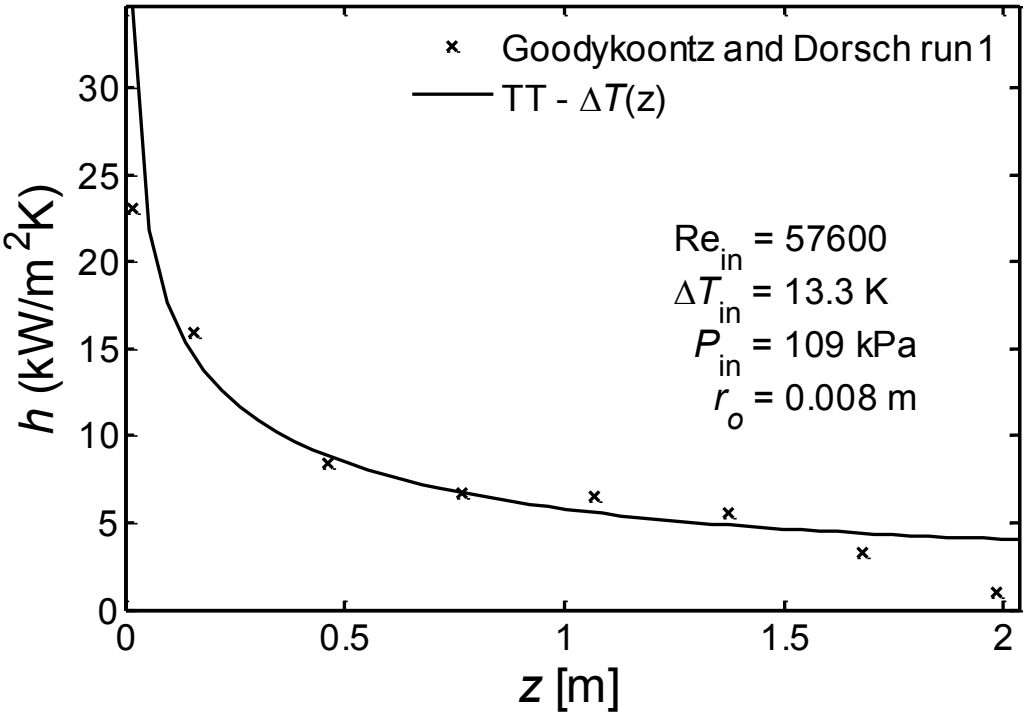

Figure 7.38: Goodykoontz-Dorsch run 1 - Local heat transfer coefficient

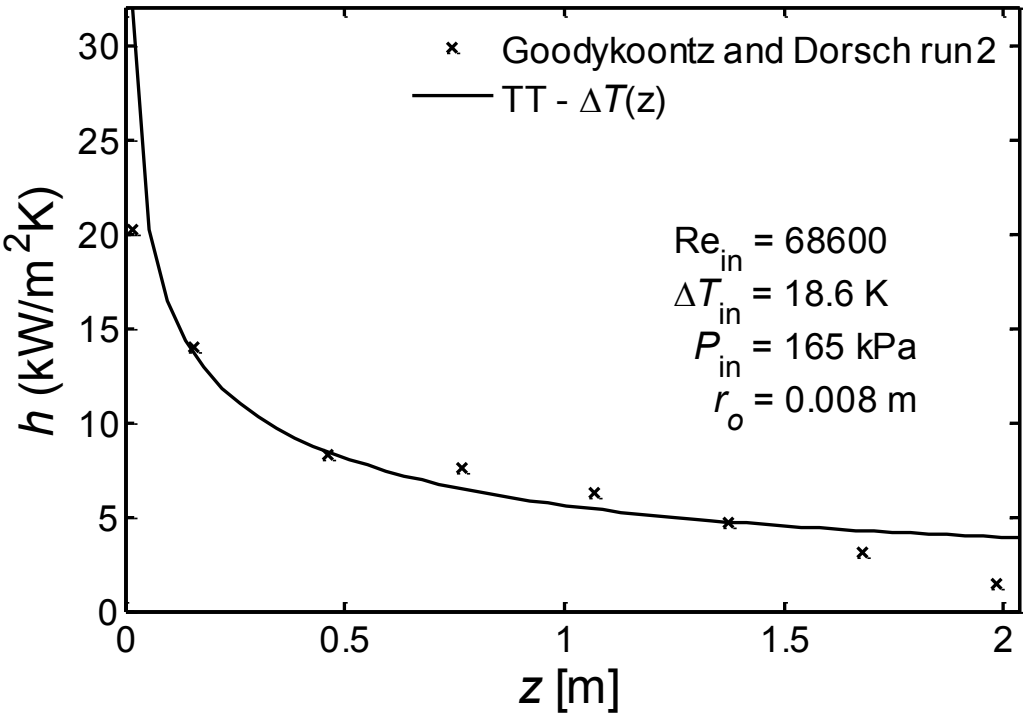

Figure 7.39: Goodykoontz-Dorsch run 2 - Local heat transfer coefficient

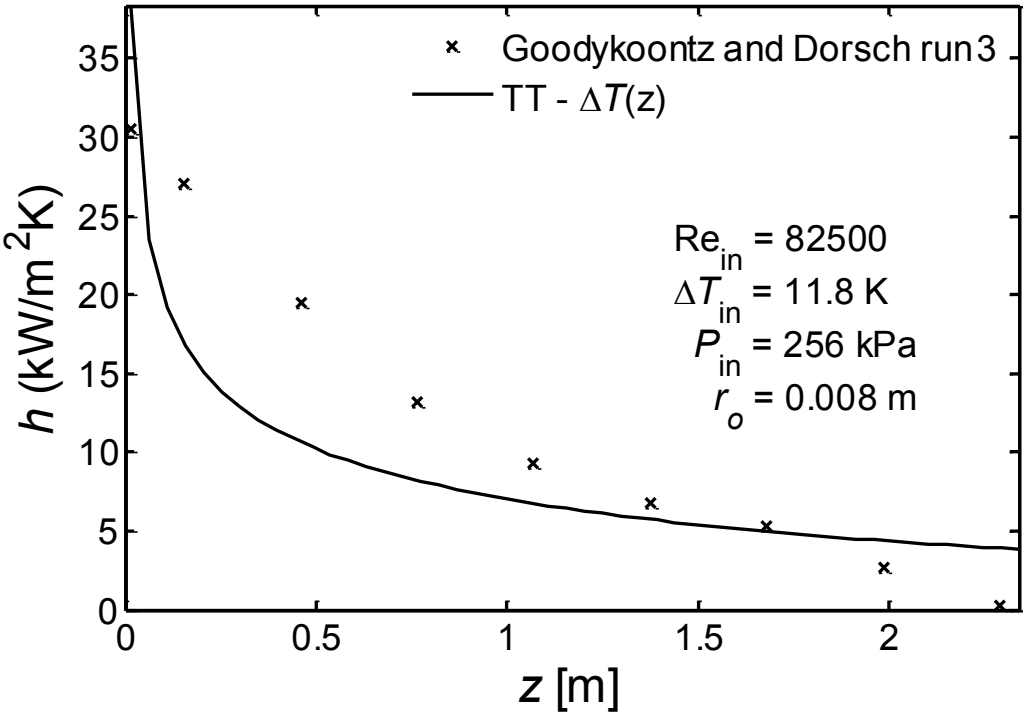

Figure 7.40: Goodykoontz-Dorsch run 3 - Local heat transfer coefficient

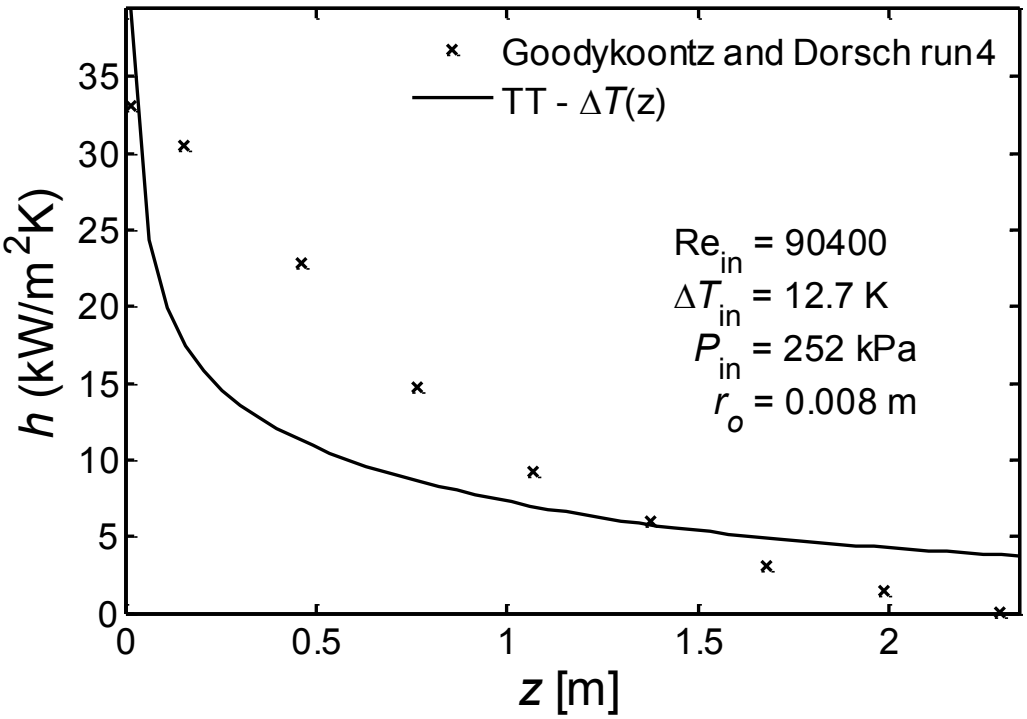

Figure 7.41: Goodykoontz-Dorsch run 4 - Local heat transfer coefficient

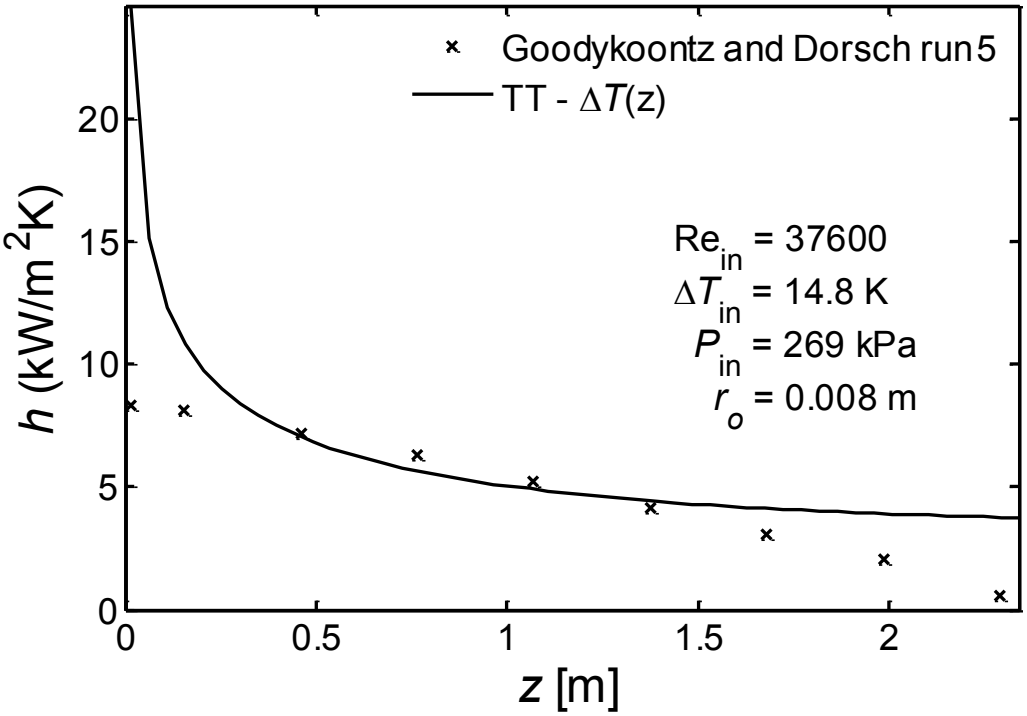

Figure 7.42: Goodykoontz-Dorsch run 5 - Local heat transfer coefficient

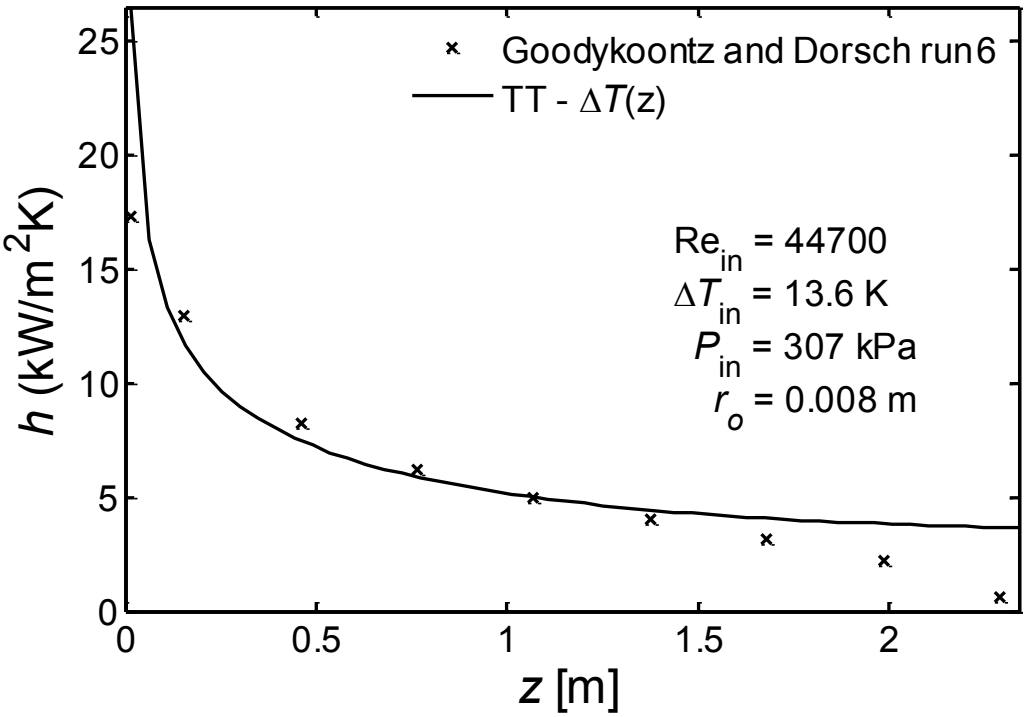

Figure 7.43: Goodykoontz-Dorsch run 6 - Local heat transfer coefficient

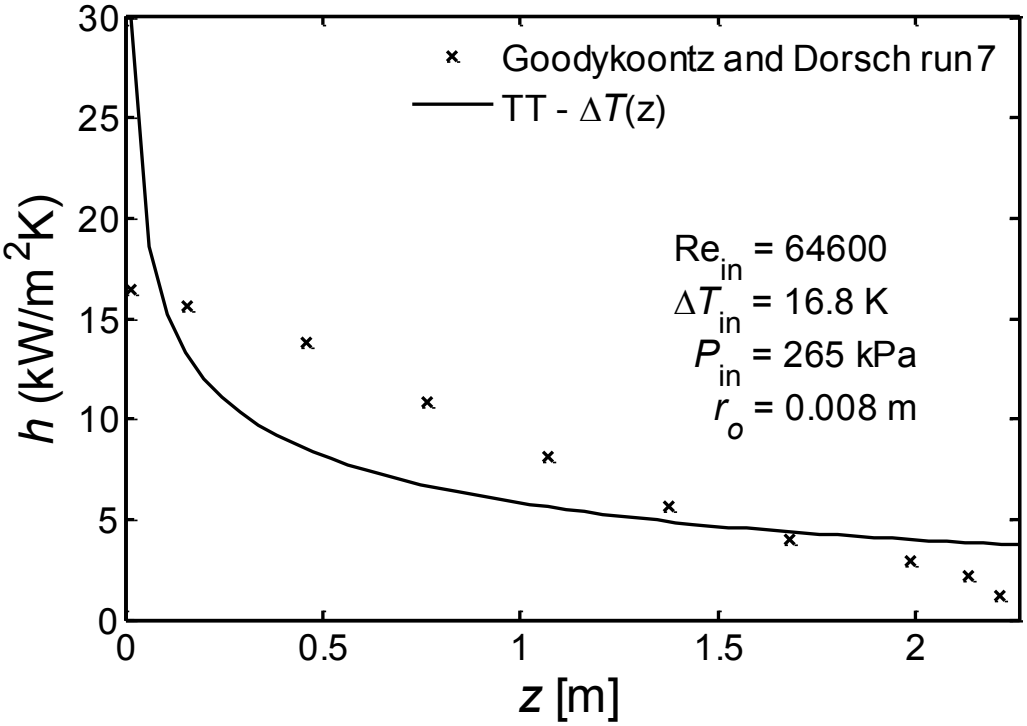

Figure 7.44: Goodykoontz-Dorsch run 7 - Local heat transfer coefficient

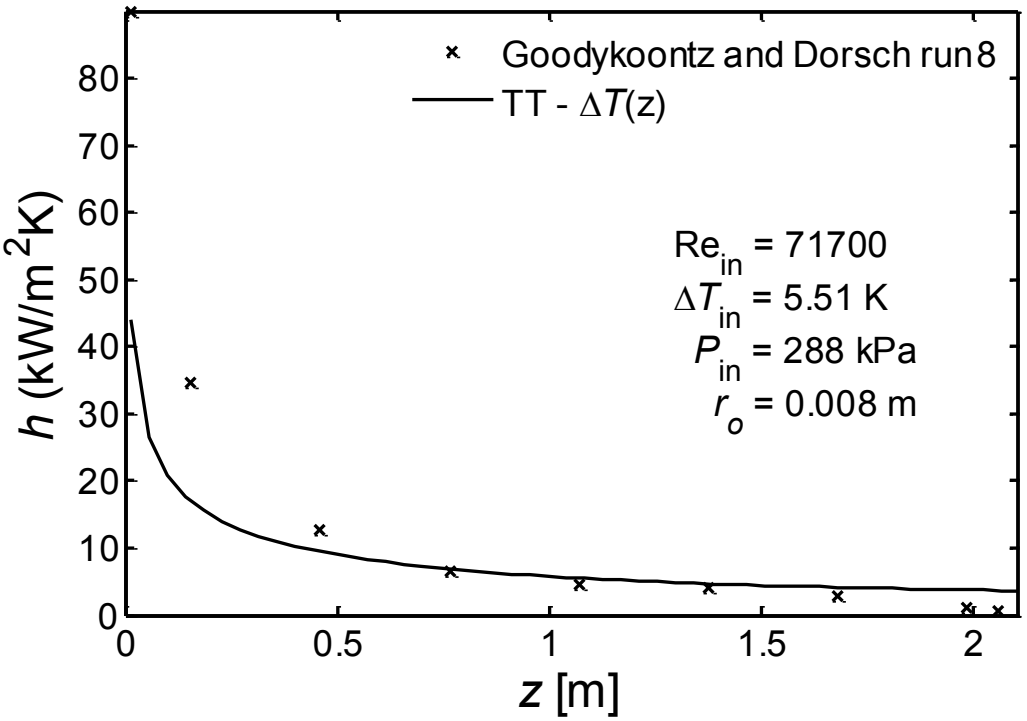

Figure 7.45: Goodykoontz-Dorsch run 8 - Local heat transfer coefficient

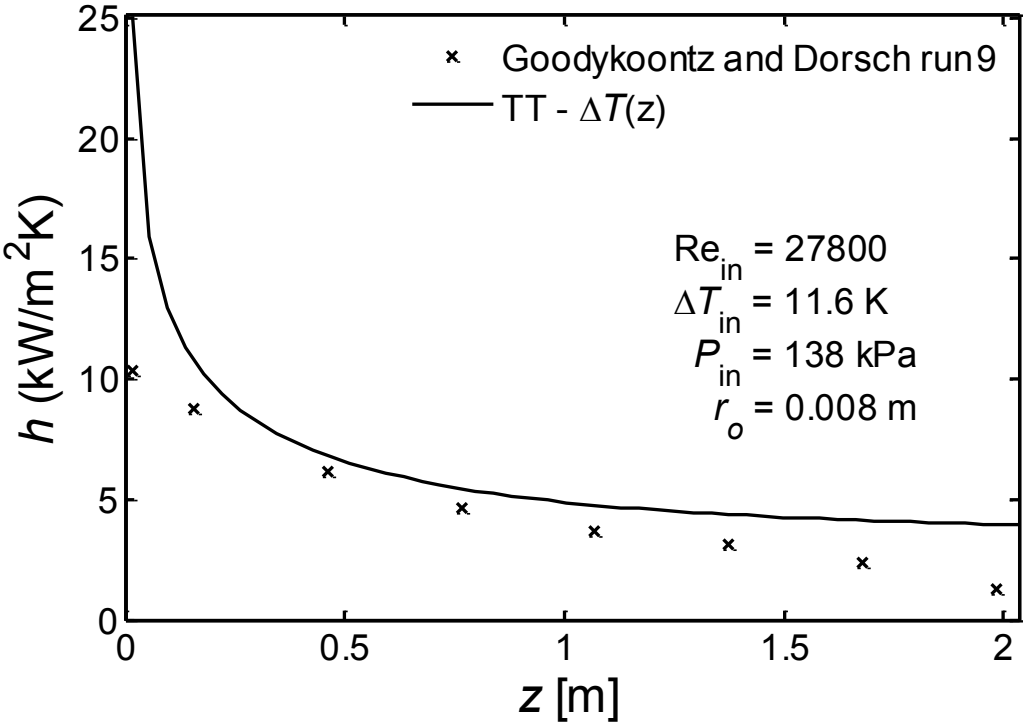

Figure 7.46: Goodykoontz-Dorsch run 9 - Local heat transfer coefficient

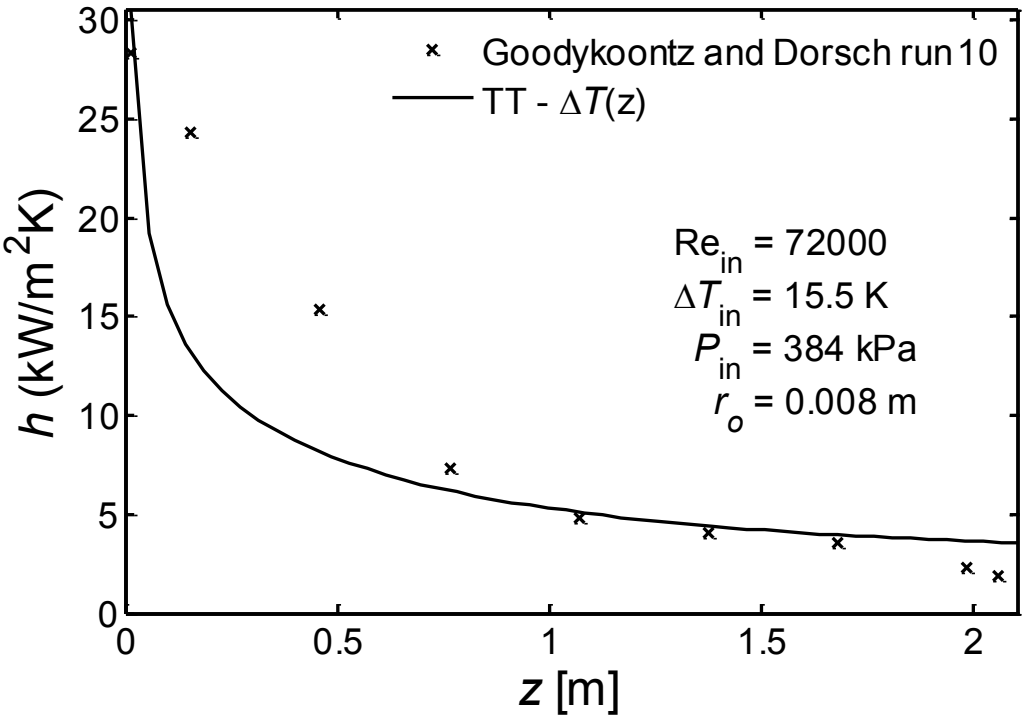

Figure 7.47: Goodykoontz-Dorsch run 10 - Local heat transfer coefficient

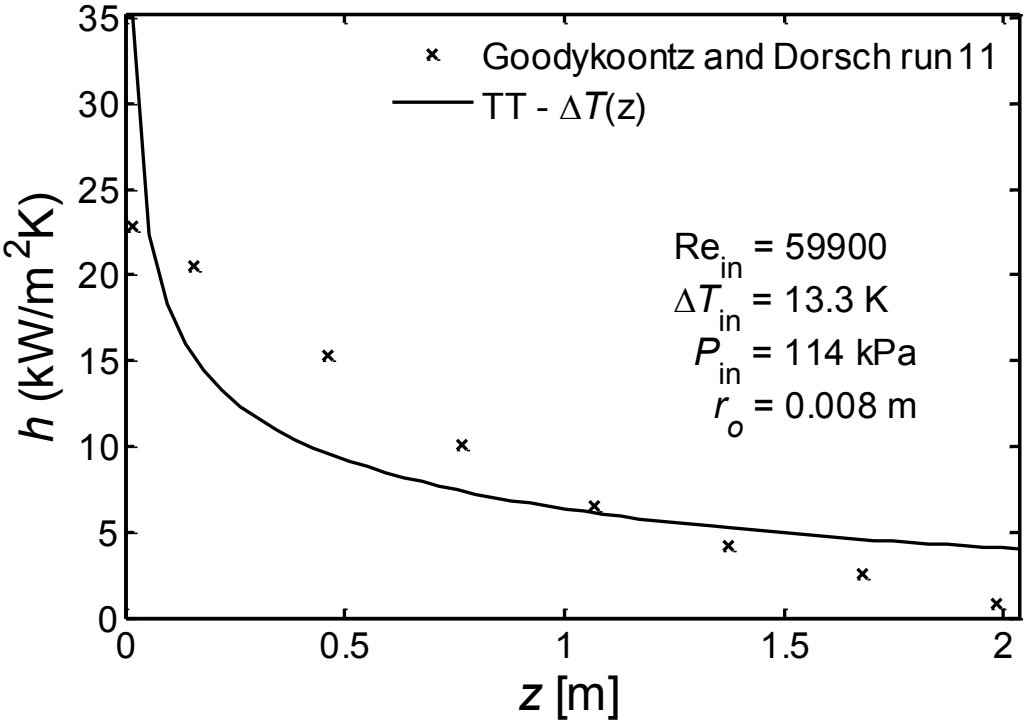

Figure 7.48: Goodykoontz-Dorsch run 11 - Local heat transfer coefficient

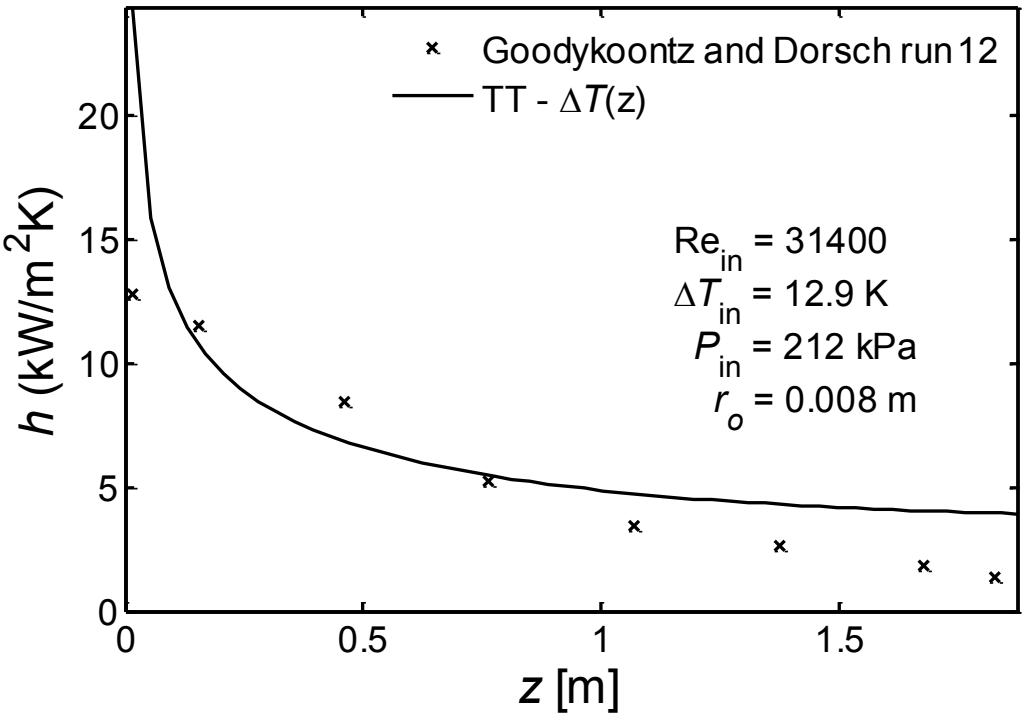

Figure 7.49: Goodykoontz-Dorsch run 12 - Local heat transfer coefficient

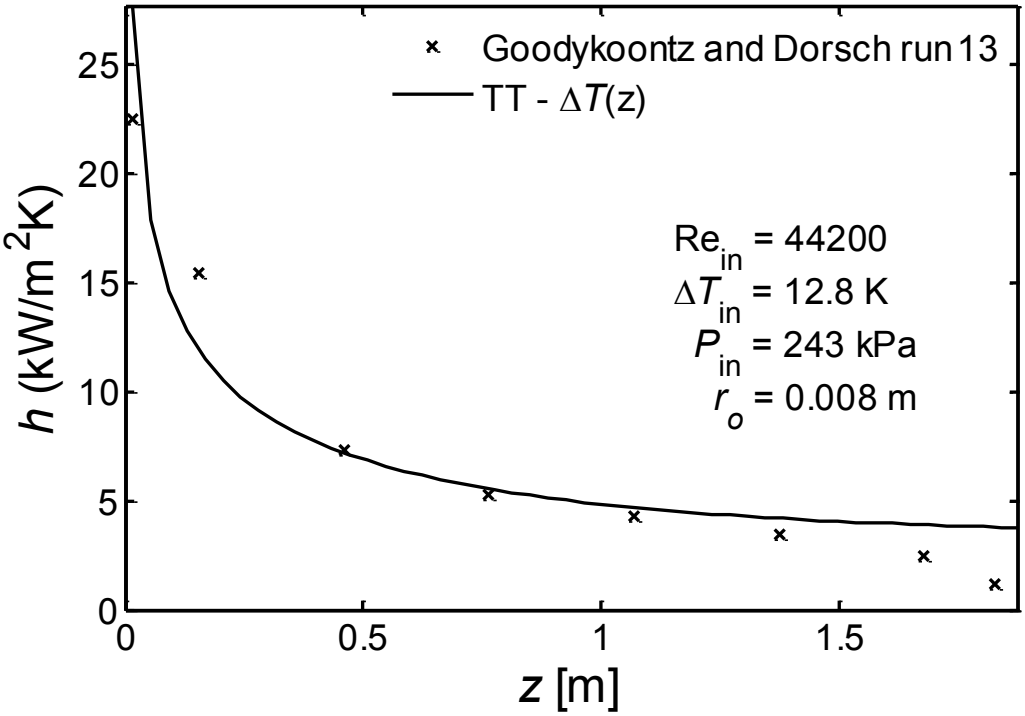

Figure 7.50: Goodykoontz-Dorsch run 13 - Local heat transfer coefficient

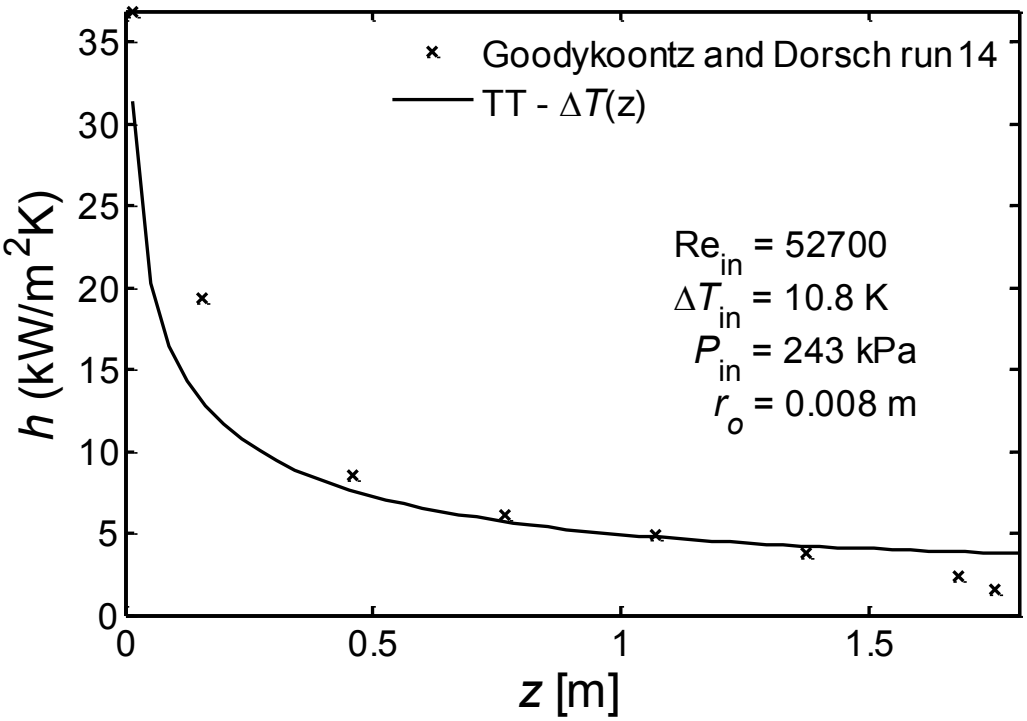

Figure 7.51: Goodykoontz-Dorsch run 14 - Local heat transfer coefficient

CHAPTER 8

SUMMARY, CONCLUSION AND RECOMMENDATIONS

8.1. Summary

The present work developed a closed-form solution procedure to calculate the axial variation of the film thickness for condensation from a pure vapor in mixed convection flow downward in a vertical tube. The new solution procedure was developed in three parts. Part one was the solution of the film thickness for condensation from a quiescent vapor on a curved vertical surface. This solution is very similar to Nusselt's solution for film condensation on vertical flat plate. The key feature of this part was a new form of the dimensionless film thickness variable δ_+ which greatly simplified an otherwise complex expression and procedure. An exact explicit solution for δ_+ was found using the Lambert W-function. An approximate closed-form solution was also obtained by using an approximation to the natural logarithm function. This approximate solution converged exactly to Nusselt's vertical flat plate solution in the limit when the wall radius of curvature approached infinity and compared very well with the exact solution. The analysis in part two included the interfacial shear stress in laminar vapor and laminar condensate flow. The key feature of this second part was a new definition of pressure gradient that combined the momentum and frictional components of the pressure gradient using a new function of vapor density. With this vapor density function, its approximate functions, and the approximation technique of part one, an approximate closed-form solution for the condensate film thickness was obtained. In part three, this solution approach in part two was extended to model turbulent flows of vapor and liquid.

Turbulent effects were modeled using an eddy viscosity assumption and turbulent viscosities for vapor and liquid were introduced. The turbulent viscosities were correlated by comparison with the data produced by the numerical model of Groff (2005). These correlations extended the approximate closed-form solution into the turbulent flow regime. A solution procedure involved variable wall temperature was also developed, which was useful for comparisons with experimental data. Comparisons were made with the experimental data of Kuhn (1995), Yuann (1993), and Goodykoontz and Dorsch (1966).

8.2. Conclusion

With the input parameters of the tube radius, the inlet Reynolds number, the inlet saturation temperature or pressure, and the constant or variable wall temperature, the present solution procedure can easily compute the condensate film thickness at any axial location with acceptable accuracy. This condensate film thickness can then be used to compute other required quantities such as the local heat transfer coefficient, the vapor and liquid velocity profiles, the vapor and liquid mass flow rates, the vapor and liquid Reynolds numbers, the interfacial shear stress, and the pressure gradient. The computation can be done manually for few local quantities or using spreadsheet if more extensive computations are required.

8.3. Recommendations

The following topics are recommended for future works:

1. Find the turbulent viscosities by solving turbulent transport equations.

2. Include the effects of noncondensable gas by solving the mixture energy and diffusion equations.
3. Extend the method to the condensation on the outside of vertical tubes.

REFERENCES

Aglar, F., and Tanrikut, A., 2008, "A New Heat Transfer Correlation for Condensation in the Presence of Air and Its Implementation into RELAP5/MOD3.3", *Nuclear Technology*, Vol. 161, pp. 286-298.

Bronstein, M., Corless, R.M., Davenport, J.H., and Jeffrey, D.J., 2008, "Algebraic properties of the Lambert *W* function from a result of Rosenlicht and of Liouville", *Integral Transforms and Special Functions,* Vol. 19, pp. 709–712.

Barry, D.A., Barry, S.J., and Culligan-Hensley, P.J., 1995, "Algorithm 743: WAPR: A Fortran Routine for Calculating Real Values of the W-Function", *ACM Transactions on Mathematical Software*, Vol. 21, No. 2, pp. 172-181.

Barry, D.A., Culligan-Hensley, P.J., and Barry, S.J., 1995, "Real Values of the W-Function", *ACM Transactions on Mathematical Software*, Vol. 21, No. 2, pp. 161-171.

Barry, D.A., Parlange, J.Y., Li, L., Prommer, H., Cunningham, C.J., and Stagnitti, F., 2000, "Analytical approximations for real values of the Lambert W-Function", *Mathematics and Computers in Simulation*, Vol. 53, pp. 95-103.

Blangetti, F., Krebs, R., Schlünder, E.U., 1982, "Condensation in Vertical Tubes – Experimental Results and Modelling", *Chemical Engineering Fundamentals*, Vol. 1, pp. 20-63.

Boyd, J.P., 1998, "Global Approximations to the Principal Real-Valued Branch of the Lambert W-Function", *Applied Mathematics Letters*, Vol. 11, No. 6, pp.27-31.

Carey, V.P., 1992, *Liquid-Vapor Phase-Change Phenomena: An Introduction to the Thermophysics of Vaporization and Condensation Processes in Heat Transfer Equipment*, Hemisphere Publishing Corporation.

Chen, S.J., 1986, "Turbulent Film Condensation on a Vertical Plate", *Proceeding of the 8th International Heat Transfer Conference*, pp. 1601-1606.

Chen, S.L., Gerner, F.M., and Tien, C.L., 1987, "General Film Condensation Correlations", *Experimental Heat Transfer*, Vol. 1, pp. 93-107.

Chen, S.L., and Ke, M.T., 1993, "Forced Convective Film Condensation Inside Vertical Tubes", *International Journal Multiphase Flow*, Vol. 19, pp. 1045-1060.

Chin, Y.S., 1995, "Numerical Solution of the Complete Two-Phase Model for Laminar Film Condensation with a Noncondensable Gas", M.Sc. Thesis, University of Manitoba.

Chin, Y.S., Ormiston, S.J., and Soliman, H.M., 1998, "A Two-Phase Boundary-Layer Model for Laminar Mixed-Convection Condensation with a Noncondensable Gas on Inclined Plates", *Heat and Mass Transfer*, Vol. 34, pp. 271-277.

Chow, T.Y., 1999, "What is a Closed-Form Number", *The American Mathematical Monthly*, Vol. 106, pp. 440-448.

Corless, R.M., Gonnet, G.H., Hare, D.E.G., Jeffrey, D.J., and Knuth, D.E., 1996, "On the Lambert W Function", *Advances in Computational Mathematics*, Vol. 5, pp.329-359.

Dalkilic, A.S., and Wongwises, S., 2009, "Intensive Literature Review of Condensation Inside Smooth and Enhanced Tubes", *International Journal of Heat and Mass Transfer*, Vol. 52, pp. 3409-3426.

Dalkilic, A.S., Yildiz, S., and Wongwises, S., 2009, "Experimental investigation of convective heat transfer coefficient during downward laminar flow condensation of R134a in a vertical smooth tube", *International Journal of Heat and Mass Transfer*, Vol. 52, pp. 142-150.

Denny, V.E., Mills, A.F., and Jusionis, V.J., 1971, "Laminar Film Condensation From a Steam-Air Mixture Undergoing Forced Flow Down a Vertical Surface", *Journal of Heat Transfer*, pp. 297-304.

Dobran, F., and Thorsen, R.S., 1980, "Forced Flow Laminar Filmwise Condensation of a Pure Saturated Vapor in a Vertical Tube", *International Journal of Heat and MassTransfer*, Vol. 23, pp. 161-177.

Du, X.Z., and Wang, B.X., 2003, "Study on transport phenomena for flow film condensation in vertical mini-tube with interfacial waves", *International Journal of Heat and MassTransfer*, Vol. 46, pp. 2095-2101.

Fujii, T., Lee, B., and Shinzato, K., 1996, "Laminar Forced Convection Condensation of Saturated Vapors in the Near-Critical Region", *Numerical Heat Transfer, Part A*, Vol. 30, pp. 799-813.

Fujii, T., Lee, B., Shinzato, K., and Makishi, O., 1997, "Laminar Free Convection Condensation of Saturated Vapors in the Near-Critical Region", *Numerical Heat Transfer, Part A*, Vol. 31, pp. 373-385.

Fujii, T., and Uehara, H., 1972, "Laminar Filmwise Condensation on a Vertical Surface", *International Journal of Heat and MassTransfer*, Vol. 15, pp. 217-233.

Ghiaasiaan, S.M., 2008, *Two-Phase Flow, Boiling and Condensation in Conventional and Miniature Systems*, Cambridge University Press.

Goodykoontz, J.H., and Dorsch, R.G., 1966, "Local Heat-Transfer Coefficients for Condensation of Steam in Vertical Downflow within a 5/8-Inch-Diameter Tube", NASA Technical Note D-3326.

Groff, M.K., 2005, "Numerical Solution for Turbulence Film Condensation from Vapor-Gas Mixture in Vertical Tubes", M.Sc. Thesis, University of Manitoba.

Groff, M.K., Ormiston, S.J., and Soliman, H.M., 2007, "Numerical solution of film condensation from turbulent flow of vapor-gas mixtures in vertical tubes", *International Journal of Heat and Mass Transfer*, Vol. 50, pp. 3899-3912.

Incropera, F.P., and DeWitt, D.P., 2002, *Fundamentals of Heat and Mass Transfer*, Fifth Ed., John Wiley & Sons.

Jacobs, H.R., 1966, "An Integral Treatment of Combined Body Force and Forced Convection in Laminar Film Condensation", *International Journal of Heat and Mass Transfer*, Vol. 9, pp. 637-648.

Jones, W.P., and Launder, B.E., 1972, "The Prediction of Laminarization with a Two-Equation Model of Turbulence", *International Journal of Heat and Mass Transfer*, Vol. 15, pp. 301-314.

Kim, D.E., Yang, K.H., Hwang, K.W., Ha, Y.H., and Kim, M.H., 2011, "Simple heat transfer model for laminar film condensation in a vertical tube", *Nuclear Engineering and Design*, Vol. 241, pp. 2544-2548.

Kim, S.J., and No, H.C., 2000, "Turbulent Film Condensation of High Pressure Steam in a Vertical Tube", *International Journal of Heat and Mass Transfer*, Vol. 43, pp. 4031-4042.

Koh, J.C.Y., Sparrow, E.M., and Hartnett, J.P., 1961, "The Two Phase Boundary Layer in Laminar Film Condensation", *International Journal of Heat and Mass Transfer*, Vol. 2, pp. 69-82.

Kuhn, S.Z., 1995, *Investigation of Heat Transfer from Condensing Steam-GasMixtures and Turbulent Film Flowing Downward Inside a Vertical Tube*, PhD Thesis, University of California at Berkeley.

Kuhn, S.Z., Schrock, V.E., and Peterson, P.F., 1997, "An Investigation of Condensation from Steam-Gas Mixtures Flowing Downward Inside a Vertical Tube", *Nuclear Engineering and Design*, Vol. 177, pp. 53-69.

Kutateladze, S.S., and Gogonin, I.I., 1979, "Heat Transfer in Film Condensation of Slowly Moving Vapor", *International Journal of Heat and Mass Transfer*, Vol. 22, pp. 1593-1599.

Kutateladze, S.S., Gogonin, I.I., Grigor'eva, N.I., and Dorokhov, A.R., 1980, "Determination of Heat Transfer Coefficient with Film Condensation of Stationary Vapor on a Vertical Surface", *Thermal Engineering*, Vol. 27, pp. 184-186.

Labuntsov, D.A., 1957, "Heat Transfer in Film Condensation of Pure Steam on Vertical Surfaces and Horizontal Tubes", *Teploenergetika*, Vol. 4, pp. 72.

Lee, J., 1964, "Turbulent Film Condensation", *A.I.Ch.E. Journal*, Vol. 10, pp. 540-544.

Lee, KY., and Kim, M.H. 2008, "Effect of an Interfacial Shear Stress on Steam Condensation in the Presence of a Noncondensable Gas in a Vertical Tube", *International Journal of Heat and Mass Transfer*, Vol. 51, pp. 5333-5343.

Lucas, K., and Moser, B., 1979, "Laminar Film Condensation of Pure Vapours in Tubes", *International Journal of Heat and Mass Transfer*, Vol. 22, pp. 431-435.

Muñoz-Cobo, J.L., Herranz, L., Sancho, J., Tkachenko, I., and Verdu, G., 1996, "Turbulent Vapor Condensation with Noncondensable Gases in Vertical Tubes", *International Journal of Heat and Mass Transfer*, Vol. 39, pp. 3249-3260.

No, H.C., and Park, S.H., 2002, "Non-Iterative Condensation Modeling for Steam Condensation with Non-Condensable Gas in a Vertical Tube", *International Journal of Heat and Mass Transfer*, Vol. 45, pp. 845-854.

Nusselt, W., 1916, "Die Oberflachenkondensation des Wasserdampfes", *Z. Ver. Deut. Ing.*, Vol. 2, 69.

Oh, S., and Revankar, S.T., 2005, "Analysis of the complete condensation in a vertical tube passive condenser", *International Communications in Heat and Mass Transfer*, Vol. 32, pp. 716-727.

Park, S.H., and No, H.C., 1999, "A Condensation Experiment in the Presence of Noncondensables in a Vertical Tube of a Passive Containment Cooling System and Its Assessment with RELAP5/MOD3.2", *Nuclear Technology*, Vol. 127, pp. 160-169.

Panday, P.K., 2003, "Two-dimensional turbulent film condensation of vapours flowing inside a vertical tube and between parallel plate: a numerical approach", *International Journal of Refrigeration*, Vol. 26, pp. 492-503.

Pletcher, R.H., 1974, "Prediction of Transpired Turbulent Boundary Layers", *Transactions of ASME Heat Transfer*, 96C, pp. 89-94.

Pohner, J.A., and Desai, P.V., 1989, "A Two-Fluid Analysis of Filmwise Condensation in Tubes", *International Journal of Engineering Science*, Vol. 27, pp. 549-564.

Revankar, S., Oh, S., and Zhou, W., 2010, "Condensation Correlation for a Vertical Passive Condenser System", *Nuclear Technology*, Vol. 170, pp. 28-39.

Rohsenow, W.M., 1956, "Heat Transfer and Temperature Distribution in Laminar Film Condensation", *Transaction of ASME*, Vol. 78, pp. 1645-1656.

Rohsenow, W.M., Webber, J.H., and Ling, A.T., 1956, "Effect of Vapor Velocity on Laminar and Turbulent Film Condensation", *Transaction of ASME*, Vol. 78, pp. 1637-1643.

Shah, M.M., 1978, "A General Correlation for Heat Transfer During Film Condensation Inside Pipes", *International Journal of Heat and Mass Transfer*, Vol. 22, pp. 547-556.

Shah, M.M., 2009, "An Improved and Extended General Correlation for Heat Transfer During Condensation in Plain Tubes", *HVAC&R Research*, Vol. 15, pp. 889-913.

Shang, D.Y., and Wang, B.X., 1997, "An extended study on steady-state laminar film condensation of a superheated vapour on an isothermal vertical plate", *International Journal of Heat and Mass Transfer*, Vol. 40, pp. 931-941.

Sparrow, E.M., and Gregg, J.L., 1959, "A Boundary-Layer Treatment of Laminar Film Condensation", *Journal of Heat Transfer*, Vol. 81, pp. 13-18.

Spiegel, M.R., 1968, *Mathematical Handbook of Formulas and Tables*, First Ed., McGraw-Hill Book Company.

Shu, J.J., and Wilks, G., 1995, "An accurate numerical method for systems of differentio-integral equations associated with multiphase flow", *Computer and Fluids*, Vol. 24, pp. 625-652.

Siddique, M., Golay, M.W., and Kazimi, M.S., 1993, "Local Heat Transfer Coefficients for Forced-Convection Condensation of Steam in a Vertical Tube in the Presence of a Noncondensable Gas", *Nuclear Technology*, Vol. 102, pp. 386-402.

Ünsal, M., 1988, "A closed form solution for average heat transfer coefficient during forced vapour flow condensation on inclined surfaces", *International Journal of Heat and Mass Transfer*, Vol. 31, pp. 1613-1617.

Vierow, K.M., and Schrock, V.E., 1991, "Condensation in a natural circulation loop with noncondensable gases: Part 1 – Heat transfer", *Proceeding of the International Conference on Multiphase Flow*, Tsukuba, Japan, pp. 183-186.

Winkler, C.M., Chen, T.S., and Minkowycz, W.J., 1999, "Film Condensation of Saturated and Superheated Vapors along Isothermal Vertical Surfaces in Mixed Convection", *Numerical Heat Transfer, Part A*, Vol. 36, pp. 375-393.

Xu, H., You, X.C., and Pop, I., 2008, "Analytical approximation for laminar film condensation of saturated stream on an isothermal vertical plat", *Applied Mathematical Modelling*, Vol. 32, pp. 738-748.

Yao, G.F., and Ghiaasiaan, S.M., 1996, "Numerical modeling of condensing two-phase flows", *Numerical Heat Transfer*, Vol. 30, pp. 137-159.

Yuann, R.Y., 1993, *Condensation from Vapor-Gas Mixtures for Forced Downflow Inside a Tube*, PhD Thesis, University of California at Berkeley.

Zhou, W., Henderson, G., and Revankar, S.T., 2010, "Condensation in a vertical tube bundle passive condenser – Part 1: Through flow condensation", *International Journal of Heat and Mass Transfer*, Vol. 53, pp. 1146-1155.

APPENDIX A

MATLAB LISTINGS

This appendix lists major MATLAB files used in the present work. The names of functions and variables are self-explanatory. If additional clarifications are required, comments are inserted only at the first appearance. All thermodynamic tables and functions required to look up or compute the fluid properties are also listed.

```
% main script file: compute/plot delta and h
clear;
g=9.81;
Re=30000;            % inlet Reynolds number
dt=40;               % inlet-to-wall ΔT (K)
ro=0.01;             % tube radius (m)
Tin=373.15;          % inlet saturation temperature (K)
Pin=f_h2o_Psat(Tin); % inlet saturation pressure (Pa)
Twall=Tin-dt;        % wall temperature (K)
Tfilm=Twall+0.31*dt; % liquid film temperature (K)
[klqd, rolqd, romix, vislqd, vismix, hfg, CPlqd]= ...
     f_h2o_get_properties(Tin,Tfilm);
[EndZ,p0,d0] = f_end_z(Tin,Tfilm,Re,ro,0,0,dt);
n=50;
z=linspace(0,EndZ,n);
for i=1:n
  [pLL(i),dLL(i),hLL(i)]=f_deltaX_quartic_varT( ...
      1,Tin,Tfilm,Re,ro,z(i),0,0,dt);
  [mVdot(i),mLdot(i),uVbar(i),uLbar(i),ReV(i),ReL(i)]= ...
      f_MVR_varT(0,Tin,Tfilm,Re,ro,pLL(i),0,0);
  [visturV(i),visturL(i)]=f_get_VisTur( ...
      vismix,vislqd,Re,dt,ro,Pin,ReV(i),ReL(i));
  [pTL(i),dTL(i),hTL(i)]=f_deltaX_quartic_varT( ...
      1,Tin,Tfilm,Re,ro,z(i),0,visturV(i),dt);
  [pLT(i),dLT(i),hLT(i)]=f_deltaX_quartic_varT( ...
      1,Tin,Tfilm,Re,ro,z(i),visturL(i),0,dt);
  [pTT(i),dTT(i),hTT(i)]=f_deltaX_quartic_varT( ...
      1,Tin,Tfilm,Re,ro,z(i),visturL(i),visturV(i),dt);
end;
hold on;
box on;
axis([0 Inf 0 Inf]);
set(gca,'FontName','FixWidth', ...
     'FontSize',14,'LineWidth',1.5);
set(gcf,'DefaultLineLineWidth',1.5);
xlabel('z*','FontSize',18);
ylabel('\delta*','FontSize',18);
plot(z/ro,dLL/ro,'k');
plot(z/ro,dTL/ro,'k--');
plot(z/ro,dLT/ro,'k:');
plot(z/ro,dTT/ro,'k-.');
legend('LL','TL','LT','TT','Location','SE');
legend('boxoff');
```

```
function [deltaX,deltaD,h] = f_deltaX_quartic_varT ...
     (num,TV,TL,Re,ro,z,visLT,visVT,chat)
% deltaX = δ+
% deltaD = δ
% h = heat transfer coefficient
% num = 1,2 : closed-form solution or poly root search
% TV, TL = T saturation and T film to compute properties
% Re = inlet Reynolds number
% ro = tube radius
% z = axial location
% visLT = liquid turbulent viscosity (0 for laminar)
% visVT = vapor turbulent viscosity (0 for lamninar)
% chat = [ao a1 ...] variable T OR [dt] constant T
  g=9.81;
  [klqd, rolqd, romix, vislqd, vismix, hfg, CPlqd] = ...
     f_h2o_get_properties(TV,TL);
  visLeff=vislqd+visLT;
  visVeff=vismix+visVT;
  kLeff=klqd+visLT*CPlqd;
  B=2*Re*vismix*visVeff/(g*romix*(rolqd-romix)*ro^3);
  dtZ=0;
  for i=1:size(chat,2)
    dtZ=dtZ+chat(i)*(z^i)/i;
  end;
  C=4*kLeff*visLeff*dtZ/(g*hfg*rolqd*(rolqd-romix)*ro^4);
  if (num==1)
    y1=nthroot(C*(sqrt(64*C/27+0.25*B^4)-0.5*B^2),3)- ...
       nthroot(C*(sqrt(64*C/27+0.25*B^4)+0.5*B^2),3);
    X=-0.25*(B+sqrt(B^2+4*y1))+ ...
       0.5*sqrt(0.5*B^2+0.5*B*sqrt(B^2+4*y1)-y1+ ...
                2*sqrt(y1^2+4*C));
  end;
  if (num==2)
    Xv=roots([1 B 0 0 -C]);
    X=Xv(4);
  end;
  deltaX=1-2*X;
  deltaD=ro*(1-sqrt(deltaX));
  h=-2*kLeff/(ro*log(deltaX));
end
```

```
function [mVdot,mLdot,uVbar,uLbar,ReV,ReL] = ...
     f_MVR_varT(num,TV,TL,Re,ro,Xi,visLT,visVT)
%mVdot, mLdot = vapor and liquid mass flow rate
%uVbar, uLbar = vapor and liquid average velocity
%ReV, ReL = vapor and liquid Reynolds number
%num = 0,1,2: compute by ρ+ , ρ+1 , ρ+2
%Xi = specific δ+ = Xi
  g=9.81;
  [klqd, rolqd, romix, vislqd, vismix] = ...
     f_h2o_get_properties(TV,TL);
  visLeff=vislqd+visLT;
  visVeff=vismix+visVT;
  fd=f_density_varT(num,TV,TL,Re,ro,Xi,visLT,visVT);
  dd=ro*(1-sqrt(Xi));
  mvs=(-fd*pi*g*romix/8)*ro^4* ...
      (Xi^2/visVeff+2*Xi*(1-Xi)/visLeff);
  mvo=(pi*romix*g*(rolqd-romix)/(4*visLeff))*ro^4* ...
      (Xi*(1-Xi)+Xi^2*log(Xi));
  mVdot=(mvs+mvo);
  uVbar=(mVdot/(romix*pi*(ro-dd)^2));
  ReV=(romix*2*(ro-dd)*uVbar/visVeff);
  m1=pi*rolqd*g*(rolqd-romix)*ro^4/(8*visLeff);
  m2=-fd*(1-2*Xi+Xi^2)/(rolqd-romix);
  m3=1-4*Xi+3*Xi^2-2*Xi^2*log(Xi);
  mLdot=m1*(m2+m3);
  if (mLdot==0)
    uLbar=0;
  else
    uLbar=mLdot/(rolqd*pi*(ro^2-(ro-dd)^2));
  end;
  ReL=2*mLdot/(pi*visLeff*(ro-dd));
end
```

```
function [frho,dPdz,Xrho0,Drho0] = ...
     f_density_varT(num,TV,TL,Re,ro,Xi,visLT,visVT)
%frho = density function
%dPdz = pressure gradient
%Xrho0 = delta plus at end of condensation
%Drho0 = film thickness at end of condensation
  g=9.81;
  [klqd, rolqd, romix, vislqd, vismix] = ...
     f_h2o_get_properties(TV,TL);
  visLeff=vislqd+visLT;
  visVeff=vismix+visVT;
  a=romix/rolqd;
  b=a*visLeff/visVeff;
  M=2*visLeff*vismix*Re/(g*rolqd*(rolqd-romix)*ro^3);
  %the numerator and denominator of density function
  fdn=@(X)2*M-1+2*(2-a)*X+(2*a-3)*X^2+2*(1-a)*X^2*log(X);
  fdd=@(X)1+2*(a-1)*X+(1-2*a+b)*X^2;
  if (num==0), frho=-(rolqd-romix)*fdn(Xi)/fdd(Xi); end;
  if (num==1), frho=-(rolqd-romix)*2*M/b; end;
  if (num==2), frho=-(rolqd-romix)*fdn(Xi)/b; end;
  dPdz=g*(romix+frho);
  Xrho0=fzero(fdn,1);
  Drho0=ro*(1-sqrt(Xrho0));
end
```

```
function [EndZ,Xd0,dd0] = ...
     f_end_z(TV,TL,Re,ro,visLT,visVT,dt)
%EndZ = z at end of condensation
%Xd0 = delta plus at end of condensation
%dd0 = film thickness at end of condensation
  g=9.81;
  [klqd, rolqd, romix, vislqd, vismix, hfg] = ...
     f_h2o_get_properties(TV,TL);
  visLeff=vislqd+visLT;
  visVeff=vismix+visVT;
  a=romix/rolqd;
  b=a*visLeff/visVeff;
  M=2*visLeff*vismix*Re/(g*rolqd*(rolqd-romix)*ro^3);
  [fd,dPdz,Xd0,dd0]= ...
     f_density_varT(2,TV,TL,Re,ro,1,visLT,visVT);
  %delta functions
  b1=(2/b)*(3-a-2*M)-4;
  b2=(2/b)*(5*a+2*M-11)+4;
  b3=(2/b)*(13-7*a);
  b4=(2/b)*(3*a-5);
  b5=(4/b)*(1-a)-4;
  b6=(12/b)*(a-1);
  b7=(8/b)*(1-a);
  f1=@(X)b1*(X*log(X)-X+1);
  f2=@(X)b2*(X^2*log(X)/2-X^2/4+1/4);
  f3=@(X)b3*(X^3*log(X)/3-X^3/9+1/9);
  f4=@(X)b4*(X^4*log(X)/4-X^4/16+1/16);
  f5=@(X)b5*(X^2*log(X)^2/2-X^2*log(X)/2+X^2/4-1/4);
  f6=@(X)b6*(X^3*log(X)^2/3-2*X^3*log(X)/9+2*X^3/27-2/27);
  f7=@(X)b7*(X^4*log(X)^2/4-X^4*log(X)/8+X^4/32-1/32);
  EdNuS4=(-(f1(Xd0)+f2(Xd0)+f3(Xd0)+f4(Xd0)+ ...
         f5(Xd0)+f6(Xd0)+f7(Xd0))/8);
  EndZ=EdNuS4*ro^4*g*hfg*rolqd*(rolqd-romix)/ ...
       (4*klqd*dt*vislqd);
end
```

```
function [visturV,visturL] = . . .
     f_get_VisTur(vismix,vislqd,Re,dt,ro,Pin,ReV,ReL)
%visturV : vapor turbulent viscosity
%visturL : liquid turbulent viscosity
%vismix : vapor molecular viscosity
%vislqd : liquid molecular viscosity
%ReV : local vapor Reynolds number
%ReL : local liquid Reynolds number
  cV1=120*(ro-5.5*ro.^2)*dt*(1-Re/90000)+Re/3000;
  visturV=vismix*cV1*(ReV/Re)^4;
  cL1=0.003*(Pin^-0.5)*(1/ro+12)*dt*((Re+2300)^-0.5);
  visturL=vislqd*cL1*ReL;
end
```

```
function [deltaX,deltaD] = f_deltaX ...
     (num,dt,Re,ro,z,visLT,visVT,file_loc)
% deltaX = δ+
% deltaD = δ
% num = 1,2 : root search by ρ+1 or ρ+2
% file_loc = user supply property file
  g=9.81;
  [klqd, rolqd, romix, vislqd, vismix, hfg, CPlqd] = ...
     f_properties(file_loc);
  a=romix/rolqd;
  visLeff=vislqd+visLT;
  visVeff=vismix+visVT;
  kLeff=klqd+visLT*CPlqd;
  b=a*visLeff/visVeff;
  M=2*visLeff*vismix*Re/(g*rolqd*(rolqd-romix)*ro^3);
  B=M/b;
  %delta functions
  b1=(2/b)*(3-a-2*M)-4;
  b2=(2/b)*(5*a+2*M-11)+4;
  b3=(2/b)*(13-7*a);
  b4=(2/b)*(3*a-5);
  b5=(4/b)*(1-a)-4;
  b6=(12/b)*(a-1);
  b7=(8/b)*(1-a);
  f1=@(X)b1*(X*log(X)-X+1);
  f2=@(X)b2*(X^2*log(X)/2-X^2/4+1/4);
  f3=@(X)b3*(X^3*log(X)/3-X^3/9+1/9);
  f4=@(X)b4*(X^4*log(X)/4-X^4/16+1/16);
  f5=@(X)b5*(X^2*log(X)^2/2-X^2*log(X)/2+X^2/4-1/4);
  f6=@(X)b6*(X^3*log(X)^2/3-2*X^3*log(X)/9+2*X^3/27-2/27);
  f7=@(X)b7*(X^4*log(X)^2/4-X^4*log(X)/8+X^4/32-1/32);
  dNuS=((4*kLeff*dt*visLeff*z/ ...
       (g*hfg*rolqd*(rolqd-romix)))^0.25)/ro;
  fX1=@(X)2*X^2*log(X)^2+2*(2*(1+B)*X-(2+B)*X^2)*log(X)+...
      2+3*B-4*(1+B)*X+(2+B)*X^2-8*dNuS^4;
  fX2=@(X)f1(X)+f2(X)+f3(X)+f4(X)+f5(X)+f6(X)+f7(X)+...
      8*dNuS^4;
  if (num==1),
    deltaX=fzero(fX1,1); deltaD=ro*(1-sqrt(deltaX)); end;
  if (num==2),
    deltaX=fzero(fX2,1); deltaD=ro*(1-sqrt(deltaX)); end;
end
```

```
function [klqd,rolqd,romix,vislqd,vismix,hfg,CPlqd]= ...
     f_h2o_get_properties(TV,TL)
%klqd: liquid thermal conductivity
%rolqd: liquid density
%romix: vapor density
%vislqd: liquid molecular viscosity
%vismix: vapor molecular viscosity
%hfg: latent heat of vaporization
%CPlqd: liquid specific heat
%TV,TL: vapor saturation T, liquid film T
  [TTBL,ROLTBL,ROVTBL,HfgTBL,CPLTBL,CPVTBL,VILTBL, ...
     VIVTBL,KLTBL,KVTBL] = f_h2o_set_table();
  klqd=interp1(TTBL,KLTBL,TL);
  rolqd=f_h2o_liquid_density(TL);
  romix=f_h2o_Psat(TV)*18.015/(TV*8314.5);
  vislqd=interp1(TTBL,VILTBL,TL);
  vismix=interp1(TTBL,VIVTBL,TV);
  hfg=f_h2o_latent_heat(TL);
  CPlqd=interp1(TTBL,CPLTBL,TL);
end
```

```
function rolqd = f_h2o_liquid_density( Temp )
%liquid density
  A = 1.d0;
  B = -1.9153882d0;
  C = 1.2015186d1;
  D = -7.8464025d0;
  E = [-3.888614d0 2.0582238d0 -2.0829991d0 ...
       8.2180004d-1 4.7549742d-1 0.d0 0.d0];
  VFCR = 3.155d-3;
  TCR = 647.3d0;
  TC = (TCR-Temp)/TCR;
  SUM = 0.d0;
  for N=1:7
    SUM = SUM + E(N)*TC^N;
  end;
  YS = A + B*TC^(1/3) + C*TC^(5/6) + D*TC^(8.75d-1) + SUM;
  rolqd = 1.d0/(YS*VFCR);
end
```

```
function Psat = f_h2o_Psat(Tsat)
%Find saturation P by known saturation T
%Valid for the temperature range 273.16 < T(K) < 647.3
  if (Tsat<600)
    A = 0.4267760e2;
    B = -0.389270e4;
    C = -0.948654e1;
  else
    A = -0.3875992e3;
    B = -0.1258750e5;
    C = -0.1525780e2;
  end;
  Psat = exp(B./(Tsat-A)-C)*1e6;
end
```

```
function Tsat = f_h2o_Tsat(Psat)
% Find saturation T by known saturation P
% 6.11e2 < Psat < 22.1e6
  if (Psat < 12.33e6)
    A = 0.426776e2;
    B = -0.38927e4;
    C = -0.948654e1;
  else
    A = -0.3875992e3;
    B = -0.125875e5;
    C = -0.152578e2;
  end;
  Tsat = A + B./(log(Psat*1e-6)+C);
end
```

```
function Hfg = f_h2o_latent_heat( Temp )
  A = 0.d0;
  B = 7.79221d-1;
  C = 4.62668d0;
  D = -1.07931d0;
  E = [-3.87446d0 2.94553d0 -8.06395d0 1.15633d1 ...
       -6.02884d0 0.d0 0.d0];
  HfgTP = 2.5009d3;
  TCR = 647.3d0;
  TC = (TCR-Temp)/TCR;
  SUM = 0.d0;
  for N=1:7
    SUM = SUM + E(N)*TC^N;
  end;
  YS = A + B*TC^(1.d0/3.d0) + C*TC^(5.d0/6.d0) + ...
       D*TC^0.875d0 + SUM;
  Hfg = YS*HfgTP*1.d3;
end
```

```
function [TTBL,ROLTBL,ROVTBL,HfgTBL,CPLTBL,CPVTBL, ...
          VILTBL,VIVTBL,KLTBL,KVTBL,PrLTBL,PrVTBL] = ...
          f_h2o_set_table()
% properties by table
%temperature
TTBL = [273.15 275.0 280.0 285.0 290.0 ...
        295.0 300.0 305.0 310.0 315.0 ...
        320.0 325.0 330.0 335.0 340.0 ...
        345.0 350.0 355.0 360.0 365.0 ...
        370.0 373.15 375.0 380.0 385.0 ...
        390.0 400.0 410.0 420.0 430.0 ...
        440.0 450.0 460.0 470.0 480.0 ...
        490.0 500.0 510.0 520.0 530.0 ...
        540.0 550.0 560.0 570.0 580.0 ...
        590.0 600.0 610.0 620.0 625.0 ...
        630.0 635.0 640.0 645.0 647.3];
%liquid specific volume and density
VOLTBL=1e-3*[1.000 1.000 1.000 1.000 1.001 ...
             1.002 1.003 1.005 1.007 1.009 ...
             1.011 1.013 1.016 1.018 1.021 ...
             1.024 1.027 1.030 1.034 1.038 ...
             1.041 1.044 1.045 1.049 1.053 ...
             1.058 1.067 1.077 1.088 1.099 ...
             1.110 1.123 1.137 1.152 1.167 ...
             1.184 1.203 1.222 1.244 1.268 ...
             1.294 1.323 1.355 1.392 1.433 ...
             1.482 1.541 1.612 1.705 1.778 ...
             1.856 1.935 2.075 2.351 3.170];
ROLTBL=1./VOLTBL;
%vapor specific volume and density
VOVTBL=1e-3*[206.3 181.7 130.4 99.4 69.7 ...
             51.94 39.13 29.74 22.93 17.82 ...
             13.98 11.06 8.82 7.09 5.74 ...
             4.683 3.846 3.180 2.645 2.212 ...
             1.861 1.679 1.574 1.337 1.142 ...
             0.98 0.731 0.553 0.425 0.331 ...
             0.261 0.208 0.167 0.136 0.111 ...
             0.0922 0.0766 0.0631 0.0525 0.0445 ...
             0.0375 0.0317 0.0269 0.0228 0.0193 ...
             0.0163 0.0137 0.0115 0.0094 0.0085 ...
             0.0075 0.0066 0.0057 0.0045 0.0032];
ROVTBL=1./VOVTBL;
%heat of vaporization
HfgTBL = 1e3*[2502 2497 2485 2473 2461 ...
              2449 2438 2426 2414 2402 ...
              2390 2378 2366 2354 2342 ...
              2329 2317 2304 2291 2278 ...
```

```
              2265 2257 2252 2239 2225 ...
              2212 2183 2153 2123 2091 ...
              2059 2024 1989 1951 1912 ...
              1870 1825 1779 1730 1679 ...
              1622 1564 1499 1429 1353 ...
              1274 1176 1068 941 858 ...
              781 683 560 361 0];
%liquid specific heat
CPLTBL = 1e3*[4.217 4.211 4.198 4.189 4.184 ...
              4.181 4.179 4.178 4.178 4.179 ...
              4.180 4.182 4.184 4.186 4.188 ...
              4.191 4.195 4.199 4.203 4.209 ...
              4.214 4.217 4.220 4.226 4.232 ...
              4.239 4.256 4.278 4.302 4.331 ...
              4.36  4.40  4.44  4.48  4.53 ...
              4.59  4.66  4.74  4.84  4.95 ...
              5.08  5.24  5.43  5.68  6.00 ...
              6.41  7.00  7.85  9.35 10.6 ...
              12.6  16.4  26.0  90.0   1.0d10];
%vapor specific heat
CPVTBL = 1e3*[1.854 1.855 1.858 1.861 1.864 ...
              1.868 1.872 1.877 1.882 1.888 ...
              1.895 1.903 1.911 1.920 1.930 ...
              1.941 1.954 1.968 1.983 1.999 ...
              2.017 2.029 2.036 2.057 2.080 ...
              2.104 2.158 2.221 2.291 2.369 ...
              2.46 2.56 2.68 2.79 2.94 ...
              3.10 3.27 3.47 3.70 3.96 ...
              4.27 4.64 5.09 5.67 6.40 ...
              7.35 8.75 11.1 15.4 18.3 ...
              22.1 27.6 42.0 1.0d10 1.0d10];
%liquid viscosity
VILTBL = 1e-6*[1750.0 1652.0 1422.0 1225.0 1080.0 ...
               959.0 855.0 769.0 695.0 631.0 ...
               577.0 528.0 489.0 453.0 420.0 ...
               389.0 365.0 343.0 324.0 306.0 ...
               289.0 279.0 274.0 260.0 248.0 ...
               237.0 217.0 200.0 185.0 173.0 ...
               162.0 152.0 143.0 136.0 129.0 ...
               124.0 118.0 113.0 108.0 104.0 ...
               101.0 97.0 94.0 91.0 88.0 ...
               84.0 81.0 77.0 72.0 70.0 ...
               67.0 64.0 59.0 54.0 45.0];
%vapor viscosity
VIVTBL = 1e-6*[8.02 8.09 8.29 8.49 8.69 ...
               8.89 9.09 9.29 9.49 9.69 ...
               9.89 10.09 10.29 10.49 10.69 ...
```

```
              10.89 11.09 11.29 11.49 11.69 ...
              11.89 12.02 12.09 12.29 12.49 ...
              12.69 13.05 13.42 13.79 14.14 ...
              14.50 14.85 15.19 15.54 15.88 ...
              16.23 16.59 16.95 17.33 17.72 ...
              18.1 18.6 19.1 19.7 20.4 ...
              21.5 22.7 24.1 25.9 27.0 ...
              28.0 30.0 32.0 37.0 45.0];
%liquid thermal conductivity
KLTBL = 1e-3*[569.0 574.0 582.0 590.0 598.0 ...
             606.0 613.0 620.0 628.0 634.0 ...
             640.0 645.0 650.0 656.0 660.0 ...
             668.0 668.0 671.0 674.0 677.0 ...
             679.0 680.0 681.0 683.0 685.0 ...
             686.0 688.0 688.0 688.0 685.0 ...
             682.0 678.0 673.0 667.0 660.0 ...
             651.0 642.0 631.0 621.0 608.0 ...
             594.0 580.0 563.0 548.0 528.0 ...
             513.0 497.0 467.0 444.0 430.0 ...
             412.0 392.0 367.0 331.0 238.0];
%vapor thermal conductivity
KVTBL = 1e-3*[18.2 18.3 18.6 18.9 19.3 ...
             19.5 19.6 20.1 20.4 20.7 ...
             21.0 21.3 21.7 22.0 22.3 ...
             22.6 23.0 23.3 23.7 24.1 ...
             24.5 24.8 24.9 25.4 25.8 ...
             26.3 27.2 28.2 29.8 30.4 ...
             31.7 33.1 34.6 36.3 38.1 ...
             40.1 42.3 44.7 47.5 50.6 ...
             54.0 58.3 63.7 76.7 76.7 ...
             84.1 92.9 103.0 114.0 121.0 ...
             130.0 141.0 155.0 178.0 238.0];
%liquid Prandtl number
PrLTBL = [12.99 12.22 10.26 8.81 7.56 ...
          6.62 5.83 5.2 4.62 4.16 ...
          3.77 3.42 3.15 2.88 2.66 ...
          2.45 2.29 2.14 2.02 1.91 ...
          1.8 1.76 1.7 1.61 1.53 ...
          1.47 1.34 1.24 1.16 1.09 ...
          1.04 0.99 0.95 0.92 0.89 ...
          0.87 0.86 0.85 0.84 0.85 ...
          0.86 0.87 0.9 0.94 0.99 ...
          1.05 1.14 1.3 1.52 1.65 ...
          2 2.7 4.2 12 1e10];
%vapor Prandtl number
PrVTBL = [0.815 0.817 0.825 0.833 0.841 ...
          0.849 0.857 0.865 0.873 0.883 ...
```

```
            0.894 0.901 0.908 0.916 0.925 ...
            0.933 0.942 0.951 0.960 0.969 ...
            0.978 0.984 0.987 0.999 1.004 ...
            1.013 1.033 1.054 1.075 1.1 ...
            1.12 1.14 1.17 1.2 1.23 ...
            1.25 1.28 1.31 1.35 1.39 ...
            1.43 1.47 1.52 1.59 1.68 ...
            1.84 2.15 2.6 3.46 4.2 ...
            4.8 6 9.6 26 1e10];
end
```

APPENDIX B

EXAMPLE OF CALCULATION USING EXCEL

A sample computation using Excel and the resulting plot are shown in Figures B.1 to B.7. They are self-explanatory and are from a single spreadsheet that is divided into six computing groups for clarity. The Excel formulas in all computing cells, which are formatted for easy drag/copy/paste to the end of condensation, are also shown. Note that the fluid properties are looked up or computed elsewhere to match the input parameters. For the laminar LL flows, the computation in Figure B.1 is all that required. For the turbulent TT flows, the computation is from Figures B.1 to B.4. Figures B.5 and B.6 are for the asymptotic TL and LT flows.

	A	B	C	D	E	F	G	H	I
1	Re=	30000	kL=	6.68E-01	hfg=	2.33E+06			
2	dt=	40	ρL=	9.76E+02	ρV=	5.86E-01			
3	ro=	0.01	μL=	3.86E-04	μV=	1.20E-05			
4	g=	9.81	CPlqd=	4.19E+03					
5	Pin=	1.01E+05							
6									
7					Laminar Vapor, Laminar Liquid				
8	z	z*	B	C	y1	X	δ+	δ_LL	δ*_LL
9	0.000	0.00	1.54E-03	0.00E+00	0.00E+00	0.00E+00	1.00E+00	0.00E+00	0.00E+00
10	0.050	5.00	1.54E-03	9.49E-09	-5.96E-07	9.51E-03	9.81E-01	9.55E-05	9.55E-03
11	0.100	10.00	1.54E-03	1.90E-08	-5.96E-07	1.14E-02	9.77E-01	1.14E-04	1.14E-02

Figure B.1: Excel computation: input parameters and LL flows

```
B9    =A9/$B$3

C9    =2*$F$3*$F$3*$B$1/($B$4*($D$2-$F$2)*$F$2*$B$3^3)

D9    =4*$D$3*$D$1*$B$2*A9/
       ($B$3^4*$F$1*$B$4*$D$2*($D$2-$F$2))

E9    =(D9*(SQRT((64/27)*D9+0.25*C9^4)-0.5*C9^2))^(1/3)-
       (D9*(SQRT((64/27)*D9+0.25*C9^4)+0.5*C9^2))^(1/3)

F9    =-0.25*(C9+SQRT(C9^2+4*E9))+0.5*SQRT(0.5*C9^2+
       0.5*C9*SQRT(C9^2+4*E9)-E9+2*SQRT(E9^2+4*D9))

G9    =1-2*F9

H9    =$B$3*(1-SQRT(G9))

I9    =H9/$B$3
```

	J	K	L	M	N
1	α=	6.01E-04			
2	β=	1.93E-02			
3	M=	2.98E-05			
4					
5					
6					
7	Selected additional quantities				
8	ρ+	mL	mV	ReV	ReL
9	-3.01E+00	0.00E+00	5.66E-03	3.00E+04	0.00E+00
10	-2.82E+00	5.37E-04	5.13E-03	2.74E+04	8.93E+01
11	-2.64E+00	8.82E-04	4.78E-03	2.56E+04	1.47E+02

Figure B.2: Excel computation: additional quantities of interest

```
K1    =F2/D2

K2    =K1*D3/F3

K3    =2*D3*F3*B1/(B4*D2*(D2-F2)*B3^3)

J9    =-($D$2-$F$2)*(2*$K$3-1+2*(2-$K$1)*G9+(2*$K$1-3)*G9^2+
       2*(1-$K$1)*G9^2*LN(G9))/(1+2*($K$1-1)*G9+
       (1+$K$2-2*$K$1)*G9^2)

K9    =(0.125*PI()*$B$4*$D$2*$B$3^4/$D$3)*(-J9*(1-G9)^2+
       ($D$2-$F$2)*(1-4*G9+3*G9^2-2*G9^2*LN(G9)))

L9    =(PI()*$B$4*$F$2*$B$3^4)*
       (-0.125*J9*(G9^2/$F$3+2*G9*(1-G9)/$D$3)+
       0.25*($D$2-$F$2)/$D$3*(G9*(1-G9)+G9^2*LN(G9)))

M9    =2*L9/(PI()*$F$3*($B$3-H9))

N9    =2*K9/(PI()*$D$3*($B$3-H9))
```

	O	P	Q	R	S	T	U
1	Cv=	40.24					
2	CL=	2.35E-04					
3							
4							
5							
6							
7	Turbulent parameters						
8	μVt	μV,eff	μLt	μL,eff	kL,eff	B,tur	C,tur
9	4.84E-04	4.96E-04	0.00E+00	3.86E-04	6.68E-01	6.37E-02	0.00E+00
10	3.38E-04	3.50E-04	8.12E-06	3.94E-04	7.02E-01	4.49E-02	1.02E-08
11	2.57E-04	2.69E-04	1.34E-05	4.00E-04	7.24E-01	3.46E-02	2.13E-08

Figure B.3: Excel computation: turbulent viscosities correlation

```
P1    =120*($B$3-5.5*$B$3^2)*$B$2*(1-$B$1/90000)+
       $B$1/3000

P2    =0.003*(1/SQRT($B$5))*(1/$B$3+12)*$B$2*
       (1/SQRT($B$1+2300))

O9    =$F$3*$P$1*(M9/$B$1)^4

P9    =$F$3+O9

Q9    =$D$3*$P$2*N9

R9    =$D$3+Q9

S9    =$D$1+Q9*$D$4

T9    =2*P9*$F$3*$B$1/($B$4*($D$2-$F$2)*$F$2*$B$3^3)

U9    =4*R9*S9*$B$2*A9/($B$3^4*$F$1*$B$4*$D$2*($D$2-$F$2))
```

	V	W	X	Y	Z
1					
2					
3					
4					
5					
6					
7	Turbulent Vapor, Turbulent Liquid				
8	y1	X	δ+	δ_TT	δ*_TT
9	0.00E+00	0.00E+00	1.00E+00	0.00E+00	0.00E+00
10	-2.25E-04	5.85E-03	9.88E-01	5.87E-05	5.87E-03
11	-2.02E-04	7.94E-03	9.84E-01	7.97E-05	7.97E-03

Figure B.4: Excel computation: TT flows

```
V9   =(U9*(SQRT((64/27)*U9+0.25*T9^4)-0.5*T9^2))^(1/3)-
      (U9*(SQRT((64/27)*U9+0.25*T9^4)+0.5*T9^2))^(1/3)

W9   =-0.25*(T9+SQRT(T9^2+4*V9))+0.5*SQRT(0.5*T9^2+
      0.5*T9*SQRT(T9^2+4*V9)-V9+2*SQRT(V9^2+4*U9))

X9   =1-2*W9

Y9   =$B$3*(1-SQRT(X9))

Z9   =Y9/$B$3
```

	AA	AB	AC	AD	AE
1					
2					
3					
4					
5					
6					
7	Turbulent Vapor, Laminar Liquid				
8	y1	X	δ+	δ_TL	δ*_TL
9	0.00E+00	0.00E+00	1.00E+00	0.00E+00	0.00E+00
10	-2.21E-04	5.72E-03	9.89E-01	5.74E-05	5.74E-03
11	-1.98E-04	7.66E-03	9.85E-01	7.69E-05	7.69E-03

Figure B.5: Excel computation: TL flows

```
AA9  =(D9*(SQRT((64/27)*D9+0.25*T9^4)-0.5*T9^2))^(1/3)-
      (D9*(SQRT((64/27)*D9+0.25*T9^4)+0.5*T9^2))^(1/3)

AB9  =-0.25*(T9+SQRT(T9^2+4*AA9))+0.5*SQRT(0.5*T9^2+
      0.5*T9*SQRT(T9^2+4*AA9)-AA9+2*SQRT(AA9^2+4*D9))

AC9  =1-2*AB9

AD9  =$B$3*(1-SQRT(AC9))

AE9  =AD9/$B$3
```

	AF	AG	AH	AI	AJ
1					
2					
3					
4					
5					
6					
7	Laminar Vapor, Turbulent Liquid				
8	y1	X	δ+	δ_LT	δ*_LT
9	0.00E+00	0.00E+00	1.00E+00	0.00E+00	0.00E+00
10	-5.96E-07	9.68E-03	9.81E-01	9.73E-05	9.73E-03
11	-5.96E-07	1.17E-02	9.77E-01	1.18E-04	1.18E-02

Figure B.6: Excel computation: LT flows

```
AF9  =(U9*(SQRT((64/27)*U9+0.25*C9^4)-0.5*C9^2))^(1/3)-
      (U9*(SQRT((64/27)*U9+0.25*C9^4)+0.5*C9^2))^(1/3)

AG9  =-0.25*(C9+SQRT(C9^2+4*AF9))+0.5*SQRT(0.5*C9^2+
      0.5*C9*SQRT(C9^2+4*AF9)-AF9+2*SQRT(AF9^2+4*U9))

AH9  =1-2*AG9

AI9  =$B$3*(1-SQRT(AH9))

AJ9  =AI9/$B$3
```

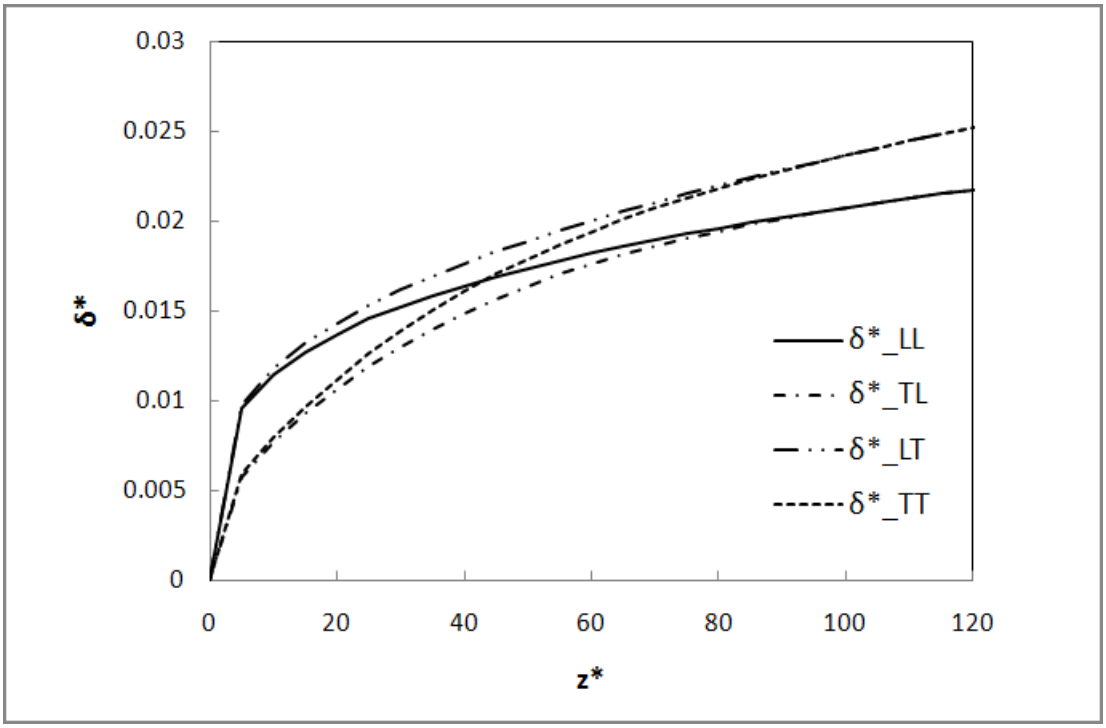

Figure B.7: Excel computation: resulting chart